THE UNIVERSITY OF CHICAGO

DELINEATING THE DEVELOPMENT AND TRANSCRIPTIONAL REGULATION OF THE INNATE LYMPHOCYTE LINEAGE

A DISSERTATION SUBMITTED TO
THE FACULTY OF THE DIVISION OF THE BIOLOGICAL SCIENCES
AND THE PRITZKER SCHOOL OF MEDICINE
IN CANDIDACY FOR THE DEGREE OF
DOCTOR OF PHILOSOPHY

COMMITTEE ON IMMUNOLOGY

BY
DARSHAN NATARAJ KASAL

CHICAGO, ILLINOIS
AUGUST 2021

CONTENTS

LIST OF FIGURES

LIST OF TABLES

LIST OF ABBREVIATIONS

αLP	$\alpha 4\beta 7^+$ Lymphoid Progenitor
AhR	Aryl hydrocarbon Receptor
AREG	Amphiregulin
Arg1	Arginase 1
ATAC-seq	Assay for Transposase Accessible Chromatin with sequencing
BAC	Bacterial Artificial Chromosome
bHLH	basic Helix-Loop-Helix
BM	Bone Marrow
CD4SP	CD4 single-positive
CD8SP	CD8 single-positive
CHILP	Common Helper Innate Lymphoid Precursor
ChIP-seq	Chromatin Immunoprecipitation sequencing
CLP	Common Lymphoid Precursor
CNS	Conserved Non-coding Sequence
CR	Cryptopatch
CRISPR	Clustered Regularly Interspaced Short Palindromic Repeats
DC	Dendritic Cell
DN	Double Negative
DP	Double Positive
E#	Embryonic Day #
EGFP	Enhanced Green Fluorescent Protein
EILP	Early Innate Lymphoid Precursor
ETP	Early Thymic Progenitor
EYFP	Enhanced Yellow Fluorescent Protein
FL	Fetal Liver

GATA3	Gata binding protein 3
ID2	Inhibitor of DNA binding 2
iILCP	Incipient Innate Lymphoid Cell Precursor
iLTiP	Incipient Lymphoid Tissue-inducer Precursor
IFNγ	Interferon-γ
ILC	Innate Lymphoid Cell
ILC2P	Innate Lymphoid Cell 2 Precursor
ILCP	Innate Lymphoid Cell Precursor
ILF	Isolated Lymphoid Follicles
IRES	Internal Ribosome Entry Site
lncRNA	Long non-coding RNA
LTi	Lymphoid Tissue-inducer
LTiP	Lymphoid Tissue-inducer Precursor
MCMV	Mouse Cytomegalovirus
NCR	Natural Cytotoxicity Receptor
NK cell	Natural Killer Cell
NKT cell	Natural Killer T Cell
PLZF	Promyelocytic Leukemia Zinc Finger
pre-NKP	Pre-Natural Killer cell Precursor
RA	Retinoic Acid
rNKP	Refined Natural Killer cell Precursor
SI LP	Small Intestinal Lamina Propria
SG	Salivary Gland
TCF1	T cell factor 1
T_h	T helper
TF	Transcription Factor

TNFα	Tumor Necrosis Factor-α
TSLP	Thymic Stromal Lymphopoietin
UTR	Untranslated Region
VIP	Vasoactive Intestinal Peptide
WAT	White Adipose Tissue

ACKNOWLEDGMENTS

First and foremost I must thank my advisor Dr. Albert Bendelac. Over the course of my graduate studies, he has fostered an environment ripe for discovery by promoting projects tailored towards independent investigation, providing the resources for scientific inquiry, and pushing for rigorous interrogation and representation of results. Through his guidance I have grown tremendously as a scientist and advanced considerably in my ability to conduct research and publish findings.

It is my privilege to thank the Committee on Immunology for accepting me into the community at the University of Chicago. The regular seminars, presentations, and events made the COI program stand out and made it an association I appreciate being a part of. I would also like to thank my thesis committee members, Dr. Peter Savage, Dr. Fotini Gounari, and Dr. Anindita Basu for contributing their time and insight to help make my thesis project a success.

To the former lab members I've had the pleasure of working with over the years, thank you. I have Dr. Isabel Ishizuka to thank predominately for my early training in the lab, for getting me onto the right path, and for experimental assistance. Similarly, Dr. Ai-ping Mao offered her time to teach me ATAC-seq methodology and get me acclimated to the lab. Their work together served as the foundation for my project, which was successful in no small part to their endeavors. To my contemporary, Dr. Steven Erickson, I owe a great amount to the immense effort he put into advancing CRISPR/Cas9 methodologies in the lab. Moreover, I will be ever grateful for the long scientific discussions we had and for his companionship in lab, sometimes extending into the late night and early morning hours. I would like to thank Dr. Christoph Drees for, though I did not work with him directly, I appreciate our conversations and having had him as a colleague. To our lab manager, Crystal O'Leary, thank you for the work you did in organizing the lab, for the experimental help, and for the enjoyable chats at the bench. Lastly, I will acknowledge Zhitao Liang, who joined

the lab most recently, training him has been an informative experience and I appreciate his assistance with experiments.

At the University of Chicago, I profusely thank members of the Transgenics, Flow Cytometry, DNA Sequencing and Genotyping, Genomics, Human Tissue Resource Center, and Integrated Microscopy core facilities who have been instrumental in the completion of my research. Specifically, I would like to thank Linda Degenstein of the Transgenics core who shouldered our constant pursuits with CRISPR/Cas9 transgenesis and helped to create the myriad reporter and deletion mice necessary for these studies. In the Flow Cytometry core, David Leclerc and Michael Olson helped train me in cell sorting and provided endless technical assistance when things invariably went wrong.

I owe my deepest thanks to my friends and family who have been so supportive and caring throughout my time at the University of Chicago.

I would specifically like to acknowledge Liana, Lydia, and Brendan, my friends in Chicago who have been there from the very beginning; Chris, my longstanding roommate who put up with all my antics over the years; and Ryan, Alex, and Becca, who complete the fellowship of friends. All of you have been an immense source of fun, laughter, and levity. There are also so many others involved in the COI graduate student community that have made this experience worthwhile, and I thank you for that.

Finally, for their endless love and encouragement, I thank my family, my parents Nataraj and Rebecca, and my siblings, Lalitha, Meghann, and Ross. I could not have done this without you.

ABSTRACT

In the past decade, our appreciation of the contribution of innate lymphoid cells (ILCs) towards homeostatic and inflammatory responses has advanced tremendously; however, because ILCs and T cells both rely on a highly overlapping set of genes for development, models of ILC-specific deficiency have lagged. To establish selective tools requires an understanding of the shared and distinct regulators of ILC development. Recent work from our lab and others has advanced an understanding of the precursors that comprise the ILC developmental hierarchy and the expression of transcription factors driving this progression. Analysis of chromatin accessibility and genome editing via CRISPR/Cas9 have also enabled the identification of *cis*-regulatory elements governing ILC development. Yet, many of the ILC precursors described to date have been recognized as far more heterogeneous populations than initially proposed, a result of the limitation in available tools to resolve such complexity. Moreover, the general lack of clarity has hindered an assessment of the dynamic changes in genome accessibility occurring between precursor and product. We utilized CRISPR/Cas9-mediated transgenesis to generate novel combinatorial transcription factor reporters to address precursor heterogeneity and uncovered intermediate specified precursors to the ILC and Lymphoid Tissue-inducer lineages. From these results, we established a revised hierarchy of ILC development and used our multi-transcription factor reporter mice to isolate refined precursor populations and compare changes in chromatin accessibility over developmental time. At the *Gata3* locus, we discovered a dynamic region responsible for regulating the high level of GATA3 expression in ILC2s that is necessary for their proper development and function at homeostasis and following type 2 inflammation. In sum, the revised hierarchy of ILC development and chromatin accessibility data for intermediate ILC precursors will enable the identification of crucial regulators of ILC development and inform the generation of models to better understand ILC biology.

CHAPTER 1

INTRODUCTION

1.1 Innate Lymphoid Cells (ILCs)

Cells of the immune system are typically categorized in to two distinct arms, adaptive and innate, with lymphoid lineage cells existing on a spectrum between these two classifications. Adaptive lymphocytes include classical $\alpha\beta$ T cells and B cells that are highly diverse due to the expression of unique antigen recognition receptors, a result of somatic recombination. As such, adaptive lymphoid cells are initially slow to react, but consequently develop antigen-specific memory and enact a highly focused response. Innate lymphoid cells (ILCs) on the other hand lack expression of somatically rearranged receptors and instead respond more broadly and quickly to a given homeostatic or inflammatory context.

Generally considered to be tissue-resident sentinel cells, ILCs are situated to rapidly respond to local signals within barrier tissues, such as the skin, lung, and intestine, as well as more distal sites including the liver, adipose tissue, and salivary glands. Several groups and subsets have been described for ILCs, which correspond to cytotoxic and T helper (Th) cell subsets, based on key commonalities including transcription factor expression profile, response stimuli, and cytokine production.[1,2] Interest in understanding ILC biology and function has exploded in the past decade following the discovery of their involvement in a host of different contexts including lymphoid tissue development, tissue homeostasis and repair, tumors, allergens, and metabolism.

Though demonstrably shown to contribute to homeostatic and inflammatory responses, the exact role of ILCs in the context of an uncompromised adaptive immune response is poorly understood, as T cells are often impacted by strategies that modulate ILCs. Therefore, in order to devise precise models to address their function, it is necessary to delineate the development and transcriptional regulation of the ILC lineage.

1.2 ILC subsets

Though extensive heterogeneity has been documented among the ILC subsets within and between tissues[3], evidence derived from studies of ILC development, transcription factor expression, tissue-specific phenotype, and function at homeostasis and following inflammatory challenge supports a five subset model for the ILC lineage (**Fig.1.1**).

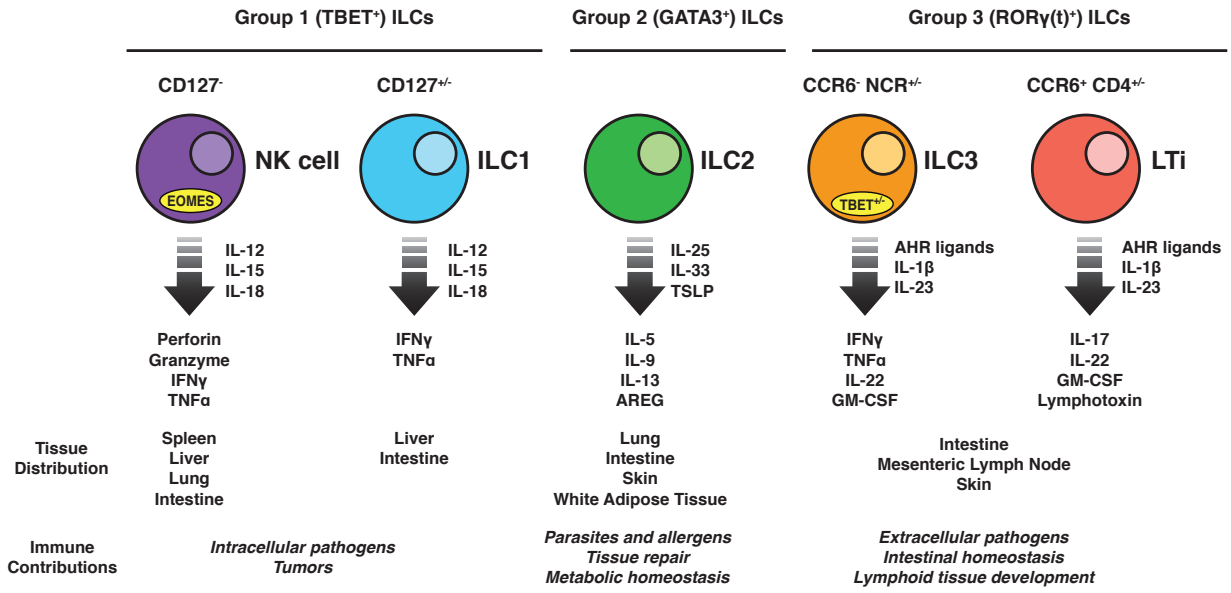

Figure 1.1: Group 1, 2, and 3 ILC subsets and function. ILCs are subdivided into groups based on the expression pattern of cell surface markers, transcription factors, and effector cytokines akin to T helper cell subsets. Each group characteristically responds to a set of stimuli under unique contexts of immune activation during inflammation or at homeostasis.

1.2.1 Group 1 ILCs (NK cell and ILC1)

Group 1 ILCs comprise both the prototypical Natural Killer (NK) cell and the more recently described ILC1 subsets.[1,2] The shared type 1 effector program expressed by NK cells and ILC1s is driven by the signature "master" transcription factor TBET (encoded by *Tbx21*)[4,5], and mirrors the programs expressed by cytotoxic $CD8^+$ T cells and Th1 cells, respectively (**Fig.1.1**). The inflammatory mediators IL-12, IL-15, and IL-18 produced by epithelial and myeloid cells upon exposure to and detection of intracellular pathogens (e.g.

Toxoplasma gondii[5] and mouse cytomegalovirus (MCMV)[6]), act on group 1 ILCs to drive the expression of several effector cytokines, most notably IFNγ and TNFα. In mice, NK cells and ILC1s are commonly characterized by surface expression of NK1.1, though expression of this marker is strain specific, and the natural cytotoxic receptor (NCR) CD335 (NKp46). NK cells and ILC1 are found across a wide variety of tissues including the spleen, liver, lung, gut, and skin where viral and intracellular bacterial infections may occur.

Though shared transcriptional and effector commonalities exist, several key features generally distinguish NK cells from ILC1s. NK cells are predominately circulating cells[7], imbued with steady-state cytotoxic potential via high levels of Perforin and Granzyme expression[8], are marked by surface expression of CD49b (DX5) in a majority of tissues[9], and are dependent on the transcription factor EOMES (encoded by *Eomes*) for development and acquisition of effector function.[4] Conversely, ILC1s are tissue-resident cells devoid of EOMES expression with more limited cytotoxic capacity and preferentially express CD49a, TRAIL, CD200R, and CD127 (IL-7Rα)[8,9], though expression of these surface markers varies depending on activation state and tissue of origin. Notably, transgene-enforced expression of EOMES alone is sufficient to drive expression of an NK cell-like phenotype in ILC1s.[10] Lastly, ILC1s arise prior to NK cells during ontogeny and are detectable before birth in the murine fetal liver (FL), whereas NK cells appear two to three weeks after birth.[11] While the aforementioned features are commonly used to distinguish NK cells from ILC1s, the extent of heterogeneity and overlap of markers within the group 1 ILC lineage has only recently been appreciated. For example, salivary gland (SG) group 1 ILCs express features associated with both the NK cell lineage (EOMES and DX5) and ILC1 lineage (CD49a and TRAIL).[12,13] The mixed SG NK/ILC1 phenotype has been ascribed to TGF-β-mediated suppression of EOMES function[13,14], and is observable in the spleen, liver, and lung following *T. gondii* infection.[15]

While numerous studies have expanded our understanding of the role NK cells and ILC1s

play during type 1 immune responses, characterization of the distinct contribution of each subset towards various immunological challenges remains difficult and has been hampered in part by the lack of sufficient tools for lineage-specific ablation. Nonetheless, several reports have ascribed unique roles in the contexts of specific models. Mice deficient in Hobit (encoded by *Zfp683*), a gene necessary for liver ILC1 tissue-residency[16], were found to be highly susceptible to MCMV infection, a result attributed to impaired early IFNγ production from ILC1s at initial sites of infection.[6] In mice and humans, a unique NK cell subset accumulates within the decidua during pregnancy and has been proposed to promote fetal development through the secretion of angiogenic and growth-promoting factors.[17–19]

1.2.2 Group 2 ILCs (ILC2)

Group 2 ILCs consist solely of the ILC2 subset that shares an effector program with Th2 cells.[1,2] The "master" transcription factor GATA3 (encoded by *Gata3*) is necessary for expression of a type 2 helper effector program in ILC2s, which is characterized by the expression of RORα, BCL11B, and GFI1 (encoded by *Rora*, *Bcl11b*, and *Gfi1* respectively) and the secretion of type 2 cytokines IL-5, IL-9, IL-13, and amphiregulin (AREG) (**Fig.1.1**).[20–22] Disparate inflammatory stimuli, ranging from large extracellular helminths (*Nippostrongylus brasiliensis*) to small protease allergens (papain), initiate the release of the type 2 mediators thymic stromal lymphopoietin (TSLP), IL-25, and/or IL-33 from non-immune cells that act on and activate ILC2s, which are predominately found within barrier tissues including the lung, gut, and skin. Similar to ILC1s, ILC2s are classically considered to be a tissue-resident population[7,23,24], though it has recently been appreciated that ILC2s can migrate from the gut to the lung in the context of helminth infection.[25–27] At homeostasis, ILC2s are also found in the white adipose tissue (WAT) and beige fat where they sustain eosinophil numbers[28], and can regulate beige fat biogenesis through IL-4Rα, the common IL-4/IL-13 receptor subunit, and STAT6 signaling in adipocyte precursors.[29,30] Gut ILC2s

can separately contribute to diet-induce obesity.[31]

Notably, whether TSLP, IL-25, or IL-33 are the primary mediators of ILC2 activation is often tissue-specific, though these cytokines are not required for ILC2 tissue-specific identity.[32] In the lung and WAT, adventitial stromal cell derived IL-33 activates ILC2s through IL-33Rα (ST2, encoded by *Il1rl1*).[28,33] However, in the gut, tuft cell derived IL-25 drives a feed-forward circuit with ILC2s through IL-25R (IL-17RB, encoded by *Il17rb*)[34–37], while in the skin IL-18, classically associated with type 1 immunity, mediates ILC2 activation through CD218a (IL-18R1).[32]

Though TSLP, IL-25, and IL-33 are considered classical mediators of ILC2 activation, recent work has identified a role for lipids and neuropeptides in controlling ILC2 activation and function, underscoring the unique position ILC2s have as integrators of tissue-derived signals. Leukotrienes amplify ILC2 activation in conjunction with primary IL-25 or IL-33 signals through CYSLTR1 while prostaglandins promote tissue accumulation of ILC2s through CRTH2 following type 2 inflammation.[38–40] Vasoactive intestinal peptide (VIP) and neuromedin U similarly enhance ILC2 activation[41–44], while *Calca*-encoding calcitonin gene-related peptide limits ILC2 function.[45,46]

1.2.3 Group 3 ILCs (Lymphoid Tissue-inducer and ILC3)

Group 3 ILCs consist of the Lymphoid Tissue-inducer (LTi) and ILC3 subsets that, like Th17 cells, express a common type 3 effector program driven by the "master" transcription factor RORγ(t) (RORγ and RORγt isoforms, encoded by *Rorc*).[1,2] LTis and ILC3s are abundantly found within the adult gut lamina propria where, in response to the epithelial-, immune-, microbial-, or dietary-derived signals such as IL-1β, IL-23, or retinoic acid (RA), they are stimulated to produce several soluble factors including TNFα, GM-CSF, IL-17, and IL-22 (**Fig.1.1**).[47] At steady state, LTis and ILC3s are the primary producers of IL-22[48,49], which acts on epithelial cells to promote wound healing and the production of antimicro-

bial peptides at the expense of lipid absorption and metabolism.[47,50] Production of IL-22 from group 3 ILC subsets, at least in the context of *Citrobacter rodentium* infection, may be partially redundant.[51] Expression of the aryl hydrocarbon receptor (AhR, encoded by *Ahr*) within LTis and ILC3s is critical for their expansion in the adult gut lamina propria and for formation of isolated lymphoid follicles (ILFs) and cryptopatches (CRs) in response to dietary AhR ligands.[49,52–54] Similar to ILC2s, LTi and ILC3 activity is regulated by neuropeptides, such as VIP and Glial Cell-line Derived Neurotrophic Factors, that suppress or activate IL-22 production through VIPR2 or RET receptor respectively.[50,55]

LTis are likely the most recently evolved ILC subset[56], as they are necessary and responsible for the development and formation of secondary lymphoid organs and intestinal Peyer's patches through their interaction with endothelial lymphoid tissue-organizers and provision of lymphotoxin (LTα1β2) and RANK ligand during early embryogenesis.[57,58] Fetal derived LTi and post-natal LTi-like cells are commonly distinguished from ILC3s based on the expression of CCR6, cKit, Neuropilin-1 (NRP-1, encoded by *Nrp1*), and CD4, though only a proportion of LTis are marked by CD4 expression.[8,57–59] Throughout fetal ontogeny, LTis are found in abundance at lymph node anlagen[58], and their development and function is highly dependent upon the cell-autonomous activity of maternally derived RA.[60,61] In the adult mouse, LTi-like cells are principally located within ILFs and CRs in the gut, drawn in to clusters through CXCR5 and CCR6 chemokine receptor signaling.[62] Though predominately found in the gut, a population of LTi-like cells was recently described in the skin epidermis where they regulated sebaceous gland size and antimicrobial lipid production.[63]

ILC3 are traditionally subdivided based on the expression of NCRs into NKp46$^+$ and NKp46$^-$CCR6$^-$ (double negative, DN) ILC3s. In contrast to LTi, NKp46$^+$ and DN ILC3s appear later in ontogeny and only begin to accumulate in the gut after birth in response to the microbiota.[52,54,59] ILC3 localization in the gut lamina propria is depend on expression of CXCR6, the absence of which impairs IL-22 mediated barrier integrity.[64] NKp46$^+$ ILC3s

develop from the pool of DN ILC3s in a process dependent on the transcription factors TBET and GATA3, Notch signaling, and the microbiota.[54,65–68] In this process, RORγ(t) expression in DN ILC3s is repressed by TBET and GATA3, resulting in a concomitant increase in IFNγ and NKp46 expression. Continued and complete suppression of RORγ(t) expression results in a loss of the type 3 phenotype in NKp46$^+$ ILC3s and conversion to ILC1s, or "ex-ILC3s".[5,54]

1.3 ILC Progenitors

While demonstrably shown to contribute to homeostatic maintenance and pathogen resistance, the exact role of ILCs in the context of an uncompromised adaptive immune response is poorly understood.[1,69] An evaluation of ILC importance is hindered by a deficiency in models for the specific depletion of ILCs and ILC subsets. As such, it is of interest to the field at large to determine specific factors involved in ILC development, persistence, and function. ILC precursors in the murine adult bone marrow (BM), FL, and peripheral tissue have been described by several groups, including ours, using a combination of transcription factor reporter mice and lineage potential analysis. These publications have lead to the development of a hierarchical model of ILC development (**Fig.1.2**).

1.3.1 The Innate Lymphoid Cell Precursor (ILCP)

A restricted precursor to murine helper ILC1/2/3 but not LTis or NK cells was identified by our lab through the application of a Natural Killer T (NKT) cell transcription factor reporter strain for PLZF (encoded by *Zbtb16*; *Zbtb16*$^{\text{EGFPCre}}$).[78] Initial fate-mapping experiments using *Zbtb16*$^{\text{EGFPCre}}$ x ROSA26$^{\text{floxSTOP-EYFP}}$ reporter mice revealed that, akin to NKT cells, ILC1, ILC2, and ILC3 in numerous tissues were EYFP$^+$, whereas LTi and NK cells showed little to no fate-mapping. Notably, EYFP fate-mapped mature ILC1/2/3 populations did not express EGFP, in contrast with NKT cells, suggesting the existence of

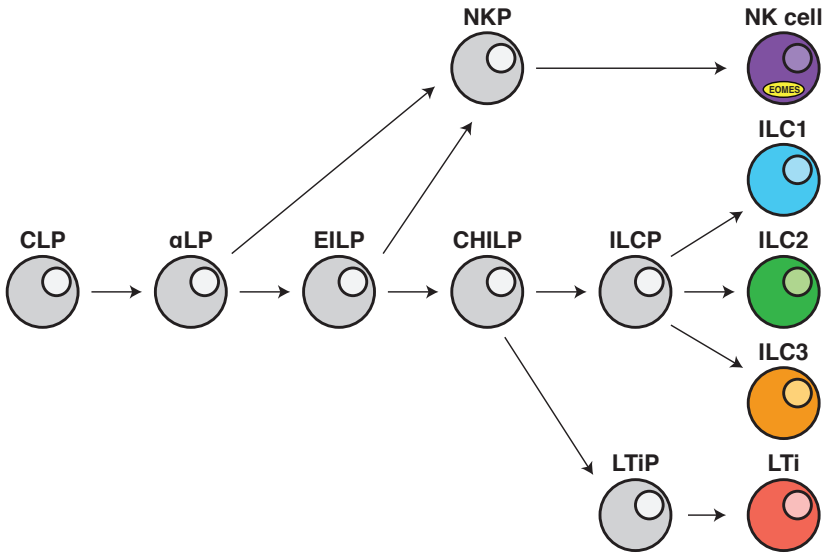

Figure 1.2: Current model of ILC development. In the mouse, all ILCs develop from the CLP (common lymphoid precursor), which is shared with the B cell and T cell lineages.[70] CLP give rise to αLP ($\alpha4\beta7^+$ lymphoid precursor) and the downstream EILP (early innate lymphoid precursor), both of which are capable of differentiating into NK cells through an intermediate NKP (NK cell precursor). EILP then give rise to a CHILP (common helper innate lymphoid precursor) with ILC1/2/3 and LTi potential. Lastly an ILCP (innate lymphoid cell precursor) committed to the ILC1/2/3 lineage and an LTiP (LTi precursor) committed to the LTi lineage arise from the CHILP before final lineage differentiation.

an earlier *Zbtb16*-expressing progenitor. Indeed, upon examination of adult BM or embryonic day 14 (E14) FL cells negative for myeloid and adaptive lineage markers (Lin^-), a rare $EGFP^+$ population was identified that expressed several markers previously used to characterize LTi precursors (LTiP) (detailed below), such as $\alpha4\beta7$, IL-7Rα, and CD117 (cKit, encoded by *Kit*).[59,72,73] Intriguingly, whereas NKT cells express *Zbtb16* throughout development[85], *Zbtb16* was only transiently expressed during ILC development, as indicated by the fact that mature peripheral ILC1/2/3 are incompletely fate-mapped ($\sim$65% $EYFP^+$) and that precursors committed to the ILC2 lineage (detailed below) rapidly downregulated *Zbtb16* expression.[78,79,86] $Lin^-\alpha4\beta7^+$IL-7Rα^+*Zbtb16*-$EGFPCre^+$ cells also expressed transcription factors previously reported to be necessary for ILC-lineage development including *Id2*, *Tcf7*, *Gata3*, *Rorα*, and *Tox*, but did not express markers associated with mature peripheral NK cells and ILC1s[83,84,87], ILC2s[21,22,81,88,89], or ILC3 and LTis[59,73,90], such as NK1.1, NKp46, IL-25R, IL-33Rα, CCR6, and CD4.[78] Subsequent reports have since observed that

Table 1.1: Defining surface markers and transcription factors of ILC precursors and the reporter strain used to characterize each precursor.

Precursor	Expression Profile	Reporter Strains	References
CLP	Lin$^-$IL-7Rα^+Flt3$^+$cKit$^+$Sca-1$^+$	—	71
αLP	Lin$^-\alpha4\beta7^+$IL-7Rα^+Flt3$^{+/-}$	RORγt^{EGFP}, ID2^{EGFP}	72–74
EILP	Lin$^-\alpha4\beta7^+$IL-7Rα^-CD90.2$^-$TCF1$^+$	*Tcf7*^{EGFP}	75–77
CHILP	Lin$^-\alpha4\beta7^+$IL-7Rα^+Flt3$^-$CD25$^-$ID2$^+$	ID2^{EGFP}	5
ILCP	Lin$^-\alpha4\beta7^+$IL-7Rα^+PD-1$^+$PLZF$^+$	*Zbtb16*^{EGFPCre}	78–80
ILC2P	Lin$^-$IL-7Rα^+Sca-1$^+$ ICOS$^+$ID2$^+$GATA3$^+$	GATA3^{EGFP}, ID2^{EGFP}	78,81
LTiP	Lin$^-\alpha4\beta7^+$IL-7Rα^+cKit$^+$ CCR6$^+$CXCR5$^+$RORγ(t)$^+$	RORγt^{EGFP}	58,59,73,82
NKP	Lin$^-$2B4$^+$CD27$^+$IL-7Rα^+ CD122$^+$Flt3$^-$ID2$^+$	ID2^{EGFP}	83,84

Zbtb16 expression in these BM precursors is highly correlated with CD279 (PD-1, encoded by *Pdcd1*) expression.[79,80,91]

Further characterization of the Lin$^-\alpha4\beta7^+$IL-7Rα^+*Zbtb16*-EGFPCre$^+$ population following bulk transfer into Rag1$^{-/-}\gamma c^{-/-}$ immunodeficient mice in competition with congenically marked CLP revealed the restricted differentiation potential of these precursors. Lin$^-\alpha4\beta7^+$ IL-7Rα^+*Zbtb16*-EGFPCre$^+$ cells readily generated mature ILC1/2/3 in several distinct tissues yet displayed a limited potential for NK cells and no potential for LTis or adaptive lymphocytes (B and T cells).[78] Moreover, NK-like cells derived from Lin$^-\alpha4\beta7^+$IL-7Rα^+*Zbtb16*-EGFPCre$^+$ cells were distinct from CLP-derived NK cells in their augmented expression of NKp46. Results from the *in vivo* transfer experiment were confirmed through clonal analysis where individual Lin$^-\alpha4\beta7^+$IL-7Rα^+*Zbtb16*-EGFPCre$^+$ cells differentiated into single ILC1/2/3 progeny or multi-potential ILC1/2/3 colonies at a lower frequency. Importantly, *Zbtb16*-EGFPCre$^+$ cells arose from short-term *in vitro* cultures of Lin$^-\alpha4\beta7^+$IL-

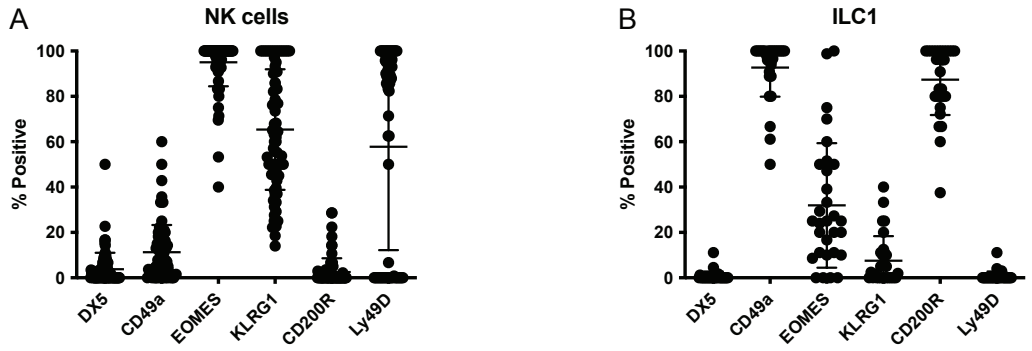

Figure 1.3: Stability of NK cell and ILC1 distinguishing markers *in vitro*. (**A**) Liver NK cells (CD45$^+$CD3ϵ^-TCRβ^- NK1.1$^+$DX5+CD49a$^-$*Eomes*-EGFP$^+$) and (**B**) Liver ILC1 (CD45$^+$CD3ϵ^-TCRβ^- NK1.1$^+$DX5-CD49a$^+$*Eomes*-EGFP$^-$) were isolated from *Eomes*$^{\text{EGFP}/+}$ reporter mice and single-cell sorted into wells containing OP9 stromal cells supplemented with IL-2, IL-7, and SCF. Mature group 1 ILCs were cultured for 6 days and the expression of identifying markers associated with Liver NK cells (DX5, *Eomes*, KLRG1, Ly49D) and Liver ILC1s (CD49a, CD200R) was assessed.[6]

7Rα^+*Zbtb16*-EGFPCre$^-$ cells, indicating their appearance downstream of an $\alpha4\beta7^+$ lymphoid precursor (detailed below). Based on the aforementioned parameters, Lin$^-\alpha4\beta7^+$IL-7Rα^+*Zbtb16*-EGFPCre$^+$ cells were termed the Innate Lymphoid Cell Precursor (ILCP) (**Table1.1**).

Of note, LTi potential was not addressed at the single-cell level in our initial study.[78] However, our group later confirmed and extended the initial clonal analysis of the ILCP by staining for CD4 in single-cell cultures as a marker for LTis, confirming that the ILCP does not efficiently give rise to LTis at the clonal level.[92] Though the ILCP was devoid of numerous mature ILC markers, a fraction of ILCPs in the murine adult BM expressed the ILC2-lineage marker ICOS, suggesting that there is early acquisition of lineage markers prior to terminal differentiation.[78] As a matter of fact, our group later documented multi-lineage priming within FL ILCPs, noting that there were cells that coexpressed transcription factors commonly associated with discrete mature ILC lineages, including *Tbx21*, *Bcl11b*, and *Rorc*.[92]

Contrary to our initial findings, two recent publications reported that adult BM ILCPs retain substantial NK cell potential.[93,94] Through the combination of a novel *Id2*$^{\text{RFP}}$ reporter

in conjunction with the *Zbtb16*$^{\text{EGFPCre}}$ reporter, Xu et al. (2019) found that *Id2*-RFP^{+} *Zbtb16*-EGFPCre^{+} ILCPs were able to give rise to NK cells, identified by EOMES and/or Perforin expression, following *in vivo* transfer and *in vitro* culture.[93] Similar observations were made by Walker et al. (2019) using 5x polychromILC mice (ID2$^{\text{BFP/+}}$GATA3$^{\text{hCD2/+}}$ ROR$\alpha^{\text{Teal/+}}$*Bcl11b*$^{\text{tdTomato/+}}$RORγt$^{\text{Katushka/+}}$).[94] Given the potential for impurities in cell sorting prior to *in vivo* transfer studies, *in vitro* clonal analysis provides a more optimal means to distinguish a populations lineage potential. However, when assessing potential *in vitro*, care must be taken to assure the stability of distinguishing markers commonly used during *ex vivo* analysis. Though EOMES serves as a distinct marker for NK cells *ex vivo*, as detailed above, we have observed the upregulation of *Eomes*$^{\text{EGFP}}$ expression within *in vitro* cultured ILC1s, calling into question the results presented by Xu et al. (2019) and Walker et al. (2019) (**Fig.1.3**).[93,94] Thus, whether the ILCP is a committed precursor to ILC1/2/3 cells distinct from an NK cell precursor (detailed below) or the ILCP retains some not-insignificant NK cell potential, and the relevance of said potential *in vivo*, remains to be determined.

1.3.2 The Common Helper Innate Lymphoid Precursor (CHILP)

Coinciding with the identification of the ILCP, a separate precursor, termed the Common Helper Innate Lymphoid Precursor (CHILP) was identified in the adult BM through the use of an ID2$^{\text{EGFP}}$ reporter line.[5,95] The CHILP, defined as a Lin$^{-}\alpha4\beta7^{+}$IL-7Rα^{+}CD25^{-}Flt3^{-} ID2-EGFP^{+} population (**Table1.1**), was described as a precursor capable of generating ILC1/2/3 and LTis but not NK cells or adaptive lymphocytes following *in vivo* transfer and *in vitro* culture, placing this progenitor upstream of the ILCP in the ILC developmental hierarchy (**Fig.1.2**). Early models of ILC development predicted the existence of an *Id2*-expressing precursor such as the CHILP given that all mature ILCs (ILC1/2/3, LTis, and NK cells) express the transcription factor ID2 and depend on it for proper develop-

ment through the suppression of adaptive-lineage promoting E-proteins.[21,96,97] The role of E-proteins and ID2 as countervailing forces promoting T cell or ILC development respectively was underscored using a mixed reporter system to demonstrate an inverse correlation between E2A (encoded by *Tcf3*)-EGFP expression and ID2-EYFP expression during ILC development.[86,98] Moreover, ID2 expression level in ILC precursors is highly indicative of T cell potential when cultured with exogenous Notch ligand from OP9-DL1 stromal cells.[92] Nonetheless, as the CHILP was incapable of generating NK cells under the assayed conditions, the observations made by Klose et al. (2014) suggested the existence of an even earlier *Id2* expressing progenitor capable of generating all ILC subsets.[5]

Several outstanding issues remained following the initial identification of the CHILP. First, though the CHILP was negative for EOMES, TBET, and RORγ(t) expression, as defined the CHILP was heterogeneous and partially overlapped with the ILCP, displaying a bimodal expression pattern of PLZF.[5] Second, LTis were not distinguished from ILC3s following *in vitro* single-cell culture. Lastly, the CHILP was isolated from the murine adult BM, which inefficiently generates LTis and contains very few RORγ(t)$^+$ cells when compared to the FL.[73] As such, a CHILP equivalent within the FL is commonly assumed to contain a RORγ(t)$^+$ LTiP; however, whether the CHILP as defined contains a shared precursor to both ILCs and LTis or comprises a mixture of distinct progenitors remains unclear without clonal analysis.

The proposed identity of the CHILP was further complicated by Xu et al. (2019) and Walker et al. (2019) who documented substantial NK cell potential from the CHILP, comparable to their observations made with the ILCP as noted above.[93,94] Though the aforementioned issue of *in vitro* NK cell identification still applies in these contexts (**Fig.1.3**), the differing conclusion of Xu et al. (2019) at least may be partly explained by the design of the *Id2*$^{\mathrm{RFP}}$ reporter used in this study.[93] The ID2$^{\mathrm{EGFP}}$ reporter first used to characterize the CHILP is a weakly expressed knock-in knock-out reporter that closely reflects ID2 protein expression whereas the *Id2*$^{\mathrm{RFP}}$ reporter is very brightly expressed and employs an

internal ribosome entry site (IRES) to track *Id2* mRNA expression.[5,93,95] Thus it is possible that early ILC-lineage precursors with broader lineage potential and lower levels of *Id2* expression, that would have been excluded with the ID2^{EGFP} reporter, were included in the analysis of total *Id2*-RFP^{+} precursors.

1.3.3 The α4β7^{+} Lymphoid Precursor (αLP)

An early precursor to LTis and NK cells that had lost B cell potential but retained T cell and dendritic cell (DC) potential was originally identified in the murine FL among CLP-like cells based on the expression of integrin $\alpha4\beta7$.[72] Later termed the $\alpha4\beta7^{+}$ lymphoid precursor (αLP), this population was minimally defined by a Lin$^{-}\alpha4\beta7^{+}$IL-7Rα^{+}Flt3$^{+/-}$ expression profile, with Flt3 expression marking cells immediately downstream of the CLP (**Fig.1.2**; **Table1.1**). Iterative refinement through the exclusion of cells expressing surface markers and transcription factors now associated with more differentiated precursors, such as the LTiP and ILCP, has since limited the αLP to include only the earliest progenitors that are negative for *Rorc*, *Gata3*, *Zbtb16*, and *Tcf7* and express low levels of *Id2*.[73,74,91,92,99] Expression of CXCR6, which coincided with a loss of T cell potential among LTi precursors[73], was used by Yu et al. (2014) to distinguish a subset of αLP in ID2^{EGFP} reporter mice capable of generating all known ILC subsets (ILC1/2/3, LTis, and NK cells) upon *in vivo* transfer.[74] At the clonal level, CXCR6^{+} αLP readily generated multi-lineage wells (ILC1s, ILC2s, ILC3s, and/or NK cells), albeit LTis were not distinguished from ILC3s and EOMES, which is unstable *in vitro* (**Fig.1.3**), was used to identify NK cells.[74] However, in both the adult BM and FL of *Cxcr6*^{EGFP} reporter mice, EGFP expression in the αLP was associated with the expression of the maturation markers RORγ(t) and CD90.2 (Thy1, congenic alleles 1 and 2) as well as elevated ID2, suggesting that CXCR6 expression marks already differentiated precursors within the αLP.[73,99] We have similarly observed that CXCR6 expression, as determined by surface staining, coincides with the expression of ILC development markers

PLZF, *Tcf7*, CD90.2, PD-1, and CCR6 in the FL (unpublished observations).

Recently, our group evaluated the lineage potential and transcription factor expression of FL αLPs through single-cell analysis.[92] When expression of *Zbtb16*-EGFP and CXCR5 were used to exclude the ILCP and LTiP, respectively, from the FL Lin$^-\alpha4\beta7^+$IL-7Rα^+Flt3$^{+/-}$ population, we found that early immature Flt3$^{+/-}$ αLP contained a common precursor to the ILC and LTi lineages and was marked by upregulation of transcription factors necessary for early ILC development, including *Tox*, *Nfil3*, *Sox4*, and *Runx1*. Similar results have been reported for adult BM αLP using single-cell RNA-seq[79,91,99]; however, αLPs are orders of magnitude rarer in the adult BM compared to the FL and have a lower comparative cell plating efficiency (unpublished observations), indicating the possible existence of a separate pan-ILC precursor in adult mice.

1.3.4 The Early Innate Lymphoid Precursor (EILP)

Most recently, a novel ILC precursor was identified in the BM of TCF1 (encoded by *Tcf7*) EGFP reporter mice based on a Lin$^-\alpha4\beta7^+$CD90.2$^-$IL-7Rα^- *Tcf7*-EGFP$^+$ expression profile and was designated the Early Innate Lymphoid Precursor (EILP) (**Table1.1**).[75] The EILP showed high expression of the early transcription factors *Tox* and *Nfil3*, akin to the αLP, but expressed low levels of the transcription factors *Id2* and *Zbtb16* that are associated with the CHILP and ILCP, respectively. Following transfer into Rag1$^{-/-}\gamma c^{-/-}$ mice, the EILP efficiently generated all known ILC subsets but not adaptive lymphocytes. Moreover, EILPs generated ILC1/2/3 and NK cells at the clonal level with a high frequency of multi-lineage wells, though DX5 was employed as an NK cell marker and is unreliable *in vitro* (**Fig.1.3**). In addition, LTi were not identified at the single-cell level. Thus, whether the EILP contains a shared precursor to all ILCs or is a mixture of precursors to ILC1/2/3, LTis, and/or NK cells remains unresolved.

Most strikingly, the EILP was characterized as an IL-7Rα^- population, in contrast to

all previously identified ILC precursor populations (**Table1.1**).[5,59,73–75,78,81] This observation raised the question of whether the EILP represented a precursor downstream of the IL-7Rα^+ CLP or was derived from an alternate IL-7Rα^- precursor capable of generating ILCs. A follow-up paper by Harly et al. (2018) utilized *Tcf7*$^{\text{EGFP}}$IL-7Rα^{Cre} x ROSA26$^{\text{floxSTOP-EYFP}}$ reporter mice to demonstrate that EILPs were indeed fate-mapped for IL-7Rα expression.[76] Furthermore, CLP transferred from *Tcf7*$^{\text{EGFP}}$ BM into irradiated wild-type hosts gave rise to *Tcf7*-EGFP$^+$ EILPs 7-days after injection, confirming that the EILP arises downstream of the CLP (**Fig.1.2**). EILPs were found to reexpress IL-7Rα in culture, when exogenous IL-7 was excluded, and upregulate PLZF expression, demonstrating that the EILP is capable of differentiating into ILCPs *in vitro*. However, BM EILPs express some low level of PLZF[75,76]; as such, it is unclear whether ILCPs derived from the EILP are an expanded population of cells already expressing PLZF or whether ILCPs can arise *de novo*.

Interestingly, Yang et al. (2015) noted that, under specific *in vitro* culture conditions permissive for DC development, EILPs are capable of differentiating into CD11c$^+$ I-A$^{\text{b}}$ (MHC-II)$^+$ DC-like cells.[75] Through single-cell RNA-seq analysis of *Tcf7*-EGFP$^+$ adult BM precursors, Harly et al. (2019) observed that a fraction of EILPs expressed transcripts associated with the DC lineage, enabling the EILP to be split into three subsets: an ILC/DC-specified EILP, an ILC-biased EILP, and a DC-biased EILP.[77] Shared ILC- and DC-lineage potential from the specified EILP, though rare, was evident at the clonal level. Nevertheless, alternate DC-lineage potential diminished upon *Zbtb16* expression in the ILC-biased EILP and was undetectable in the downstream ILCP, coinciding with an upregulation of *Tcf7* expression. These results are notable as they indicate that, similar to developing T cells, ILC precursors first lose B cell potential and then gradually lose DC potential.[72,100]

1.3.5 The ILC2 Precursor (ILC2P)

The first precursor to the helper ILC lineage was identified in the murine adult BM as a committed ILC2 precursor (ILC2P), defined as a Lin$^-$ population with surface expression of Sca-1 (Ly6A/E), IL-7Rα, and CD25 (IL-2Rα) and intracellular expression of *Id2* and *Gata3* (**Table1.1**).[81] The ILC2P, which exclusively generated ILC2 following *in vivo* transfer or *in vitro* culture, expressed several markers associated with ILC2-lineage function, including IL-33Rα and IL-25R, yet this population differed from mature ILC2s in several ways. The BM ILC2P showed considerable expression of the early ILC-lineage marker $\alpha4\beta7$ without expression of the mature ILC2 markers cKit and KLRG1; was extremely limited in its ability to produce the type 2 cytokines IL-5 and IL-13 following stimulation; and displayed marked proliferative potential after *in vivo* transfer, all in stark contrast to mature ILC2s.[20–22,81,89,101] These metrics formed the basis for classifying this BM population as a bona fide ILC2P.

The extent to which the BM ILC2P seeds peripheral tissues to replace or replenish mature ILC2 populations has been a matter of intense scrutiny given the limited turnover and migration of tissue-resident ILCs at steady state.[7] Recent work using inducible fate-mapping experiments has revealed a critical neonatal window for tissue seeding of ILC2s at homeostasis.[24] When ILC2s were lineage traced via tamoxifen treatment of *Arg1*$^{\text{CreERT2}}$ x ROSA26$^{\text{floxSTOP-EYFP}}$ or ID2$^{\text{CreERT2}}$ x ROSA26$^{\text{floxSTOP-EYFP}}$ reporter mice during the neonatal period (postnatal day 10-12), fate-mapped ILC2s persisted in multiple tissues for the majority of the lifespan of the mouse (1 year). Nevertheless, the contribution if any of BM ILC2P to peripheral mature ILC2 populations particularly during inflammatory contexts remains controversial with evidence for and against.[24,27]

1.3.6 Lymphoid Tissue-inducer Precursor (LTiP)

An early progenitor to the LTi lineage was first identified among the αLP in the murine FL[72,102], and later refined using RORγt^{EGFP} reporter mice.[58,59,73,82] Unlike precursors to NK, ILC1, and ILC2, ILC3 and LTi precursors are incredibly rare in the murine adult BM, exemplified by a near absence of RORγ(t) expression in the BM.[5,73,94] FL RORγ(t)$^+$ cells, which critically depend on *Id2* and *Rorc* for development, were defined by a Lin$^-$NKp46$^-$ $\alpha4\beta7^+$IL-7Rα^+cKit$^+$RORγt-EGFP$^+$ expression profile and generated both LTis and ILC3s following *in vivo* transfer or culture *in vitro* (identified by CD4$^+$ and NKp46$^+$ respectively).[58,59,82] In addition to RORγ(t), FL precursors to both the LTi and ILC3 lineage were found to be enriched among CXCR5$^+$ and CXCR6$^+$ cells, while CCR6 expression was limited to LTi-lineage cells.[59,73,82,92] Most recently, our lab utilized the *Zbtb16*^{EGFPCre} reporter to distinguish early CXCR5$^+$*Zbtb16*$^+$ ILC3 precursors (ILC3P) from CXCR5$^+$*Zbtb16*$^-$ LTi precursors (LTiP) in the FL, a distinction that was corroborated by single-cell multiplex transcriptional analysis.[78,92] However, to date, a clonal assessment of the proposed LTiP has not been performed.

1.3.7 The Natural Killer cell Precursor (NKP)

A BM precursor to NK cells downstream of the common lymphoid progenitor (CLP) and devoid of adaptive lymphocyte potential was first identified among CD3ϵ^-CD122 (IL-2Rβ)$^+$NK1.1$^-$DX5$^-$ cells.[87] These NK cell precursors (NKP) were principally characterized by CD122 expression and an absence of mature NK cell phenotypic markers such as expression of activating and inhibitory receptors and cytolytic potential via Granzyme and Perforin release *in vitro*. The identity of the NKP was later refined (rNKP) through the inclusion of IL-7Rα and *Id2*-EGFP as defining markers, which subsequently led to the identification of an even earlier pre-NKP that was phenotypically similar to the rNKP but lacked CD122 expression.[83,84] Following *in vivo* transfer and *in vitro* culture, the rNKP and pre-NKP

both generated CD3ϵ^-NK1.1$^+$ cells at a high frequency, though the potential for alternate ILC lineages was not addressed at this time. More recently, our lab revisited the identity of the rNKP and pre-NKP using *Zbtb16*$^{\text{EGFPCre}}$ x ROSA26$^{\text{floxSTOP-EYFP}}$ reporter mice and found that both populations were highly heterogeneous and overlapped extensively with the newly discovered ILCP and ILC1-lineage cells. Both the rNKP and pre-NKP contained subpopulations with substantial *Zbtb16*-EGFPCre expression, a hallmark of the ILCP, and EYFP fate-mapping, indicative of substantial ILC1-lineage overlap or an ill-defined low level expression of *Zbtb16* in the NK cell lineage. Thus the early development of the NK cell lineage and the identity of a committed NK cell precursor that lacks ILC1 potential remains poorly understood.

1.3.8 Peripheral Tissue ILC Precursors

Precursors to the ILC lineage have principally been identified in the adult BM and FL, sites of lymphocyte hematopoiesis, though the extent of their contribution to the maintenance of peripheral populations is an area of active study. The replenishment and replacement of peripheral ILC populations by adult BM precursors appears to be rather limited.[7,23,24] However, several publications have identified populations of multi-potent or restricted ILC precursors, indicating that the pool of tissue-resident ILCs may primarily be replenished by ILC precursors that seed the tissue during the fetal or post-natal window.[27,103–105]

By crossing a reporter strain for the urea cycle enzyme Arginase-1 (ARG1; *Arg1*$^{\text{EYFP}}$), which was known to map BM ILC2P, with a RORγt$^{\text{Cre}}$ x ROSA26$^{\text{floxSTOP-RFP}}$ fate-mapper mouse, Bando et al. (2015) identified an ILC precursor in the fetal intestine capable of generating ILC1/2/3 after *in vitro* clonal culture.[103] Intriguingly, this Lin$^-$IL-7Rα^+ $\alpha4\beta7^+$ *Arg1*-EYFP$^+$RORγt-RFP$^-$NK1.1$^-$IL-33Rα^- population of ILC precursors coexpressed TBET, GATA3, and RORγ(t) at low levels, reminiscent of multi-lineage priming observed in the FL ILCP.[92,103] However, while the *Arg1*$^+$ fetal intestine ILC precursor was capable

of generating ILC1/2/3, very few multi-lineage wells were observed, suggesting that this precursor likely follows the ILCP in the developmental hierarchy and is a recent emigrant to the gut from the FL. A similar, albeit more restricted precursor to ILC1s and ILC3s was identified after hematopoietic deletion of the transcription factor *Runx3* resulted in their accumulation within the adult gut.[104]

More recently, a tissue-resident precursor was identified in the lung of neonatal and adult mice.[27,105] By performing single cell analysis on lung Lin$^-$CD45$^+$IL-7Rα^+ ILCs, two groups independently observed a population of IL-18Rα^+IL-33Rα^- cells that expressed features characteristic of adult BM and FL ILCPs, including *Tcf7*, *Zbtb16*, *Ror*α, and *Kit*. Trajectory analysis indicated that IL-18Rα^+IL-33Rα^- ILCs differentiated into IL-18Rα^-IL-33Rα^+ ILC2s in the lung. When compared to adult BM ILCPs, adult lung IL-18Rα^+IL-33Rα^- ILC precursors were capable of generating multi-lineage wells, yet demonstrated biased differentiation towards the ILC2 lineage following *in vivo* transfer and *in vitro* culture.[27,105]

1.3.9 Human ILC Precursors

Equivalents to murine ILC1s, ILC2s, ILC3s, LTis, and NK cells have been identified in humans based on the expression of similar core transcription factors (i.e., TBET, GATA3, RORγ(t), and EOMES), cytokines, and surface markers, though several defining markers are poorly conserved.[2,106] In humans, as in mice, all ILC subsets arise at multiple stages of life from distinct anatomical sites, such as the yolk sac, fetal liver, and bone marrow, where they arise from a common lymphoid progenitor.[2,107] However, while numerous advances have contributed towards an understanding of murine ILC development and its intermediate precursors, human ILC development remains less well characterized in part due to limitations of tissue availability and appropriate tools.

A Lin$^-$CD34$^+$CD45RA$^+$CD117$^+$IL-1R1$^+$ precursor capable of generating all human ILCs, but not alternate lineages, was identified as a population exclusively present within secondary

lymphoid tissues.[108] Notably, this human ILC progenitor expressed low to intermediate levels of RORγ(t), which contrasts with observations made in mice that found no evidence of a history of RORγ(t) expression among NK cells.[109] It was later determined that *RORC*-deficient patients capably generated NK cells, ILC1s, and ILC2s, suggesting that RORγ(t)$^+$ precursors were not the exclusive and/or primary intermediate for human ILC development, or that RORγ(t) expression in these cells was not essential.[110]

Recently, a CD117$^+$ ILCP with restricted ILC potential was characterized in peripheral blood of healthy human adults.[110] These ILCPs were also found in several lymphoid and non-lymphoid tissues including the fetal liver, cord blood, adult lung, and adult tonsils. Akin to ILCPs in the mouse, these cells expressed *ZBTB16*, *TCF7*, *ID2*, *GATA3*, and *IL7R* and did not express factors associated with mature ILC subsets. Likewise, human ILCPs were multipotent and capable of generating ILC1, ILC2, ILC3, and NK cells at a clonal level *in vitro* and following *in vivo* transfer into BALB/c *Rag2*$^{-/-}$*Il2rg*$^{-/-}$*Sirpa*^{NOD} immunodeficient mice. Though the identification of ILCPs in circulation differs from studies in mice, and NK cell potential from the murine ILCPs remains controversial, the functional similarities between human and mouse ILCPs highlights the value of studies in mice that provide a framework to understand human ILC development and biology.

1.4 Regulation of core factors in ILC development

Conditional knockout strategies have illustrated that numerous lineage-determining transcription factors that drive T cell development similarly promote ILC development[70], though how a shared collection of transcription factors and receptors ultimately drives the development of similar cells with divergent states of responsiveness remains an enigma. TOX (encoded by *Tox*)[111,112], E4BP4/NFIL3 (encoded by *Nfil3*)[74,113–118], and TCF1[88,90,119] are required for the development of all ILC subsets. More selectively, GATA3[68,120–122], ID2[21,58,96,97], and RUNX1 (encoded by *Runx1)*[123,124] are necessary for helper ILC and

LTi-lineage development but are not required for NK cell development and instead contribute to NK cell maturation. Whereas the prior transcription factors have broad roles in ILC development, PLZF[11,78], BCL11B[79,125–127], RORγ(t)[58,59,65], TBET[4,5,9,128], and others are more restricted in their contributions.[104,129,130]

While the precise function of each transcription factor is poorly understood, several studies have contributed to the field's understanding of the regulatory network constructed by these transcription factors during ILC development. Groups including ours have identified changes in transcript induction during development and after maturation[3,8,79,91,92], providing insight into the timeline of expression.[70] For example, mechanistically, NFIL3, TOX, and ID2 are proposed to act in concert to promote ILC development. In accordance with the observations that retroviral overexpression of ID2 or TOX virtually restores the ILC developmental deficiency observed in *Nfil3* knockouts, NFIL3 was able to bind within the *Id2* locus and to the promoter of *Tox*.[74,118] While informative, this approach does not necessarily identify or recapitulate spatial and temporal transcription factor binding during development nor does it indicate the necessity or sufficiency of particular enhancers. More recently, an alternative approach combining the Assay for Transposase Accessible Chromatin with sequencing (ATAC-seq) and CRISPR/Cas9 has been used to identify specific regulatory regions that contribute to stage- or subset-specific expression of a transcription factor.

1.4.1 Inhibitor of DNA binding 2 (ID2)

The transcriptional regulator ID2, a member of the inhibitor of DNA binding (ID) family of proteins, has long been recognized as a necessary factor in development of all ILC subsets, as mice deficient in ID2 display an NK cell maturation defect and are devoid of LTis and ILC1/2/3.[21,96,97] ID2 and its family members antagonize the function of E-protein family members, such as E2A, that would induce *Rag1* expression in order to suppress adaptive lymphocyte development.[131] Mechanistically, E-proteins contain DNA binding domains and

basic helix-loop-helix (bHLH) domains, the latter of which permits the formation of homo- or heterodimers, while ID2, which contains a similar bHLH domain and no DNA binding capability, inhibits E-protein function by forming heterodimers. Though ID2 is the predominantly expressed ID family member in ILCs, compensatory expression of ID1 and ID3 has been observed in the absence of ID2 without restoration of ILC development, indicating a non-redundant role for these transcription factors in suppressing E-protein function.[75,97,132] Curiously, while a pronounced defect in NK cell maturation, characterized by CD27 down-regulation and CD11b upregulation[133], is observed in $ID2^{-/-}$ mice, residual NK cells are detectable and display an immature phenotype as a result of compensatory ID3 expression.[97,132,134] In the absence of both ID2 and ID3, a naïve T cell program is induced in NK cells, revealing a critical role for E-protein suppression during NK cell maturation.[132]

How *Id2* expression is induced in the ILC lineage and what factors regulate its expression remain poorly understood. Recently, Mowel et al. (2017) identified a distal *cis*-regulatory element that specifically controlled *Id2* expression in group 1 ILCs, leaving group 2 and 3 ILCs unperturbed.[135] The region regulating *Id2* expression was demarcated by a long non-coding RNA (lncRNA) termed *Rroid* that was necessary for group 1 ILC homeostasis and function. The *Rroid* locus was found to induce *Id2* expression in part by promoting STAT5 deposition at the *Id2* promoter. Interestingly, early group 1 ILC precursors including the ILCP and NKP developed normally in mice lacking the *Rroid* locus, while NK cells displayed a cell-intrinsic impairment in maturation. These results suggested that the *Rroid* locus may play an important role in suppressing E-protein function by promoting *Id2* expression during NK cell maturation[132,134], and indeed, *Rroid*-deficient NK cells expressed higher levels of T and B cell specific genes compared *Rroid*-sufficient NK cells.[135]

1.4.2 Promyelocytic Leukemia Zinc Finger (PLZF)

PLZF was first characterized as a transcription factor necessary for NKT cell development and acquisition of effector function, and has more recently been used to characterize a committed ILC1/2/3 precursor.[78,85] The precise mechanistic function of PLZF in the ILC lineage remains uncharacterized, though insight may be gained from studies performed in T cells. Within $CD4^+$ T cells, transgenic overexpression of PLZF is sufficient to promote the acquisition of an NKT-like effector phenotype with IL-4 and IFNγ expression[85], and in both NKT cells and PLZF transgenic thymocytes, PLZF directly binds the gene locus of several key helper T cell surface receptors (e.g., *Icos*, *Sell*, *Ifngr*, and *Il4ra*) and transcription factors (e.g., *Gata3*, *Rora*, *Rorc*, and *Runx3*).[136] The effects of *Zbtb16* deletion are most pronounced in ILC2s and ILC1s, with little impact on ILC3s despite all three subsets proceeding through the PLZF-expressing ILCP.[11] *Zbtb16*-deficient mice are impaired in their ability to mount type 2 inflammatory responses in the lung as a result of reduced numbers of ILC2s.[137]

A specific *cis*-regulatory element governing *Zbtb16* expression in the ILC and NKT cell lineage was recently discovered by our lab.[80] By combining ATAC-seq and CRISPR/Cas9-mediated deletion, it was observed that mice containing a deletion in the intronic region of *Zbtb16*, either +18/32 or +21/23, failed to upregulate PLZF expression in adult BM ILCPs and thymic NKT precursors. Several RUNX motifs were present within the +21/23 region of *Zbtb16*, which, when individually removed, were found to synergistically contribute to the function of the enhancer.

1.4.3 T cell factor 1 (TCF1)

Initially characterized as a transcription factor critically required for thymocyte development and establishment of the T cell identity[138,139], TCF1 is now recognized as being similarly important for the development of all ILCs and for enforcing commitment to the ILC lineage.[77] Mice deficient in *Tcf7* were first documented to have defects in NK cell de-

velopment at steady-state.[140] The impact of *Tcf7* deletion was subsequently extended to ILC2s and NKp46$^+$ ILC3s, with *Tcf7*-deficient mice presenting impaired responses to the allergen papain and *C. rodentium* respectively.[88,90] The establishment of mixed BM chimeras later confirmed the extent of *Tcf7* requirement in all ILC subsets, including ILC1s and LTis, given the observation that TCF1 expressing ILC precursors (NKP, CHILP, and ILCP) are undetectable in *Tcf7*$^{-/-}$ mice.[75,78,119] In addition to the requirement for TCF1 during the development of all ILCs, ILC3s and NK cells rely on TCF1 for proper function, differentiation, and/or maturation. ILC3s deficient in *Tcf7* more readily produce IL-17 and IL-22 following stimulation, indicating that TCF1 acts to constrain ILC3 function.[141] Interestingly, *Tcf7*-deficient ILC3s also display elevated expression levels of RORγ(t), which supports the reported pronounced defect in NKp46$^+$ ILC3 development[90], as RORγ(t) dose regulates NKp46$^+$ ILC3 differentiation from DN ILC3s[68], and suggests that TCF1 might suppress RORγ(t) downstream of Notch signaling.[54,67] In NK cells, TCF1 promotes the survival of immature NK cells and, in contrast to NKp46$^+$ ILC3s, acts to restrain NK cell maturation, which is supported by the observation that NK cells with elevated levels of TCF1 expression arrest at the CD27$^+$CD11b$^-$ immature NK cell stage.[119,142]

Until recently, a *cis*-regulatory element controlling *Tcf7* expression in the T cell lineage had not been described, though a prime candidate had been identified at an evolutionarily conserved site ~31.5 kb upstream of the gene that was bound by numerous T cell lineage transcription factors including TCF1, Notch-1/CSL, and RUNX1.[143,144] Subsequent interrogation of this element via CRISPR/Cas9-mediated deletion revealed that *Tcf7* +30/32 kb controlled *Tcf7* expression in both T cells and ILCs[145], a finding we have independently confirmed. Deletion of *Tcf7* +30/32 resulted in diminished thymic cellularity and TCF1 expression in thymocytes comparable to germline *Tcf7* knockouts. Similar developmental impairments were observed in the ILC lineage with reduced numbers of EILP, ILCP, and ILC2P as well as lower TCF1 expression, indicating there is a shared dependence on this

Tcf7 enhancer in both ILCs and T cells.

1.4.4 GATA binding protein 3 (GATA3)

GATA3 is a pleiotropic transcription factor with notable roles not only at several stages of ILC and T cell development, but also throughout organismal development[146], such as in the craniofacial ganglia[147], central nervous system, endocardium, urogenital system[148], kidney[149], inner ear[150], and embryonic lens.[151] Generally, in T cells, GATA3 controls the development of early thymic progenitors (ETPs) and thymopoiesis[152,153], CD4-CD8 T cell lineage commitment[154], T cell homeostasis[155], and Th2 cell differentiation and function.[156–158]

As indicated, GATA3 performs similarly broad roles during ILC development, differentiation, and function. GATA3 is necessary for the development, maintenance, and function of ILC2s, akin to its well-established role in Th2 cells.[81,159] However, the effects of GATA3 extend beyond type 2 lymphocytes, as the transcription factor was shown to control the appearance and development of ILC precursors in the adult BM and FL, as well as the peripheral maintenance of all IL-7Rα-expressing ILCs (ILC1/2/3 and LTi) but not NK cells.[68,76,120–122,160] Incidentally, the requirement for GATA3 during helper ILC development resembles its function in promoting helper T cell development during CD4-CD8 T cell lineage commitment. Building upon initial observations, Zhong et al. (2020) demonstrated that GATA3 was largely dispensable for the differentiation of LTis, and was instead principally involved in the acquisition of LTi function.[161] These results suggested that GATA3 likely functions upstream of a shared precursor to ILCs and LTis after the NK cell branch point, coinciding with PLZF expression[78], and may contribute to the ILC vs. LTi lineage fate decision.[161]

Numerous enhancers have been reported to regulate *Gata3* expression in non-lymphoid tissues.[146–151] Yet to date, only one enhancer has been identified that regulates the expression of *Gata3* within the immune system.[162,163] Using a bacterial artificial chromosome (BAC)

reporter system, Hosoya et al. (2011) first identified a 7.1 kb enhancer ∼280 kb downstream of *Gata3* within a gene desert based on EGFP expression in thymocytes and naïve $CD4^+$ T cells, for which they termed it the T cell enhancer 7.1 kb (TCE7.1).[162] A subsequent study by Ohmura et al. (2016) utilized CRISPR/Cas9 to generate mice with a germline deletion of TCE7.1 in which they observed impaired development of CD4 single-positive (CD4SP) T cells in the thymus that extended into peripheral naïve $CD4^+$ T cells.[163] It was originally reported that Th2 cells did not express EGFP in the TCE7.1 BAC reporter system[162], suggesting that Th2 cells differentiated independently of this enhancer, however these results were not explored in the context of an *in vivo* type 2 inflammatory model or through the use of mice deficient in the enhancer, the latter of which would be confounded by early defects in $CD4^+$ T cell development. Moreover, while the TCE7.1 BAC reporter was used to indicate that thymic NK cells utilized this enhancer, these results were not corroborated in the TCE7.1 deletion mouse nor have they been extended to the ILC family as a whole. Only recently has in been shown that TCF1 is capable of binding to TCE7.1 within the EILP[77], suggesting that TCE7.1 may regulate *Gata3* expression during ILC development as it does in thymocytes.

1.4.5 Interleukin-7 Receptor (IL-7R)

The surface receptor for the cytokine IL-7, IL-7R, comprises the IL-7R α-chain (IL-7Rα) and the common cytokine receptor γ-chain (IL-2Rγc). Genomic deletion of IL-7Rα severely impairs the maintenance and development of adaptive lymphocytes, halting early thymocyte and pro-B cell progression[164], as well as ILC1/2/3 and LTi development from their IL-7Rα-expressing precursors.[5,21,65,76,81,109,165] IL-7Rα is expressed during B cell, T cell, and ILC development, starting from the CLP. In the B cell lineage, IL-7Rα expression progressively decreases as the cells develop into immature B cells.[166] However, in both thymocytes and ILC precursors IL-7Rα expression is transiently downregulated at the double-positive (DP)

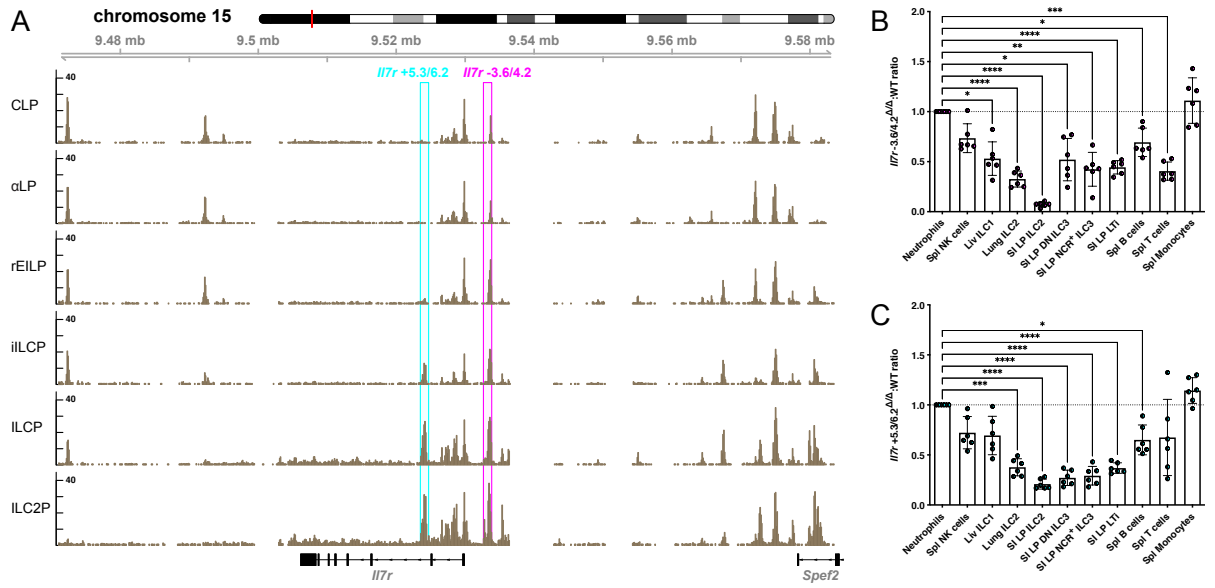

Figure 1.4: Chromatin accessibility at the *Il7r* locus and impact of *Il7r* -3.6/4.2 and *Il7r* +5.3/6.2 deletion. (**A**) ATAC-seq accessibility coverage tracks in sequential BM progenitors to the ILC lineage, including CLP, αLP, rEILP, iILCP, ILCP and ILC2P (detailed in **Chapter 3.1**). Magenta and cyan windows represent *Il7r* -3.6/4.2 and *Il7r* +5.3/6.2 regions respectively. (**B**) *Il7r* -3.6/4.2$^{\Delta/\Delta}$:WT and (**C**) *Il7r* +5.3/6.2$^{\Delta/\Delta}$:WT reconstitution ratio for the indicated populations in mixed BM chimeric mice.

thymocyte stage and the EILP respectively before being reexpressed.[75,167] The purpose and reason behind the transient loss of IL-7Rα expression in the ILC and T cell lineage is unknown. In B cells, the downregulation of IL-7Rα expression coincides with a migration away from IL-7 producing stromal cells in the BM[166], indicating that ILC precursors may migrate away from and back into an IL-7 rich niche. Alternatively, in T cells, IL-7 signaling is capable of regulating the expression of its own receptor[168], suggesting that the EILP might have low IL-7Rα expression as a result of IL-7 signaling.

Whether or not distinct regulatory elements underlie the dynamic expression pattern of IL-7Rα and the transient trough of expression in T cell and ILC development compared to B cell development remains largely unexplored. A conserved non-coding sequence (CNS) element containing consensus binding motifs for several T cell and ILC lineage transcription factors, including GATA and RUNX, was identified ~3.6 kb upstream of the *Il7r* start codon (**Fig.1.4A**, magenta window).[169] Yang et al. (2013) later identified a TCF motif present within this region, which was necessary for TCF1 induced luciferase reporter activ-

ity and was bound by TCF1 in *ex vivo* expanded ILC2s.[88] Deletion of this region, designated CNS-1, resulted in a cell-intrinsic impairment in $CD4^+$ and $CD8^+$ T cell maintenance and IL-7Rα expression, but was dispensable for both thymocyte and BM B cell development in unperturbed mice.[170] Apart from peripheral NK cells, ILC development and maintenance was not addressed. We have found, through the establishment of mixed BM chimeras, that CNS-1 (*Il7r* -3.6/4.2) was intrinsically required for the development and/or maintenance of several ILC subsets as well as in adaptive lymphocytes (**Fig.1.4B**). These results suggest that similar to T cells, ILCs rely on *Il7r* -3.6/4.2 for optimal IL-7Rα expression and indicate that while *Il7r* -3.6/4.2 deficient B cells arise normally at steady-state, their development is partially impaired in competition.

An additional putative enhancer was identified within the second intron of *Il7r* using Chromatin Immunoprecipitation sequencing (ChIP-seq) analysis (**Fig.1.4A**, cyan window).[68] Zhong et al. (2016) observed an enrichment of GATA3 binding at the conserved genomic region *Il7r* +5.3/6.2 in ILC2s, ILC3s, and Th2 cells. When we generated mixed BM chimeras for *Il7r* +5.3/6.2, we observed that this region was intrinsically required for the development and/or maintenance of both ILC subsets and adaptive lymphocytes, similar to *Il7r* -3.6/4.2 (**Fig.1.4C**). As with the deletion of *Il7r* -3.6/4.2, deletion of *Il7r* +5.3/6.2 only partially compromised the development of ILCs, T cells, and B cells, but had the largest impact on the *Il7r* expressing ILC2s and ILC3s. Thus, at least two elements, *Il7r* -3.6/4.2 and *Il7r* +5.3/6.2. appear to regulate *Il7r* expression throughout the lymphocyte lineage.

1.5 Aims and Significance

All murine ILCs, comprising helper ILC1, 2, and 3, LTis, and NK cells, are derived from the CLP.[1,69] ILCs, though lymphoid in origin, lack somatically rearranged antigen recognition receptors, which are defining features of B and T cells. Still, extensive similarities exist between ILCs and T cells, including a reliance on similar factors and stimuli for their development; the transcription factors TCF1 and GATA3 as well as signaling via IL-7Rα are crucial for ILC and T cell development, while additional factors contribute to a greater extent towards ILC development, namely ID2 and PLZF.[1,69] Despite their involvement in ILC development, a comprehensive understanding of how each transcription factor or signaling receptor is regulated and in turn contributes to the specification of the ILC lineage is lacking.

In addition to the parallels between ILCs and T cells, a level of similarity exists within subsets of ILCs, as is the case with NK cells and ILC1s or LTis and ILC3s.[1,4,5,9,11,58,69] While similar in their requirement for a "master regulator", TBET or RORγ(t) respectively, the use of conditional knockouts and fate mapping reveals a differential reliance on specific transcription factors and branch points whose precise positions during ILC development remain to be defined. This model is further substantiated by the identification of intermediate ILC precursors in the mouse adult BM and FL, such as the ILCP, that give rise to restricted subsets of mature ILCs.[5,73–75,78] However, many proposed precursors are still ill-defined or have apparent heterogeneity[5,11,70,76,77,93,94], and a systematic approach to addressing precursor-product relationship has not been performed. Thus, the lineage progression and bifurcation during ILC development are matters of great interest in the field.

Binding of temporally-regulated transcription factors within *cis*-regulatory modules (e.g. enhancers and silencers), provides a level of specificity for gene expression necessary to determine cell fate. Given that numerous transcription factors are shared between T cells and ILCs as well as among mature and precursor ILCs, we expect the availability of binding sites

within *cis*-regulatory elements to govern the lineage-specific expression of crucial transcription factors, which would then instruct the development and maturation of ILCs. Thus the overarching hypothesis is that a combined approach based on new combinatorial transcription factor reporter strains and epigenetic analysis will clarify the developmental progression of ILCs and help elucidate the regulation of ILC transcription factors.

Aim 1: Generate novel transcription factor reporter strains for use in combination to identify and isolate putative ILC precursors.

Aim 2: Delineate the developmental progression and intermediate precursors of the ILC lineage.

Aim 3: Discern regions of dynamic chromatin accessibility and identify putative *cis*-regulatory elements throughout ILC development.

Aim 4: Assess the activity of putative *cis*-regulatory elements during ILC development to address the role of these elements in driving lineage progression and expression of proximal genes.

These studies will 1) generate tools that enable the characterization of ILC precursors, 2) clarify the developmental progression of the ILC lineage, 3) provide a resource for understanding the regulation of genes during ILC development, and 4) lay the foundation for dissecting the *cis*-regulatory network that governs the lineage- and stage-specific expression of key transcription factors during ILC development. As the ablation of shared factors leads to defects in both the development and function of ILCs and T cells, there has been no definitive assessment of homeostatic or inflammatory responses sans ILCs. The results of this study will serve to inform the generation of better tools (e.g. selective knockouts) to determine and influence the contribution of ILCs to homeostatic and inflammatory responses.

CHAPTER 2

MATERIALS AND METHODS

2.0.1 Mice

C57BL/6J (CD45.2+; Stock No. 000664) and B6.SJL-Ptprca Pepcb/Boy (CD45.1+; Stock No. 002014) mice were purchased from The Jackson Laboratory and maintained in house. *Zbtb16*$^{\text{EGFPCre}}$ mice were generated as previously described (Stock No. 024529).[78] ID2$^{\text{EYFP}}$ mice were a gift from Ananda Goldrath (University of California, San Diego, La Jolla, CA) and were described previously.[171] RORγt$^{\text{EGFP}}$ mice were described previously (Stock No. 007572).[58] *Tcf7*$^{\text{EGFP}}$ mice were a gift from Avinash Bhandoola (National Institutes of Health, Bethesda,MD) and were described previously (Stock No. 030909).[75] For FL experiments, the morning after timed pregnancy setup was considered as E0. For enhancer deletion analysis (detailed below), male and female littermate mice ranging from 6 to 8 weeks were used in all experiments of the study. Novel reporter mice and enhancer deletion mice (detailed below) were maintained on the C57BL/6J background. All mice were bred and housed in the specific pathogen-free facility at the University of Chicago. Experiments were conducted under the guidelines of the University of Chicago Institutional Animal Care and Use Committee.

2.0.2 Generation of reporter and enhancer deletion mice

Tcf7$^{\text{mCherry}}$, *Rorc*$^{\text{Thy1.1}}$, *Gata3*$^{\text{Citrine}}$, and *Zbtb16*$^{\text{hCD4}}$ mice were generated via CRISPR/Cas9-mediated insertion. Guide sites targeting the 3' UTR of each gene were designed using the Broad Institute or IDT design tools. Regions flanking the cut site were amplified to generate 1 kb and 3 kb asymmetric homology arms. Homology arms were cloned into a pUC19 vector along with a minimal IRES sequence and reporter sequence using NEB Hi-Fi DNA Assembly Master Mix (NEB). The vector was amplified, purified with

the Thermo Purelink HiPure Plasmid Filter Kit (ThermoFisher), and the sequence was verified by Sanger sequencing. Alt-R CRISPR-Cas9 crRNA, tracrRNA, and Cas9 nuclease were purchased from IDT. The following sequences were used for each crRNA: 5'-CGACCTGAGAATGTTGGTGC-3' (*Tcf7*), 5'-GTCCTACAAGGCAAGCCTAG-3' (*Rorc*), 5'-GGAGGAACTCTTCGCACACT-3' (*Gata3*), and 5'-CGAGCTAGAACCAGACAAAG-3' (*Zbtb16*). For microinjections, gRNA was assembled with crRNA and tracrRNA according to the manufacturer's instructions and added to the final injection mix at 20 ng/μl along with 50 ng/μl Cas9 nuclease and 12.5 ng/μl plasmid in embryo-grade water. Mixes were injected into the nuclei of C57BL/6J embryos (detailed below). Successful integrations were determined by targeting PCR using two primer sets that generate a product spanning the insert out beyond the homology arms, which was sequence verified.

Gata3 +674/762$^{\Delta/\Delta}$, *Gata3* +674/710$^{\Delta/\Delta}$, *Gata3* +710/762$^{\Delta/\Delta}$, and *Gata3* +278/285$^{\Delta/\Delta}$ mice were generated via CRISPR/Cas9-mediated deletion. Guide sites were selected using IDT design tools and Alt-R CRISPR/Cas9 crRNA, tracrRNA, and Cas9 nuclease were purchased from IDT. Targeting strategies and crRNA sequences are displayed in **Fig.3.14C**, **Fig.3.17A**, and **Fig.3.22B**. For microinjections, guide RNA (gRNA) was assembled with crRNA and tracrRNA according to the manufacturer's instructions and added to the final injection mix at 50 ng/μL and 50 ng/μL Cas9 per guide in embryo grade water. Mixes were injected into the nuclei of C57BL/6J embryos (detailed below). Successful deletions were determined by PCR and sequence verified. Deletion mice were maintained on the C57BL/6J background and backcrossed for four generations unless otherwise indicated. *H11* enhancer reporter mice were generated via CRISPR/Cas9 mediated insertion as before (**Fig.3.22E**).[172] Targeting strategy and crRNA sequence are displayed in **Fig.3.22E**. Briefly, the *Gata3* +761/762 sequence was cloned upstream of the murine minHSP68 promoter and EGFP, which was then inserted into a pUC19 vector between 1 kb and 3 kb asymmetric homology arms. Microinjection mixes were assembled as above with 20 ng/μL

gRNA, 50 ng/μL Cas9 nuclease, and 12.5 ng/μL plasmid in embryo grade water. Successful integrations were determined by targeting PCR using two primer sets that generate a product spanning the insert out beyond the homology arms, which was sequence verified.

Table 2.1: List of CRISPR/Cas9-generated mice.

Strain	Type	Reporter
Tcf7$^{\text{mCherry}}$	Transcription Factor Reporter	mCherry
Rorc$^{\text{Thy1.1}}$	Transcription Factor Reporter	Thy1.1
Gata3$^{\text{mCitrine}}$	Transcription Factor Reporter	mCitrine
Zbtb16$^{\text{hCD4}}$	Transcription Factor Reporter	hCD4
Tcf7 +30/32	Deletion	—
Il7r -3.6/4.2	Deletion	—
Il7r +5.3/6.2	Deletion	—
Gata3 +674/762	Deletion	—
Gata3 +674/710	Deletion	—
Gata3 +710/762	Deletion	—
Gata3 +278/285	Deletion	—
H11 Gata3 +761/762	Enhancer Reporter	EGFP
H11 Gata3 +283/284	Enhancer Reporter	EGFP
H11 Zbtb16 +21/23	Enhancer Reporter	EGFP
H11 Tcf7 +30/32	Enhancer Reporter	EGFP
H11 Il7r -3.6/4.2	Enhancer Reporter	EGFP
H11 Il7r +5.3/6.2	Enhancer Reporter	EGFP
H11 Tcrb Eb	Enhancer Reporter	EGFP

2.0.3 Embryo microinjection

C57BL/6 J female mice in diestrus ranging from 9 and 16 weeks were selected for superovulation. Mice were injected with 5-7 IU of PMSG (Millipore #367222 or BioVendor

#RP1782721000) via intraperitoneal (i.p.) injection at 2:50-3:05 PM depending on age and size of the mice, followed by HCG 5-7 IU (Sigma CG5) 47 hours later. C57BL/6J males were introduced one hour later. The next morning, females were examined for evidence of a mating plug, and harvested for fertilized eggs if a plug was present. Harvested eggs were cultured for 1-3 hours in KSOMaa Evolve Bicarb +BSA (Zenith Biotech #ZEKS-050) and then placed on the injection slide in KSOMaa Evolve HEPES +BSA (Zenith Biotech #ZEHP-050). Glass needles loaded with the aforementioned injection mixes were placed on ice until ready for injection. An Eppendorf FemtoJet apparatus was used to inject mixes into fertilized eggs, which were then returned to the incubator and cultured until embryo transfer into 0.5 day pseudopregnant CD-1 females. Implanted females were monitored daily and separated 2 days before the pups were due to deliver. Tail and toe samples were taken from pups at 2 weeks for genotyping.

2.0.4 Preparation of cell suspensions

FLs were passed through a 70-μm cell strainer and re-suspended in FACS buffer (1X HBSS [Gibco], 0.25% BSA [Millipore-Sigma], 50 ng/ml DNase, and 5 mM sodium azide [Millipore-Sigma]). BM was collected from the femur, tibia, and ilium (six bones in total), crushed with the syringe plunger flange, passed through a 70-μm cell strainer, and re-suspended in FACS buffer. Spleens and thymi were prepared in the same manner as FLs. Adult livers were passed through a 70-μm cell strainer and re-suspended in FACS buffer. Fat was removed by centrifugation in 0.45% Percoll (Millipore-Sigma). RBCs were removed with 1× RBC lysis buffer (ThermoFisher). The lung was perfused with 1× PBS (Corning), chopped into small pieces, and digested by shaking (250 rpm) at 37°C for 15 min in RPMI (Hyclone) with 650 U/ml collagenase A (Roche) and 0.01% DNase (Millipore- Sigma). The SI LP was prepared by removing Peyer's patches, washing out intestinal contents with ice-cold 1X PBS, and cutting length- and widthwise into small pieces. Intraepithelial lymphocytes were

removed by two 37°C 15-min shakes (250 rpm) in RPMI with 5 mM EDTA (ThermoFisher) and 1% FBS (Atlanta Biologicals), and lamina propria was digested by shaking (250 rpm) at 37°C for 30 min in RPMI with 20% FBS, 0.5 mg/ml collagenase A, and 0.17 mg/ml DNase. Visceral WAT (vWAT) was digested by shaking (250 rpm) at 37°C for 45 min in RPMI with 1mg/mL Collagenase A. Digests for the lung, SI LP, and vWAT were passed through 70 μm or 100 μm cell strainers, followed by excess fat removal and RBC lysis as above. BAL was prepared by inserting a cannula into the trachea followed by flushing of the lungs 4 times with 1X PBS 5 mM EDTA to collect a total of 3.5 mL BAL fluid.

2.0.5 Flow cytometry

Single-cell suspensions were incubated with BD FcBlock for 15 min on ice. All FL cells were lineage depleted with CD3ϵ, CD11c, CD19, GR-1, NK1.1, TCRβ, and Ter119, while BM depletions additionally contained B220, CD4, CD8α, and CD11b. Lineage antibodies conjugated to APC-Cy7 or Biotin were incubated with cells for 30 min on ice, then subsequently incubated with anti-Cy7 or anti-streptavidin microbeads (Miltenyi Biotec) for an additional 30 min. Bead-bound cells were depleted with an autoMACS (Miltenyi Biotec) using the depletion-sensitive program. The following fluorochrome- or biotin-conjugated antibodies were used: $\alpha4\beta7$ (DATK32), CCR6 (29-2L17), CD11c (N418), CD19 (6D5), CD45.1 (A20), CD45.2 (104), CD90.2 (Thy-1.2; 53–2.1), CD127 (IL-7Rα; A7R34), CXCR5 (L138D7), GR-1 (RB6-8C5), ICOS (C398.4A), IL-4 (11B11), IL-17RB (9B10), IL-33Rα (DIH9), KLRG1 (MAFA), NK1.1 (PK136), NKp46 (29A1.4), PD-1 (29F.1A12), TCR$\gamma\delta$ (GL3), Ter119 (TER-119), mouse IgG1 κ-chain (MG1-45), mouse IgG2a κ-chain (MG2a-53), rat IgG1 κ-chain (RTK20-71), rat IgG2a κ-chain (RTK27-58) and rat IgG2b κ-chain (RTK45-30) (all from BioLegend); B220 (RA3-6B2), CD3ϵ (145-2C11), CD4 (GK1.5), CD8α (53–6.7), CD11b (M1/70), CD11c (HL3), CD19 (1D3), CD25 (PC61), CD45.2 (104), CD49a (Ha31/8), CD117 (cKit, 2B8), CD121a (35F5), Flt3 (A2F10.1), GR-1 (RB6-8C5), IL-5 (TRFK5), Ly6A/E

(Sca-1, D7), NK1.1 (PK136), Siglec-F (E50-2440), TCRβ (H57-597), Thy1.1 (OX-7), Ter119 (TER-119), RORγ(t) (Q31-378), and PLZF (R17-809; all from BD Biosciences); GATA3 (TWAJ), IL-13 (eBio13A), and FOXP3 (FJK-16s) (all from ThermoFisher); NRP-1 (761705) from R&D Systems; TCF1 (Cell Signaling Technologies); and polyclonal goat α-Rb IgG (Abcam). To exclude dead cells, Zombie NIR, Yellow, or Violet Fixable Viability Dye (BioLegend) was added to live cells. Intracellular staining was performed using the Foxp3 Transcription Factor Staining Buffer Kit (ThermoFisher) according to the manufacturer's instructions. Cells were blocked with unlabeled isotype-matched antibody (above) and negative controls were prepared using 20-fold excess unlabeled antibody to the TF (cold competitor). Samples were acquired on a four-laser LSRII (BD Biosciences) or sorted on a FACSAriaII or FACSAria Fusion (BD Biosciences) and analyzed using FlowJo software (TreeStar). Unless otherwise indicated, cell populations were lineage negative and identified as follows for Chapter 3.1: ILC2P ($\alpha4\beta7^+$IL-7Rα^+CD90.2$^+$ICOS$^+$ *Zbtb16*$^-$), ILCP ($\alpha4\beta7^+$IL-7Rα^+CCR6$^-$ *Zbtb16*$^+$ or $\alpha4\beta7^+$IL-7Rα^+CCR6$^-$ *Tcf7*$^+$ *Zbtb16*$^+$), LTiP ($\alpha4\beta7^+$IL-7Rα^+CCR6$^+$ *Zbtb16*$^-$ or $\alpha4\beta7^+$IL-7Rα^+CCR6$^+$ *Tcf7*$^+$ *Zbtb16*$^-$ *Rorc*$^+$), iILCP ($\alpha4\beta7^+$IL-7Rα^-CD90.2$^-$ *Tcf7*$^+$ *Zbtb16*$^+$ *Rorc*$^-$), iLTiP ($\alpha4\beta7^+$IL-7Rα^-CD90.2$^-$ *Tcf7*$^+$ *Zbtb16*$^-$ *Rorc*$^+$), rEILP ($\alpha4\beta7^+$IL-7Rα^-CD90.2$^-$ *Tcf7*$^+$ *Zbtb16*$^-$ *Rorc*$^-$), *Rorc*$^+$ αLP ($\alpha4\beta7^+$IL-7Rα^+CD90.2$^-$PD-1$^-$ *Tcf7*$^-$ *Zbtb16*$^-$ *Rorc*$^+$), Flt3$^-$ αLP ($\alpha4\beta7^+$IL-7Rα^+CD90.2$^-$PD-1$^-$Flt3$^-$ *Tcf7*$^-$ *Zbtb16*$^-$), Flt3$^+$ αLP ($\alpha4\beta7^+$IL-7Rα^+CD90.2$^-$PD-1$^-$Flt3$^+$ *Tcf7*$^-$ *Zbtb16*$^-$), CLP ($\alpha4\beta7^-$IL-7Rα^+CD90.2$^-$PD-1$^-$Flt3$^+$), and CHILP ($\alpha4\beta7^+$IL-7Rα^+ID2$^+$CD25$^-$Flt3$^-$).

Unless otherwise indicated, cell populations were identified as follows while excluding alternate lineages for Chapter 3.2: BM CLP (Lin$^-$IL-7Rα^+Flt3$^+$Sca-1$^+$cKit$^+$), BM αLP (Lin$^-\alpha4\beta7^+$CD90.2$^-$IL-7Rα^+ *Tcf7*$^{\text{mCherry-}}$PD-1$^-$Flt3$^+$) BM rEILP (Lin$^-\alpha4\beta7^+$CD90.2$^-$IL-7Rα^- *Tcf7*$^{\text{mCherry+}}$PD-1$^-$); BM iILCP (Lin$^-\alpha4\beta7^+$CD90.2$^-$IL-7Rα^- *Tcf7*$^{\text{mCherry+}}$PD-1$^+$); BM ILCP (Lin$^-\alpha4\beta7^+$IL-7Rα^+ *Tcf7*$^{\text{mCherry+}}$PD-1$^+$); BM ILC2P (Lin$^-\alpha4\beta7^+$IL-7Rα^+ CD90.2$^+$ICOS$^+$PD-1$^-$); splenic NK cells (CD45.2$^+$CD19$^-$CD3ϵ^-TCRβ^-NK1.1$^+$); liver NK

cells ($CD45.2^+CD19^-CD3\epsilon^-TCR\beta^-NK1.1^+DX5^+CD49a^-$); liver ILC1 ($CD45.2^+CD19^-CD3\epsilon^-TCR\beta^-NK1.1^+DX5^-CD49a^+$); lung and vWAT NK/ILC1 ($CD45.2^+CD19^-CD11c^-CD3\epsilon^-TCR\beta^-NK1.1^+$); lung and BAL ILC2 ($CD45.2^+CD19^-CD11c^-CD3\epsilon^-TCR\beta^-IL\text{-}7R\alpha^+CD90.2^+CD25^+IL\text{-}33R\alpha^+$); vWAT ILC2 ($CD45.2^+CD19^-CD11c^-CD3\epsilon^-TCR\beta^-IL\text{-}7R\alpha^+CD90.2^+CD25^+IL\text{-}33R\alpha^+KLRG1^+$); SI LP ILC2 ($CD45.2^+CD19^-CD11c^-CD3\epsilon^-TCR\beta^-IL\text{-}7R\alpha^+CD90.2^+KLRG1^+Sca\text{-}1^+IL\text{-}17RB^+$); SI LP NCR^+ ILC3 ($CD45.2^+CD19^-CD11c^-CD3\epsilon^-TCR\beta^-IL\text{-}7R\alpha^+CD90.2^+CD121a^+CCR6^-NKp46^+$); SI LP LTi ($CD45.2^+CD19^-CD11c^-CD3\epsilon^-TCR\beta^-IL\text{-}7R\alpha^+CD90.2^+CD121a^+CCR6^+NKp46^-NRP1^+$); SI LP ILC3 ($CD45.2^+CD19^-CD11c^-CD3\epsilon^-TCR\beta^-IL\text{-}7R\alpha^+CD90.2^+CD121a^+$); Thy ETP ($B220^-CD11b^-CD11c^-CD19^-GR\text{-}1^-CD4^-CD8\alpha^-TCR\gamma\delta^-CD1d\text{-}Tet^-TCR\beta^-CD25^-CD44^+$); Thy CD4SP ($B220^-CD11b^-CD11c^-CD19^-GR\text{-}1^-CD4^+CD8\alpha^-TCR\gamma\delta^-CD1d\text{-}Tet^-$); Thy CD8SP ($B220^-CD11b^-CD11c^-CD19^-GR\text{-}1^-CD4^-CD8\alpha^+TCR\gamma\delta^-CD1d\text{-}Tet^-TCR\beta^+$); splenic T cells ($CD45.2^+CD3\epsilon^+TCR\beta^+$, $CD4^+$ or $CD8\alpha^+$); Lung and BAL Th2 cells ($CD45.2^+CD3\epsilon^+TCR\beta^+CD90.2^+CD4^+IL\text{-}33R\alpha^+GATA3^+$); medLN Th2 cells ($CD45.2^+CD3\epsilon^+TCR\beta^+CD90.2^+CD4^+GATA3^+$); splenic B cells ($CD45.2^+B220^+CD19^+$); splenic neutrophils ($CD45.2^+CD11b^+GR\text{-}1^+FSC^{Hi}SSC^{Hi}$); Lung, vWAT, BAL, and medLN eosinophils ($CD45.2^+Siglec\text{-}F^+SSC^{Hi}$); Lung and BAL AMac ($CD45.2^+CD11c^+Siglec\text{-}F^+$), vWAT $GATA3^+$ Treg cells ($CD45.2^+CD3\epsilon^+TCR\beta^+CD90.2^+CD4^+FOXP3^+GATA3^+IL\text{-}33R\alpha^+KLRG1^+$), and vWAT $GATA3^-$ Treg cells ($CD45.2^+CD3\epsilon^+TCR\beta^+CD90.2^+CD4^+FOXP3^+GATA3^-$).

2.0.6 OP9 and OP9-DL1 stromal cell culture

Stocks of OP9 and OP9-DL1 stromal cells were a gift from J.C. Zúñiga-Pflücker (University of Toronto, Toronto, Canada). All experiments were performed in Opti-MEM with GlutaMAX (Gibco) containing heat-inactivated 10% FBS, 1% penicillin-streptomycin (Gibco), and 60 μM 2-mercaptoethanol (Millipore- Sigma) and were maintained in a 37°C incubator

(ThermoFisher) with 5% CO_2. Stromal cells were plated at a density of 10,000 cells per well of a 96-well plate, allowed to grow overnight, and then irradiated (1500 rad). Before sorting lymphocytes, the media was replaced and supplemented with murine stem cell factor (25 ng/ml; BioLegend), IL-7 (25 ng/ml; BioLegend), and IL-2 (25 ng/ml; BioLegend). FL cells were lineage depleted as described, stained, and single cells were sorted. Cultures were analyzed after 6 d, and colonies with five or more $CD45^+$ cells were considered. Cell populations were defined as follows for single-cell cultures: ILC1 ($NK1.1^+ICOS^-\alpha4\beta7^-$), ILC2 ($NK1.1^-ICOS^+\alpha4\beta7^-$), ILC3/$LTi_0$ ($NK1.1^-ICOS^{+/-}\alpha4\beta7^+CD4^-$), and/or LTi_4 ($NK1.1^-ICOS^{+/-}\alpha4\beta7^+CD4^+$). Wells were categorized as LTi_4 if >8% of $NK1.1^-ICOS^{+/-}\alpha4\beta7^+$ cells were $CD4^+$; no frequency was used to categorize ILC1, ILC2, or ILC3/LTi_0. Early T cells were identified in OP9-DL1 cultures by high expression of CD25. For bulk cultures, stromal cells were plate at a density of 24,000 cells per well of a 48-well plate, grown overnight, and irradiated as above. Media was replaced and supplemented with stem cell factor (25 ng/ml), IL-7 (25 ng/ml), IL-2 (25 ng/ml), and Flt3-L (25 ng/ml; BioLegend). Cells were sorted, and 500 cells of each precursor population were plated and allowed to grow for 48 h before analysis. $CD45^+$ cell populations were defined as follows for bulk cell cultures: ILC1 ($NK1.1^+ICOS^-$), ILC2 ($NK1.1^-ICOS^+$), ILC3/LTi_0 ($NK1.1^-ICOS^-$*Rorc*-$Thy1.1^+CD4^-$), and/or LTi_4 ($NK1.1^-ICOS^-$*Rorc*-$Thy1.1^+CD4^+$).

2.0.7 Mixed Bone Marrow Chimeras

To generate mixed chimeras, bone marrow was isolated as described above for *Gata3* $+674/762^{\Delta/\Delta}$ (CD45.2) mice and WT (CD45.1 or CD45.1/.2) mice, depleted of T cells, and mixed at a 50:50 ratio. 10 million mixed cells were injected retro-orbitally into lethally irradiated (1000 rad) CD45.1/.2 or CD45.1 recipients to allow for discrimination of donor *Gata3* $+674/762^{\Delta/\Delta}$ and WT cells from host cells. Host mice were allowed to recover for 6 weeks prior to analysis or treatment. Populations were normalized to the reconstitution

frequency of splenic neutrophils or splenic B cells.

2.0.8 IL-33 challenge

500 ng of IL-33 (Biolegend) in PBS was administered i.n. in 40 μL to Isoflurane (Henry Schein) anesthetized mice on days 0, 1, and 2, followed by analysis on day 3 (**Fig.3.14L**). Control mice were administered PBS alone.

2.0.9 House Dust Mite challenge

HDM extracts (Stallergenes Greer Lenoir) were suspended in 1X sterile endotoxin free PBS (Sigma) to a concentration of 4 mg/mL. Lots are titrated to induce a minimum of 2 X 10^6 eosinophils in the BAL of C57BL/6 mice on day 13 using an i.t. challenge model (**Fig.3.18A** and **Fig.3.20A**). Briefly, mice were anesthetized with i.p. injection of ketamine/xylazine (Covetrus) and sensitized via administration of 50 μg HDM extract in 50 μL 1X sterile endotoxin free PBS through i.t. instillation on day 0. After 7 days, mice were challenged i.t. with 25 μg HDM extract in 50 μL 1X sterile endotoxin free PBS on days 7, 8, 9, and 10 followed by analysis on day 13. Control mice were treated with PBS alone during the sensitization and challenge phases.

2.0.10 Strongyloides venezuelensis passage and infection

S. venezuelensis was propagated in NSG mice (The Jackson Laboratory) by s.c. infection with 10,000 larvae. Prior to infection of mice, feces were collected and spread on Whatman paper, and the paper was placed into a beaker with 28°C water. Hatching live larvae were collected after 4 days. Mice were s.c. infected with 700 L3 larvae per mouse. For egg count, feces were collected, weighed, and homogenized with counts normalized to feces weight.

2.0.11 OVA-Alum challenge

Mice were treated using a 23-day model of sensitization and challenge as previously described (**Fig.3.18I**).[137] Briefly, 50 μL of 1 mg/mL Grade V OVA (Sigma) in 1X PBS was mixed with 50 μL of Imject Alum (ThermoFisher), and 100 μL of the mixture was injected i.p. on days 0, 7, and 14 for sensitization. Subsequently, mice were challenged i.n. with 100 μg OVA in 40 μL of 1X PBS or PBS only on days 20, 21, and 22 and analyzed on day 23.

2.0.12 Histology

Subsequent to perfusion, as described above, the left lobe of the lung was removed and fixed in 10% neutral buffered formalin (Azer Scientific) for a minimum of 24 hours before transfer to 70% Ethanol (Fisher Scientific) for storage. Lobes were embedded in paraffin and cut into 5 μm sections before staining with PAS. Histology slides were scanned using the Pannoramic SCAN 40x Whole Slide Scanner and analyzed with QuPath whole slide image analysis software (https://qupath.github.io/). Histology slides were blinded for PAS scoring and scored on a scale from 0-5 as follows: 0 = No PAS staining, 1 = 0-25% PAS^+ cells, 2 = 26-50% PAS^+ cells, 3 = 51-75% PAS^+ cells, 4 = 76-100% PAS^+ cells, and 5 = 100% PAS^+ cells and evidence of mucus plugs.

2.0.13 ATAC-seq sample preparation

ATAC-seq was performed as described in the published Omni-ATAC protocol.[173] Briefly, 5,000–10,000 cells were sorted into FACS buffer and washed twice with 1 ml ice cold ATAC-seq re-suspension buffer (RSB; 10 mM Tris, pH 7.4 [Invitrogen], 10 mM NaCl [Millipore-Sigma], 3 mM $MgCl_2$ [Millipore-Sigma]) by centrifugation at 0.5 xg for 5 min at 4°C. After centrifugation, the supernatant was carefully removed to avoid the cell pellet, which was then gently re-suspended in 50 μl ATAC-seq RSB containing 0.1% NP-40 (Roche), 0.1% Tween-20 (Millipore-Sigma), and 0.1% digitonin (Millipore-Sigma). The lysis reaction was

incubated on ice for 3 min, 1 ml ATAC-seq RSB containing 0.1% Tween-20 was added, and the nuclei were centrifuged at 0.5 xg for 10 min at 4°C. The supernatant was subsequently removed, and the pelleted nuclei were gently re-suspended in 50 μl transposition mix (25 μl 2x Tagment DNA buffer [Illumina], 2.5 μl Tn5 transposase [Illumina], 16.5 μl 1× PBS, 0.5 μl 1% digitonin, 0.5 μl 1% Tween-20, and 5 μl water). Transposition reactions were incubated for 30 min in a 37°C water bath. Zymo DNA Clean and Concentrator kits were used to clean up the transposition reactions, and libraries were prepared as previously described.[174] Libraries were sequenced by 50 bp single-end, dual-index sequencing on an Illumina HiSeq 4000.

2.0.14 ATAC-seq analysis (Chapter 3.1)

ATAC-seq reads were aligned to the mouse genome (mm10) with Bowtie, and duplicate reads were removed using Picard Tools. A pooled bam file was generated from all samples, including replicates (n = 2), and peaks were called on the pooled bam file with MACS2 to control for type I error.[175] Called peaks were filtered through a modified blacklist, and mitochondrial and Y chromosome peaks were removed (n = 214,321).[176] ATAC-seq read counts for all samples, including replicates, were determined via bedtools multiBamCov, and peaks with low read counts were removed (n = 122,250). Quantile normalization, GC content normalization, and peak length normalization were performed using the CQN R package.[177] Peaks were filtered to select for the top peaks (n = 100,000) with the highest variance. Heatmap generation and principal component analysis were performed on normalized data. Generation of normalized bigWig files for data visualization was performed by first generating normalized bedGraph files with bedtools genomecov, where the sum of reads within peaks associated with transcription start sites was used as a scaling factor, followed by file conversion using the University of California, Santa Cruz, bedGraphToBigWig program. Motif enrichment analysis was performed using HOMER.[178] The R package Gviz was used

for coverage track visualization.

2.0.15 Bioinformatic analysis (Chapter 3.2)

Publicly available data was downloaded from the NCBI SRA database.[68,129,179–183] Reads were aligned to the mouse genome (mm10) with Bowtie and duplicate reads were removed using Picard Tools. Bedgraphs were generated using HOMER[178], and files were converted to bigWig format for visualization using the UCSC bedGraphToBigWig program. The R package Gviz was used for coverage track visualization.

2.0.16 Statistical analysis

Single-cell indexing, Chi-Square Test for Independence followed by post-hoc analysis with Bonferroni correction, hierarchical clustering by Pearson correlation as the distance metric, heatmap generation, and principal component analysis were all performed in R. Student's t-test, multiple t-tests controlling for False Discovery Rate, and One-way ANOVA with Tukey's multiple comparisons test were performed in GraphPad Prism 8.

2.0.17 Accession codes

Chapter 3.1 GEO: ATAC-seq data, GSE150763 and Chapter 3.2 GEO: ATAC-seq data, GSE169542

CHAPTER 3

RESULTS

3.1 Multi-transcription factor reporter mice delineate early precursors to the ILC and LTi lineages

Darshan N. Kasal[1,2] and Albert Bendelac[1,2]

[1] *Committee on Immunology, University of Chicago, Chicago, IL 60637, USA*

[2] *Department of Pathology, University of Chicago, Chicago, IL 60637, USA*

Published online in the Journal of Experimental Medicine

26 October 2020; doi:10.1084/jem.20200487

3.1.1 Abstract

Transcription factor (TF) reporter mice have proved integral to the characterization of murine innate lymphoid cell (ILC) development and function. Here, we implemented a CRISPR/Cas9-generated combinatorial reporter approach for the simultaneous resolution of several key TFs throughout ILC development in both the fetal liver and adult bone marrow. We demonstrate that the *Tcf7*-expressing early innate lymphoid precursor (EILP) and the common helper ILC precursor (CHILP) both contain a heterogeneous mixture of specified ILC and lymphoid tissue inducer (LTi) precursors with restricted lineage potential rather than a shared precursor. Moreover, the earliest specified precursor to the LTi lineage was identified upstream of these populations, before *Tcf7* expression. These findings match dynamic changes in chromatin accessibility associated with the expression of key TFs (i.e., GATA3 and RORγ(t)), highlighting the distinct origins of ILC and LTi lineages at the epigenetic and functional levels, and provide a revised map for ILC development.

3.1.2 Introduction

Innate lymphoid cells (ILCs) are a diverse lineage classically divided into ILC1, ILC2, ILC3, lymphoid tissue inducer (LTi) cells, and natural killer (NK) cells based on developmental origin, phenotype, and function.[69] Studies identifying restricted precursors provide a basis for the delineation of ILCs into distinct developmental origins, and transcription factor (TF) reporter mice have served as critical tools for these studies.[70] LTi precursors (LTiPs) were identified in the fetal liver (FL) of RORγt$^{\mathrm{EGFP}}$ mice.[58,59,73] The ILC precursor (ILCP), which generated ILC1/2/3 but not LTi or NK cells, was characterized in *Zbtb16*$^{\mathrm{EGFPCre}}$ mice.[78] Concurrently, the common helper ILC precursor (CHILP) was described in ID2$^{\mathrm{EGFP}}$ mice and generated ILC1/2/3 and LTi but not NK cells.[5] Early work found that a shared precursor to all ILCs resides downstream of the common lymphoid precursor (CLP) within the $\alpha4\beta7^{+}$ lymphoid precursor (αLP).[72–74,91] More recently, however, studies using *Tcf7*$^{\mathrm{EGFP}}$ mice defined an early innate lymphoid precursor (EILP) that resides downstream of the αLP as the common precursor to all ILCs (**Fig.3.1A**).[75,76]

Several models have been proposed for ILC development based on precursor fates; nevertheless, outstanding questions remain regarding precursor ontogeny, heterogeneity, and hierarchy. First, neither the CHILP nor the EILP were characterized in the FL, the dominant source of LTi during ontogeny, and furthermore, LTi were not distinguished from ILC3 in clonal cultures.[5,75,76] Second, both the CHILP and EILP are heterogeneous and contain a *Zbtb16*$^{+}$ subpopulation.[5,76,77] Thus, whether these populations contain a shared precursor to the ILC and LTi lineages (ILC-LTi) or are an amalgamation of distinct precursors remains unresolved. Finally, though studies on ILC progenitor fates have prompted their hierarchical placement, a contemporaneous comparison of precursor potential has not been conducted.

Recent reports have applied polychromatic reporter mice to examine bone marrow (BM) ILC progenitors.[77,93,94] To better address the aforementioned questions, we implemented a multi-TF reporter strategy to evaluate ILC progenitors in the FL and BM. We established a

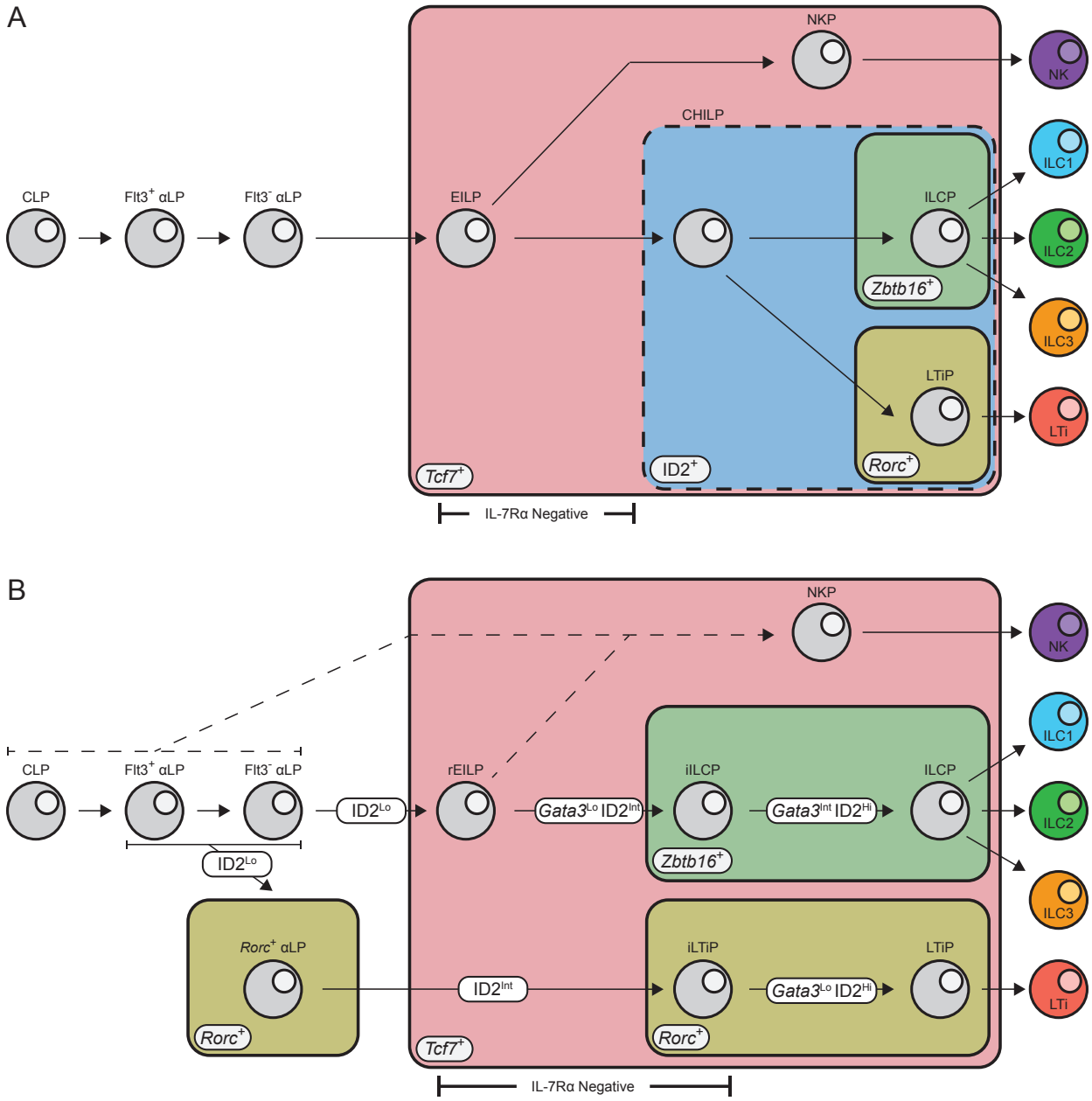

Figure 3.1: Current and revised models for ILC development. (**A**) In the current model, CLP give rise to αLP, gaining $\alpha4\beta7$ expression and progressively losing Flt3. The EILP, identified by *Tcf7* expression and the lack of IL-7Rα, arises downstream of the αLP generating all known ILC subsets. The CHILP, identified by high ID2 expression, is downstream of the EILP generating ILC and LTi lineage cells. The ILCP, identified by *Zbtb16* expression, and LTiP, identified by *Rorc*, both arise from the CHILP and generate ILC1/2/3 or LTi, respectively. (**B**) In the revised model, CLP give rise to αLP, gaining $\alpha4\beta7$ expression and progressively losing Flt3. Bifurcation into the ILC and LTi lineage occurs within the αLP stage and is marked by low expression of ID2 and the early expression of *Rorc* within the αLP. Expression of ID2 increases to intermediate levels as cells mature, coinciding with the transient down-regulation of IL-7Rα expression. Expression of *Zbtb16* in the iILCP and further up-regulation of *Rorc* in the iLTiP along with differential *Gata3* up-regulation mark the restriction of cellular potential. High expression of ID2 and augmented *Gata3* expression coincides with IL-7Rα re-expression as cells further differentiate toward the ILCP and LTiP.

method for site-specific integration using CRISPR/Cas9-mediated transgenesis that enables the rapid generation of compatible TF reporter mouse lines expressing distinct reporters[184] These novel reporters were combined with preexisting reporters to interrogate ILC developmental stages. Our studies revealed that both the EILP and CHILP were heterogeneous mixtures of ILC and LTi lineage progenitors with restricted lineage potential. Furthermore, we identified a new early LTi-specified precursor upstream of the EILP, before *Tcf7* expression. Chromatin accessibility in FL precursors supports the proposed cellular identity for each new ILC and LTi lineage precursor, and TF motif enrichment across developmental trajectories implicates GATA3 and RORγ(t) as major TFs in establishing ILC and LTi lineage identity, respectively. Together, these findings warrant a revised map of ILC and LTi lineage developmental progression and highlight the value of using a combinatorial TF reporter system for resolving complex developmental processes.

3.1.3 Results

3.1.3.1 Generation of novel TF reporter lines

Enhanced characterization of ILC development necessitates the combined use of reporter lines for the simultaneous resolution of key TFs. However, because many previously generated strains used enhanced GFP (EGFP) to report on TF expression, these lines could not be combined for multi-TF analysis.[5,58,75,78] To overcome this limitation, we employed CRISPR/Cas9-mediated transgenesis for the rapid generation of new designer transgenic lines with distinct reporters (**Fig.3.2A**).[184] TCF1 (*Tcf7*), RORγ(t) (RORγ and RORγt isoforms, *Rorc*), and GATA3 (*Gata3*) were of particular interest for addressing ILC development; therefore, we generated three novel reporter lines: *Tcf7*$^{\text{mCherry}}$, *Rorc*$^{\text{Thy1.1}}$, and *Gata3*$^{\text{Citrine}}$. An internal ribosome entry site (IRES)-reporter sequence was inserted into the 3' UTR of each gene; as such, reporter expression closely reflects mRNA expression (**Fig.3.2A**).[185] To confirm the fidelity of each novel TF reporter, we compared the pat-

tern of reporter expression to previously characterized EGFP reporter lines, intracellular TF staining, and/or known population expression. *Tcf7*-mCherry expression in lineage-

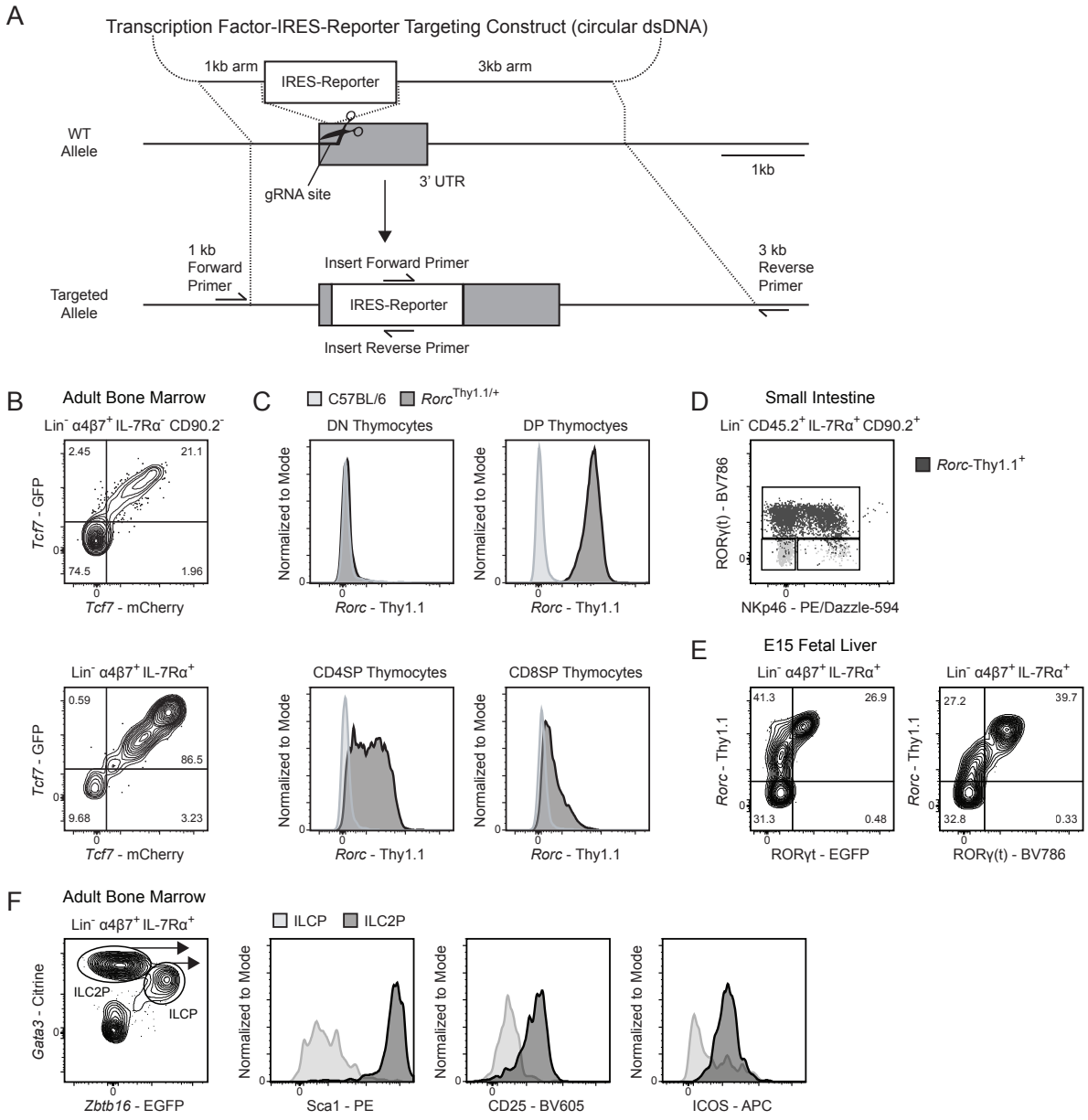

Figure 3.2: Generation of the novel TF reporter mice. (**A**) Design of CRISPR/Cas9 knock-in strategy. (**B-F**) Representative flow plots of ILC progenitors from a *Tcf7*$^{\text{EGFP}}$ x *Tcf7*$^{\text{mCherry}}$ adult BM (B), thymocytes from a *Rorc*$^{\text{Thy1.1}}$ adult thymus (C), mature ILCs from a *Rorc*$^{\text{Thy1.1}}$ SI lamina propria with *Rorc*-Thy1.1^{+} cells overlaid in dark gray and total ILCs in light gray (D), ILC progenitors from a *Rorc*$^{\text{Thy1.1}}$ x RORγt$^{\text{EGFP}}$ E15 FL with RORγ(t) intracellular staining (E), and ILC progenitors from *Gata3*$^{\text{Citrine}}$ adult BM (F). Data are representative of at least two independent experiments (B-F). DN, double negative; DP, double positive; dsDNA, double-strand DNA.

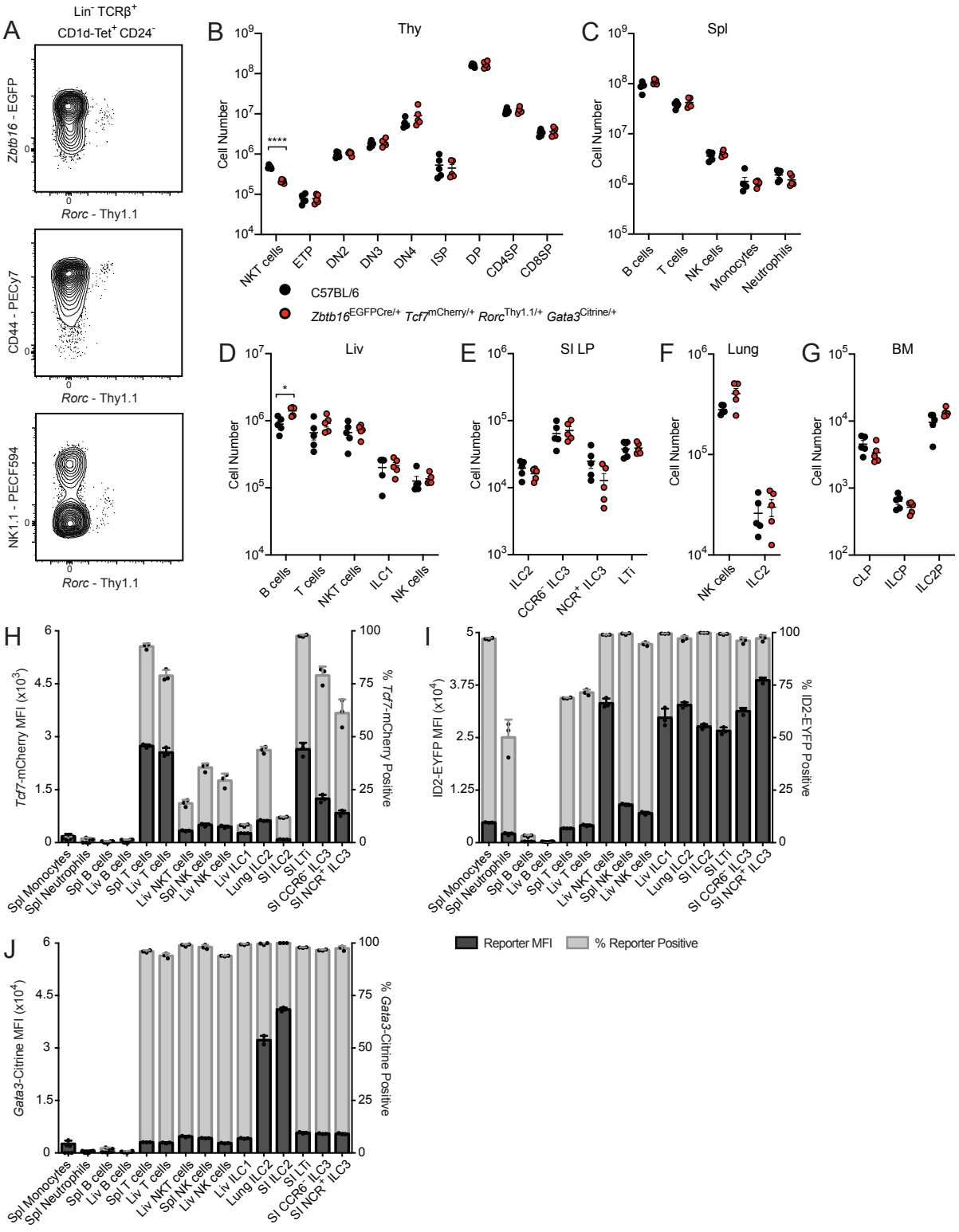

Figure 3.3: Immune phenotyping of *Tcf7*$^{\mathbf{mCherry}}$, *Rorc*$^{\mathbf{Thy1.1}}$, *Gata3*$^{\mathbf{Citrine}}$, and ID2$^{\mathbf{EYFP}}$ reporters.

Figure 3.3, continued. (**A**–**G**) Expression of *Rorc*-Thy1.1 in thymic NKT cells from *Zbtb16*$^{\text{EGFPCre}}$ *Tcf7*$^{\text{mCherry}}$ *Rorc*$^{\text{Thy1.1}}$ adult mice. Cell numbers from adult C57BL/6 and *Zbtb16*$^{\text{EGFPCre/+}}$ *Tcf7*$^{\text{mCherry/+}}$ *Rorc*$^{\text{Thy1.1/+}}$ *Gata3*$^{\text{Citrine/+}}$ mice taken from the thymus (Thy; B), spleen (Spl; C), liver (Liv; D), SI (E), lung (F), and BM (G; n = 5). Each symbol represents an individual mouse; data are presented as mean ± SEM. Q-values were calculated with multiple t tests controlling for false discovery rate. (**H**–**J**) Reporter MFI and frequency of reporter positive cells in the indicated populations from select tissues of *Zbtb16*$^{\text{EGFPCre}}$ *Tcf7*$^{\text{mCherry}}$ (H), *Zbtb16*$^{\text{EGFPCre}}$ *Tcf7*$^{\text{mCherry}}$ID2$^{\text{EYFP}}$ (I), and *Zbtb16*$^{\text{EGFPCre}}$ *Tcf7*$^{\text{mCherry}}$ *Gata3*$^{\text{Citrine}}$ (J) adult mice (n = 3). Each symbol represents an individual mouse. Data are representative of (A) or pooled from (B–J) at least two independent experiments. *, Q < 0.05; ****, Q < 0.0001. ETP, early thymic precursor; DN, double negative; ISP, immature single positive; DP, double positive; SP, single positive.

negative (Lin$^-$) $\alpha4\beta7^+$ populations in the BM was identical to *Tcf7*-EGFP expression in Tcf7$^{\text{EGFP/mCherry}}$ mice (**Fig.3.2B**).[75] To circumvent known issues related to hypomorphic expression of RORγt in knock-in knock-out reporters, we elected to report on both RORγ(t) isoforms using a novel *Rorc*$^{\text{Thy1.1}}$ reporter.[58,68,94] Thymocytes from *Rorc*$^{\text{Thy1.1/+}}$ mice displayed dynamic reporter expression consistent with RORγt$^{\text{EGFP/+}}$ mice (**Fig.3.2C**).[58] Intracellular staining for RORγ(t) in the small intestine (SI) lamina propria demonstrated that *Rorc*-Thy1.1 expression coincides with protein expression in mature group 3 ILCs (**Fig.3.2D**), while FL *Rorc*-Thy1.1 expression precedes protein expression, likely reflecting the difference in mRNA and protein expression kinetics (**Fig.3.2E**).[185] Notably, the *Rorc*-Thy1.1 reporter captures rare thymic NKT17 cells (**Fig.3.3A**). Lastly, Citrine expression in *Gata3*$^{\text{Citrine/+}}$ reporter mice brightly marked BM immature ILC2 (**Fig.3.2F**).[81] To establish parity with wild-type mice, we evaluated major hematopoietic cell populations in C57BL/6 and *Zbtb16*$^{\text{EGFPCre/+}}$ *Tcf7*$^{\text{mCherry/+}}$ *Rorc*$^{\text{Thy1.1/+}}$ *Gata3*$^{\text{Citrine/+}}$ mice. No significant differences were observed in cell number apart from the expected reduction in thymic NKT cells, resulting from a hypomorphic *Zbtb16* allele, and marginally elevated numbers of liver B cells in compound heterozygotes (**Fig.3.3B-G**).[186] Overall, the novel *Tcf7*$^{\text{mCherry}}$, *Rorc*$^{\text{Thy1.1}}$, and *Gata3*$^{\text{Citrine}}$ reporters reflect TF expression patterns without altering lymphocyte development.

To catalog reporter expression across tissues, we isolated mature ILCs and reference populations from the novel *Tcf7*$^{\text{mCherry}}$ and *Gata3*$^{\text{Citrine}}$ reporters and the previously generated ID2$^{\text{EYFP}}$ reporter. The ID2$^{\text{EYFP}}$ reporter is a knock-in knock-out expressing enhanced

YFP (EYFP), akin to the ID2^{EGFP} reporter used to characterize the CHILP, αLP, and ILC2 precursor (ILC2P).[5,81,91,93,95,171] Unsurprisingly, peripheral T cells expressed substantial levels of *Tcf7*-mCherry, though some population-level heterogeneity was observed (**Fig.3.3H**). Conversely, most mature ILCs, apart from SI LTi, expressed low or negligible levels of *Tcf7*-mCherry. ID2-EYFP was uniformly expressed across mature ILC populations (**Fig.3.3I**). However, NK cells displayed markedly lower levels of ID2-EYFP compared with the ILC1/2/3 and LTi. This observation is consistent with the ID2^{EGFP} reporter and the novel ID2^{TagBFP} reporter but contrasts with the recently described *Id2*^{RFP} reporter, where *Id2*-RFP expression is equivalent in all ILCs.[81,93,94] Lastly, *Gata3*-Citrine expression was predictably high in lung and SI ILC2, while T cells and all other ILCs expressed low to intermediate levels (**Fig.3.3J**).[68,81] Expectedly, B cells were devoid of reporter expression in *Tcf7*^{mCherry}, ID2^{EYFP}, and *Gata3*^{Citrine} mice.

3.1.3.2 FL EILPs are transcriptionally heterogeneous

The EILP is the critical stage in which TCF1 expression promotes ILC lineage fate decisions, and was initially overlooked given its unexpected placement at a stage of transient IL-7Rα down-regulation, a marker commonly used to identify mature and developing ILCs.[75–77] To date, the EILP has only been characterized in the BM, and the existence of an equivalent precursor in the FL has not been reported. Although the BM EILP is considered multipotent for all ILC lineages (**Fig.3.1A**), its ability to generate LTi at a clonal level remains unresolved, as LTi arise almost exclusively during the fetal period.[58,59,73,75,78] To this end, we performed intracellular staining for TCF1, PLZF (*Zbtb16*), and RORγ(t) within embryonic day 15 (E15) FL ILC progenitors and divided Lin$^-\alpha4\beta7^+$TCF1$^+$ cells into non-EILP (IL-7Rα^+) and EILP (IL-7Rα^-CD90.2$^-$) populations, conforming to the gating strategy used to identify the BM EILP (**Fig.3.4A**).[75] This result supports the existence of an EILP within the FL. The non-EILP comprises the previously defined ILCP and LTiP (**Fig.3.4A**, lower

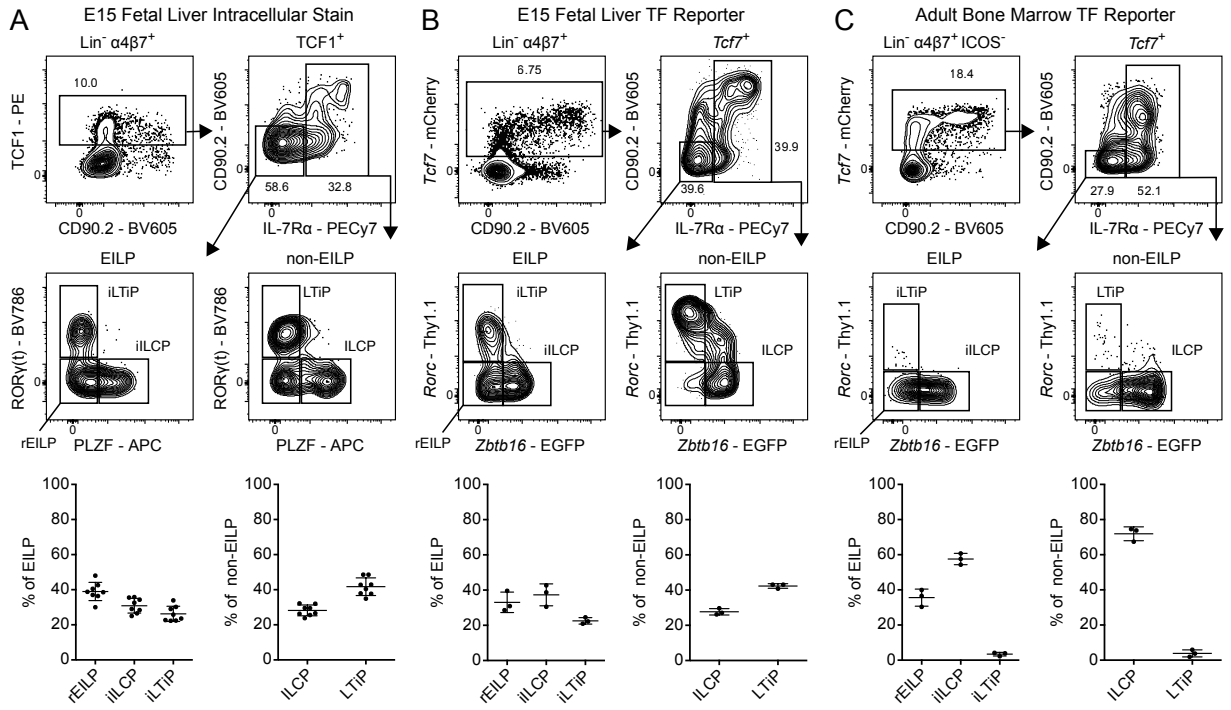

Figure 3.4: Characterization of TF expression in the FL EILP. (**A**) Intracellular staining for TCF1, PLZF, and RORγ(t) TFs in C57BL/6 E15 FL (n = 8). (**B**) Representative flow cytometry plots of ILC progenitors from a *Zbtb16*$^{\text{EGFPCre}}$ *Tcf7*$^{\text{mCherry}}$ *Rorc*$^{\text{Thy1.1}}$ mice E15 FL (n = 3). (**C**) Representative flow cytometry plots of ILC progenitors from a *Zbtb16*$^{\text{EGFPCre}}$ *Tcf7*$^{\text{mCherry}}$ *Rorc*$^{\text{Thy1.1}}$ mice adult BM (n = 3). Associated plots reflect population frequencies; each symbol represents an individual FL or BM; data are presented as mean ± SEM. Data are representative of or pooled from at least two independent experiments.

right panel). A fraction of PLZF^{-}RORγ(t)$^{-}$ non-EILP expresses low levels of IL-7Rα and is negative for CD90.2, which may reflect TCF1 expression before IL-7Rα down-regulation. Surprisingly, we observed substantial heterogeneity among the EILP. The EILP displayed a remarkably similar pattern of PLZF and RORγ(t) expression compared with non-EILP cells, mirroring the ILCP and LTiP, respectively (**Fig.3.4A**, lower left panel). A subset of BM EILP expresses PLZF; however, RORγ(t) expression has not been reported in this population, ostensibly due to the paucity of RORγ(t)$^{+}$ BM cells.[5,75,78,94] Given the striking similarities of the PLZF^{+} EILP and RORγ(t)$^{+}$ EILP with the ILCP and LTiP, respectively, hereafter we refer to the PLZF^{+} EILP as the incipient ILCP (iILCP), the RORγ(t)$^{+}$ EILP as the incipient LTiP (iLTiP), and the remaining PLZF^{-}RORγ(t)$^{-}$ EILP as the refined EILP (rEILP).

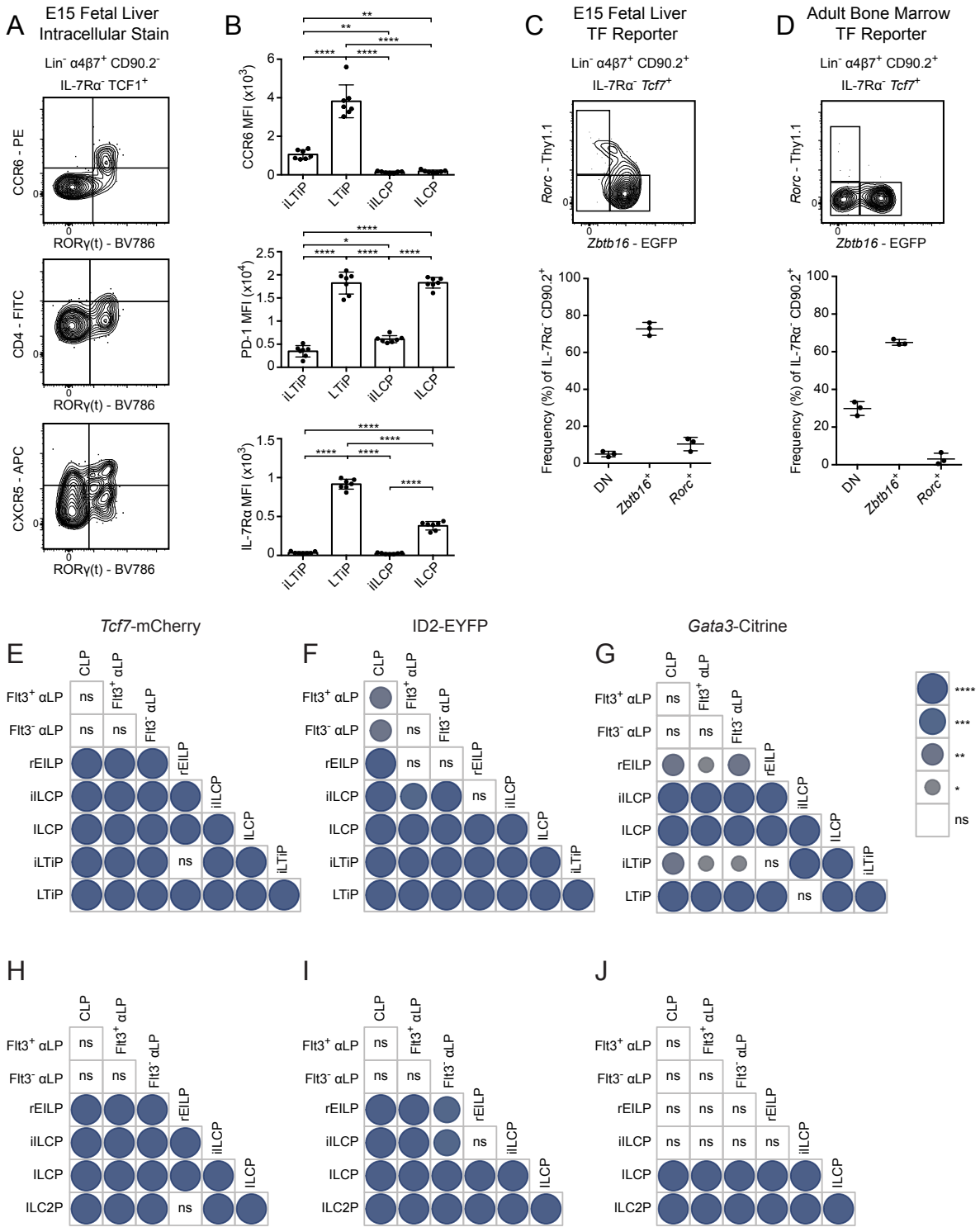

Figure 3.5: Analysis of ILC and LTi maturation markers on iILCP and iLTiP.

Figure 3.5, continued. (A) Representative flow cytometry plots of the EILP from a C57BL/6 E15 FL stained for the indicated surface markers and intracellular RORγ(t) (n = 4). (B) MFI of CCR6, PD-1, and IL-7Rα on the iLTiP, LTiP, iILCP, and ILCP from a *Zbtb16*$^{\text{EGFPCre}}$ *Tcf7*$^{\text{mCherry}}$ *Rorc*$^{\text{Thy1.1}}$ E15 FL (n = 7). Each symbol represents an individual FL; data are presented as mean ± SEM. (C) Representative flow cytometry plots of ILC progenitors from a *Zbtb16*$^{\text{EGFPCre}}$ *Tcf7*$^{\text{mCherry}}$ *Rorc*$^{\text{Thy1.1}}$ E15 FL (n = 3). (D) Representative flow cytometry plots of ILC progenitors from a *Zbtb16*$^{\text{EGFPCre}}$ *Tcf7*$^{\text{mCherry}}$ *Rorc*$^{\text{Thy1.1}}$ adult BM (n = 3). Associated plots reflect population frequencies; each symbol represents an individual FL or BM; data are presented as mean ± SEM. (E–J) Pairwise comparisons of *Tcf7*-mCherry, ID2-EYFP, and *Gata3*-Citrine reporter expression MFI from Fig. 3 plots for FL (E–G) and BM (H–J) precursors. Circle size and color denote level of significance. Data are representative of (A) or pooled from (B–J) at least two independent experiments. Pairwise comparison P values were calculated by one-way ANOVA with Tukey's multiple comparisons test *, $P < 0.05$; **, $P < 0.01$; ***, $P < 0.001$; ****, $P < 0.0001$; ns, not significant.

Phenotypic analysis supported the notion that the iLTiP was more immature than the LTiP. A small fraction of iLTiP express CCR6 and CXCR5 but were devoid of CD4 expression, all of which are markers up-regulated during LTi maturation (**Fig.3.5A**).[58,59,73,92] Furthermore, CCR6, PD-1, a marker correlated with ILCP maturation, and IL-7Rα were expressed at lower levels on the iLTiP compared with the LTiP (**Fig.3.5B**).[79,80,91] These results suggested that the iLTiP could represent an early precursor upstream of the LTiP.

3.1.3.3 Triple transgenic reporter mice reflect EILP heterogeneity

While TF staining facilitates the simultaneous detection of PLZF, RORγ(t), and TCF1, this method precludes live cell sorting for functional analysis. By breeding the novel *Tcf7*$^{\text{mCherry}}$ and *Rorc*$^{\text{Thy1.1}}$ mice with existing *Zbtb16*$^{\text{EGFPCre}}$ mice to generate *Zbtb16*$^{\text{EGFPCre}}$ *Tcf7*$^{\text{mCherry}}$ *Rorc*$^{\text{Thy1.1}}$ mice, we successfully recapitulated FL EILP heterogeneity observed via intracellular staining (**Fig.3.4B**). We principally observed *Zbtb16*$^{+}$ and *Zbtb16*$^{-}$*Rorc*$^{-}$ cells among adult BM EILP and non-EILP, consistent with the diminished capacity of BM precursors to generate ILC3 and LTi (**Fig.3.4C**).[5,73,78] Nevertheless, we discerned a rare *Rorc*-Thy1.1$^{\text{Hi}}$ fraction among the non-EILP (**Fig.3.4C**, lower right plot). Compared with TCF1 in the FL, *Tcf7*-mCherry expression increased with CD90.2 expression in both FL and BM reporter mice, a facet shared with the *Tcf7*-EGFP reporter (**Fig.3.4A-C**, upper left panels).[75–77] This observation may result from a difference in the half-life of the reporter versus protein.[185] While not noted in previous reports, we consistently

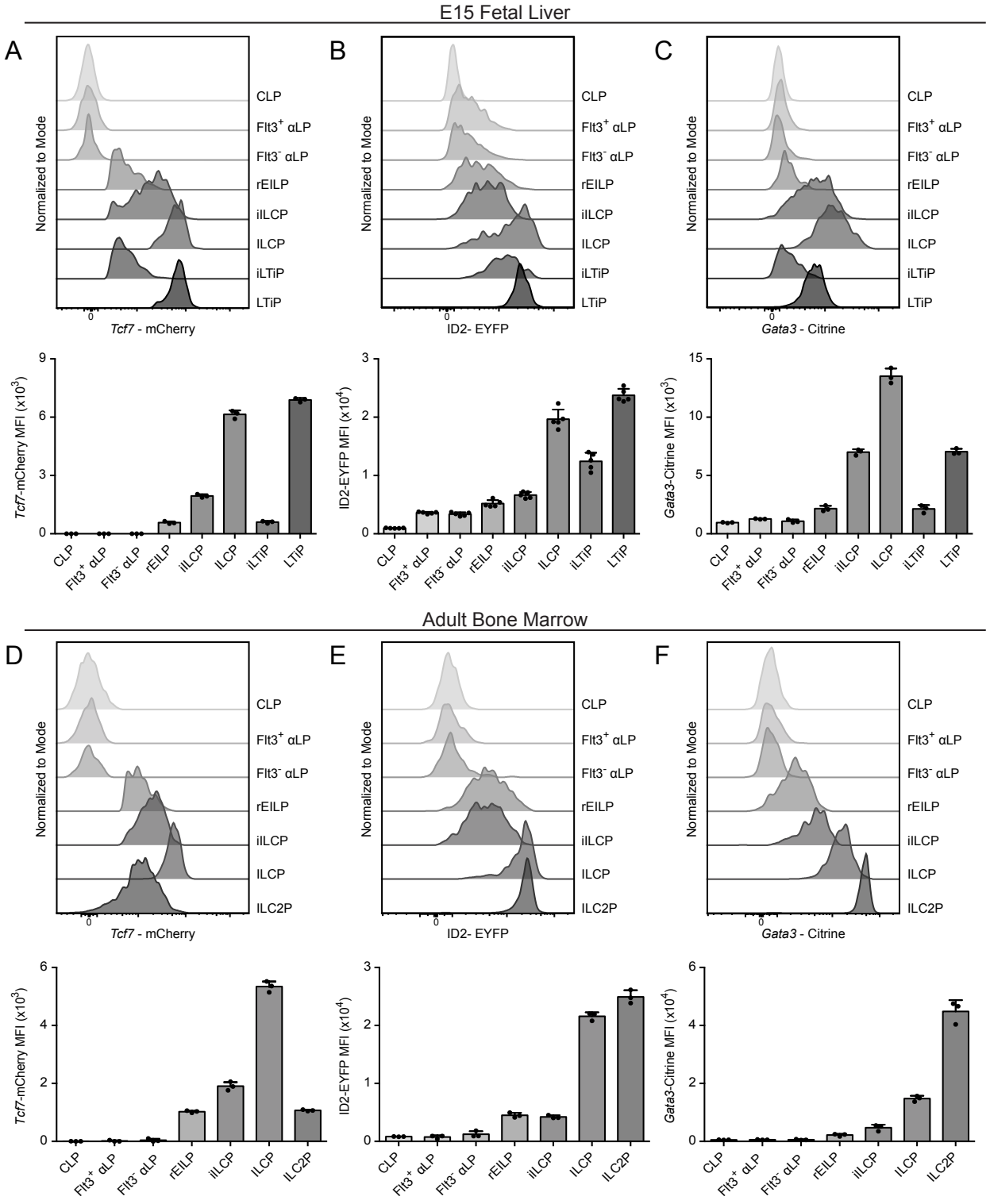

Figure 3.6: TF reporter expression in FL and adult BM ILC progenitors.

Figure 3.6, continued. (**A**–**F**) Representative histogram plots of *Tcf7*-mCherry, ID2-EYFP, and *Gata3*-Citrine reporter expression in the indicated ILC progenitors from (**A**) *Zbtb16*$^{\text{EGFPCre}}$ *Tcf7*$^{\text{mCherry}}$ *Rorc*$^{\text{Thy1.1}}$ E15 FLs (n = 3), (**B**) *Zbtb16*$^{\text{EGFPCre}}$ *Tcf7*$^{\text{mCherry}}$ *Rorc*$^{\text{Thy1.1}}$ID2$^{\text{EYFP}}$ E15 FLs (n = 6), (**C**) *Zbtb16*$^{\text{EGFPCre}}$ *Tcf7*$^{\text{mCherry}}$ *Rorc*$^{\text{Thy1.1}}$ *Gata3*$^{\text{Citrine}}$ E15 FLs (n = 3), (**D**) *Zbtb16*$^{\text{EGFPCre}}$ *Tcf7*$^{\text{mCherry}}$ adult BM, (**E**) *Zbtb16*$^{\text{EGFPCre}}$ *Tcf7*$^{\text{mCherry}}$ *Rorc*$^{\text{Thy1.1}}$ID2$^{\text{EYFP}}$ adult BM (n = 3), and (**F**) *Zbtb16*$^{\text{EGFPCre}}$ *Tcf7*$^{\text{mCherry}}$ *Rorc*$^{\text{Thy1.1}}$ *Gata3*$^{\text{Citrine}}$ adult BM (n = 3). Associated plots reflect population median fluorescent intensity (MFI); each symbol represents an individual FL or BM; data are presented as mean ± SEM; pairwise comparison P values are presented in **Fig.3.5 E–J**, and were calculated by one-way ANOVA with Tukey's multiple comparisons test. Data are representative of or pooled from at least two independent experiments.

observed a population of TCF1^{+}/*Tcf7*$^{+}$IL-7Rα^{-}CD90.2^{+} cells in both the FL and BM (**Fig.3.4A-C**, upper right panels).[75–77] These cells were predominantly *Zbtb16*-EGFP^{+}, though *Rorc*-Thy1.1^{+} and double-negative populations were discernable in the FL and BM, respectively (**Fig.3.5C and D**). Taken together, through the combinatorial use of novel TF reporters, we can reconstruct EILP heterogeneity observed via TF staining.

Given the combinatorial nature of the novel and existing TF reporters, we incorporated *Gata3*$^{\text{Citrine}}$ or ID2$^{\text{EYFP}}$ reporters with *Zbtb16*$^{\text{EGFPCre}}$ *Tcf7*$^{\text{mCherry}}$ *Rorc*$^{\text{Thy1.1}}$ mice to gauge the hierarchical placement of the rEILP, iILCP, and iLTiP through TF expression patterns. E15 FL rEILP, iILCP, and iLTiP expressed intermediate levels of *Tcf7*-mCherry and ID2-EYFP relative to the earliest precursors (CLP, Flt3^{+} αLP, and Flt3^{-} αLP) and the later ILCP and LTiP (**Fig.3.6A and B**; and **Fig.3.5E and F**). A fraction of FL αLP expressed low/intermediate levels of ID2-EYFP compared with the ILCP and LTiP, in accordance with a previous report.[99] *Gata3*-Citrine expression was higher in both the iILCP and ILCP compared with the iLTiP and LTiP, respectively, suggesting that early up-regulation of *Gata3* coincides with *Zbtb16* expression (**Fig.3.6C** and **Fig.3.5G**). *Tcf7*, ID2, and *Gata3* expression increases from early to late ILC progenitors, though expression levels vary in mature ILCs (**Fig.3.3H-J**).[70,76,78,79,91,92] In support of a linear maturation program, expression of *Tcf7*-mCherry, ID2-EYFP, and *Gata3*-Citrine all progressively increased from the rEILP to iILCP to ILCP. Likewise, these reporters increased from the iLTiP to the LTiP. The adult BM displayed comparable *Tcf7*-mCherry and *Gata3*-Citrine expression patterns, though low ID2 expressers were absent from the αLP (**Fig.3.6D-F**; and **Fig.3.5H-J**). As expected, *Tcf7*-mCherry expression decreased while *Gata3*-Citrine expression increased as

cells matured into ILC2P.[78,93] In summary, the transcriptional states of the rEILP, iILCP, and iLTiP indicate that these precursors may arise before the ILCP and LTiP in developmental time (**Fig.3.1B**).

3.1.3.4 The iILCP and iLTiP are restricted precursors to the ILCP and LTiP

To formally determine the cellular potential of the FL rEILP, iILCP, and iLTiP in comparison with the earlier αLP and the later ILCP and LTiP, we performed clonal analysis using *Zbtb16*$^{\mathrm{EGFPCre}}$ *Tcf7*$^{\mathrm{mCherry}}$ *Rorc*$^{\mathrm{Thy1.1}}$ mice. Precursors were cultured on OP9 stromal cells and assessed for the ability to differentiate into ILC1/2/3 and/or LTi (**Fig.3.7** and **Table3.1-3.7**). CCR6 identifies LTi *in vivo*; however, CCR6 proved unreliable *in vitro* (unpublished observations). Therefore, we used CD4 as a marker of LTi potential. While CD4 expression is characteristic of a majority of LTi (LTi_4), ~40% of LTi lack CD4 (LTi_0) and are indistinguishable from CD4$^-$ ILC3 *in vitro* and *in vivo*; this uncertainty is acknowledged as ILC3/LTi_0.[59,92] Single clones were index sorted from the EILP to facilitate the unbiased assessment of cell potential. In short, EILP were sorted based on the minimal set of identifying markers used in **Fig.3.4B** (bottom left panel). Following *in vitro* differentiation, wells were computationally assigned to a subset (rEILP, iILCP, or iLTiP) based on *Zbtb16*-EGFP and *Rorc*-Thy1.1 expression at the time of sorting. As expected, the ILCP and LTiP gave rise almost exclusively to ILC1/2 and ILC3/LTi_0 or to LTi_4 and ILC3/LTi_0, respectively. The iLTiP were already largely LTi lineage restricted, displaying a striking bias toward LTi_4 and ILC3/LTi_0 akin to the LTiP ($P = 1$). The iILCP exhibited a similar differentiation potential as the ILCP ($P = 0.22$), generating primarily ILC1/2 and ILC3/LTi_0, with a reduced frequency of ILC2, presumably due to the premature interruption of Notch signals required for efficient ILC2 differentiation.[92] The iLTiP generated a fraction of ILC1, and the iILCP generated a fraction of LTi_4 (~11% each, **Table3.4** and **3.6**), distinguishing them from their

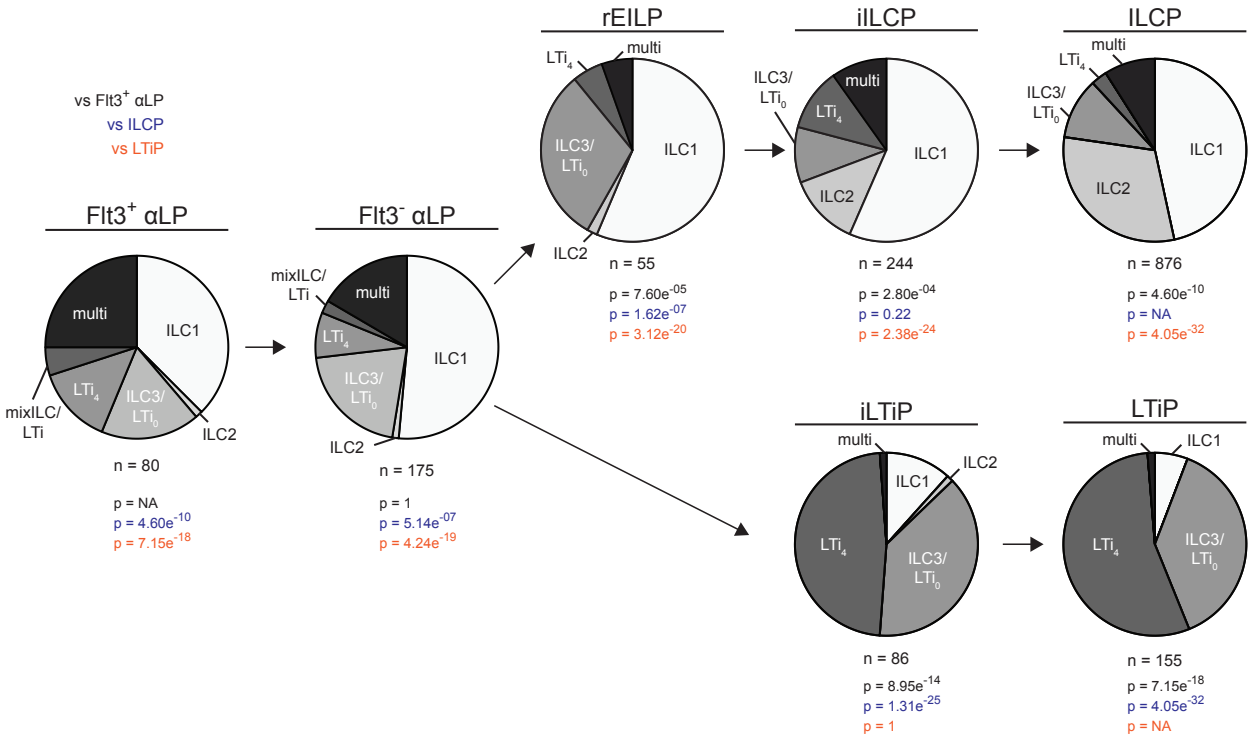

Figure 3.7: Clonal potential of FL ILC progenitors. Single-cell potential of the indicated ILC progenitors sorted from *Zbtb16*$^{\text{EGFPCre}}$ *Tcf7*$^{\text{mCherry}}$ *Rorc*$^{\text{Thy1.1}}$ E14-E16 FLs onto OP9 stromal cells. Pie charts represent the frequency of single ILC1 (NK1.1^{+}ICOS$^{-}\alpha4\beta7^{-}$), ILC2 (NK1.1^{-}ICOS$^{+}\alpha4\beta7^{-}$), and ILC3/LTi$_0$ (NK1.1^{-}ICOS$^{+/-}\alpha4\beta7^{+}$CD4^{-}); two or more ILC subsets (multi); LTi$_4$ (NK1.1^{-}ICOS$^{+/-}\alpha4\beta7^{+}$CD4^{+}); and mixed ILC1/2/3/LTi$_0$ and LTi$_4$ (mixILC/LTi). Data are pooled from >20 independent experiments. P values for pie charts were calculated using Chi-Square Test for Independence followed by post-hoc analysis with Bonferroni correction; comparisons were made against the Flt3^{+} αLP (black), ILCP (blue), and LTiP (orange).

downstream counterparts, indicating incomplete lineage commitment under our culture conditions. Taken as is, evidence from cell phenotype, transcriptional state, and differentiation potential are consistent with a model wherein the iILCP and iLTiP arise upstream of the ILCP and LTiP and have diminished alternate lineage potential downstream of the common ILC-LTi precursor (**Fig.3.1B**).

BM rEILP generate *Zbtb16*-EGFP^{+} cells in short-term culture.[77] As the FL rEILP appeared to represent a common ILC-LTi precursor downstream of the αLP, we evaluated its clonal potential with respect to the αLP. Previous work from our laboratory suggested that the αLP represents the stage of bifurcation into the ILC and LTi lineages.[92] The rEILP generated ILC1/2 and ILC3/LTi$_0$ progeny similar to the iILCP, with a more pronounced

decrease in ILC2 (**Fig.3.7**). Few LTi_4 arose from the rEILP, and no mixed ILC and LTi lineage wells were observed, which stands in contrast to the $Flt3^+$ αLP and $Flt3^-$ αLP.[92] Thus, the rEILP likely represents a precursor upstream of the iILCP, before expression of the ILC lineage marker *Zbtb16*.[77] Taken together, these findings indicate that the ILC-LTi precursor resides upstream of the EILP (**Fig.3.1B**).

3.1.3.5 The CHILP is a heterogeneous mixture of ILC and LTi progenitors

The CHILP, characterized in the BM by high ID2 expression upstream of the ILCP, was proposed to be the common ILC-LTi precursor (**Fig.3.1A**).[5,69,92] However, whether the CHILP is a shared ILC-LTi precursor or a heterogeneous mixture of ILCP and LTiP has not been tested. As such, we performed index-based clonal analysis on the CHILP population isolated from the BM of *Zbtb16*$^{\text{EGFPCre}}$ID2$^{\text{EYFP}}$ mice. Cells were seeded onto OP9 or OP9-DL1 stroma, as Notch ligand is required for efficient generation of group 3 ILCs from BM precursors.[73] The BM CHILP comprised a mixture of *Zbtb16*$^+$ ILCP, ICOS$^+$*Zbtb16*$^-$ ILC2P, and *Zbtb16*$^-$ID2$^+$ cells (**Fig.3.8A**). The latter subset primarily generated single wells of ILC1, ILC2, or ILC3/LTi_0, with a fraction of multi ILC1/2 and ILC3/LTi_0 wells arising in cultures with Notch ligand. (**Fig.3.8B and C**; and **Table3.8-3.13**). Given the limited ability of BM ILC progenitors to generate group 3 ILCs *in vitro*, we extended our analysis by index sorting the CHILP from the FL of *Zbtb16*$^{\text{EGFPCre}}$ID2$^{\text{EYFP}}$ mice. The FL CHILP comprised *Zbtb16*$^+$ ILCP and *Zbtb16*$^-$ID2$^+$ cells, similar to the BM, in addition to CCR6-expressing LTiP (**Fig.3.8D**). FL CHILP subsets did not generate mixed wells of ILC and LTi on either OP9 or OP9-DL1 stroma (**Fig.3.8E and F**; and **Table3.14-3.19**). Thus, in both the BM and FL the CHILP, like the EILP, represents a mixture of ILC and LTi lineage progenitors downstream of a shared ILC-LTi precursor (**Fig.3.1A and B**).

3.1.3.6 An early *Rorc*-expressing αLP marks the bifurcation between ILC and LTi lineages

As both the EILP and the CHILP contain separate precursors to the ILC and LTi lineages, we examined the upstream αLP for the presence of an earlier precursor in *Zbtb16*$^{\text{EGFPCre}}$

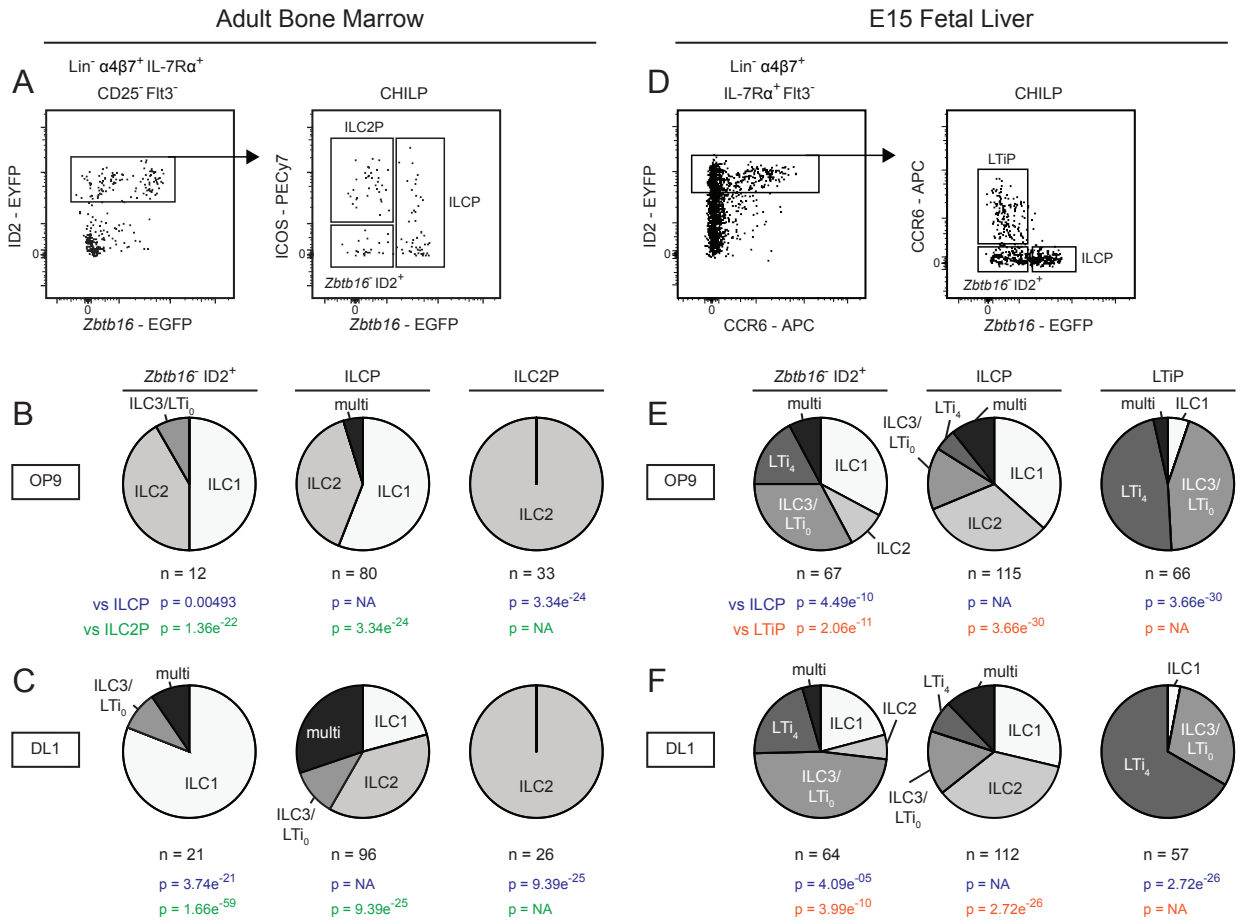

Figure 3.8: Clonal analysis of the CHILP from adult BM and FL. (**A-C**) Index gating strategy for the CHILP from *Zbtb16*$^{\text{EGFPCre}}$ID2$^{\text{EYFP}}$ adult BM. Pie charts represent the frequency of single ILC1, ILC2, ILC3/LTi$_0$; two or more ILC subsets (multi); LTi$_4$; and mixed ILC1/2/3/LTi$_0$ and LTi$_4$ (mix-ILC/LTi) on OP9 (B) and OP9-DL1 (C) stromal cells. (**D**) Index gating strategy for the CHILP from *Zbtb16*$^{\text{EGFPCre}}$ID2$^{\text{EYFP}}$ E14-E16 FL. (**E and F**) Pie charts represent the frequency of single ILC1, ILC2, ILC3/LTi$_0$; two or more ILC subsets (multi); LTi$_4$; and mixed ILC1/2/3/LTi$_0$ and LTi$_4$ (mixILC/LTi) on (E) OP9 and (F) OP9-DL1 stromal cells. Early T cells were identified in OP9-DL1 cultures by high expression of CD25$^+$; T cell-only wells were excluded from pie charts, while ILC+T cell wells were included with the appropriate ILC classification. Data are representative of (A and D) or pooled from (B, C, E, and F) four independent experiments. P values for pie charts were calculated using Chi-Square Test for Independence followed by post-hoc analysis with Bonferroni correction; comparisons were made against the ILCP (blue), ILC2P (green), and LTiP (orange).

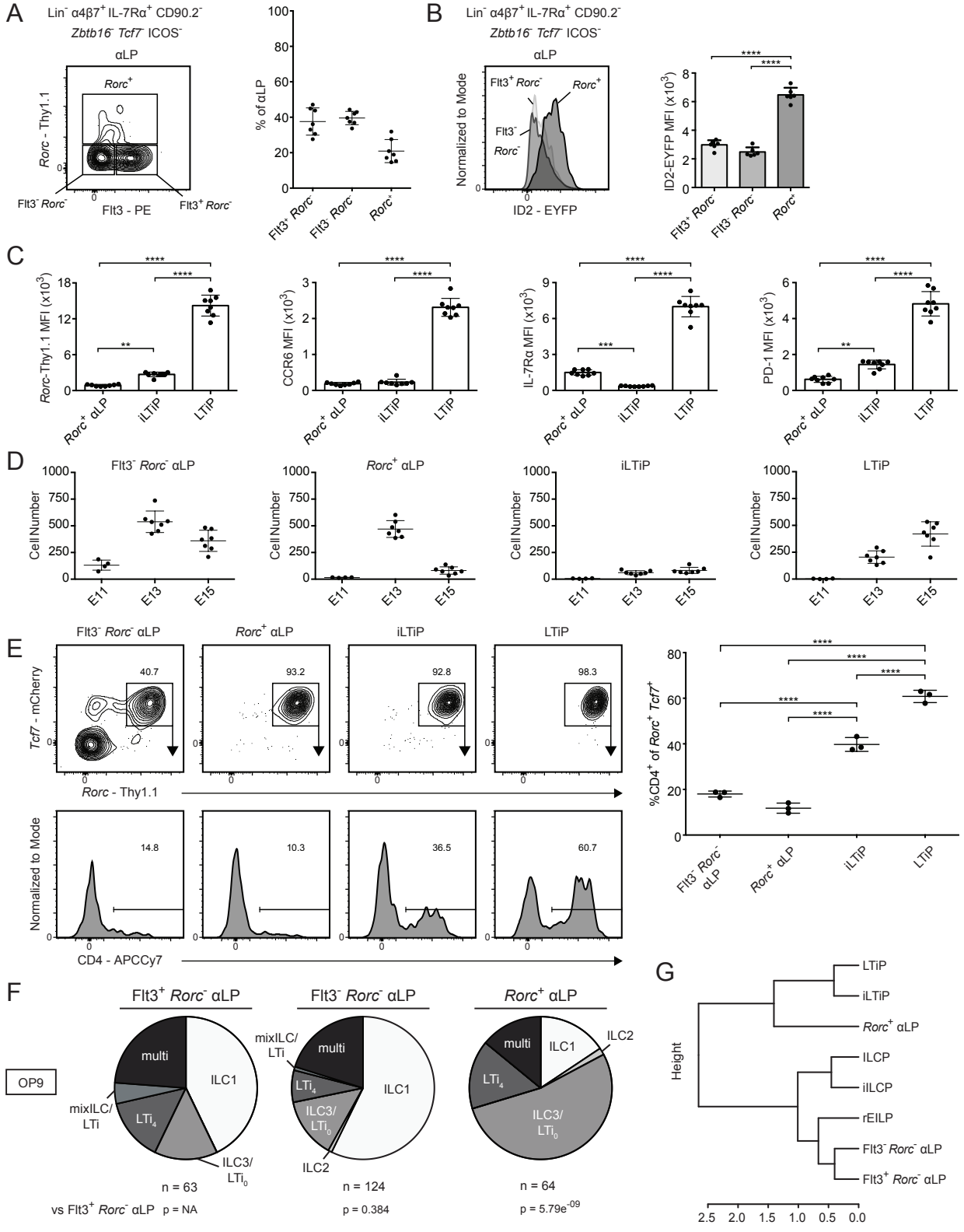

Figure 3.9: Identification of *Rorc* expression in the FL αLP.

Figure 3.9, continued. (**A**) Representative flow cytometry plot of αLP from *Zbtb16*$^{\text{EGFPCre}}$ *Tcf7*$^{\text{mCherry}}$ *Rorc*$^{\text{Thy1.1}}$ E15 FL (n = 7). Adjacent plot reflects population frequencies. (**B**) Representative histogram plot of ID2-EYFP expression in the indicated ILC progenitors from *Zbtb16*$^{\text{EGFPCre}}$ *Tcf7*$^{\text{mCherry}}$ *Rorc*$^{\text{Thy1.1}}$ ID2$^{\text{EYFP}}$ E15 FL (n = 6). Associated plots reflect population MFI. (**C**) MFI of *Rorc*-Thy1.1, CCR6, IL-7Rα, and PD-1 on *Rorc*$^{+}$ αLP, iLTiP, and LTiP from *Zbtb16*$^{\text{EGFPCre}}$ *Tcf7*$^{\text{mCherry}}$ *Rorc*$^{\text{Thy1.1}}$ E15 FL (n = 8). (**D**) Quantification of Flt3^{-}*Rorc*$^{-}$ αLP, *Rorc*$^{+}$ αLP, iLTiP, and LTiP from *Zbtb16*$^{\text{EGFPCre}}$ *Tcf7*$^{\text{mCherry}}$ *Rorc*$^{\text{Thy1.1}}$ FL at E11, E13, and E15. (**E**) Representative flow plots and histograms of bulk cultured Flt3^{-}*Rorc*$^{-}$ αLP, *Rorc*$^{+}$ αLP, iLTiP, and LTiP from *Zbtb16*$^{\text{EGFPCre}}$ *Tcf7*$^{\text{mCherry}}$ *Rorc*$^{\text{Thy1.1}}$ E15 FL cultured for 2 d on OP9 stromal cells (n = 3). Adjacent plot reflects CD4^{+} frequency among *Rorc*$^{+}$ *Tcf7*$^{+}$ cells. (**F**) Single-cell potential of the indicated αLP precursors sorted from *Zbtb16*$^{\text{EGFPCre}}$ *Tcf7*$^{\text{mCherry}}$ *Rorc*$^{\text{Thy1.1}}$ E15 FL onto OP9 stromal cells. (**G**) Hierarchical clustering dendrogram of ILC progenitor clonal potential on OP9 stromal cells calculated from Pearson correlation. For plots, each symbol represents an individual FL; data are presented as mean ± SEM; and P values were determined by one-way ANOVA with Tukey's multiple comparisons test. P values for pie charts were calculated using Chi-Square Test for Independence followed by post-hoc analysis with Bonferroni correction; comparisons were made against the Flt3^{+}*Rorc*$^{-}$ αLP (black). Data are pooled from at least two independent experiments. **, P < 0.01; ***, P < 0.001; ****, P < 0.0001.

Tcf7$^{\text{mCherry}}$ *Rorc*$^{\text{Thy1.1}}$ mice. A subset of αLP expressed *Rorc*-Thy1.1 (*Rorc*$^{+}$ αLP), despite lacking *Tcf7*-mCherry expression (**Fig.3.9A**). This population was absent from the adult BM (**Fig.3.10A**). The *Rorc*$^{+}$ αLP represented the majority of ID2-EYFP$^{\text{Lo/Int}}$ cells among the FL αLP (**Fig.3.9B** and **Fig.3.6B**). Compared with the iLTiP and LTiP, the *Rorc*$^{+}$ αLP expressed less *Rorc*-Thy1.1 and PD-1, while being low for CCR6 and intermediate for IL-7Rα (**Fig.3.9C**). We then examined the ontogeny and immediate potential of the *Rorc*$^{+}$ αLP. The iLTiP was detectable as early as E13 alongside the LTiP, and both increased until E15 (**Fig.3.9D**). The *Rorc*$^{+}$ αLP was maximally present at E13, in greater numbers than either the iLTiP or LTiP, but decreased by E15, while the Flt3^{-}*Rorc*$^{-}$ αLP was detectable as early as E11. The phenotype and rapid expansion and contraction indicated that the *Rorc*$^{+}$ αLP might precede the iLTiP and LTiP in a developmental wave during ontogeny. In a short-term *in vitro* culture assay, the *Rorc*$^{+}$ αLP, iLTiP, and LTiP rapidly and almost exclusively generated *Tcf7*$^{+}$ *Rorc*$^{+}$ cells; however, only the iLTiP and LTiP generated a substantial frequency of LTi$_4$ cells by 2 d (**Fig.3.9E**). Notably, while both the Flt3^{-}*Rorc*$^{-}$ αLP and *Rorc*$^{+}$ αLP promptly up-regulated *Tcf7*-mCherry expression, only a fraction of Flt3^{-}*Rorc*$^{-}$ αLP expressed *Rorc*-Thy1.1. These results suggested that the *Rorc*$^{+}$ αLP could represent a very early precursor biased toward the LTi lineage.

We further addressed the clonal potential of the *Rorc*$^{+}$ αLP through index-based sort-

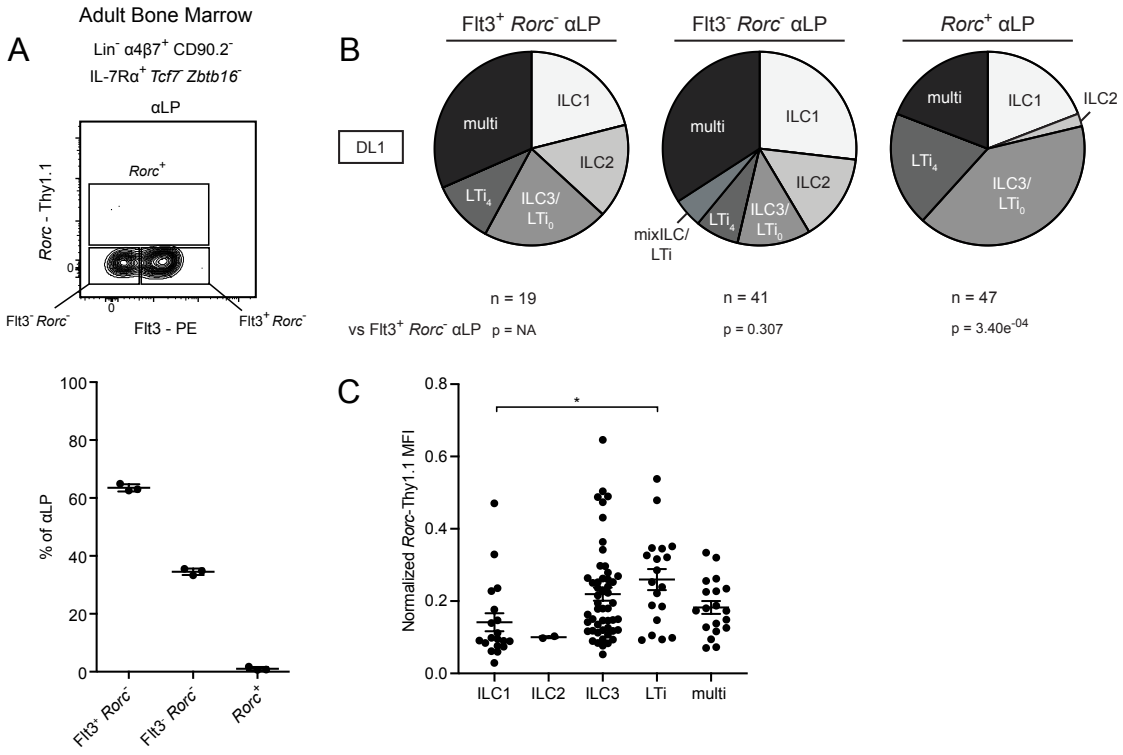

Figure 3.10: Analysis of *Rorc*$^+$ αLP. (**A**) Representative flow cytometry plot of αLP from *Zbtb16*$^{\text{EGFPCre}}$ *Tcf7*$^{\text{mCherry}}$ *Rorc*$^{\text{Thy1.1}}$ adult BM (n = 3). Associated plot reflects population frequencies; each symbol represents an individual BM; data are presented as mean ± SEM. (**B**) Single-cell potential of the indicated αLP precursors sorted from *Zbtb16*$^{\text{EGFPCre}}$ *Tcf7*$^{\text{mCherry}}$ *Rorc*$^{\text{Thy1.1}}$ E15 FL onto OP9-DL1 stromal cells. Early T cells were identified in OP9-DL1 cultures by high expression of CD25$^+$; T cell-only wells were excluded from charts, while ILC+T cell wells were included with the appropriate ILC. (**C**) Normalized *Rorc*-Thy1.1 MFI of index-sorted single *Rorc*$^+$ αLP categorized by *in vitro* potential on OP9 and OP9-DL1. Data were normalized by experiment to average LTiP *Rorc*-Thy1.1 MFI; data are presented as mean ± SEM; and P values were determined by one-way ANOVA with Tukey's multiple comparisons test. Data are pooled from two (A and B) or four (C) independent experiments. P values for pie charts were calculated using Chi-Square Test for Independence followed by post-hoc analysis with Bonferroni correction; comparisons were made against the Flt3$^+$*Rorc*$^-$ αLP (black). *, P < 0.05.

ing of the αLP onto OP9 and OP9-DL1 stromal cells, subdividing into Flt3$^+$*Rorc*$^-$ αLP, Flt3$^-$*Rorc*$^-$ αLP, and *Rorc*$^+$ αLP. Regardless of the culture condition, the *Rorc*$^+$ αLP predominantly generated ILC3/LTi$_0$ and LTi$_4$, though the large fraction of ILC3/LTi$_0$ may indicate that additional signals are required for efficient CD4 expression (**Fig.3.9F**, **Fig.3.10B**, and **Table3.20-3.25**). Nevertheless, the *Rorc*$^+$ αLP retained multipotentiality similar to the Flt3$^+$*Rorc*$^-$ and Flt3$^-$*Rorc*$^-$ αLP. Multipotentiality was independent of initial *Rorc*-Thy1.1 expression level in index-sorted *Rorc*$^+$ αLP (**Fig.3.10C**). Hierarchical clustering by clonal

potential on OP9 stroma revealed that the *Rorc*$^{+}$ αLP was more similar to the iLTiP and LTiP than it was to the Flt3^{+}*Rorc*$^{-}$ and Flt3^{-}*Rorc*$^{-}$ αLP (**Fig.3.9G**). Based on these results, the *Rorc*$^{+}$ αLP appears to be an early LTi-specified precursor before LTi lineage restriction.

3.1.3.7 ATAC-seq reinforces ILC and LTi lineage progression and reveals differential use of TF modules

To gain further insight into the lineage relationship between the newly identified FL ILC and LTi lineage intermediates, we profiled their chromatin accessibility landscape using ATAC-seq. Unsupervised hierarchical clustering separated the progenitors into roughly three groups. Common precursors (CLP, Flt3^{+} *Rorc*$^{-}$ αLP, and Flt3^{-}*Rorc*$^{-}$ αLP) clustered together away from ILC and LTi lineage progenitors (**Fig.3.11A**). Consistent with its transitional placement, the *Rorc*$^{+}$ αLP clustered with the iLTiP while exhibiting high correlation with the common αLPs. Notably, ILC and LTi lineage progenitors did not cleanly separate into two groups. Though the iILCP and ILCP formed a distinct cluster separate from the *Rorc*$^{+}$ αLP and iLTiP, the LTiP clustered with the ILCP, despite strong correlation with LTi lineage progenitors. Clustering of the LTiP with the ILCP may result from an oversized influence of principal component 1 on the correlation analysis that reflects lineage maturation and/or the appearance of common type 3 signatures in a heterogeneous ILCP (**Fig.3.11B**).[92] Additionally, the rEILP clustered with the common precursors away from the iILCP and ILCP, mirroring the hierarchical clustering based on differentiation potential (**Fig.3.9G**).

We then examined chromatin accessibility data tracks near genes associated with ILC and LTi lineage differentiation. Though the *Rorc*$^{+}$ αLP is only specified toward the LTi lineage, accessibility at the *Rorc* locus was comparable to that observed in the iLTiP and LTiP (**Fig.3.11C**). ILC lineage progenitors, in contrast, only showed increased accessibility at the *Rorc* locus within the ILCP, the stage in which multi-transcriptional priming and

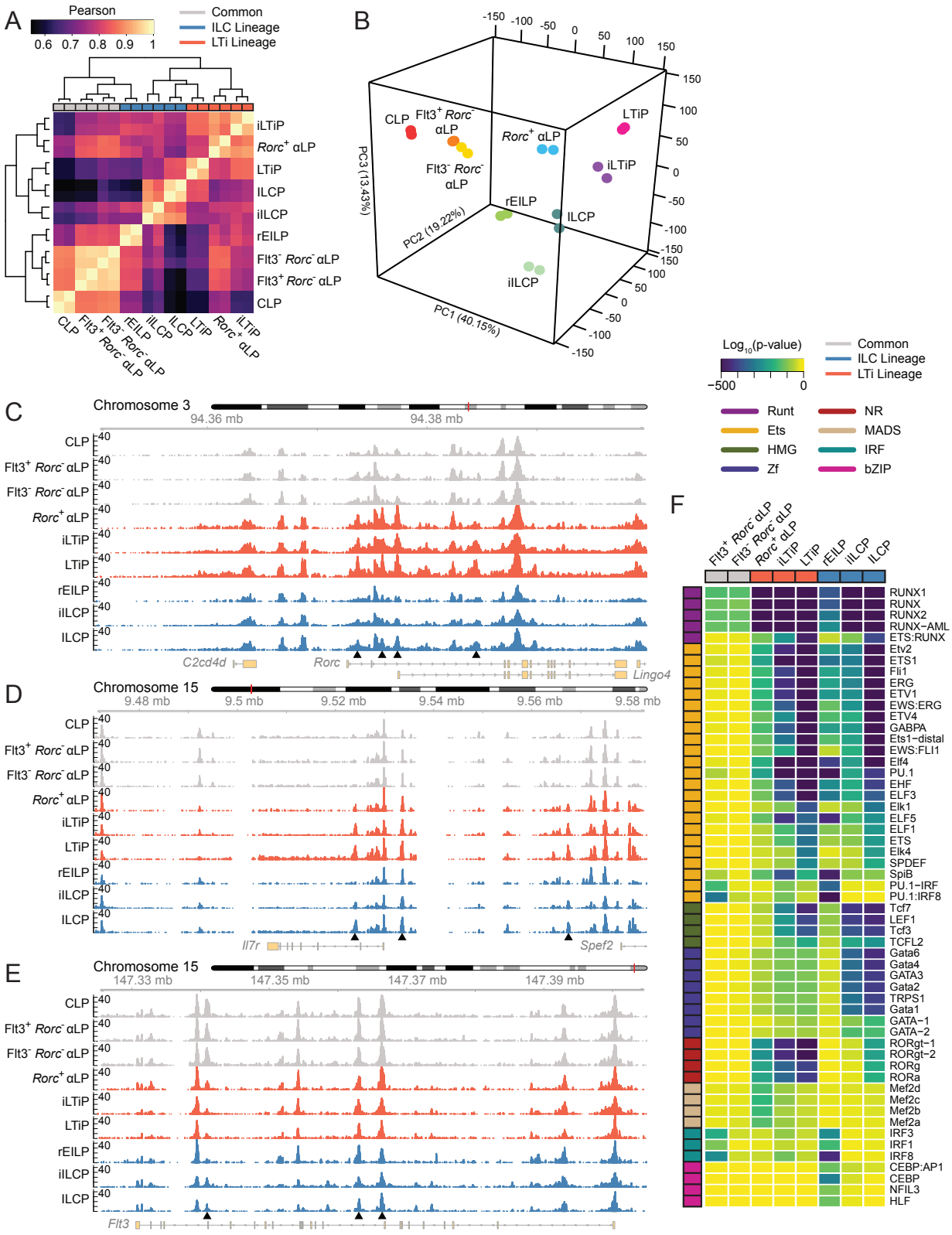

Figure 3.11: Chromatin accessibility of FL ILC progenitors.

Figure 3.11, continued. (**A**) Correlation heatmap for FL ILC progenitor ATAC-seq samples (n = 2). Precursors are categorized by *in vitro* clonal potential. (**B**–**E**) 3D principal component (PC) analysis of ATAC-seq data. Accessibility coverage tracks at the indicated loci in FL ILC progenitors: *Rorc* (C), *Il7r* (D), and *Flt3* (E). Black arrow heads indicate regions of dynamic chromatin accessibility. (**F**) Developmental trajectory heatmap of TF motif enrichment derived from comparing the indicated FL ILC progenitor to the CLP. Motifs were plotted if they exhibited a log10(P value) $\leq$ -100 and a signal-to-noise ratio $\geq$1.5 in at least one comparison. Data represents two samples per cell type and were collected across seven independent experiments.

ILC1/2/3 subset differentiation occurs.[92] This pattern of accessibility was mirrored at the *Il17a/Il17f* locus (**Fig.3.12A**). Increasing accessibility was observed in the *Il7r* locus at two sites bound by TCF1 (-3.6 kb) and GATA3 (+5.3 kb), tracking IL-7Rα re-expression (**Fig.3.11D**).[68,88] Similarly, accessibility at a *Tcf7* enhancer (-31 kb) progressively increased before the expression of *Tcf7* (**Fig.3.12B** and **Fig.3.6A**). Examination of the *Flt3* locus showed that regions accessible in common precursors were either unchanged or moderately reduced in accessibility within the *Rorc*$^+$ αLP and rEILP but were diminished in later progenitors (**Fig.3.11E**). Taken together, comparison of the chromatin accessibility landscape between FL precursors reinforces the hierarchical placement of each precursor during ILC development (**Fig.3.1B**).

The molecular determinants that govern the distinct differentiation of the ILC and LTi lineages are poorly understood. To determine the TFs important for ILC and LTi lineage differentiation across the FL developmental trajectory, we identified statistically enriched TF motifs in ATAC-seq peaks with increased accessibility in each common αLP, ILC, or LTi lineage progenitor in comparison to the CLP. Peaks were robustly and predictably enriched for Runt and ETS motifs in both the ILC and LTi lineages, starting in the common αLPs and progressively increasing in enrichment along each developmental trajectory (**Fig.3.11F**).[80,104,130] While the rEILP showed similar enrichment for Runt and ETS motifs, there was distinguishable motif enrichment for the bZIP member CEBP, several IRF factors, and myeloid-expressed ETS factors (i.e., PU.1 and SpiB), consistent with a recent report demonstrating that this population expresses several of these factors and retains dendritic cell (DC) potential.[77] Binding motifs for TCF1 and other high-mobility group family

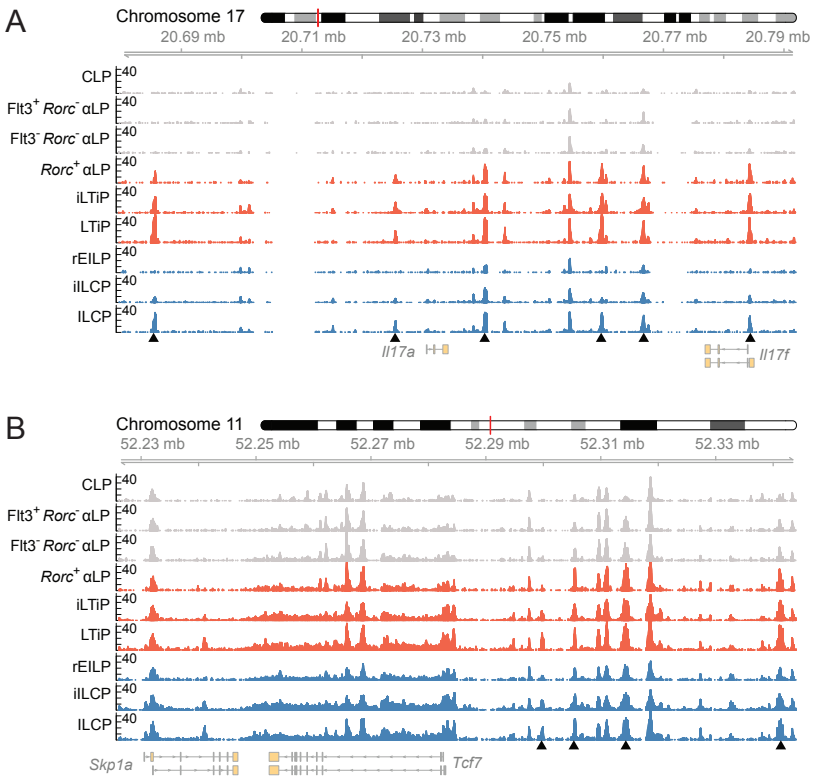

Figure 3.12: Chromatin accessibility profiles of FL ILC progenitors. (**A and B**) Accessibility coverage tracks at the (A) *Il17a*/*Il17f* and (B) *Tcf7* loci in FL ILC progenitors. Black arrow heads indicate regions of dynamic chromatin accessibility. Data represents two samples per cell type and were collected across seven independent experiments.

members were comparably enriched in both the ILC and LTi lineages; motif enrichment followed the known pattern of *Tcf7* expression in these cells (**Fig.3.6A**). More notable was the differential enrichment for zinc finger and nuclear receptor TF motifs between the ILC and LTi lineage, respectively. Whereas motifs for GATA3 and similar zinc finger family members were greatly enriched in the ILC lineage, maximally within the ILCP, the LTi lineage displayed a markedly lower enrichment, mirroring *Gata3* expression (**Fig.3.6C**). Conversely, the LTi lineage was significantly enriched in nuclear receptor motifs comprising the TFs RORγ, RORγt, and RORα, while these motifs only showed enrichment late in ILC lineage development in the ILCP. In summary, the patterns uncovered through TF motif enrichment analysis provide insight into the shared and distinct usage of TFs throughout ILC and LTi lineage development.

3.1.4 Discussion

Using a novel combination of CRISPR/Cas9-generated TF reporter lines, we have identified and resolved population-level heterogeneity within FL ILC progenitors. The EILP is present within the FL and comprises a previously unappreciated mixture of PLZF- and RORγ(t)-expressing cells, herein termed the iILCP and iLTiP, respectively. Although PLZF expression in the BM EILP has been described before, RORγ(t) expression in the FL EILP was overlooked due to the exclusive focus on the adult BM.[75–77] Functional assessment of precursor potential using the combination reporter mice revealed that the EILP and CHILP contained discrete precursors to the ILC and LTi lineages. The sensitivity and deliberate selection of our reporter combination also enabled the identification of a *Rorc*$^+$ population before *Tcf7* expression, marking the earliest known precursor to the LTi lineage. Analysis of the chromatin accessibility landscape in precursors re-enforces the lineages distinctions reached through phenotypic, transcriptional, and *in vitro* clonal analysis and implicates the differential usage of GATA3 and RORγ(t) in the development of the ILC and LTi lineages, respectively. These results warranted a revised model for ILC development that accounts for the newly discovered heterogeneity and places the common ILC-LTi precursor upstream of its previously assumed position within the *Tcf7*$^+$ compartment (**Fig.3.1B**).

Conventional TF staining captures the cellular heterogeneity present within the FL EILP, yet functional analysis necessitated the use of TF reporters. Compared with previous reports that have relied on single TF reporters and surface markers to make claims about ILC development, the multi-TF reporter system enables the simultaneous resolution of several TFs throughout development while permitting the functional assessment of lineage potential. Several recent reports have implemented combinatorial reporters, generated through standard transgenic methods, to interrogate ILC development in the adult BM.[77,93,94] The novel application of CRISPR/Cas9-mediated transgenesis in this study stands out as a rapid and flexible method for the generation of custom reporter lines that can be used to evaluate

or discover cellular complexity.

The EILP and the CHILP were identified in previous reports using *Tcf7*$^{\text{EGFP}}$ and ID2$^{\text{EGFP}}$ mice respectively, and both precursors were reported to generate restricted ILC subsets (**Fig.3.1A**).[5,75,76] The observations made herein suggest a different model for ILC development (**Fig.3.1B**). Clonal analysis performed with *Zbtb16*$^{\text{EGFPCre}}$ *Tcf7*$^{\text{mCherry}}$ *Rorc*$^{\text{Thy1.1}}$ mice demonstrates that the FL EILP is not a precursor to all ILCs but instead contains distinct intermediates to the ILC and LTi lineages upstream of the ILCP and LTiP. Our discovery of an iILCP and iLTiP within the EILP suggested several surprising implications. First, precursors to the ILC and LTi lineage both transiently down-regulate IL-7Rα expression.[76] The consequence of reduced IL-7Rα expression during ILC and LTi development remains to be determined. Continuous IL-7Rα expression via transgene only marginally impairs thymocyte development, potentially by inhibiting TCF1 up-regulation, though group 3 ILCs appear unperturbed by sustained IL-7Rα expression.[100,167] Second, the existence of intermediate precursors to the ILCP and LTiP intermediate for ID2 expression called into question the identity of the CHILP. Using *Zbtb16*$^{\text{EGFPCre}}$ID2$^{\text{EYFP}}$ reporter mice to isolate the *Zbtb16*$^{-}$ID2^{+} fraction of the CHILP, we provide evidence through index-based clonal analysis that the CHILP is not a shared ILC-LTi precursor as formerly suggested, but actually comprises an admixture of restricted precursors in both the BM and FL, similar to the EILP, and is unlikely to be a discrete precursor.

Another inference that can be made from EILP heterogeneity is that the bifurcation of the ILC and LTi must occur earlier in development. Despite looking like a shared ILC-LTi precursor, the rEILP appears to represent a stage before the iILCP, preceding *Zbtb16* expression with negligible LTi potential. This observation is in line with the recent study that found that a BM specified EILP, equivalent to the rEILP here, generated *Zbtb16*$^{+}$ cells in short-term culture.[77] Instead, we discerned an earlier multipotent *Rorc*$^{+}$ αLP in the FL of *Zbtb16*$^{\text{EGFPCre}}$ *Tcf7*$^{\text{mCherry}}$ *Rorc*$^{\text{Thy1.1}}$ mice that was devoid of several maturation markers,

including *Tcf7*, but was already biased toward LTi differentiation. Sawa et al. (2010) proposed the existence of two FL $\alpha4\beta7^{+}$RORγt-EGFP^{+} populations that generated LTi almost exclusively. RORγt-EGFP$^{\text{high}}$ cells noted in that study likely represent the LTiP, while the RORγt-EGFP$^{\text{mid}}$ cells likely represent a mixture of both iLTiP and *Rorc*$^{+}$ αLP, as these two populations were indistinguishable in the absence of *Tcf7* and IL-7Rα assessment. The absence of *Rorc*$^{+}$ αLP and diminished output of LTi from adult BM may result from a failure to up-regulate ID2 in αLP (**Fig.3.6E**), as sequential expression of ID2 and RORγ(t) was proposed to facilitate LTi development.[82] Taken together, our results suggest a model in which a shared ILC-LTi precursor within the αLP expresses *Rorc*, diminishing ILC lineage potential, followed closely by *Tcf7* expression and down-regulation of IL-7Rα giving rise to the iLTiP. In parallel, *Tcf7* and subsequent *Zbtb16* and *Gata3* expression in the iILCP defines the reduction in LTi lineage potential.

ATAC-seq assessment of FL ILC progenitors reinforced the cellular identity and lineage classification of the newly characterized rEILP, iILCP, *Rorc*$^{+}$ αLP, and iLTiP. The *Rorc*$^{+}$ αLP categorically presented a transitional chromatin accessibility landscape between common precursors and the more mature iLTiP and LTiP. ILC lineage and LTi lineage progenitors largely clustered together apart from two exceptions. First, the rEILP clustered with common precursors and displayed aspects of alternate lineage potential, including CEBP, IRF8, PU.1, and SpiB motif enrichment. Harly et al. (2019) found that rEILP from BM generated DCs *in vitro* under permissive conditions and established TCF1 as the key factor in driving ILC lineage commitment. Our results indicate that, like BM rEILP, FL rEILP may retain DC potential, emulating in the ILC lineage the progressive loss of B cell and then myeloid cell potential observed during thymocyte development.[72,100] Second, notwithstanding the disparate phenotype, transcriptional state, and cellular potential of the ILCP and LTiP, clustering of these precursors revealed that a similar accessibility landscape was acquired during cellular maturation, and that only a fraction of accessible regions contributed

to their distinct cellular identity. The similarity may result from the appearance of shared type 3 signatures, as the ILCP contains ILC3-biased cells.[92] Future characterization of the chromatin accessibility landscape will benefit from the isolation of homogenous populations of ILC1, ILC2, and ILC3 precursors. Nevertheless, TF motif enrichment across the developmental trajectories suggests a markedly differential usage of GATA3 and RORγ(t) in establishing ILC and LTi lineage cellular identity, respectively. Moreover, our *Gata3*-Citrine reporter indicated that expression of *Gata3* in the LTi lineage is delayed when comparing the iLTiP to the iILCP and does not reach the expression level observed in the ILCP. Zhong et al. (2020) demonstrated a differential reliance on the TF GATA3 for the development of ILC1/2/3 and LTi cells; whereas ILC1/2/3 require GATA3 for development, LTi develop in the absence of GATA3, albeit while exhibiting functional defects. The results presented herein highlight the role GATA3 plays as a defining factor governing the distinct development of these two lineages.

The model proposed herein conforms with our earlier observations using single-cell analysis that implicated the αLP as the point of lineage bifurcation between the ILC and LTi lineage, based on the generation of mixed colonies.[92] The frequency of mixed colonies was notably low, possibly resulting from a lack of critical factors necessary for the overall survival of early multipotent αLPs given that our culture system supports ample LTi generation. Furthermore, the window to capture large numbers of ILC-LTi precursors among the αLP may be earlier than E14-16, as suggested by the early wave of *Rorc*$^{+}$ αLP at E13 (**Fig.3.9D**). In stark contrast to previous findings and the work presented here, Walker et al. (2019) generated a novel PLZF$^{\text{tdTomato}}$ reporter and observed PLZF$^{\text{tdTomato}}$ expression in peripheral LTi-like cells and in CD4^{+} LTiP from the FL.[78,92] These incongruous findings may be explained by the design of each *Zbtb16* reporter. The *Zbtb16*$^{\text{EGFPCre}}$ reporter was constructed by inserting an IRES-EGFPCre sequence downstream of the *Zbtb16* stop codon.[78] The PLZF$^{\text{tdTomato}}$ reporter, on the other hand, was constructed by inserting a T2A-tdTomato polyA sequence

before the *Zbtb16* stop codon.[94] While the T2A sequence enables precise expression of td-Tomato during protein translation, the incorporation of an exogenous polyA bypasses the endogenous polyA signal sequence and may disrupt any 3' UTR regulatory mechanisms that could govern the stability or turnover of *Zbtb16* mRNA.[186,187] Altered post-transcriptional regulation of *Zbtb16* mRNA, potentially resulting in exaggerated expression, may explain the observation that the PLZF$^{\text{tdTomato}}$ reporter does not reflect *Zbtb16*$^{\text{EGFPCre}}$ fate mapping and known intracellular staining patterns for PLZF in the LTiP, ILC2P, or mature ILC populations.[5,78,91,92,161]

In summary, our study has highlighted the value of applying a multi-TF reporter approach, specifically to the dissection of ILC and LTi lineage progression. Moreover, we have identified several unappreciated precursors along both the ILC and LTi development pathways. Delineation of these early intermediates will facilitate the molecular interrogation of factors and mechanisms that govern ILC development and lineage progression.

Author Contributions

D.N. Kasal and A. Bendelac conceived the study and wrote the manuscript. D.N. Kasal designed experiments; generated reporter constructs; performed flow cytometry, single-cell sorting, and culture experiments; and conducted ATAC-seq computational analysis. A. Bendelac supervised experiments.

Acknowledgments

We thank A. Goldrath for the ID2$^{\text{EYFP}}$ mice and A. Bhandoola for the *Tcf7*$^{\text{EGFP}}$ mice; J.C. Zúñiga-Pflücker for stocks of OP9 and OP9-DL1 stromal cells; S. Erickson (University of Chicago) for productive discussion of CRISPR/Cas9 methodology; and B. Kee (University of Chicago) and F. Gounari (University of Chicago) for critical reading of the manuscript. We are grateful to L. Degenstein (University of Chicago) and the University of Chicago

Transgenics Core for support with microinjections; the University of Chicago DNA Sequencing and Genotyping Core for sequencing of reporter plasmid constructs; the University of Chicago Flow Cytometry Core for technical assistance with cell sorting; and the University of Chicago Genomics Core for sequencing of ATAC-seq samples.

This work was supported by the National Institutes of Health (R37 AI127518, R01 AI144094, and U01 AI125250) and support funds from the University of Chicago Dean's office.

3.1.5 Appendix

Table 3.1: Fetal Liver Flt3$^+$ αLP
OP9 culture
n = 80, Plating Efficiency: 37.91%

	Wells Grown	% of Wells Grown	μ Col. Size	σ Col. Size
ILC1	30	37.50	867.92	431.55
ILC2	1	1.25	9.00	0
ILC3	14	17.50	100.21	38.97
LTi_4	11	13.75	136.08	37.99
mixLTi	4	5.00	112.24	37.14
multi	20	25.00	571.49	237.36

Table 3.2: Fetal Liver Flt3$^-$ αLP
OP9 culture
n = 175, Plating Efficiency: 40.60%

	Wells Grown	% of Wells Grown	μ Col. Size	σ Col. Size
ILC1	90	51.43	547.53	224.39
ILC2	2	1.14	262.00	284.25
ILC3	36	20.57	206.27	71.57
LTi_4	14	8.00	170.92	88.53
mixLTi	4	2.28	457.25	472.42
multi	29	16.57	450.93	195.88

Table 3.3: Fetal Liver rEILP
OP9 culture
n = 55, Plating Efficiency: 21.82%

	Wells Grown	% of Wells Grown	μ Col. Size	σ Col. Size
ILC1	31	56.36	982.39	189.21
ILC2	1	1.82	48.00	0
ILC3	17	30.91	128.76	29.59
LTi_4	3	5.45	32.33	10.33
mixLTi	0	0.00	0	0
multi	3	5.45	869.67	777.90

Table 3.4: Fetal Liver iILCP
OP9 culture
n = 244, Plating Efficiency: 52.54%

	Wells Grown	% of Wells Grown	μ Col. Size	σ Col. Size
ILC1	138	56.56	450.28	53.56
ILC2	31	12.70	44.32	6.62
ILC3	24	9.84	59.29	12.27
LTi_4	27	11.07	68.19	11.70
mixLTi	0	0.00	0	0
multi	24	9.84	187.79	64.26

Table 3.5: Fetal Liver ILCP
OP9 culture
n = 876, Plating Efficiency: 53.27%

	Wells Grown	% of Wells Grown	μ Col. Size	σ Col. Size
ILC1	408	46.58	189.87	140.02
ILC2	269	30.71	38.84	27.09
ILC3	95	10.84	51.15	31.54
LTi_4	25	2.85	54.67	20.26
mixLTi	0	0.00	0	0
multi	79	9.02	61.45	52.60

Table 3.6: Fetal Liver iLTiP
OP9 culture
n = 86, Plating Efficiency: 55.23%

	Wells Grown	% of Wells Grown	μ Col. Size	σ Col. Size
ILC1	10	11.63	463.59	313.78
ILC2	1	1.16	35	0
ILC3	33	38.37	119.54	37.26
LTi_4	41	47.67	50.97	20.90
mixLTi	0	0.00	0	0
multi	1	1.16	1103.00	0

Table 3.7: Fetal Liver LTiP
OP9 culture
n = 155, Plating Efficiency: 55.20%

	Wells Grown	% of Wells Grown	μ Col. Size	σ Col. Size
ILC1	9	5.81	166.77	154.52
ILC2	0	0.00	0	0
ILC3	59	38.06	61.37	52.68
LTi_4	85	54.84	49.08	27.27
mixLTi	0	0.00	0	0
multi	2	1.29	393.5	207.18

Table 3.8: Bone Marrow *Zbtb16*$^-$ID2$^+$
OP9 culture
n = 12, Plating Efficiency: 49.06%

	Wells Grown	% of Wells Grown	μ Col. Size	σ Col. Size
ILC1	6	50.00	89.50	48.43
ILC2	5	41.67	16.60	5.10
ILC3	1	8.33	9.00	0
LTi_4	0	0.00	0	0
mixLTi	0	0.00	0	0
multi	0	0.00	0	0

Table 3.9: Bone Marrow ILCP *Zbtb16*$^+$ID2$^+$
OP9 culture
n = 80, Plating Efficiency: 76.11%

	Wells Grown	% of Wells Grown	μ Col. Size	σ Col. Size
ILC1	47	55.95	142.34	22.99
ILC2	33	39.29	17.00	2.01
ILC3	0	0.00	0	0
LTi_4	0	0.00	0	0
mixLTi	0	0.00	0	0
multi	4	4.76	37.25	26.28

Table 3.10: Bone Marrow ILC2P *Zbtb16*$^{-}$ID2^{+}
OP9 culture
n = 33, Plating Efficiency: 53.12%

	Wells Grown	% of Wells Grown	μ Col. Size	σ Col. Size
ILC1	0	0.00	0	0
ILC2	33	100.00	9.70	0.97
ILC3	0	0.00	0	0
LTi_4	0	0.00	0	0
mixLTi	0	0.00	0	0
multi	0	0.00	0	0

Table 3.11: Bone Marrow *Zbtb16*$^{-}$ID2^{+}
OP9-DL1 culture
n = 21, Plating Efficiency: 36.56%

	Wells Grown	% of Wells Grown	μ Col. Size	σ Col. Size	μ Tcell Col. Size	σ Tcell Col. Size
ILC1	15	71.43	50.27	12.35	3.00	1.32
ILC1+Tcell	2	9.52	186.00	71.00	69.50	5.50
ILC2	0	0.00	0	0	0	0
ILC3	1	4.76	39.00	0	3.00	0
ILC3+Tcell	1	4.76	505.00	0	67.00	0
LTi_4	0	0.00	0	0	0	0
mixLTi	0	0.00	0	0	0	0
multi	1	4.76	103.00	0	0.00	0
multi+Tcell	1	4.76	79.00	0	28.00	0

Table 3.12: Bone Marrow ILCP *Zbtb16*$^{+}$ID2^{+}
OP9-DL1 culture
n = 96, Plating Efficiency: 62.90%

	Wells Grown	% of Wells Grown	μ Col. Size	σ Col. Size	μ Tcell Col. Size	σ Tcell Col. Size
ILC1	15	15.62	44.20	9.78	4.67	1.55
ILC1+Tcell	5	5.21	188.40	33.27	95.40	29.16
ILC2	36	37.5	34.31	5.86	0.94	0.25
ILC3	6	6.25	21.00	6.89	6.50	3.28
ILC3+Tcell	5	5.21	97.60	10.10	54.00	4.30
LTi_4	0	0.00	0	0	0	0
mixLTi	0	0.00	0	0	0	0
multi	20	20.83	105.65	27.66	8.75	3.91
multi+Tcell	9	9.38	198.77	61.35	80.77	74.58

Table 3.13: Bone Marrow ILC2P *Zbtb16*$^{-}$ID2^{+}
OP9-DL1 culture
n = 26, Plating Efficiency: 26.67%

	Wells Grown	% of Wells Grown	μ Col. Size	σ Col. Size	μ Tcell Col. Size	σ Tcell Col. Size
ILC1	0	0.00	0	0	0	0
ILC2	26	100.00	9.85	0.81	0.04	0.04
ILC3	0	0.00	0	0	0	0
LTi_4	0	0.00	0	0	0	0
mixLTi	0	0.00	0	0	0	0
multi	0	0.00	0	0	0	0

Table 3.14: Fetal Liver *Zbtb16*$^{-}$ID2^{+}
OP9 culture
n = 67, Plating Efficiency: 84.62%

	Wells Grown	% of Wells Grown	μ Col. Size	σ Col. Size
ILC1	14	20.90	119.57	24.21
ILC2	4	5.97	21.00	8.65
ILC3	32	47.76	46.62	10.70
LTi_4	14	20.90	39.07	8.08
multi	3	4.48	692.00	395.55

Table 3.15: Fetal Liver ILCP *Zbtb16*$^{+}$ID2^{+}
OP9 culture
n = 115, Plating Efficiency: 73.73%

	Wells Grown	% of Wells Grown	μ Col. Size	σ Col. Size
ILC1	33	28.70	177.91	40.31
ILC2	41	35.65	34.98	3.01
ILC3	18	15.65	49.39	6.87
LTi_4	9	7.83	40.00	11.47
multi	14	12.17	78.64	31.72

Table 3.16: Fetal Liver LTiP *Zbtb16*$^{-}$ID2^{+}
OP9 culture
n = 66, Plating Efficiency: 67.16%

	Wells Grown	% of Wells Grown	μ Col. Size	σ Col. Size
ILC1	2	3.03	25.50	8.50
ILC2	0	0.00	0	0
ILC3	20	30.30	21.55	3.37
LTi_4	44	66.67	25.84	3.60
multi	0	0.00	0	0

Table 3.17: Fetal Liver *Zbtb16*$^{-}$ID2^{+}
OP9-DL1 culture
n = 65, Plating Efficiency: 75.00%

	Wells Grown	% of Wells Grown	μ Col. Size	σ Col. Size	μ Tcell Col. Size	σ Tcell Col. Size
ILC1	21	32.31	62.10	14.24	2.19	1.03
ILC2	6	9.23	46.33	20.44	3.17	1.82
ILC3	20	30.77	27.25	4.80	0.20	0.09
ILC3+Tcell	1	1.54	1137.00	0	183.00	0
LTi_4	11	17.19	24.45	7.22	0.36	0.20
multi	3	4.62	65.33	20.34	5.33	5.33
multi+Tcell	2	3.08	308.00	161.00	133.00	98.00
Tcell	1	1.54	444.00	0	177.00	0

Table 3.18: Fetal Liver ILCP *Zbtb16*$^{+}$ID2^{+}
OP9-DL1 culture
n = 57, Plating Efficiency: 83.15%

	Wells Grown	% of Wells Grown	μ Col. Size	σ Col. Size	μ Tcell Col. Size	σ Tcell Col. Size
ILC1	39	34.82	92.74	14.27	2.23	0.55
ILC1+Tcell	2	1.78	478.50	189.50	41.50	9.50
ILC2	34	30.36	37.76	5.11	1.21	0.28
ILC2+Tcell	2	1.78	132.50	3.50	36.50	11.50
ILC3	17	15.18	51.18	14.57	1.24	1.24
LTi_4	6	5.35	31.83	14.36	0.17	0.17
multi	7	6.25	82.42	23.05	3	2.6012
multi+Tcell	5	4.46	680.4	387.21	238.6	333.62

Table 3.19: Fetal Liver LTiP *Zbtb16*$^{-}$ID2^{+}
OP9-DL1 culture
n = 112, Plating Efficiency: 65.09%

	Wells Grown	% of Wells Grown	μ Col. Size	σ Col. Size	μ Tcell Col. Size	σ Tcell Col. Size
ILC1	3	5.26	15.33	4.91	0.33	0.33
ILC2	0	0.00	0	0	0	0
ILC3	24	42.10	21.54	3.68	0.42	0.21
ILC3+Tcell	1	1.75	71.00	0	33.00	0
LTi_4	27	47.37	19.93	2.55	0.30	0.12
multi	2	3.51	102.50	45.50	3.50	3.50

Table 3.20: Fetal Liver Flt3^{+} *Rorc*$^{-}$ αLP
OP9 culture
n = 30, Plating Efficiency: 44.44%

	Wells Grown	% of Wells Grown	μ Col. Size	σ Col. Size
ILC1	27	42.86	1175.66	383.46
ILC2	0	0.00	0	0
ILC3	9	14.29	136.11	113.19
LTi_4	9	14.29	131.99	46.64
mixLTi	3	4.76	122.33	38.20
multi	15	23.81	588.39	279.66

Table 3.21: Fetal Liver Flt3^{-} *Rorc*$^{-}$ αLP
OP9 culture
n = 124, Plating Efficiency: 46.90%

	Wells Grown	% of Wells Grown	μ Col. Size	σ Col. Size
ILC1	71	57.26	636.60	185.61
ILC2	1	0.81	12	0
ILC3	17	13.71	170.53	63.39
LTi_4	9	7.26	226.99	61.34
mixLTi	1	0.81	1104.00	0
multi	25	20.16	378.75	196.12

Table 3.22: Fetal Liver *Rorc*$^{+}$ αLP
OP9 culture
n = 64, Plating Efficiency: 70.75%

	Wells Grown	% of Wells Grown	μ Col. Size	σ Col. Size
ILC1	10	15.62	321.40	88.95
ILC2	1	1.56	12.00	0
ILC3	34	53.12	146.29	16.95
LTi	10	15.62	83.20	17.22
mixLTi	0	0.00	0	0
multi	9	14.06	507.33	220.38

Table 3.23: Fetal Liver Flt3^{+} *Rorc*$^{-}$ αLP
OP9-DL1 culture
n = 63, Plating Efficiency: 31.17%

	Wells Grown	% of Wells Grown	μ Col. Size	σ Col. Size	μ Tcell Col. Size	σ Tcell Col. Size
ILC1	4	13.33	187.25	85.99	8	3.02
ILC2	0	0.00	0	0	0	0
ILC2+Tcell	3	10.00	796.66	144.23	412	323.65
ILC3	1	3.33	54.00	0	12.00	0
ILC3+Tcell	3	10	1757.00	580.67	1309.00	621.90
LTi_4	1	3.33	49.00	0	5.00	0
LTi_4+Tcell	1	3.33	1012.00	0	773.00	0
mixLTi	0	0.00	0	0	0	0
multi	0	0.00	0	0	0	0
multi+Tcell	6	20.00	648.33	570.49	246.5	277.15
Tcell	11	36.67	1548.54	830.08	1140.63	574.33

Table 3.24: Fetal Liver Flt3$^-$ *Rorc*$^-$ αLP
OP9-DL1 culture
n = 41, Plating Efficiency: 40%

	Wells Grown	% of Wells Grown	μ Col. Size	σ Col. Size	μ Tcell Col. Size	σ Tcell Col. Size
ILC1	5	12.20	202.60	111.05	5.40	3.50
ILC1+Tcell	6	14.63	408	118.88	65.83	31.71
ILC2	1	2.44	215.00	0	6.00	0
ILC2+Tcell	5	12.20	2352.79	2102.03	2074.80	2103.67
ILC3	0	0.00	0	0	0	0
ILC3+Tcell	5	12.20	2133.99	1386.65	1841.4	1387.09
LTi_4	1	2.44	51.00	0	3.00	0
LTi+Tcell	2	4.88	1464.50	38.50	990.50	28.50
mixLTi	1	2.44	196.00	0	4.00	0
mixLTi+Tcell	1	2.44	3936.00	0	1311.00	0
multi	2	4.88	93.5	60.10	5	5.65
multi+Tcell	12	29.27	1271.08	949.99	609.33	743.97

Table 3.25: Fetal Liver *Rorc*$^+$ αLP
OP9-DL1 culture
n = 49, Plating Efficiency: 60.26%

	Wells Grown	% of Wells Grown	μ Col. Size	σ Col. Size	μ Tcell Col. Size	σ Tcell Col. Size
ILC1	3	6.12	253.33	41.91	8.00	2.89
ILC1+Tcell	6	12.24	526.00	131.38	83.67	33.48
ILC2	1	2.04	261.00	0	23.00	0
ILC3	16	32.65	129.31	21.78	4.25	0.93
ILC3+Tcell	3	6.12	385.00	115.02	53.00	7.51
LTi_4	9	18.37	65.00	18.38	1.78	0.64
mixLTi	0	0.00	0	0	0	0
multi	2	4.08	666.00	176.00	15.00	3.00
multi+Tcell	7	14.28	606.71	274.93	108.28	59.35
Tcell	2	4.08	133.00	109.00	98.00	74.00

3.2 A novel *Gata3* enhancer necessary for ILC2 development and function

Darshan N. Kasal[1,2], Zhitao Liang[1,2], Maile K. Hollinger[1,3], Crystal Y. O'Leary[2], Wioletta Lisicka[1,4], Anne I. Sperling[1,3], and Albert Bendelac[1,2]

[1]*Committee on Immunology, University of Chicago, Chicago, IL 60637, USA*

[2]*Department of Pathology, University of Chicago, Chicago, IL 60637, USA*

[3]*Department of Medicine, Section of Pulmonary and Critical Care, University of Chicago, Chicago, IL 60637, USA*

[4]*Department of Medicine, Section of Gastroenterology, University of Chicago, Chicago, IL 60637, USA*

Accepted for publication in the Proceedings of the National Academy of Sciences

15 June 2021; doi:10.1073/pnas.2106311118

3.2.1 Abstract

The type 2 helper effector program is driven by the master transcription factor GATA3 and can be expressed by subsets of both innate lymphoid cells (ILCs) and adaptive $CD4^+$ T helper (Th) cells. While ILC2s and Th2 cells acquire their type 2 differentiation program under very different contexts, the distinct regulatory mechanisms governing this common program are only partially understood. Here we show that the differentiation of ILC2s, and their concomitant high level of GATA3 expression, are controlled by a novel *Gata3* enhancer, *Gata3* +674/762, that plays only a minimal role in Th2 cell differentiation. Mice lacking this enhancer exhibited defects in several but not all type 2 inflammatory responses, depending on the respective degree of ILC2 and Th2 cell involvement. Our study provides molecular insights into the different gene regulatory pathways leading to the acquisition of the GATA3-driven type 2 helper effector program in innate and adaptive lymphocytes.

3.2.2 Significance Statement

Group 2 innate lymphoid cells (ILC2s) and adaptive $CD4^+$ T helper type 2 (Th2) cells express a common effector program orchestrated by the "master" transcription factor GATA3 that is acquired through development or differentiation respectively. To elucidate the regulatory mechanisms controlling the acquisition of this shared program, we used a combination of chromatin accessibility data and CRISPR/Cas9-mediated deletion, which revealed a novel *Gata3* enhancer necessary for ILC2 development and function. Notably, this enhancer was largely dispensable for Th2 cell differentiation. Thus, ILC2s and Th2 cells display different requirements for the induction of a common type 2 helper effector program.

3.2.3 Introduction

Innate lymphoid cells (ILCs) are classically considered tissue-resident lymphocytes that are functionally divided into three groups (1, 2, and 3), mirroring $CD4^+$ T helper (Th) cell subsets, in accordance with their transcription factor (TF) expression profile and rapid cytokine response under varied homeostatic and inflammatory conditions.[2] ILCs and T cells express a highly overlapping subset of TFs, yet these two lineages differ in their temporal acquisition of effector properties through development or activation respectively.[179,188] Among the shared TFs expressed in both lineages, GATA3 (encoded by *Gata3*) in particular plays a central role. GATA3 is well established as an essential regulator of both ILC and T cell development, differentiation, and function.[189,190] In T cells, GATA3 controls the development of early thymic progenitors (ETPs) and thymopoiesis[152,153], CD4-CD8 T cell lineage commitment[154], T cell homeostasis[155], and Th2 cell differentiation and function.[156–158] Akin to its functions in T cells, GATA3 regulates ILC precursor development[121,122], peripheral ILC maintenance[68,121], ILC2 differentiation and function[81,159], and may contribute to ILC vs. lymphoid tissue-inducer (LTi) lineage specification.[161,172] Importantly, GATA3 expression dramatically increases above developmental levels during type 2 lymphocyte lineage com-

mitment in both ILC2s and Th2 cells.[78,156,162,172] GATA3 up-regulation promotes ILC2 and Th2 cell differentiation by activating type 2 helper effector genes (e.g., *Il4*/*Il5*/*Il13* and *Il33ra*) and suppressing alternate lineage promoting factors (e.g., *Tbx21* and *Ifng*).[189] How exactly the expression of *Gata3* is regulated at multiple distinct stages within the ILC and T cell lineages remains poorly understood.

Proper tissue- and stage-specific regulation of gene expression is achieved partly through the combined interaction of *cis*-regulatory elements both proximal (promoters) and distal (i.e., enhancers). GATA3 is critically expressed in a variety of tissue contexts apart from the immune system. *Gata3*-null mice exhibit embryonic lethality[146], and tissue-specific enhancers regulate GATA3 expression during the development of the craniofacial ganglia[147], central nervous system, endocardium, urogenital system[148], kidney[149], inner ear[150], and embryonic lens.[151] Of particular importance to the immune system, Engel and colleagues identified a 7.1 kb T cell specific *Gata3* enhancer (TCE7.1, *Gata3* +278/285) which resides ∼280 kb downstream of *Gata3* within a 2.5 Mb gene desert.[162,163] Through a combination of bacterial artificial chromosome and CRISPR/Cas9-mediated deletion approaches, Ohmura et al. 2016 demonstrated that a core 1.2 kb element of TCE7.1, *Gata3* +283/284, was necessary for optimal *Gata3* expression in ETPs, CD4 single positive (CD4SP) thymocytes, and naïve $CD4^+$ T cells.[163] However, no element of *Gata3* +278/285 fully recapitulated the elevated pattern of *Gata3* expression seen in Th2 cells.[162,163] Furthermore, the contribution of *Gata3* +278/285 or other regulatory elements to *Gata3* expression throughout the ILC lineage remained unexplored. While it is well established that the *Gata3*-mediated type 2 helper effector program of ILC2s and Th2 cells is acquired in very different contexts, i.e., development vs. immune challenge respectively[179,188], it is unclear whether these differences are reflected in the use of or reliance on discrete *Gata3* regulatory elements. This question is of fundamental interest not only to understand the evolution of the type 2 helper effector program in these lineages, but also to develop potential strategies to selectively dissect and

manipulate the innate and adaptive arms of type 2 immunity. For example, whether an innate type 2 response by ILC2s is a prerequisite for the effective differentiation of Th2 cells remains controversial[188,191–193], and could be addressed using mice lacking an ILC2-specific enhancer.

Through a comparison of accessible chromatin regions within the *Gata3* locus gene desert, we identified a novel regulatory region 674 kb downstream of the *Gata3* gene that functions as a type 2-specific *Gata3* enhancer (*Gata3* +674/762). Deletion of this *cis*-regulatory region via CRISPR/Cas9 selectively impaired the differentiation and function of ILC2s at homeostasis as well as during type 2 inflammation. This enhancer was highly selective for ILC2s, and only partially and mostly indirectly impacted Th2 cells, resulting in variable functional defects in allergic and helminthic inflammatory responses depending on the degree of requirement for ILC2s vs. Th2 cells. Other lymphoid lineages such as group 1 (NK cell and ILC1) and group 3 (NCR^+ ILC3 and $CD4^+$ LTi) ILCs as well as undifferentiated $CD4^+$ T cells remained unperturbed. In contrast, we found that the previously identified enhancer *Gata3* +278/285 functioned mainly during the early development of ILCs but not in the differentiation or function of ILC2s, indicating distinct control of these processes. Finally, application of an *in vivo* enhancer reporter strategy in conjunction with the analysis of chromatin accessibility profiles revealed that elements of *Gata3* +674/762 and *Gata3* +278/285 are available and active at distinct stages of *Gata3* expression during ILC and T cell development, differentiation, and function.

3.2.4 Results

3.2.4.1 A distal enhancer of *Gata3* regulates ILC2 homeostasis

To identify potential *cis*-regulatory elements of *Gata3* associated with ILC2 development we examined chromatin accessibility in bone marrow (BM) ILC progenitors using the assay for transposase accessible chromatin with sequencing (ATAC-seq) (**Fig.3.13A**). Ap-

proximately 674 kb downstream of *Gata3* we identified an 88 kb region (*Gata3* +674/762) containing signatures of type 2-specific activity. Chromatin accessibility increased in this region from the common lymphoid progenitor (CLP) to the ILC2 precursor (ILC2P), coinciding with ILC2 lineage differentiation. Moreover, within the 88 kb locus, an un-characterized long non-coding RNA (lncRNA) *1700061F12Rik* was expressed specifically in peripheral ILC2s, as determined by RNA-seq data from Immgen (**Fig.3.14A**).[194] Cell-type specific transcription of lncRNAs has been increasingly recognized as a correlate of active *cis*-regulatory elements. For example, the lncRNA *Rroid* was previously found to demarcate a group 1 ILC specific enhancer of *Id2*.[135] Similarly, the *Gata3* enhancer TCE7.1 (*Gata3* +278/285) resides adjacent to the lncRNA *Dreg1*, which was co-expressed with *Gata3* in T cells (**Fig.3.13A**).[195,196] A more detailed examination of accessibility within sequential progenitors throughout BM ILC development revealed that elements within the *Gata3* +674/762 region began to show increased accessibility in the ILC precursor (ILCP), the stage in which ILC1/2/3 multilineage priming occurs, and were further augmented in the ILC2P where *Gata3* expression is maximal (**Fig.3.13B**, red window and side bar).[92,172] In contrast, there was no detectable accessibility at earlier stages such as the refined early innate lymphoid precursor (rEILP) and the incipient ILC precursor (iILCP) where *Gata3* expression was low (Fig 1B, side bar). These results stood in contrast to accessibility at the previously identified enhancer *Gata3* +278/285, which was accessible from the rEILP to the ILCP, but closed upon ILC2 differentiation (**Fig.3.13B**, purple window).

Given that *Gata3* is expressed throughout T cell development in the thymus and in mature ILCs and differentiated T cells in the periphery, we next evaluated chromatin accessibility in these populations using publicly available ATAC-seq data.[179,197] The distal *Gata3* +674/762 region was conspicuously inaccessible in thymocytes while *Gata3* +278/285 accessibility persisted throughout T cell development, consistent with previously reported

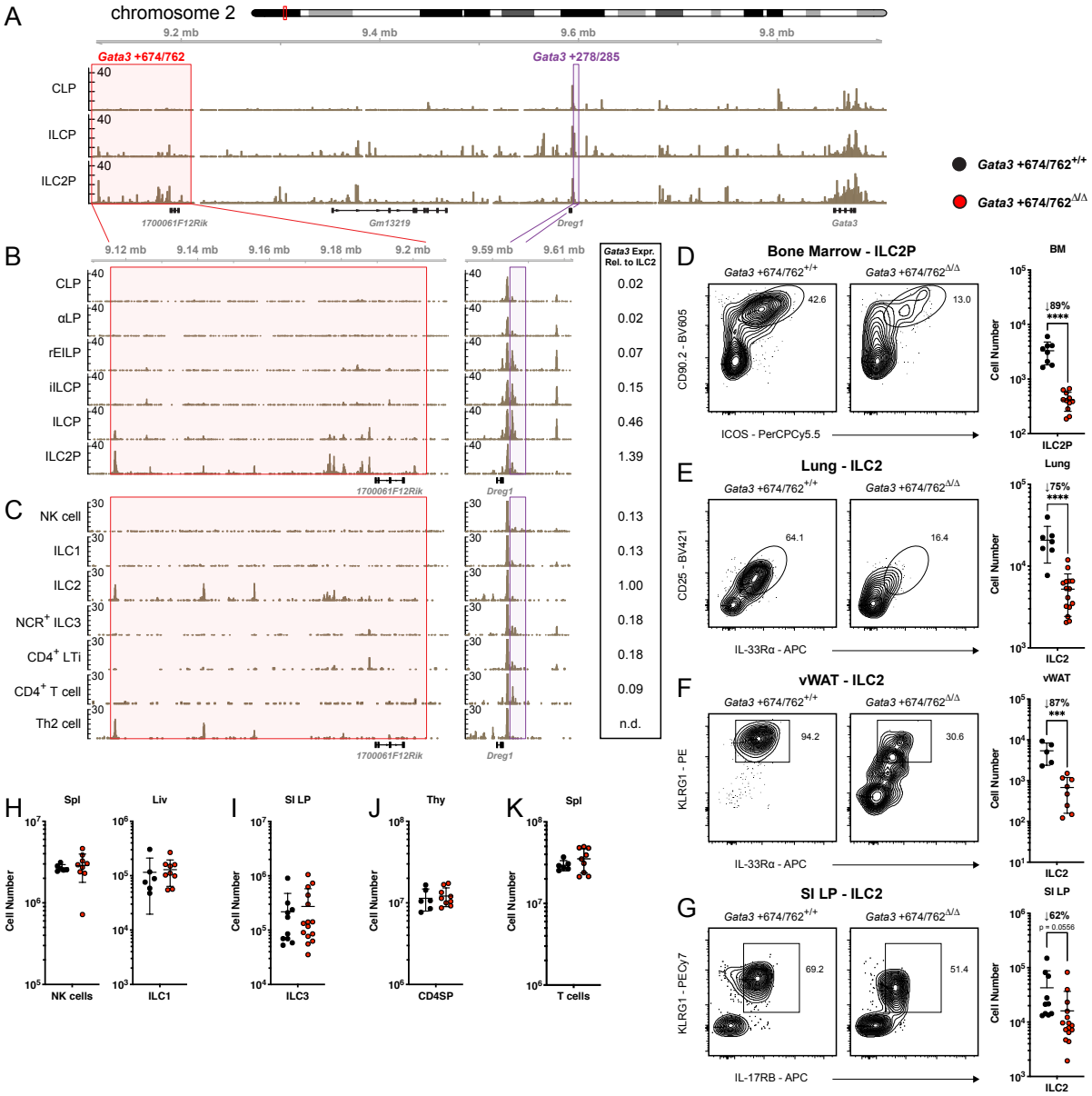

Figure 3.13: Chromatin accessibility at the *Gata3* locus and impact of *Gata3* +674/762 deletion on lymphocyte subsets. (**A**) ATAC-seq accessibility coverage tracks in BM CLP, ILCP, and ILC2P. Red and purple windows represent *Gata3* +674/762 and *Gata3* +278/285 regions respectively. (**B**) Zoomed in ATAC-seq accessibility coverage tracks for the *Gata3* +674/762 and *Gata3* +278/285 regions in sequential BM progenitors to the ILC lineage, including CLP, αLP ($\alpha4\beta7$ Lymphoid Precursor), rEILP, iILCP, ILCP and ILC2P. (**C**) Published ATAC-Seq tracks of splenic NK cells, liver ILC1, lung ILC2, SI LP NCR$^+$ ILC3, SI LP CD4$^+$ LTi, splenic CD4$^+$ T cells, and *Nippostrongylus brasiliensis*-activated lung Th2 cells.[179] Expression levels of *Gata3*-Citrine relative to lung ILC2 are shown to the right of (B) and (C).[172] Representative flow cytometry plots and summary data of cell numbers in WT vs. *Gata3* +674/762$^{\Delta/\Delta}$ mice for (**D**) BM

Figure 3.13, continued. ILC2P (pre-gated on Lin$^-$$\alpha$4$\beta$7$^+$IL-7R$\alpha^+$), (**E**) lung ILC2 (pre-gated on CD45.2$^+$ CD19$^-$CD11c$^-$CD3ϵ^-TCRβ^-IL-7Rα^+CD90.2$^+$), (**F**) vWAT ILC2 (pre-gated on CD45.2$^+$CD19$^-$CD11c$^-$CD3ϵ^- TCRβ^-IL-7Rα^+CD90.2$^+$CD25$^+$), and SI LP ILC2 (pre-gated on CD45.2$^+$CD19$^-$CD11c$^-$CD3ϵ^-TCRβ^-IL-7Rα^+CD90.2$^+$Sca-1$^+$). Summary data of cell numbers for (**H**) spleen NK cells and liver ILC1; (**I**) SI LP ILC3; (**J**) CD4SP thymocytes; and (**K**) splenic CD4$^+$ T cells in WT vs. *Gata3* +674/762$^{\Delta/\Delta}$ mice. Dots represent individual mice; n ranging from 6-15 in different groups pooled from multiple independent experiments; data are presented as mean ± SEM. Statistical comparison was performed via unpaired t-test. ***, P < 0.001; ****, P < 0.0001.

experiments (**Fig.3.14B**).[162,163,197] Among peripheral mature ILCs and T cells, only ILC2s and lung Th2 cells from *Nippostrongylus brasiliensis*-infected mice displayed sections of open chromatin within the *Gata3* +674/762 locus, coinciding with differentiation and enhanced *Gata3* expression (**Fig.3.13C**, red window and side bar).[156,172,179] A comparison of accessibility across the *Gata3* locus revealed no ILC2- vs. Th2 cell-specific peaks (**Fig.3.15**). At the *Gata3* +278/285 enhancer, however, only group 3 ILCs and CD4$^+$ T cells maintained some minor accessibility while this enhancer was closed in group 1 ILCs, ILC2s, and Th2 cells, despite continuous *Gata3* expression throughout all populations (**Fig.3.13C**, purple window and side bar). These results suggest that chromatin accessibility within the distal *Gata3* +674/762 region is regulated in a distinct manner from *Gata3* +278/285 in both ILCs and T cells, with opening of elements in *Gata3* +674/762 coinciding with the acquisition and expression of a type 2 helper effector program by developing ILC2s and differentiating and/or activated Th2 cells.

To directly evaluate the role of the *Gata3* +674/762 region *in vivo*, we employed a CRISPR/Cas9-mediated deletion strategy to generate mice lacking this locus and evaluated representative populations (**Fig.3.14C**). Strikingly, *Gata3* +674/762$^{\Delta/\Delta}$ mice displayed markedly diminished numbers of group 2 ILCs at homeostasis. ILC2P in the adult BM as well as mature ILC2 in the lung, visceral white adipose tissue (vWAT), and small intestinal lamina propria (SI LP) were reduced 62-89% compared to wild-type (WT) littermate controls (**Fig.3.13D-G**). Conversely, group 1 ILCs (NK cell and/or ILC1) in the spleen, liver, lung, and vWAT as well as ILC3s in the SI LP were preserved in the absence of the *Gata3* +674/762 region (**Fig.3.13H**, **3.13I**, and **Fig.3.14D**). Similarly, thymocytes,

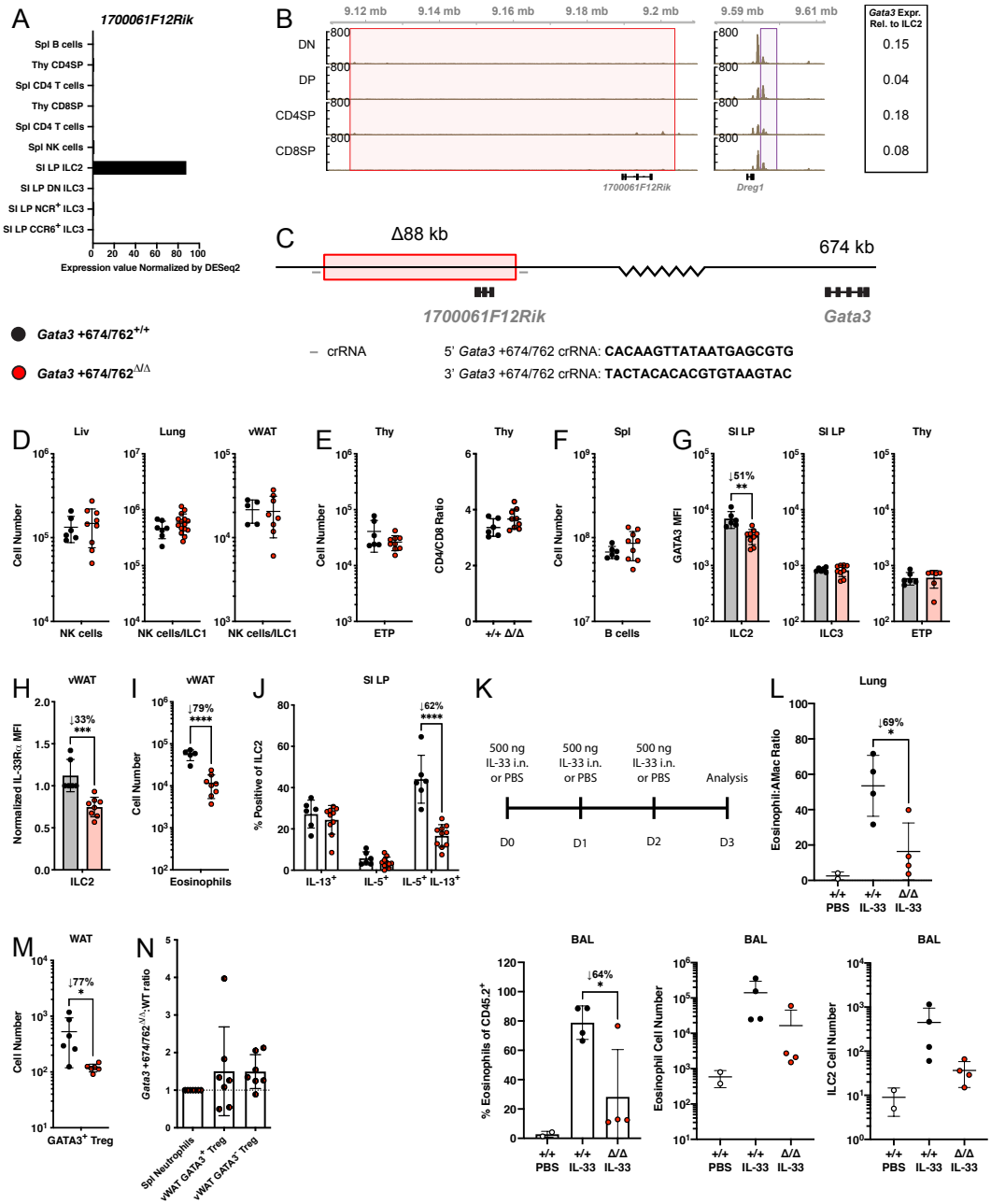

Figure 3.14: Deletion of *Gata3* +674/762 and profiling of immune cells, related to Figure 1 and 2. (**A**) *1700061F12Rik* expression data in the indicated populations from Immgen.[194] (**B**) Zoomed in ATAC-seq accessibility coverage tracks for the *Gata3* +674/762 and *Gata3* +278/285 regions in double negative (DN), double positive (DP), CD4SP, and CD8 single positive (CD8SP) thymocytes. Expression levels of *Gata3*-Citrine relative to lung ILC2 are shown to the right of (B).[172] (**C**) CRISPR/Cas9 deletion strategy for *Gata3* +674/762 with crRNA sequences. Summary data of cell numbers for (**D**) liver NK cells, lung NK/ILC1, and vWAT NK/ILC1; (**E**) ETPs and CD4/CD8 thymocyte ratio; and (**F**) splenic B cells. (**G**) Summary bar graphs of GATA3 MFI in SI LP ILC2, SI LP ILC3, and ETPs. (**H**) Summary bar graph

Figure 3.14, continued of normalized IL-33Rα MFI on vWAT ILC2. (**I**) Summary data of vWAT eosinophil cell numbers. (**J**) Summary data for frequency of IL-5 and IL-13 cytokine production from SI LP ILC2s stimulated *in vitro* with PMA and ionomycin for 4 hours. (**K**) Schematic for i.n. challenge with IL-33. (**L**) Summary data for eosinophils in the lung and BAL and ILC2 numbers in the BAL from IL-33 challenged mice. (**M**) Summary data of GATA3^{+} Treg cell numbers in the vWAT. (**N**) *Gata3* +674/762$^{\Delta/\Delta}$:WT reconstitution ratio for the indicated populations in mixed bone marrow chimeric mice. Dots represent individual mice; n ranging from 4-15 in different groups pooled from multiple independent experiments; data are presented as mean ± SEM. Statistical comparison was performed via unpaired t-test or multiple unpaired t-test. *, P < 0.05; **, P < 0.01; ***, P < 0.001; ****, P < 0.0001.

splenic T cells, and splenic B cells were also unaltered in the absence of *Gata3* +674/762 (**Fig.3.13J**, **3.13K**, **Fig.3.14E**, and **3.14F**). Taken together, these results indicate a specific reliance on the *Gata3* +674/762 region in ILC2s, which coincides with regional chromatin accessibility and heightened *Gata3* expression, that was not observed in other *Gata3* expressing cells at homeostasis. Hereafter we will refer to the deleted 88 kb region as the type 2-specific *Gata3* enhancer (*Gata3* +674/762).

3.2.4.2 ILC2s bearing a deletion of *Gata3* +674/762 are functionally impaired at homeostasis

We next evaluated the differentiation and function of residual ILC2s at homeostasis in mice lacking the *Gata3* +674/762 region. We found that *Gata3* +674/762$^{\Delta/\Delta}$ mature ILC2s expressed 50-60% less GATA3 than WT littermate ILC2s in the lung and SI LP, while SI LP ILC3s, CD4SP thymocytes, and ETPs showed no reduction in GATA3 expression (**Fig.3.16A** and **Fig.3.14G**). As GATA3 expression was significantly diminished in *Gata3* +674/762$^{\Delta/\Delta}$ ILC2s, we then examined the expression of several GATA3 target genes. The surface receptor IL-33Rα is expressed by ILC2s in peripheral tissues, such as the lung and vWAT, and its expression is regulated by GATA3 in both ILC2s and Th2 cells.[121,198,199] Relative to WT littermate controls, lung and vWAT ILC2s from *Gata3* +674/762$^{\Delta/\Delta}$ mice displayed 28-33% lower levels of surface IL-33Rα (**Fig.3.16B** and **Fig.3.14H**). GATA3 binds to several *cis*-regulatory elements within the *Il4/Il5/Il13* cytokine locus in ILC2s and Th2 cells to control locus accessibility and gene expression.[121,159,200–203] Basal production of IL-

5 by ILC2s underlies the homeostatic recruitment and maintenance of eosinophils in several tissues.[28,41] In both the lung and vWAT, eosinophil numbers were reduced 61-79% in *Gata3* $+674/762^{\Delta/\Delta}$ mice compared to WT littermate controls (**Fig.3.16C** and **Fig.3.14I**). Diminished numbers of eosinophils could result from a combined effect of reduced ILC2 numbers

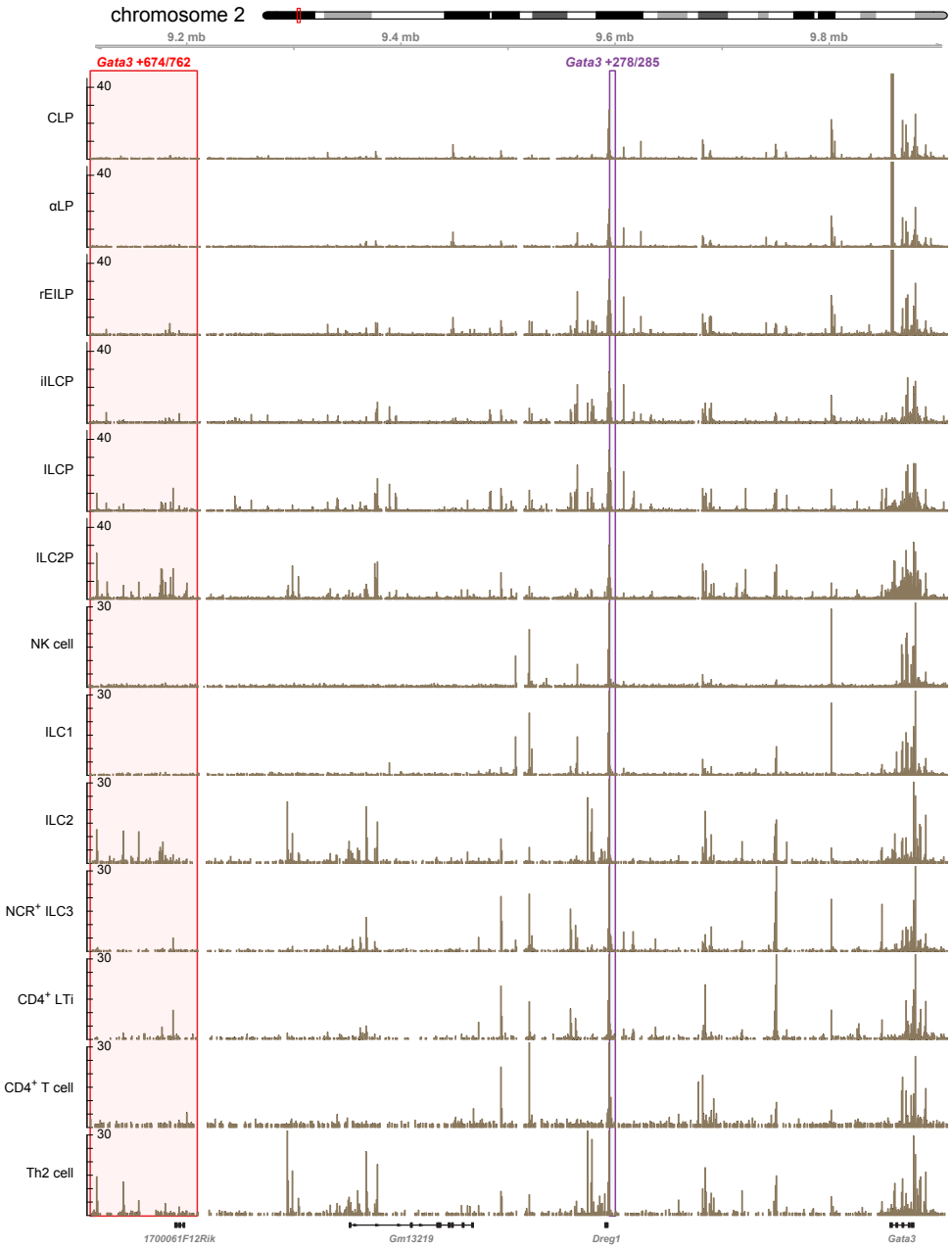

Figure 3.15: Chromatin accessibility at the *Gata3* locus. ATAC-seq accessibility coverage tracks in BM CLP, αLP, rEILP, iILCP, ILCP, ILC2P, NK cell, ILC1, ILC2, NCR^+ ILC3, $CD4^+$ LTi, $CD4^+$ T cell, and Th2 cell.[179] Red and purple windows represent *Gata3* +674/762 and *Gata3* +278/285 regions respectively.

and an impaired capacity to sense local IL-33; therefore, we addressed the intrinsic capacity of ILC2s to produce type 2 cytokines *ex vivo*. ILC2s haplo-insufficient for GATA3 produce less IL-5 and IL-13 than their WT counterparts.[159] Indeed, ILC2s from the lung and SI LP of *Gata3* $+674/762^{\Delta/\Delta}$ mice, which expressed ∼50% less GATA3, contained 64% fewer IL-5/IL-13 double-producers when stimulated *ex vivo* with phorbol myristate acetate (PMA) and ionomycin (**Fig.3.16D** and **Fig.3.14J**). In sum, the aforementioned results indicate that deletion of the *Gata3* +674/762 locus massively and globally impairs the frequency, differentiation, and function of ILC2s at homeostasis.

To ascertain the functional deficiency of *Gata3* $+674/762^{\Delta/\Delta}$ ILC2s *in vivo*, we applied a 3-day regimen of type 2 pulmonary inflammation via intranasal (i.n.) administration of IL-33 (**Fig.3.14K**).[137,204] Using this model, we found that eosinophilia was reduced in the lung and bronchoalveolar lavage (BAL) in *Gata3* $+674/762^{\Delta/\Delta}$ mice, and infiltration of ILC2s into the bronchoalveolar space did not reach levels seen in WT littermate mice (**Fig.3.14L**). Thus, the inflammatory response to i.n. IL-33 administration is impaired in *Gata3* $+674/762^{\Delta/\Delta}$ mice, likely a combined result of diminished ILC2 numbers and function.

To determine whether the observed reduction in ILC2s in *Gata3* $+674/762^{\Delta/\Delta}$ mice was cell intrinsic, we used congenically marked mice to generate mixed bone marrow chimeras containing a 50:50 ratio of *Gata3* $+674/762^{\Delta/\Delta}$ and WT bone marrow (**Fig.3.16E**). Following 6 weeks of reconstitution, ILC2s of *Gata3* $+674/762^{\Delta/\Delta}$ origin were outcompeted 1:7 in the BM, 1:11 in the lung and vWAT, and 1:14 in the SI LP by WT ILC2s (**Fig.3.16F**). In contrast, group 1 and 3 ILCs as well as eosinophils, B cells, and T cells showed comparable reconstitution between *Gata3* $+674/762^{\Delta/\Delta}$ and WT cells. From these results, we conclude that the *Gata3* +674/762 region is intrinsically required to achieve normal numbers of ILC2s.

A subset of regulatory T (Treg) cells normally present within the adipose tissue express a type 2-like program characterized by the expression of GATA3 and IL-33Rα.[28,205,206] At

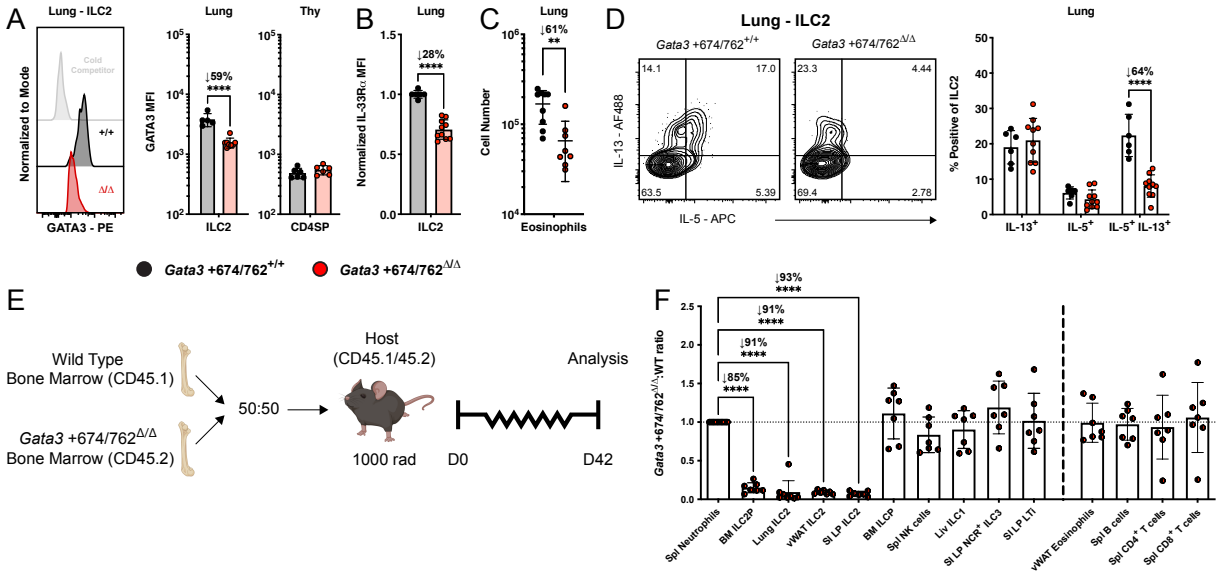

Figure 3.16: Impact of *Gata3* +674/762 deletion on homeostatic ILC2 function. (**A**) Representative histogram and summary bar graph of GATA3 median fluorescent intensity (MFI) in lung ILC2 and summary bar graph for CD4SP thymocytes. White histogram denotes lung ILC2 GATA3 stain blocked with unlabeled antibody (cold competitor). (**B**) Summary bar graph of normalized IL-33Rα MFI on lung ILC2. (**C**) Summary data of lung eosinophil cell numbers. (**D**) Representative flow cytometry plots and summary data for frequency of IL-5 and IL-13 cytokine production from lung ILC2s (pre-gated on CD45.2$^+$CD19$^-$CD11c$^-$CD3ϵ^-TCRβ^-IL-7Rα^+CD90.2$^+$CD25$^+$IL-33Rα^+) stimulated *in vitro* with PMA and ionomycin for 4 hours. (**E**) Schematic for establishing congenically marked mixed bone marrow chimeric mice. (**F**) *Gata3* +674/762$^{\Delta/\Delta}$:WT reconstitution ratio for the indicated populations in mixed bone marrow chimeric mice. Dots represent individual mice; n ranging from 6-10 in different groups pooled from multiple independent experiments; data are presented as mean ± SEM. Statistical comparison was performed via unpaired t-test, multiple unpaired t-test, or one-way ANOVA. **, P < 0.01; ****, P < 0.0001.

homeostasis, we observed a 77% reduction in GATA3$^+$ Treg cells from *Gata3* +674/762$^{\Delta/\Delta}$ mice compared to WT littermate controls (**Fig.3.14M**). Furthermore, this defect appeared to be cell-extrinsic, as it was corrected in mixed (*Gata3* +674/762$^{\Delta/\Delta}$:WT) bone marrow chimeras (**Fig.3.14N**). Given that vWAT GATA3$^+$ Treg cells proliferate in response to IL-33[206], and adventitial stromal cells produce IL-33 in response to IL-13 from ILC2s[33], the homeostatic defect in the vWAT may be secondary to the ILC2 defect in *Gata3* +674/762$^{\Delta/\Delta}$ mice.

3.2.4.3 *Gata3* +278/285 regulates pan-ILC development before differentiation

The previously identified enhancer, *Gata3* +278/285, was shown to control the development and persistence of T cells at homeostasis; however, the contribution of *Gata3* +278/285 to *Gata3* expression within the ILC lineage was not explored.[162,163] To characterize the impact of *Gata3* +278/285 on ILC development and function, we generated mice deficient in *Gata3* +278/285 via CRISPR/Cas9-mediated deletion (**Fig.3.17A**). Similar to *Gata3* +674/762$^{\Delta/\Delta}$ mice, *Gata3* +278/285$^{\Delta/\Delta}$ mice showed a dramatic reduction in the number of ILC2P in the BM and ILC2 in the lung and SI LP compared to WT littermate controls (**Fig.3.17B-D**). However, in contrast with *Gata3* +674/762$^{\Delta/\Delta}$, *Gata3* +278/285 deletion also had a broad impact on other ILCs. In the spleen, liver, and lung of *Gata3* +278/285$^{\Delta/\Delta}$ mice, group 1 ILCs were diminished, while ILC3 were overrepresented in the SI LP, possibly a result of an expanded niche from the loss of SI LP ILC2s (**Fig.3.17E** and **Fig.3.17F**).[61] Consistent with initial observations in *Gata3* +278/285$^{\Delta/\Delta}$ mice, CD4SP T cells were considerably underrepresented in the spleen and in the thymus, causing an inversion of the CD4/CD8 ratio (**Fig.3.17G** and **Fig.3.17H**).[163] Splenic B cell numbers were unaffected by the deletion of *Gata3* +278/285$^{\Delta/\Delta}$ (**Fig.3.17I**). Taken together, these results indicate a general reliance on *Gata3* +278/285 for the development or homeostatic maintenance of GATA3-expressing ILCs and CD4^{+} T cells.

We next assessed the impact of *Gata3* +278/285 deletion on the expression of GATA3 and GATA3 target genes. In striking contrast with *Gata3* +674/762$^{\Delta/\Delta}$ mice, the residual mature ILC2s in the lung and SI LP of *Gata3* +278/285$^{\Delta/\Delta}$ mice expressed unaltered levels of GATA3 compared to WT littermate ILC2s (**Fig.3.17J**). Conversely, GATA3 expression in ETPs and CD4SP thymocytes was diminished in *Gata3* +278/285$^{\Delta/\Delta}$ mice, in line with the previous publication.[163] Further contrasting observations made in *Gata3* +674/762$^{\Delta/\Delta}$ mice, IL-33Rα expression on the residual *Gata3* +278/285$^{\Delta/\Delta}$ lung ILC2s and expression

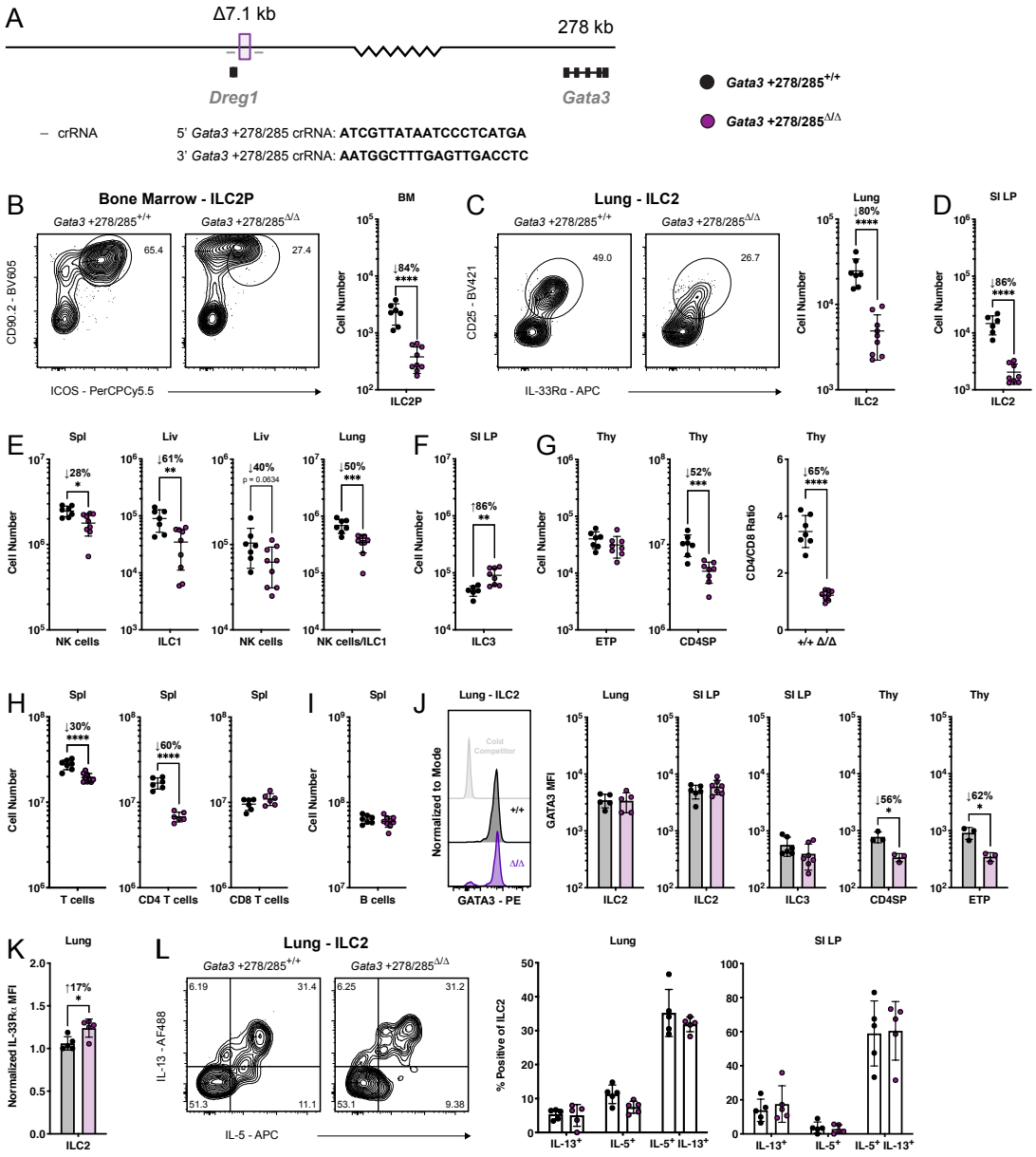

Figure 3.17: Deletion of *Gata3* +278/285 and profiling of lymphocyte subsets and homeostatic ILC2 function. (**A**) CRISPR/Cas9 deletion strategy for *Gata3* +278/285 with crRNA sequences. Representative flow cytometry plots and summary data of cell numbers in WT vs. *Gata3* +278/285$^{\Delta/\Delta}$ mice for (**B**) BM ILC2P (pre-gated on Lin$^-\alpha4\beta7^+$IL-7Rα^+) and (**C**) lung ILC2 (pre-gated on CD45.2$^+$CD19$^-$CD11c$^-$CD3ϵ^-TCRβ^-IL-7Rα^+CD90.2$^+$). Summary data of cell numbers for (**D**) SI LP ILC2; (**E**) spleen NK cells, liver ILC1, liver NK cells, and lung NK/ILC1; (**F**) SI LP ILC3; (**G**) ETPs, CD4SP thymocytes, and CD4/CD8 thymocyte ratio; (**H**) splenic T cells and split CD4$^+$ and CD8$^+$ T cells, and (**I**) splenic B cells in WT vs. *Gata3* +278/285$^{\Delta/\Delta}$ mice. (**J**) Representative histogram and summary bar graph of GATA3 MFI in lung ILC2 and summary bar graph for SI LP ILC2, SI LP ILC3, CD4SP thymocytes, and ETPs. White histogram denotes lung ILC2 GATA3 stain blocked with unlabeled antibody (cold competitor).

Figure 3.17, continued. (**K**) Summary bar graph of normalized IL-33Rα MFI on lung ILC2. (**L**) Representative flow cytometry plots of lung ILC2s (pre-gated on CD45.2$^+$CD19$^-$CD11c$^-$CD3ϵ^-TCRβ^-IL-7Rα^+CD90.2$^+$CD25$^+$IL-33Rα^+) and summary data for frequency of IL-5 and IL-13 cytokine production from lung ILC2s and SI LP ILC2s stimulated *in vitro* with PMA and ionomycin for 4 hours. Dots represent individual mice; n ranging from 3-9 in different groups pooled from multiple independent experiments; data are presented as mean ± SEM. Statistical comparison was performed via unpaired t-test or multiple unpaired t-test. *, P < 0.05; **, P < 0.01; ***, P < 0.001; ****, P < 0.0001.

of IL-5 and IL-13 from stimulated *Gata3* +278/285$^{\Delta/\Delta}$ lung and SI LP ILC2s were also unaltered compared with that of WT littermate ILC2s (**Fig.3.17K** and **Fig.3.17L**). Collectively, these results demonstrate a differential impact for *Gata3* +278/285 and *Gata3* +674/762, with the former contributing more globally to the low/medium level of GATA3 expression during the development of ILCs and T cells and the latter specifically regulating elevated levels of GATA3 expression and acquisition of the type 2 helper effector program in ILC2s. Notably these findings correlate with the temporal pattern of accessibility of these enhancers and the relative expression of *Gata3* in the different lymphocyte subsets (**Fig.3.13B**, **3.13C**, and **Fig.3.14B**).[172]

3.2.4.4 *Gata3* +674/762$^{\Delta/\Delta}$ mice have an impaired type 2 inflammatory response

Th2 cells, like ILC2s, upregulate GATA3 above their undifferentiated CD4$^+$ counterparts[156,162], and may similarly depend on *Gata3* +674/762 for this enhanced expression. Rapid challenge with IL-33 in the absence of protein antigen precludes any significant contribution of Th2 cells to type 2 pulmonary inflammation.[137] To broadly assess the impact of *Gata3* +674/762 deletion *in vivo*, we used two experimental models of type 2 airway inflammation, which elicit both ILC2 and Th2 cell responses. First, we applied a 14-day protocol of intratracheal (i.t.) allergen sensitization and challenge using house dust mite (HDM) extract (**Fig.3.18A**).[204] Following HDM challenge on days 7-10, *Gata3* +674/762$^{\Delta/\Delta}$ mice exhibited 60-78% diminished eosinophilia in the lung and BAL, while maintaining a 94-96% reduction in ILC2 numbers (**Fig.3.18B**, **3.18C**, **Fig.3.19A**, and **Fig.3.19B**). Unlike studies at

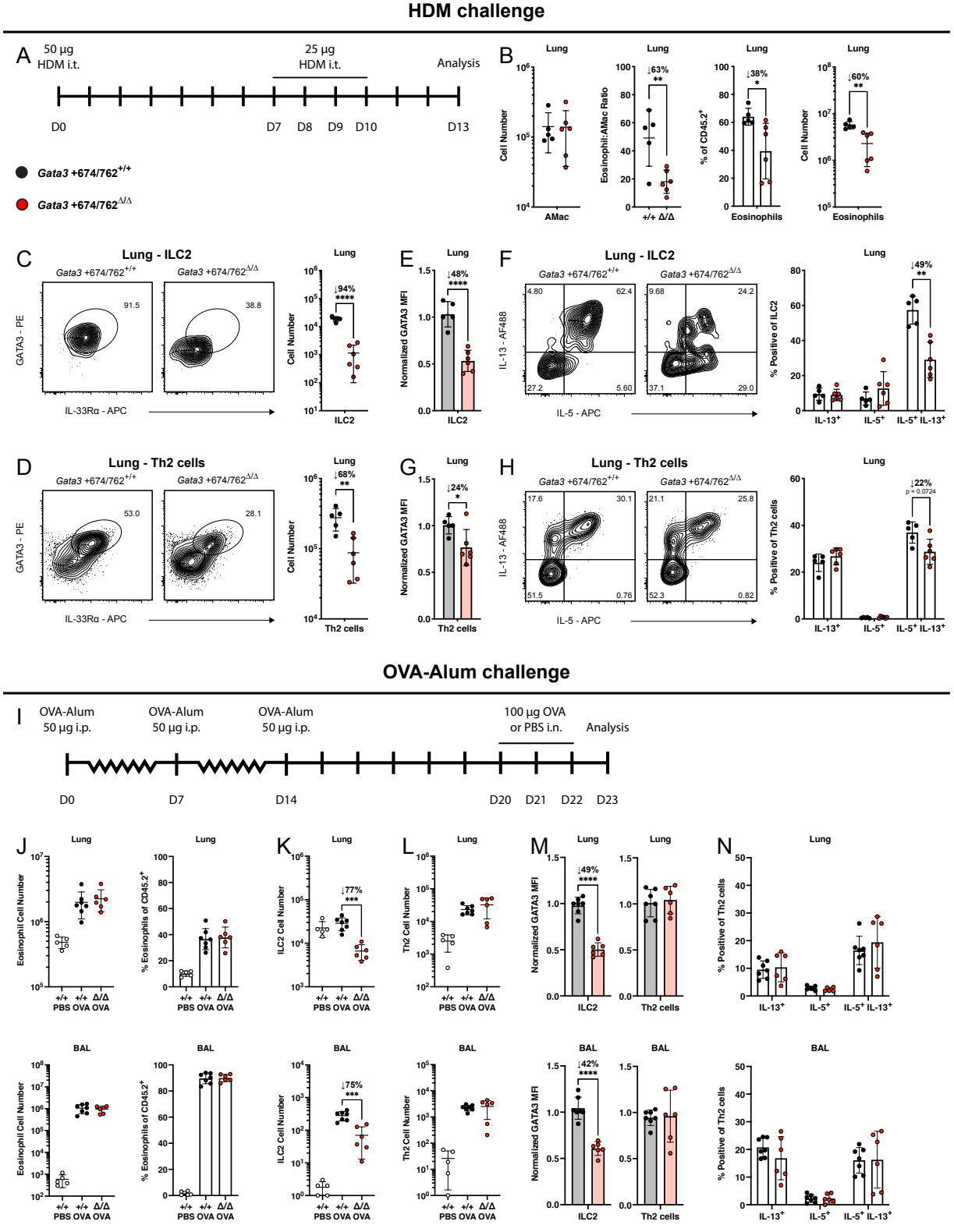

Figure 3.18: Impact of *Gata3* +674/762 deletion on allergic airway inflammation.

Figure 3.18, continued. (**A**) Schematic for i.t. sensitization and challenge with HDM extract. (**B**) Representative flow cytometry plot and summary data for alveolar macrophages (AMac) and eosinophils in the lung of HDM challenged mice. Representative flow cytometry plots and summary data of (**C**) ILC2 (pre-gated on CD45.2$^+$CD19$^-$CD11c$^-$CD3ϵ^-TCRβ^-IL-7Rα^+CD90.2$^+$CD25$^+$) and (**D**) Th2 cell (pre-gated on CD45.2$^+$CD3ϵ^+TCRβ^+CD90.2$^+$CD4$^+$) numbers in the lung. (**E**) Summary plots of GATA3 MFI in lung ILC2. (**F**) Representative flow cytometry plots and summary data for frequency of IL-5 and IL-13 cytokine production from lung ILC2s (pre-gated on CD45.2$^+$CD19$^-$CD11c$^-$CD3ϵ^-TCRβ^-IL-7Rα^+CD90.2$^+$CD25$^+$IL-33Rα^+) stimulated *in vitro* with PMA and ionomycin for 4 hours. (**G**) Summary plots of GATA3 MFI in lung Th2 cells. (**H**) Representative flow cytometry plots and summary data for frequency of IL-5 and IL-13 cytokine production from lung Th2 cells (pre-gated on CD45.2$^+$CD3ϵ^+TCRβ^+CD90.2$^+$CD4$^+$IL-33Rα^+) stimulated *in vitro* with PMA and ionomycin for 4 hours. (**I**) Schematic of the OVA-Alum model for induction of allergic airway inflammation via i.p. immunization with OVA-Alum and subsequent i.n. challenge with OVA. (**J**) Summary data for eosinophils in the lung and BAL of OVA-Alum challenged mice. Summary data of (**K**) ILC2 and (**L**) Th2 cell numbers in the lung and BAL. (**M**) Summary plots of GATA3 MFI in ILC2s and Th2 cells from the lung and BAL. (**N**) Summary data for frequency of IL-5 and IL-13 cytokine production from lung Th2 cells stimulated *in vitro* with PMA and ionomycin for 4 hours. Dots represent individual mice; n = 5 or 6 (HDM) and n = 7 or 6 (OVA-Alum) for WT or *Gata3* +674/762$^{\Delta/\Delta}$ mice. Data is pooled from multiple independent experiments and presented as mean ± SEM. Values of 0 were converted to a value of 1 on a log-scale. Statistical comparison was performed via unpaired t-test or multiple unpaired t-test. *, $P < 0.05$; **, $P < 0.01$; ***, $P < 0.001$; ****, $P < 0.0001$.

homeostasis, this model also permitted the assessment of Th2 cell generation and function, demonstrating a 68-86% impaired Th2 cell differentiation and infiltration in both the lung and BAL compared to WT littermate controls (**Fig.3.18D** and **Fig.3.19C**). Furthermore, like ILC2s, GATA3 expression and the frequency of IL-5/IL-13 double-producers were lower in *Gata3* +674/762$^{\Delta/\Delta}$ Th2 cells (**Fig.3.18E-H**, **Fig.3.19D**, and **Fig.3.19E**). Notably, however, the degree of reduction in each of these parameters was much less pronounced in Th2 cells compared to ILC2s: e.g., 94% vs. 68% for cell number, 48% vs. 24% for GATA3 expression, and 49% vs. 22% for IL-5/IL-13 double producers in lung ILC2s vs. lung Th2 cells respectively. Thus, while ILC2s were drastically impaired in both number and function, relatively large numbers of Th2 cells were preserved with near normal function. Together these results explain why hallmarks of allergic inflammation were only partially compromised, including a 60% decrease in lung eosinophilia (**Fig.3.18B**), and unaltered bronchial goblet cell hyperplasia (**Fig.3.19F**).

We confirmed the conclusions made in the HDM challenge model by employing a second model of type 2 inflammation using the helminth *Strongyloides venezuelensis*. From the site of subcutaneous (s.c.) infection, *S. venezuelensis* migrates through the lung where it

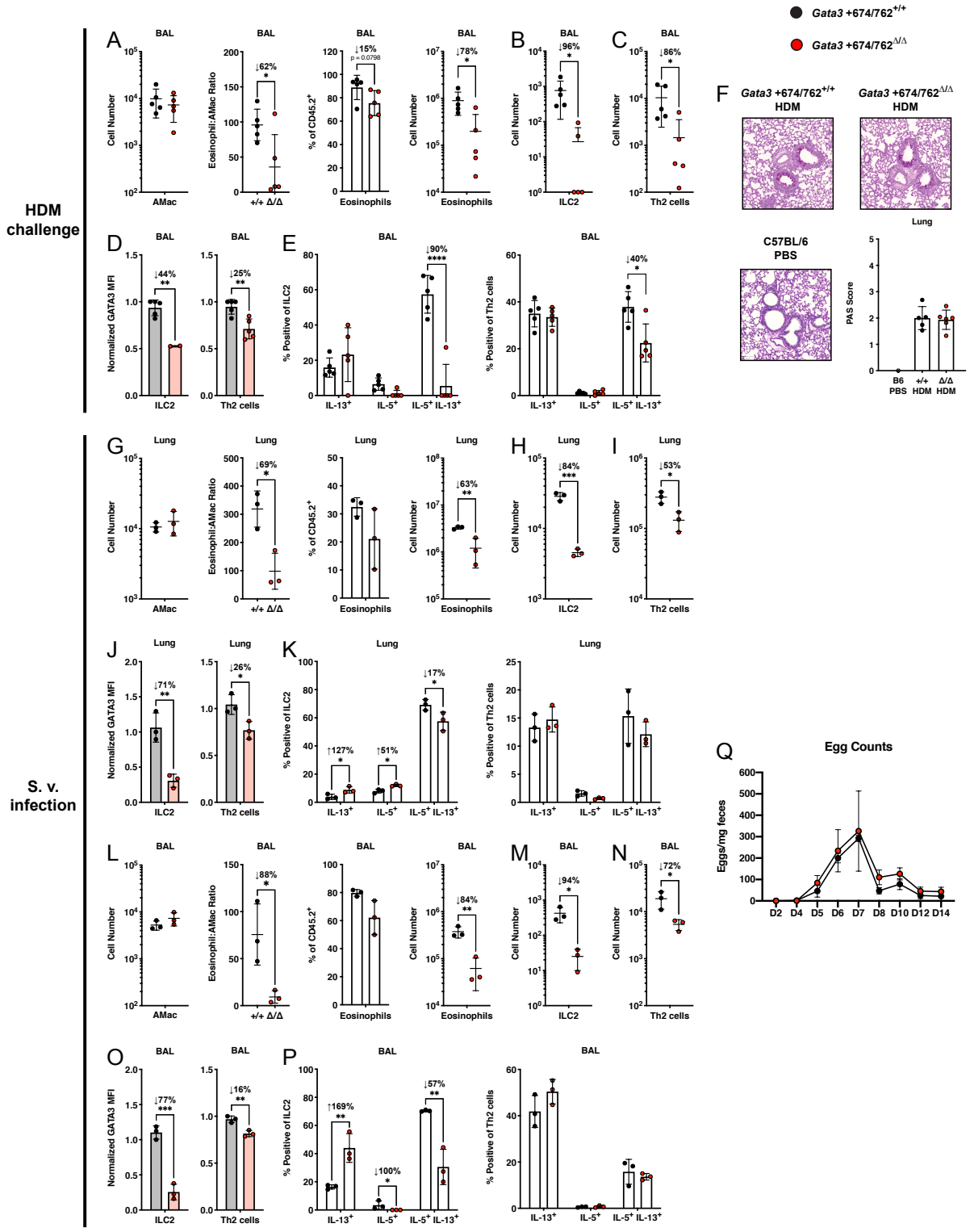

Figure 3.19: Response of *Gata3* +674/762$^{\Delta/\Delta}$ mice to type 2 inflammatory challenge, related to Figure 3.

Figure 3.19, continued. (**A**) Summary data for AMac and eosinophils in the BAL of HDM challenged mice. Summary data of (**B**) ILC2 and (**C**) Th2 cell numbers in the BAL from HDM challenged mice. (**D**) Summary plots of GATA3 MFI in BAL ILC2s and Th2 cells from HDM challenged mice. (**E**) Summary data for frequency of IL-5 and IL-13 cytokine production from BAL ILC2s and Th2 cells from HDM challenged mice stimulated *in vitro* with PMA and ionomycin for 4 hours. (**F**) PAS staining of lung sections at 40X magnification with summary bar graph of PAS scores. (**G**, **L**) Summary data for AMac and eosinophils in the lung or BAL from *S. venezuelensis* challenged mice. Summary data of (**H**, **M**) ILC2 and (**I**, **N**) Th2 cell numbers in the lung or BAL from *S. venezuelensis* challenged mice. (**J**, **O**) Summary bar graphs of GATA3 MFI in lung and BAL ILC2s and Th2 cells from *S. venezuelensis* challenged mice. (**K**, **P**) Summary data for frequency of IL-5 and IL-13 cytokine production from lung or BAL ILC2s and Th2 cells from *S. venezuelensis* challenged mice stimulated *in vitro* with PMA and ionomycin for 4 hours. (**Q**) Time course of *S. venezuelensis* egg counts in the feces of infected mice. Dots represent individual mice; data are pooled from multiple independent experiments (HDM; n = 5) or one experiment (*S. venezuelensis*; n = 3); data are presented as mean ± SEM. Values of 0 were converted to a value of 1 on a log-scale. Statistical comparison was performed via unpaired t-test or multiple unpaired t-test. *, $P < 0.05$; **, $P < 0.01$; ***, $P < 0.001$.

induces a type 2 inflammatory response via activation of ILC2s and Th2 cells before eventual maturation in the duodenum of the small intestine and clearance within ∼2 weeks in mice with a functional adaptive immune system.[193,207,208] Subsequent to the resolution of helminth infection, *Gata3* $+674/762^{\Delta/\Delta}$ mice showed weaker eosinophilia (63-84%); decreased numbers of ILC2s (84-94%) with lower expression of GATA3 (71-77%) and dual production of IL-5/IL-13 (17-57%); and blunted Th2 cell differentiation and/or infiltration (53-72%) with lower GATA3 expression (16-26%) in both the lung and BAL (**Fig.3.19G-P**). As with the HDM challenge model, the impact of *Gata3* +674/762 deletion on Th2 cells was markedly less pronounced than on ILC2s in both the lung and BAL following *S. venezuelensis* infection. These results, and the persistence of some residual ILC2s, may explain why the time-course of helminth clearance was similar in *Gata3* $+674/762^{\Delta/\Delta}$ mice compared to WT littermates (**Fig.3.19Q**). In sum, the type 2 inflammatory response following exposure to HDM extract and *S. venezuelensis* infection is defective in *Gata3* $+674/762^{\Delta/\Delta}$ mice, and the defect is more pronounced in ILC2s compared with Th2 cells.

Lastly, we used a third model of type 2 pulmonary inflammation, based on antigen adjuvanted allergen challenge via intraperitoneal (i.p.) systemic ovalbumin (OVA)-Alum administration followed by i.n. challenge with OVA (**Fig.3.18I**). The rationale for this additional model was that, unlike HDM and *S. venezuelensis*, OVA-Alum induced allergic airway inflammation was previously suggested to be largely independent of ILC2s.[137,191] Strikingly,

in contrast with HDM and *S. venezuelensis* challenged mice, the extent of eosinophilia in the lung and BAL was comparable between WT littermate and *Gata3* +674/762$^{\Delta/\Delta}$ mice treated with the OVA-Alum protocol (**Fig.3.18J**). Furthermore, despite the persistent reduction in cell numbers (∼75%) and GATA3 expression (∼45%) by ILC2s, Th2 cells showed unaltered expansion, differentiation, infiltration, GATA3 expression, and type 2 cytokine production in the lung and BAL of OVA-Alum treated *Gata3* +674/762$^{\Delta/\Delta}$ mice compared with WT littermate mice (**Fig.3.18K-N**). These results not only support prior observations that ILC2s are largely dispensable in the systemic OVA-Alum model, but also demonstrate that *Gata3* +674/762$^{\Delta/\Delta}$ Th2 cells are fully capable of eliciting a normal, robust type 2 inflammatory response.

3.2.4.5 *Gata3* +674/762$^{\Delta/\Delta}$ mice exhibit a profound cell-intrinsic ILC2 defect and a modest, partially cell-extrinsic Th2 cell defect

In *Gata3* +674/762$^{\Delta/\Delta}$ mice, extrinsic factors could contribute to the impaired differentiation and response of Th2 cells to HDM challenge and *S. venezuelensis* infection. Though CD4^{+} T cell numbers were normal and did not require *Gata3* +674/762 at homeostasis or in competition with WT cells (**Fig.3.13I** and **Fig.3.16F**), the deficiency in ILC2 numbers and early type 2 cytokine production in *Gata3* +674/762$^{\Delta/\Delta}$ mice may hinder the proper priming and progression of an adaptive type 2 response.[137,191–193] To address this possibility, we evaluated the intrinsic differentiation capacity of *Gata3* +674/762$^{\Delta/\Delta}$ Th2 cells through a competitive (*Gata3* +674/762$^{\Delta/\Delta}$:WT) mixed bone marrow chimera model where mice were sensitized and challenged i.t. with HDM extract (**Fig.3.20A**). In this model, the differentiation of *Gata3* +674/762$^{\Delta/\Delta}$ Th2 cells occurs in the presence of a WT ILC2 compartment, permitting an assessment of the intrinsic type 2 differentiation capability of WT and *Gata3* +674/762$^{\Delta/\Delta}$ CD4^{+} T cells. As expected from unchallenged mixed bone marrow chimeras, the reconstitution frequency of *Gata3* +674/762$^{\Delta/\Delta}$ and WT eosinophils and

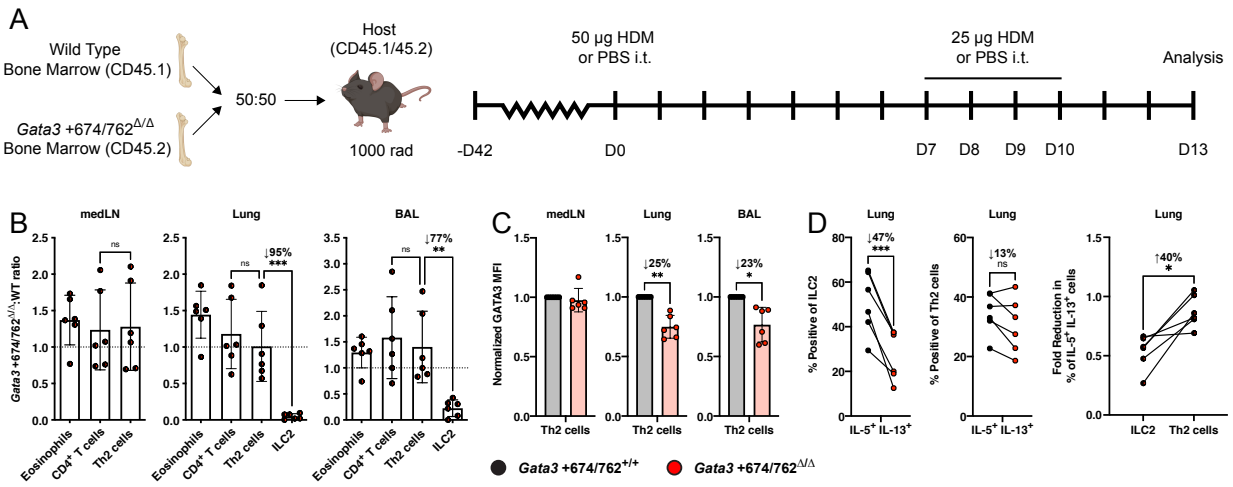

Figure 3.20: Cell-intrinsic impact of *Gata3* +674/762 deletion on Th2 cell differentiation and function. (**A**) Schematic for HDM-induced allergic airway inflammation in congenically marked mixed bone marrow chimeras. (**B**) *Gata3* +674/762$^{\Delta/\Delta}$:WT reconstitution ratio for the indicated populations in the medLN, lung, and BAL from HDM treated mixed bone marrow chimeric mice. (**C**) Summary plots of GATA3 MFI in medLN, lung, and BAL Th2 cells. (**D**) Summary data for frequency of IL-5/IL-13 cytokine double producers from lung ILC2s and Th2 cells, and summary data showing the pairwise comparison of the fold reduction in the frequency of IL-5/IL-13 cytokine double producers for lung ILC2s (*Gata3* +674/762$^{\Delta/\Delta}$:WT) vs. lung Th2 cells (*Gata3* +674/762$^{\Delta/\Delta}$:WT) in mixed bone marrow chimeras. Dots represent individual mice; n = 6 for mixed bone marrow chimeras and data is pooled from multiple independent experiments; data are presented as mean ± SEM. Values of 0 were converted to a value of 1 on a log-scale. Statistical comparison was performed via paired t-test or one-way ANOVA. *, P < 0.05; **, P < 0.01; ***, P < 0.001.

CD4$^+$ T cells was equivalent while ILC2s from *Gata3* +674/762$^{\Delta/\Delta}$ BM were profoundly outcompeted 1:20 in the lung and 1:4 in the BAL by WT ILC2s (**Fig.3.20B**). In contrast to ILC2s however, differentiated Th2 cells of both genotypes were equally represented in the mediastinal lymph node (medLN), lung, and BAL. Nevertheless, *Gata3* +674/762$^{\Delta/\Delta}$ Th2 cells expressed ∼25% lower levels of GATA3 in the lung and BAL (**Fig.3.20C**). Furthermore, while *Gata3* +674/762$^{\Delta/\Delta}$ ILC2s were intrinsically and profoundly deficient in their ability to produce both IL-5 and IL-13 (47% reduction compared to WT ILC2s), Th2 cells exhibited only a minor non-significant defect (13% reduction compared to WT Th2 cells) (**Fig.3.20D**). When the deficiency in ILC2 and Th2 cell cytokine production was directly evaluated in a pair-wise comparison, *Gata3* +674/762$^{\Delta/\Delta}$ ILC2s were found to be significantly more impaired than *Gata3* +674/762$^{\Delta/\Delta}$ Th2 cells (40% lower than Th2 cells). Taken together, these findings support the conclusion of a predominant and profound cell-intrinsic

impact of *Gata3* +674/762 deletion on ILC2 function and a modest, largely cell-extrinsic impact on Th2 cells that may be secondary to ILC2 dysfunction. This interpretation is also consistent with the preserved Th2 cell frequency and function in the ILC2-independent model of OVA:Alum allergic inflammation.

3.2.4.6 Characterization of *Gata3* +761/762, a regulatory element recapitulating *Gata3* regulation in ILC2s

Our results indicated that the *Gata3* +674/762 region controlled the proper differentiation and function of ILC2s and, to a minor degree, Th2 cells. To identify which elements within *Gata3* +674/762 contributed to the regulatory function, we utilized public ChIP-seq data to assess additional parameters typical of enhancer elements. Alignment of histone 3 K27 acetylation (H3K27Ac) and TF binding in ILC2s and Th2 cells, in addition to genomic conservation, revealed a top candidate sub-domain, *Gata3* +761/762, with enhancer-like characteristics in ILC2s and Th2 cells (**Fig.3.21A**, maroon window). *Gata3* +761/762 was conserved in placental mammalian genomes and its flanking regions accumulated H3K27Ac marks.[180,181] Furthermore, this segment was bound by several key type 2 lineage-determining TFs, including GATA3, BCL11B, GFI1, and STAT6, as well as other TFs such as RUNX1, RUNX3, and CBFB.[68,129,180–183] Another putative enhancer, *Gata3* +736/737, exhibited somewhat similar though markedly weaker features and did not show genomic conservation (**Fig.3.21A**, black window). Notably, neither H3K27Ac nor any of the analyzed TFs accumulated at the 1.2 kb core element of *Gata3* +278/285, *Gata3* +283/284, in mature ILC2s or differentiated Th2 cells, consistent with the distinct functions of these enhancer regions (**Fig.3.21A**, cornflower blue window). We next scanned for immune-specific TF motifs present within the *Gata3* +761/762, Gata3 +736/737, and *Gata3* +283/284 regions using the TRANSFAC database to gain insight into potential regulatory mechanisms (**Fig.3.22A**).[209] Strikingly, *Gata3* +761/762 contained a multitude of predicted GATA3 mo-

tifs, seven in total, while *Gata3* +736/737 and *Gata3* +283/284 only contained three and one GATA3 motif respectively. Enrichment for GATA3 motifs within *Gata3* +761/762 agrees

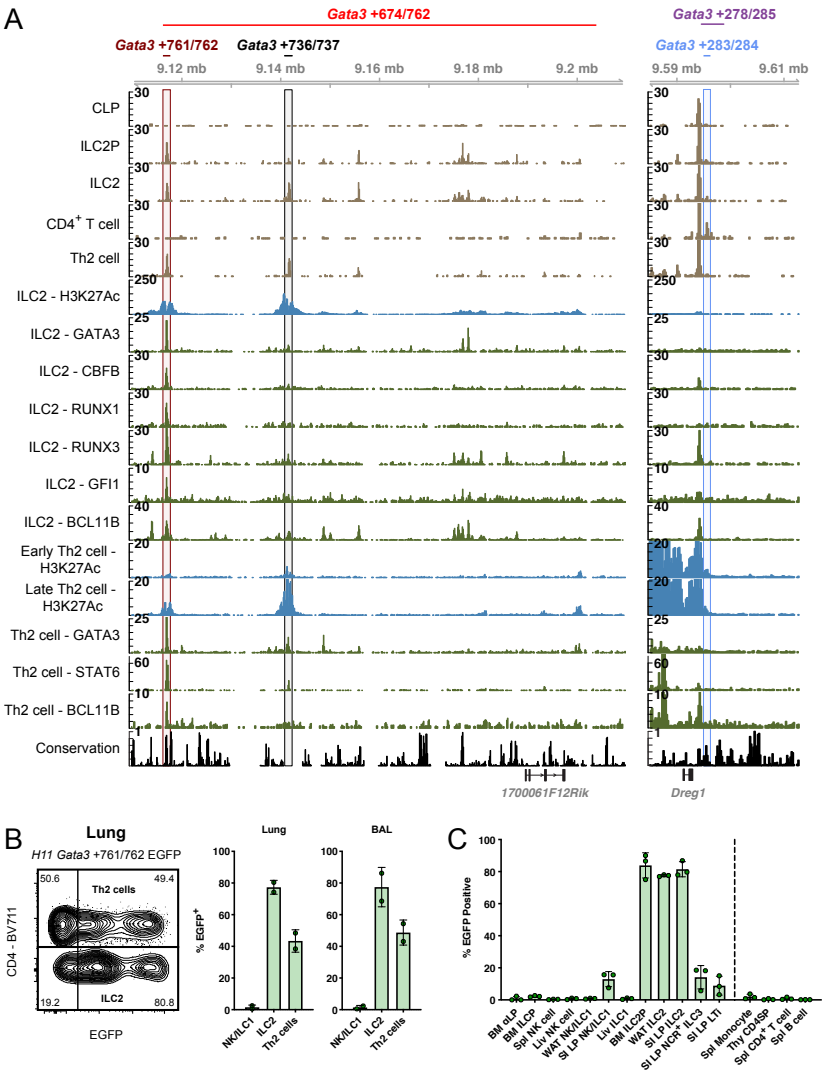

Figure 3.21: Characterization of *Gata3* +674/762, and a GATA3 binding element in *Gata3* +674/762. (**A**) ATAC-seq accessibility coverage (beige), ChIP-seq histone modification (blue), ChIP-seq transcription factor binding (green), and UCSC conservation (black) tracks for the *Gata3* +674/762 and *Gata3* +278/285 regions in the indicated populations from public sequencing data.[68,129,179–182] Maroon, black, and cornflower blue windows represent *Gata3* +761/762, *Gata3* +736/737, and *Gata3* +283/284 regions respectively. (**B**) Representative flow cytometry plot of *H11 Gata3* +761/762 EGFP reporter expression in ILC2s (pre-gated on $CD45.2^+CD19^-CD11c^-CD3\epsilon^-TCR\beta^-IL\text{-}7R\alpha^+CD90.2^+CD25^+IL\text{-}33R\alpha^+$) and Th2 cells (pre-gated on $CD45.2^+CD3\epsilon^+TCR\beta^+CD90.2^+CD4^+IL\text{-}33R\alpha^+$) from the lung following HDM challenge. Summary bar graph shows *H11 Gata3* +761/762 EGFP reporter expression in ILC2, Th2 cells and NK/ILC1 from the lung and BAL. (**C**) *H11 Gata3* +761/762 EGFP reporter expression in various lymphocyte population from different tissues as indicated. Dots represent individual mice; n ranging from 2 to 3 in one experiment from independent founder (F_0) mice; data are presented as mean ± SEM.

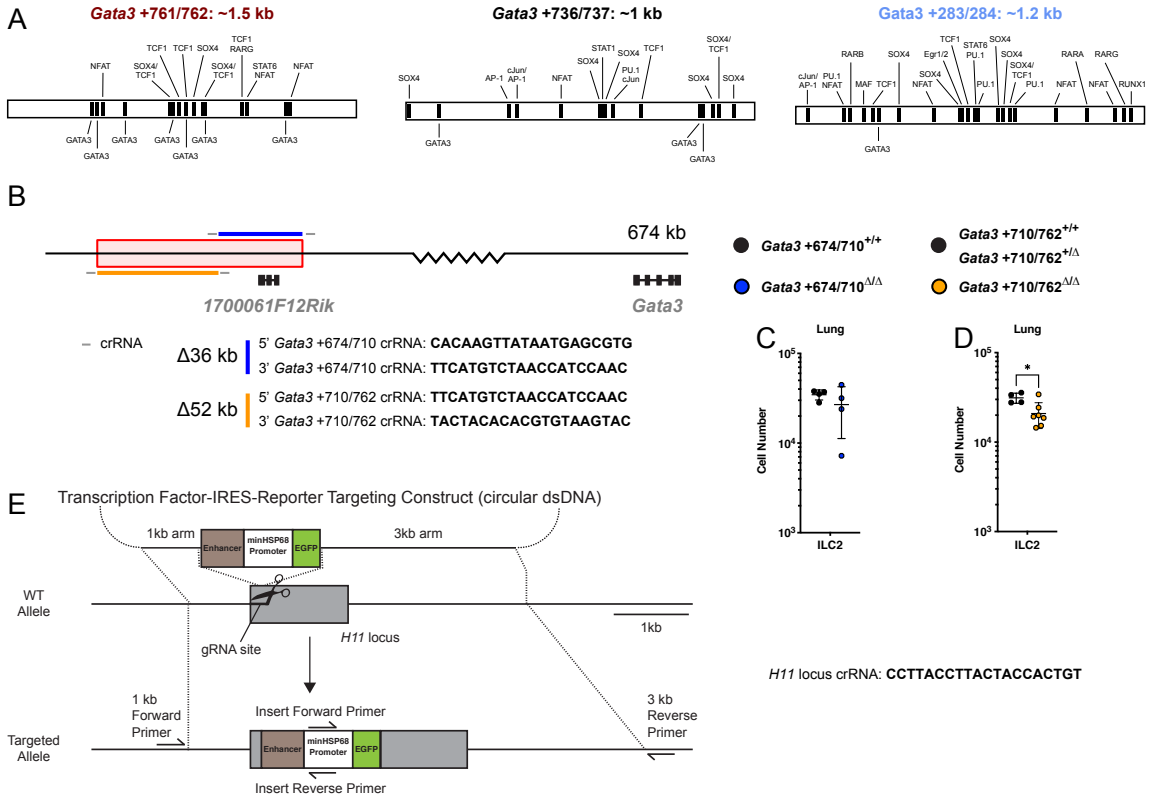

Figure 3.22: CRISPR/Cas9-mediated dissection of *Gata3* +674/762 sub-domains. (**A**) TRANSFAC predicted immune specific transcription factor binding sites for *Gata3* +761/762, *Gata3* +736/737, and *Gata3* +283/284 regions.[209] (**B**) CRISPR/Cas9 deletion strategy for *Gata3* +674/710 and *Gata3* +710/762 with crRNA sequences. Summary data of lung ILC2 numbers in WT vs. (**C**) *Gata3* +674/710$^{\Delta/\Delta}$ and (**D**) *Gata3* +710/762$^{\Delta/\Delta}$ mice. (**E**) Design of CRISPR/Cas9 knock-in strategy for enhancer reporter insertion at the *H11* locus. Dots represent individual mice; n ranging from 4 to 8 in multiple independent experiments; data are presented as mean ± SEM. *Gata3* +710/762$^{\Delta/\Delta}$ and respective control mice were pups from the cross breeding of F_0 mice.

with the observed ChIP-seq enrichment seen in ILC2s and Th2 cells (**Fig.3.21A**), suggesting a potential auto-regulatory role for GATA3 in type 2-specific *Gata3* expression.[201,210,211] In sum, these results indicate that *Gata3* +674/762, and *Gata3* +761/762 in particular, are enriched for TF binding *in vivo* and binding motifs *in silico* suggestive of type 2-specific function.

To further dissect the *Gata3* +674/762 enhancer region, we next generated deletion strains with CRISPR/Cas9 targeting (**Fig.3.22B**). However, deletion of *Gata3* +674/710 or the complementary *Gata3* +710/762 segment appeared to only marginally, or non-significantly, compromise ILC2 numbers in the lung, failing to recapitulate the magnitude of the ILC2

defect associated with the larger *Gata3* +674/762 deletion (**Fig.3.22C** and **3.22D**), indicating the presence of redundant regulatory elements, a well-established feature of many important enhancers.[212] Moreover, these results demonstrated that while lncRNA *1700061F12Rik* was expressed in ILC2s (**Fig.3.14A**), it was not necessary for ILC2 development. To determine the sufficiency of *Gata3* +761/762, the top candidate regulatory element within *Gata3* +674/762, to contribute to the regions characterized type 2-specific *Gata3* regulatory function, we generated *in vivo* enhancer reporter mice via CRISPR/Cas9-mediated integration.[172] Genomic integration of an enhancer element upstream of a minimal promoter, such as the heat shock protein 68 (HSP68) minimal promoter, has been used to track *in vivo* enhancer activity by driving the expression of Cre, lacZ, fluorescent proteins, or coding genes.[213–216] However, traditional methods used to generate transgenic mice are hampered by concerns of uncontrolled integration and multiple copy number. Site-specific integration into a safe harbor locus, such as *Rosa26* or *H11*, provides a means to control these factors while additionally increasing efficiency and minimizing time to generation.[213,217] We therefore applied a CRISPR/Cas9-mediated integration strategy to target the H11 locus (**Fig.3.22E**).[172] To this end, we generated H11 Gata3 +761/762 enhanced green fluorescent protein (EGFP) reporter mice and characterized the pattern of EGFP expression in ILCs and T cells. Following treatment of *H11 Gata3* +761/762 EGFP reporter mice with HDM extract as described before (**Fig.3.18A**), we found that ILC2s and, to a lesser degree Th2 cells, in the lung and BAL were marked by EGFP expression whereas group 1 ILCs were not (**Fig.3.21B**). More broadly, we observed high levels of EGFP expression specifically in ILC2s from the BM, SI LP, and vWAT, but not in group 1 or 3 ILCs, thymocytes, $CD4^+$ T cells, or B cells (**Fig.3.21C**). From these observations, we concluded that the *Gata3* +761/762 element is sufficient to recapitulate the pattern of type 2-specific *Gata3* enhancer activity in ILC2s and Th2 cells.

3.2.5 Discussion

ILC2s and Th2 cells express a similar GATA3-driven type 2 helper effector program and contribute to a variety of allergic and helminthic inflammatory processes, but their differentiation occurs in very different contexts.[179,188] While optimal Th2 cell differentiation from naïve $CD4^+$ T cells occurs in the lymph nodes following antigen exposure and IL-4-mediated activation of STAT6[202,211,218,219], ILC2s differentiate from precursors in the BM and peripheral tissues[70,81], and are maintained in the periphery at homeostasis independently of STAT6 or exposure to type 2 cytokines.[220] To understand the mechanisms underlying these differences, we leveraged ATAC-seq chromatin accessibility data in combination with CRISPR/Cas9-mediated deletion to identify *cis*-regulatory elements controlling the *Gata3* locus. Our studies identified a novel distal regulatory region, *Gata3* +674/762, that primarily controls the frequency and differentiation of ILC2s and, to a lesser and mostly indirect degree, Th2 cells. Chromatin accessibility within *Gata3* +674/762 coincided with elevated *Gata3* expression in ILC2s and Th2 cells[78,156,162,172,179], and deletion of this region specifically and profoundly impacted the frequency and function of ILC2s, and to a more minor extent Th2 cells, leaving group 1 and 3 ILCs as well as $CD4^+$ T cells unperturbed. In comparison, the previously identified enhancer *Gata3* +278/285 did not impact ILC2 differentiation or function, but instead contributed broadly to the development of all ILC subsets. Following HDM allergen, *S. venezuelensis* helminth, or OVA-Alum challenge, *Gata3* $+674/762^{\Delta/\Delta}$ mice were variably compromised in their ability to mount a type 2 inflammatory response. Notably, while ILC2s were profoundly and intrinsically impaired by deletion of *Gata3* +674/762 in all contexts, the impact of enhancer deletion on Th2 cells was milder or completely absent, depending on the nature of the type 2 challenge. The limited Th2 cell defect stemmed from both an extrinsic reduction in ILC2 numbers and function and a partial cell-intrinsic deficiency. The lack of a substantial Th2 cell defect explained the generally modest impact of *Gata3* +674/762 deletion on eosinophilia and goblet cell hyperplasia

that characterize the overall type 2 inflammatory response. Lastly, we identified a highly conserved element of the *Gata3* +674/762 region, *Gata3* +761/762, that was sufficient to recapitulate key features of the entire region, including its specific activity in ILC2s, upon incorporation into an *in vivo* enhancer reporter system.

Functionally, *Gata3* +674/762 controlled the number, type 2 differentiation, and function of ILC2s at homeostasis and during a variety of type 2 inflammatory challenges, including HDM, *S. venezuelensis*, and OVA-Alum. Lung ILC2s were profoundly decreased by 75-96% at homeostasis and after allergic and helminthic challenges in mice bearing a deletion of *Gata3* +674/762. Furthermore, the few residual ILC2s in *Gata3* +674/762$^{\Delta/\Delta}$ mice were impaired by ∼50% in GATA3 expression, a level previously shown to significantly alter their ability to produce type 2 cytokines[159], consistent with a 64% reduction in IL-5/IL-13 double-producer lung ILC2s. In contrast, Th2 cells showed a more limited and mostly indirect dependency on *Gata3* +674/762 for expansion and differentiation following allergic and helminthic challenge. Whereas lung ILC2s were profoundly decreased at homeostasis and after type 2 inflammatory challenges in mice bearing a deletion of *Gata3* +674/762, Th2 cells were diminished by 53-86% following HDM or *S. venezuelensis* challenge, or not decreased at all in the case of the ILC2-independent OVA-Alum challenge model.[137,191] Furthermore, this decrease in Th2 cells was largely corrected in a mixed bone marrow chimera setting, indicating a predominantly cell-extrinsic origin for the Th2 cell defect in *Gata3* +674/762$^{\Delta/\Delta}$ mice that may be secondary to the deficiency in type 2 cytokine production from ILC2s. For example, production of IL-13 by ILC2s has been suggested to promote dendritic cell migration to the draining lymph node.[192,221] Separately, production of IL-4 by Th2 cells could further enhance Th2 cell differentiation in an autocrine or paracrine manner.[211,222] Accordingly, our findings indicated that deletion of *Gata3* +674/762 induced a major numerical and functional defect in ILC2s but had only a partial, mostly indirect impact on Th2 cells, explaining the relatively minor overall functional impact of the *Gata3* +674/762

deletion on a variety of type 2 responses, particularly those, like OVA-Alum, that do not appear to involve significant ILC2 contribution.[137,191] Thus, our study provides a genetic basis for the distinct mechanisms involved in driving innate versus adaptive type 2 responses, with potential evolutionary implications for their association with distinct types of immune challenges.

Our study also established that the previously described *Gata3* +278/285 enhancer, termed TCE7.1[162,163], had a very distinct pattern of dynamic accessibility and function compared with *Gata3* +674/762. *Gata3* +278/285 appeared to control the low/medium levels of GATA3 expression required for the development of early ILC precursors and thymocytes but had little impact on the acquisition of the type 2 helper effector program in ILC2s, including the elevated GATA3, IL-33Rα, and cytokine expression that are driven instead by *Gata3* +674/762 in ILC2s.

Our efforts to further dissect the active elements in the *Gata3* +674/762 enhancer region were partially hampered by the finding that distinct portions of this region seemed to contribute to enhancer function in an apparently redundant manner (**Fig.3.22C** and **3.22D**). Deletion of either *Gata3* +674/710 or the complementary *Gata3* +710/762 segments did not significantly impair or only marginally impaired enhancer function as judged by lung ILC2 numbers remaining within 2-fold of WT littermate ILC2s. The presence of separate but redundant regulatory elements is a well characterized phenomenon across both vertebrates and invertebrates that confers robustness, patterning precision, and evolvability to gene expression.[212] Nevertheless, it was possible to characterize at least one potent regulatory element, *Gata3* +761/762, contained within *Gata3* +674/762 based on several key properties. First *Gata3* +761/762 displayed chromatin accessibility in ILC2s and exhibited markers of activation such as H3K27 acetylation.[179,180] Second, binding of GATA3, CBFB, RUNX1 and RUNX3, BCL11B, and GFI1 was enriched within *Gata3* +761/762, as determined by published ILC2 ChIP-seq data.[68,129,181,182] Lastly, *Gata3* +761/762 showed high sequence

conservation in placental mammals. Based on these suggestive features, we established an *in vivo* enhancer reporter that demonstrated specific and high levels of reporter expression in ILC2s, and to a lesser degree, Th2 cells, but not in various other innate or adaptive cell subsets. Notably, this enhancer reporter system may be exploited, for example, to drive the expression of an inducible Cre or diphtheria toxin receptor, providing "next-generation" tools to assess or manipulate the distinct contribution of ILC2s towards type 2 inflammatory challenges in the context of an unperturbed adaptive immune response.

Thus, while further dissection of the distal *Gata3* +674/762 region is warranted, our studies demonstrate and partially characterize the presence of a novel *Gata3* enhancer controlling ILC2 development and function that is largely dispensable for Th2 cells, suggest the existence of additional, distinct regulatory elements controlling *Gata3* expression in Th2 cells. Furthermore, in addition to the GATA3 binding site identified by direct ChIP-Seq analysis, motif analysis in accessible portions of this region revealed several additional putative GATA3 binding motifs. These observations support the possibility that GATA3 may exert a prominent positive feedback on its own expression[201,210,211], providing a potential mechanistic explanation for achieving the elevated levels of GATA3 required to support the type 2 helper effector program of ILC2s.

Author Contributions

D.N.K and A.B. conceived the study and wrote the manuscript. D.N.K designed experiments; generated deletion and reporter mice; performed flow cytometry; and conducted bioinformatic analysis. Z.L and C.Y.O. assisted with sample preparation. M.K.H. treated mice for HDM challenge experiments and performed blinded PAS scoring. A.S. provided support for HDM challenge experiments. W.L. infected mice with *S. venezuelensis* and determined egg counts. A.B. supervised experiments. All authors read and commented on the manuscript.

Acknowledgments

We thank D. Esterhazy (University of Chicago) for providing *S. venezuelensis* for infection experiments; A. Hoffman (University of Chicago) for technical guidance with vWAT preparation; and C. Stamper (University of Chicago) for technical guidance with i.n. treatment. We are grateful to L. Degenstein (University of Chicago) and the University of Chicago Transgenics Core for support with microinjections; the University of Chicago DNA Sequencing and Genotyping Core for sequencing of reporter plasmid constructs; the University of Chicago Genomics Core for sequencing of ATAC-seq samples; the University of Chicago Human Tissue Resource Center for processing, embedding, and staining of histology samples; and the University of Chicago Integrated Microscopy Core for whole slide scanning. Schematics in **Fig.3.16E** and **Fig.3.21A** depicting a mouse and mouse femurs were created with images from BioRender.com.

This work was supported by the US National Institutes of Health (R37 AI127518, R01 AI144094, and U01 AI125250) and support funds from the University of Chicago Dean's office.

CHAPTER 4

DISCUSSION AND FUTURE DIRECTIONS

4.1 Discussion

4.1.1 Generation and application of multi-transcription factor reporters

A majority of ILC precursors described to date have been identified and described using single transcription factor reporter mouse strains in combination with a number of distinguishing surface markers (**Table1.1**). This approach permitted the isolation and characterization of considerably more refined populations than surface markers alone permitted given the greater specificity of transcription factor expression throughout development and differentiation. However, the extent of ILC precursor population heterogeneity was often missed given the reliance on single transcription factor reporter lines. In the ILCP, which was characterized in *Zbtb16*$^{\text{EGFPCre}}$ mice[78], multi-lineage priming occurs with individual ILCP expressing transcripts for *Tbx21*, *Bcl11b*, and *Rorc*.[92] Among the CHILP, identified in ID2$^{\text{EGFP}}$ mice, nearly 50% expressed PLZF and were thus contaminated with ILCP in addition to the LTiP in the FL.[5] The αLP, already recognized as a highly heterogeneous population[70], included both the ILCP and LTiP as well as more mature cells.[73,74,91,92,99] Only after the fact was it reported that the EILP, discovered in *Tcf7*$^{\text{EGFP}}$ mice, contained a distinct PLZF-expressing sub-fraction as opposed to a broad low level of expression.[75–77] Characterization of the heterogeneity observed in these populations has been limited by the dependence on EGFP as a fluorescent reporter, which was initially used to report on RORγt, *Zbtb16*, ID2, and *Tcf7*.[5,59,73–75,78,81] Thus it was not possible to combine these strains for further refinement.

Recent implementation of combinatorial transcription factor reporter strains has highlighted the power of this approach in resolving population heterogeneity. Harly et al. (2019) utilized *Zbtb16*$^{\text{EGFPCre}}$ *Tcf7*$^{\text{EYFP}}$ mice to distinguish *Zbtb16*$^{+}$ EILP from *Zbtb16*$^{-}$

EILP in the adult BM, revealing a stage of commitment to the ILC lineage over shared ILC/DC lineage potential.[77] Both Xu et al. (2019) and Walker et al. (2019) combined a multitude of transcription factor reporter strains, *Zbtb16*$^{\text{EGFPCre}}$*Id2*$^{\text{RFP}}$*Bcl11b*$^{\text{tdTomato}}$ and ID2$^{\text{BFP/+}}$GATA3$^{\text{hCD2/+}}$ROR$\alpha^{\text{Teal/+}}$*Bcl11b*$^{\text{tdTomato/+}}$RORγt$^{\text{Katushka/+}}$ respectively, to identify adult BM populations enriched for ILC3 potential, interrogate ILCP heterogeneity, and further refine the ILC2P.[93,94]

In contrast to these three reports that utilized standard transgenic methods to generate each novel transcription factor reporter strain, we employed CRISPR/Cas9-mediated transgenesis to rapidly develop several select reporters.[172,184] Through a careful selection of specific transcription factors expressed throughout ILC development, we opted to generate *Tcf7*$^{\text{mCherry}}$, *Rorc*$^{\text{Thy1.1}}$, and *Gata3*$^{\text{Citrine}}$ reporter mice which could then be combined with existing *Zbtb16*$^{\text{EGFPCre}}$ and ID2$^{\text{EYFP}}$ lines.[78,171] By combining *Zbtb16*$^{\text{EGFPCre}}$, *Tcf7*$^{\text{mCherry}}$, and *Rorc*$^{\text{Thy1.1}}$ strains, we were able to resolve the heterogeneity of PLZF and RORγ(t) expression observed within the EILP and characterize transitional stages of transcription factor expression to support the hierarchical placement of intermediate ILC precursors.

4.1.2 Delineating ILC and LTi-lineage bifurcation

The point of ILC and LTi-lineage bifurcation has been somewhat contentious given the identification of three separate precursors with reported shared ILC-LTi lineage potential.[70] The CHILP was the first reported common ILC-LTi precursor found to generate both ILC and LTi upon *in vivo* transfer.[5] Yet, the observation of a prominent PLZF-expressing subpopulation within the CHILP, contemporaneously characterized as the ILCP[78], and the expected overlap with the FL LTiP prompted a modern reevaluation of the CHILP as a PLZF^{-}RORγ(t)$^{-}$ population with high levels of TCF1 and ID2 downstream of the αLP (**Fig.3.1A**). Utilizing an approach that combined *in vitro* clonal culture and single-cell mul-

tiplex PCR, our lab traced the last common ILC-LTi lineage precursor in the FL to the Flt3$^-$ αLP population, based on the ability to generate mixed cultures of ILC1/2 and LTi and the identification of a cell cluster with a gene expression signature characteristic of both ILCs and LTis.[92] Separately, Yang et al. (2015) characterized a population in the adult BM termed the EILP, which they found generated ILC1/2/3, LTis, and NK cells, and was suspected to arise downstream of the αLP based on the precursors gene expression profile.[75] However, placement of the EILP downstream of the CLP or parallel in development was not fully appreciated until the application of *Tcf7*$^{\text{EGFP}}$IL-7Rα^{Cre} x ROSA26$^{\text{floxSTOP-YFP}}$ reporter mice confirmed a history of *Il7r* expression.[76] Furthermore, the adult BM EILP was found to contain a fraction of PLZF-expressing cells, similar to the CHILP[5], suggesting that a common ILC-LTi precursor would likely reside within the PLZF$^-$ fraction of the EILP.[77]

The results presented herein (**Chaper 3.1**) detail the uncharacterized heterogeneity of the EILP through the evaluation of FL precursors resolved through multi-transcription factor reporter lines. We observed that the EILP contained a mixture of incipient precursors based on the mutually exclusive expression of PLZF and RORγ(t), the iILCP and iLTiP respectively, that were already specified towards the ILC and LTi lineages. Furthermore, PLZF$^-$RORγ(t)$^-$ EILP, reclassified as the rEILP, were not multipotent for ILCs and LTis, which eliminated the EILP as a candidate shared ILC-LTi lineage precursor. An assessment of the CHILP revealed the presence of contaminating ILCP and LTiP, as expected[70], and that the remaining PLZF$^-$RORγ(t)$^-$ CHILP similarly did not contain a shared ILC-LTi lineage precursor, in line with the CHILP arising downstream of the EILP. Lastly, we observed that a fraction of Flt3$^-$ αLP expressed *Rorc*, was devoid of LTi-lineage maturation markers, and displayed an increased propensity to differentiate towards ILC3/LTi in bulk and single cell culture. Moreover, the *Rorc*$^+$ αLP already contained numerous epigenetic features in common with more mature LTi-lineage precursors (iLTiP and LTiP), reinforcing our conclusion that the *Rorc*$^+$ αLP represents an early precursor in the LTi-lineage track.

These observations warranted the development of a revised hierarchical map of ILC development wherein ILC and LTi-lineage bifurcation occurs prior to the EILP at the αLP stage (**Fig.3.1B**).

Several outstanding questions remain from the study in **Chapter 3.1** regarding ILC development.[172] First, while clonal analysis of the EILP and CHILP and the identification of the LTi-specified *Rorc*$^{+}$ αLP helped to reinforce the Flt3^{-} αLP as the point of ILC-LTi lineage bifurcation[92], a refined common precursor has not been identified. *Tox*, *Nfil3*, and *Id2* were previously found to mark the earliest stages of the αLP and *Runx1* and *Sox4* were found at the transitional stage between the αLP and ILCP.[92] Therefore, a multi-transcription factor reporter approach focusing on these factors, while excluding mature populations with *Tcf7* for example, may help to identify a refined early ILC precursor within the αLP. Second, while it appears that GATA3 and RORγ(t) play important and discrete roles in promoting ILC and LTi-lineage development respectively[161], how these factors act to promote lineage bifurcation, fate, and progression and how they themselves are induced remain to be determined. Identification and refinement of a shared ILC-LTi precursor will go a long way towards addressing these questions. Additionally, advancements in low-input ChIP-seq when combined with sequential ILC and LTi-lineage chromatin accessibility data may provide insight into the binding of GATA3 and RORγ(t) across the genome. Lastly, our study did not address where NK lineage cells branch off during ILC development, as such, where the bifurcation occurs remains unclear, and other reports have proposed distinct possibilities (discussed below).

4.1.3 Epigenetic analysis of ILC precursors

How external and internal stimuli are integrated to implement the transcriptional program within ILCs is only beginning to be understood. Previous reports suggest that the majority of transcription factor binding sites are found within *cis*-regulatory elements distal

to the genes they regulate and are active in specific cell types.[178,223] Pioneering transcription factors and lineage-determining transcription factors act in concert to alter chromatin accessibility through nucleosome repositioning at *cis*-regulatory elements, which contributes to the epigenetic regulation of gene expression in eukaryotic organisms.[178,223,224] Traditional strategies to assess global accessibility and regulation, such as DNase-seq and ChIP-seq, are often prohibitively difficult for application to rare cell populations as is the case with ILC progenitors. To circumvent this issue, ATAC-seq has been used to reliably determine the chromatin accessibility landscape of mature ILCs and ILC precursors.[80,179]

By comparing chromatin accessibility between ILCs and T cells, Shih et al. (2016) demonstrated that whereas ILC subset-specific regulatory elements proximal to cytokine genes were open at homeostasis, allowing for rapid transcript expression upon infection, the same regulatory elements in naïve T cells were closed. Thus ILCs and T cells acquire their effector programs through development or differentiation respectively.[179] A comparison of chromatin accessibility between the CLP and ILCP by our lab permitted the identification of an intronic enhancer within the *Zbtb16* locus that functions as a critical regulator of PLZF expression during ILC development.[80]

Building on these studies that focused on mature ILCs and distinct stages of ILC development, chromatin accessibility data presented in **Chapter 3.1** enabled the comparison of chromatin landscapes between early, intermediate, and late progenitors, revealing differentially-accessible regions that emerged or disappeared throughout ILC development in the ILC and LTi lineages. Moreover, these findings separately reenforced the hierarchical placement of each precursor based on *in vitro* clonal culture data. Lastly, in lieu of ChIP-seq binding data, motif analysis in accessible regions across the ILC and LTi lineage uncovered a shared usage of RUNX, ETS, and TCF factors and a differential reliance on GATA and ROR factors respectively for development.

4.1.4 Identification of a novel Gata3 enhancer

Classical evaluation of a given *cis*-regulatory element's contribution to gene expression has been accomplished through the use of *in vitro* and *in vivo* reporter expression systems or *in silico* identification.[88,143,162,169] While these strategies can address whether a particular *cis*-regulatory element is active, accessible, and/or bound by transcription factors, they are each limited in scope. *In vitro* assays are rapid but neglect the context of *cis*-regulatory element activity such as tissue- or stage-specific expression. *In vivo* transgenic approaches and *in silico* identification go further to map the pattern of activity often without assessing the function of a particular *cis*-regulatory element. Our lab and others have extended these approaches via the targeted removal of *cis*-regulatory element using CRISPR/Cas9-mediated deletion.[80,135,163,184]

In our recent work, a comparison of chromatin accessibility between the CLP and ILCP followed by a systematic removal of *Zbtb16* intronic enhancer elements revealed the origin of tissue-specific expression of PLZF in the hematopoietic (ILC and NKT cell) and skeletal compartments.[80] Subsequent to the identification of the *Gata3* enhancer TCE7.1 through *in silico* and *in vivo* analysis in an earlier report[162], Ohmura et al. (2016) specifically removed this enhancer element and found that in accordance with a BAC driven reporter assay, TCE7.1 played a large role in regulating GATA3 expression during thymocyte development.[163] When scanning for accessible regions around *Id2*, Mowel et al. (2017) identified an enhancer region demarcated by a lncRNA which when removed via CRISPR/Cas9 dramatically impaired the expression of *Id2* in and development of group 1 ILCs.[135]

Characterization of the novel enhancer *Gata3* +674/762, described in **Chapter 3.2**, followed a similar approach as these three studies. Through a stage-specific comparison of chromatin accessibility at the *Gata3* locus in ILC precursors, mature ILCs, and T cells, we observed a distal region, *Gata3* +674/762, with features characteristic of a type 2-specific *Gata3* enhancer. CRISPR/Cas9-mediated deletion of *Gata3* +674/762 revealed a severe

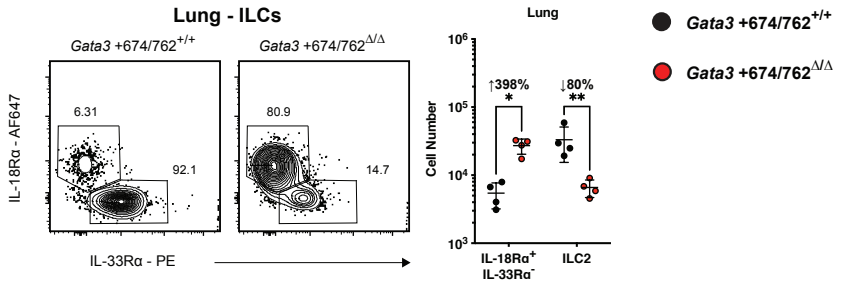

Figure 4.1: Impact of *Gata3* +674/762 deletion on lung IL-18Rα^+IL-33Rα^- ILC precursors. Representative flow cytometry plot and summary data of cell numbers in WT vs. *Gata3* +674/762$^{\Delta/\Delta}$ mice for lung IL-18Rα^+IL-33Rα^- ILC precursors and ILC2s (pre-gated on CD45.2$^+$CD19$^-$CD11c$^-$CD3ϵ^-TCRβ^-IL-7Rα^+CD90.2$^+$).

and specific impairment in ILC2 development, GATA3 expression, and IL-5/IL-13 cytokine production at homeostasis and following type 2 inflammation. Notably, while accessibility of *Gata3* +674/762 tracked with Th2 cell differentiation, deletion of *Gata3* +674/762 only had a minor largely cell extrinsic impact on Th2 cells, which suggested partial redundancy of the enhancer element. Lastly, the specific function of *Gata3* +674/762 in type 2 immune cells was confirmed using an enhancer reporter system that revealed that only ILC2s and Th2 cells expressed factors capable of binding to and activating this enhancer region. In sum, these results identified a type 2-specific regulatory element that was necessary for GATA3 transcription factor expression in ILC2s, but mostly redundant for Th2 cells.

Though deletion of *Gata3* +674/762 severely impacted GATA3 expression in ILC2s, we did not identify a discrete element within the 88 kb region that was responsible for the observed *cis*-regulatory activity. Further interrogation of *Gata3* +674/762 and the important elements within necessitates a more detailed understanding of the distal interactions made with the *Gata3* promoter element. Low-input chromatin conformation capture techniques could permit the identification of contact points within *Gata3* +674/762 that interact with the *Gata3* promoter element to regulate gene expression in ILC2s. How these interactions compare between ILC2s and Th2 cells may provide insight into the distinct usage of *Gata3*

+674/762 in these two lineages. The stage of ILC2 development in which *Gata3* +674/762 is necessary for *Gata3* expression appears to be the ILC2P when *Gata3* expression is elevated, based on the *H11 Gata3* +674/762 reporter and the pattern of GATA3 expression during ILC development. However, the ILC2P is not the exclusive contributor to peripheral ILC2 populations at homeostasis and during inflammation.[24,27,105] We documented a blockage in development from peripheral IL-18Rα^{+}IL-33Rα^{-} ILC precursors in the lung (**Fig.4.1**), suggesting that *Gata3* +674/762 is universally required for full ILC2 lineage commitment. Finally, as *Gata3* +674/762 contains numerous GATA3 binding motifs and its function coincides with type 2 upregulation of GATA3, it is possible that *Gata3* +674/762 performs an auto-regulatory role by enhancing and/or maintaining the augmented expression level of GATA3 in ILC2s. Nevertheless, a dissection of the GATA3 motifs, through deletion or replacement, and the temporal removal of *Gata3* +674/762 using the Cre-lox system will be necessary to substantiate the role of *Gata3* +674/762 in regulating *Gata3* expression.

Numerous models have been devised to target ILC function at homeostasis and during inflammation.[225] Two models in particular, *Rora*$^{\mathrm{fl/fl}}$ or *Rora*$^{\mathrm{sg/sg}}$ and *Il5*$^{\mathrm{tdTomato\text{-}Cre}}$, were designed to ascertain the specific contribution of ILC2s. Prior deletion strategies targeting ILC2s through *Rora* relied on their dependence on this transcription factor for development[22,89]; however, later discovery of more widespread expression of *Rora* in ILC3s and Th2 cells has brought to light ILC2-extrinsic issues associated with this approach.[188,226] More recently, implementation of the *Il5*$^{\mathrm{tdTomato\text{-}Cre}}$ strain in combination with a ROSA26 Diphtheria toxin (DTA) deleter allele has offered greater specificity in targeting the ILC2 lineage.[28,41,188] At steady state, ILC2s are the dominant producer of IL-5[41]; as such, the aforementioned model is highly effective in addressing ILC2 function in the absence of Th2 cell induction. Under inflammatory contexts where Th2 cell differentiation does occur however, the *Il5*$^{\mathrm{tdTomato\text{-}Cre}}$ X ROSA26$^{\mathrm{DTA}}$ system results in diminished numbers of cytokine-producing Th2 cells.[188] One workaround has been to reconstitute *Rag1*$^{-/-}$ *Il5*$^{\mathrm{tdTomato\text{-}Cre}}$ROSA26$^{\mathrm{DTA}}$

mice with unmanipulated naïve $CD4^+$ T cells, yet this approach suffers from aberrant lymph node development and impaired Th2 cell differentiation. Compared with these two models of ILC2 deficiency, deletion of *Gata3* +674/762 is highly specific for ILC2s while demonstrating a minimal impact on Th2 cells. Nevertheless, the penetrance of this phenotype is not complete in all tissues, as seen with numbers of ILC2s in the intestine, and further manipulations may be required to definitively exclude any cell-intrinsic impact in Th2 cells. Thus, *Gata3* $+674/762^{\Delta/\Delta}$ mice offer a novel system to study ILC2-specific function when outstanding issues are considered.

4.2 Future Directions

4.2.1 Enhancer reporters

It is clear from prior reports and the results presented herein that a combination of reporter strains has and will permit a more detailed refinement of ILC development. Furthermore, careful reporter design that permits combination and a selective application of reporters can enable the interrogation of distinct windows of development, as has been done for the ILCP and now the EILP and CHILP.

Integration of a novel type of reporter system based on enhancer activity will enable the identification and characterization of precursors in the process of differentiating towards a particular lineage and provide additional insight beyond chromatin accessibility as to when enhancers are active, not just accessible, during development. The latter point, when combined with gene expression and motif enrichment analysis, will not only provide information as to what stage enhancer-associated transcription factors are functioning but also what upstream network of factors may be responsible for gene induction. By redesigning the traditionally used LacZ *in vivo* enhancer reporters to use fluorescent proteins and/or surface markers[215], this approach, which is flow cytometry compatible, should offer a new layer of

refinement for ILC development and gene regulation.

As demonstrated in **Fig.3.21B** and **3.21C**, the *H11 Gata3* +761/762 enhancer reporter specifically marked ILC2s and differentiated Th2 cells following HDM challenge. Thus, enhancer reporters can be used to distinguish cells that have reached a point in maturation where a specific enhancer is active, presumably based on the expression of transcription factors capable of binding to said enhancer, which may provide insight into the induction and regulation of key transcription factors. Case in point, we have generated *H11* enhancer reporters for *Zbtb16* +21/23 and *Gata3* +283/284. For *H11 Zbtb16* +21/23, we discerned high levels of EGFP expression in the ILCP and, to a lesser degree, NKT cells, where *Zbtb16* is expressed and the region is accessible (**Fig.4.2A**).[80] Notably, a small fraction of Flt3$^+$ αLP are EGFP$^+$, which may indicate precursors within the ill-defined αLP capable of differentiation towards the ILC lineage. For *H11 Gata3* +283/284, we noted expression not only within thymocytes, as expected from previous reports[162,163], but also at the ILCP stage to an equivalent degree, consistent with the observed impact of *Gata3* +283/284 deletion on ILC development (**Fig.4.2B** and Fig.3.17). Whether this enhancer is active at the rEILP and iILCP stage, when this region initially becomes accessible (**Fig.3.13B**), can be addressed by including this enhancer reporter in existing multi-transcription factor reporter combinations.

Additional *H11* enhancer reporter lines have been generated by our lab to test the principles of this system. We generated *H11* enhancer reporters for *Il7r* -3.6/4.2 and *Il7r* +5.3/6.2 based on the previous work and data shown in (**Fig.1.4B** and **1.4C**), which identified these regions as important enhancers of *Il7r* expression in innate and adaptive lymphocyte lineages.[68,88,169,170] For *H11 Il7r* -3.6/4.2, we observed expression of EGFP in IL-7Rα expressing peripheral ILC populations, the ILCP and ILC2P, as well as CD4$^+$ and CD8$^+$ T cells in the spleen (**Fig.4.2C**). For *H11 Il7r* +5.3/6.2, we observed expression of EGFP in IL-7Rα expressing peripheral ILC populations, the ILCP, and ILC2P (**Fig.4.2D**). Notably, neither

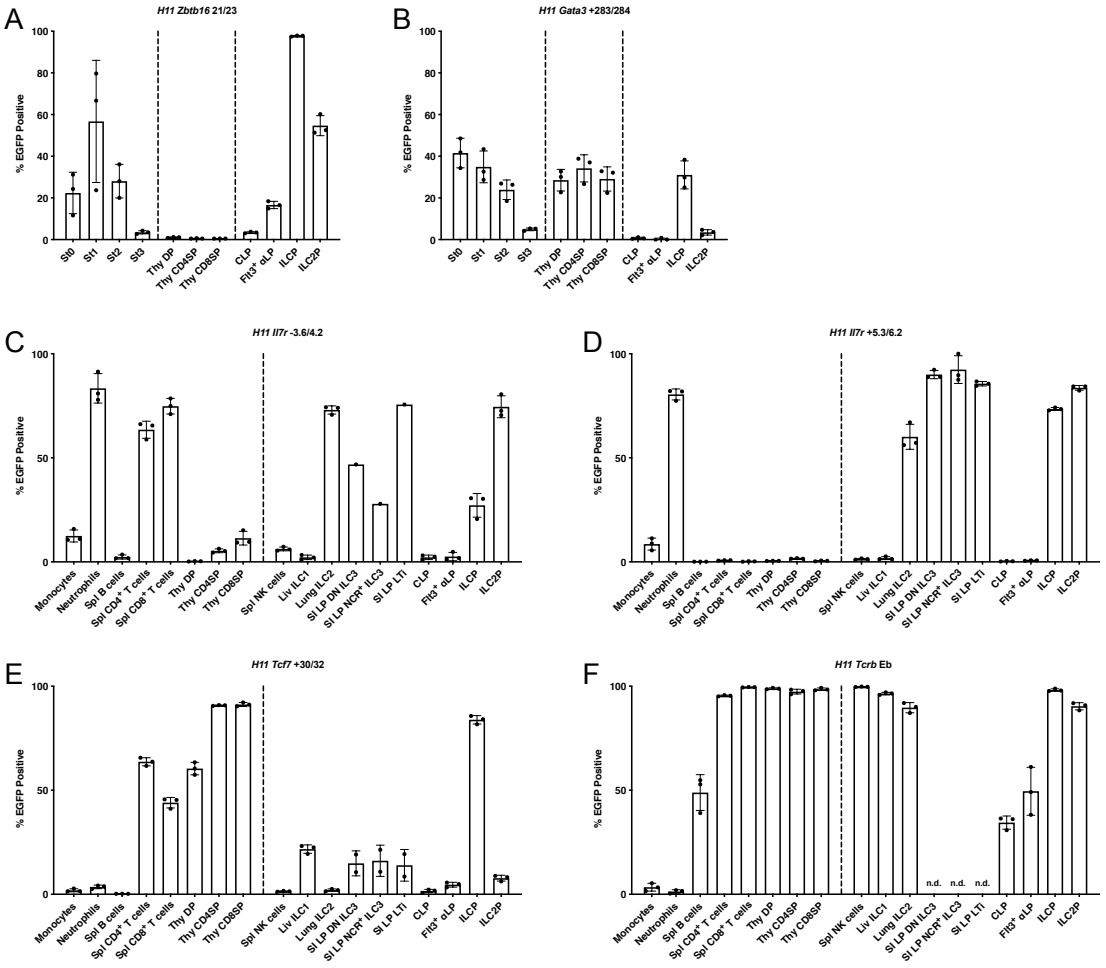

Figure 4.2: Characterization of *H11* enhancer reporters. Summary bar graph shows *H11* enhancer EGFP reporter expression in various lymphocyte populations for the enhancers (**A**) *Zbtb16* +21/23, (**B**) *Gata3* +283/284, (**C**) *Il7r* -3.6/4.2, (**D**) *Il7r* +5.3/6.2, (**E**) *Tcf7* +30/32, and (**F**) *Tcrb* Eb.

the CLP nor the Flt3$^+$ αLP were EGFP$^+$, despite expression if IL-7Rα and in accordance with chromatin accessibility, indicating that neither express factors capable of activating this enhancer (**Fig.1.4A**). A similar *H11* reporter was generated for *Tcf7* +30/32, were we documented a high level of EGFP expression in TCF1 expressing T cells, thymocytes, and the ILCP when the enhancer is accessible (**Fig.4.2D**).[145] These results highlight the power of enhancer reporters to track *in vivo* enhancer activity.

While the *H11* enhancer reporter system appears to be highly effective in mapping enhancer activity, two main caveats exist that must be considered in advance of applying this

strategy. First and foremost, while the site-specific integration of the enhancer into the *H11* locus limits multiple and off-target integration, no locus aside from that of the enhancer in question will replicate activity of insulators and appropriate 3D chromatin conformation involved in higher order enhancer regulation.[223] Second, as a safe-harbor sequence[213,217], the *H11* locus is not likely to contain the same nucleosome deposition seen at the native enhancer. These two aspects together can enable access to an enhancer that would normally be closed in a particular cell type, leading to reporter expression if the cell expresses factors capable of binding the transgenic enhancer element. This effect was observed in several of our enhancer reporters. For *H11 Il7r* -3.6/4.2 and *H11 Il7r* +5.3/6.2, we noted EGFP expression in splenic neutrophils, despite the absence of *Il7r* expression in these cells (**Fig.4.2C** and **4.2D**).[194] Similarly, for the *H11* enhancer reporter using the minimal *Tcrb* enhancer (*Tcrb* Eb)[227], we found that EGFP was expressed in mature ILCs, ILC precursors, and splenic B cells in addition to conventional TCR$\alpha\beta^+$ thymocytes and splenic T cells (**Fig.4.2F**). These results indicate that when these enhancer elements are introduced irrespective of their native genomic position and chromatin accessibility, abnormal enhancer activation can occur, perhaps due to the expression of the same or similar transcription factors capable of binding and activating the element. Thus, this enhancer reporter system is best used in conjunction with chromatin accessibility data and is most suited for tracking cells that express factors capable of enhancer activation.

4.2.2 Development of NK cell and ILC1 lineages

A major outstanding question in the field of ILC development is the resolution of NK cell precursors from ILC1 precursors, which has been hampered in large part by their highly similar gene expression pattern and parallel stages of progression. Precursors to the NK cell lineage, including the pre-NKP and rNKP[83,84,87], were and continue to be identified principally through surface marker expression, even though it is now appreciated that

ILC1s also express a majority of these same markers. Fate-mapping using *Zbtb16*$^{\text{EGFPCre}}$ x ROSA26$^{\text{floxSTOP-EYFP}}$ reporter mice and precursor transfer studies indicated that the NK cell lineage diverges prior to both the ILCP and the CHILP, presumably originating from the rEILP or Flt3$^{+/-}\alpha$LP (**Fig.3.1B**).[5,75,78] Moreover, when *Zbtb16*$^{\text{EGFPCre}}$ fate-mapping was applied specifically to interrogate NK cell lineage precursors, our lab observed that significant fractions of the pre-NKP and rNKP expressed or were fate-mapped by *Zbtb16*.[11] Therefore, a history of *Zbtb16* expression is expected to distinguish the NK cell lineage from the ILC1 lineage. However, two recent reports have applied novel *Id2*$^{\text{RFP}}$ and ID2$^{\text{TagBFP}}$ reporters to suggest that the ILCP and the CHILP both retain significant NK cell potential.[93,94] While our studies in the FL do not shed light on the point of bifurcation, as ILC1 cells predominate over NK cells during early life[11], we and others have demonstrated the need for more sophisticated tools, like multi-transcription factor reporters, to address lineage development.

A multi-transcription factor reporter strategy, similar to that used in **Chaper 3.1**, is likely to provide more robust distinction of precursor populations than surface markers alone. One approach would be to combine the existing *Eomes*$^{\text{EGFP}}$ reporter with *Tcf7*$^{\text{mCherry}}$, ID2$^{\text{EYFP}}$, and our novel *Zbtb16*$^{\text{hCD4}}$ reporter[4,171,172], which will enable the clean separation of rEILP, iILCP, and ILCP from *Eomes*-EGFP^{+} *Zbtb16*-hCD4^{-} cells that are presumably NK cell precursors. Additionally, because *Tcf7*$^{\text{mCherry}}$ captures a window of intermediate ILC precursors including the NKP (**Fig.3.6D** and **Fig.3.3I**)[75,78,119], and ID2$^{\text{EYFP}}$ appears to be more highly expressed in the ILC1 lineage compared to the NK cell lineage (**Fig.3.3H**), an *Eomes*$^{\text{EGFP}}$ *Tcf7*$^{\text{mCherry}}$ID2$^{\text{EYFP}}$ *Zbtb16*$^{\text{hCD4}}$ combination may enable the exclusion of later NK cell lineage precursors and ILC1 lineage precursors respectively. A second approach would be to design a novel compatible *Eomes* reporter for combination with the *Zbtb16*$^{\text{EGFPCre}}$ x ROSA26$^{\text{floxSTOP-EYFP}}$ fate-mapping system in order to rigorously exclude cells with a history of *Zbtb16* expression. Lastly, unbiased single-cell sequencing of

adult BM ILC precursors could be used to identify alternate transcription factors suitable for a combination reporter system while NK cell lineage-specific enhancer regions determined from differential chromatin accessibility data can be incorporated into the *H11* enhancer reporter system. Ultimately, these three possible approaches must be experimentally validated using an assay capable of distinguishing differentiated NK cells from ILC1s, yet no markers currently used for *in vitro* clonal culture offer such clarity. As such, the search for the elusive NK cell lineage-restricted precursor requires not only novel tools for identification and isolation, but also a faithful method for characterization.

4.3 Conclusion

In sum, by designing and applying a multitude of newly generated transcription factor reporter lines created via CRISPR/Cas9-mediated transgenesis, we have resolved population heterogeneity of several ILC precursors in the FL and adult BM; established a resource for understanding the dynamic change in chromatin accessibility across the ILC and LTi lineages, providing a means to dissect the regulatory network governing transcription factor expression in these cells; and identified a novel distal regulatory element controlling *Gata3* expression during ILC2 development and function.

The results of this study will bolster our understanding of the basic biology of ILCs and, in a more translational and clinically relevant context, support the generation of refined models to study ILC function, at homeostasis and following diverse inflammatory insults, that will advance an understanding of the role ILCs play in human health and disease. Our contributions to the field of CRISPR/Cas9-mediated transgenesis not only enable the rapid development of transcription factor and novel enhancer reporter mouse strains to separate distinct lineages of ILCs, but also provides insight into the application of this revolutionary technique to repair or replace sequences, such as deleterious mutations in somatic or germline human genomes. Clarification of the ILC developmental hierarchy and

collection of chromatin accessibility across developmental time permits the discovery and determination of a transcription factor's role in guiding lineage progression, and may be used to artificially influence cell fate decisions to achieve a specific course of development. Identification of the novel *Gata3* enhancer necessary for ILC2 development and function sheds light onto the origin and evolution of ILCs and T cells, how shared effector programs have emerged in both the innate and adaptive arms of the immune system, which will inform the design of tools to target and tweak these two systems to promote desirable health outcomes. It is difficult to predict how a body of work will ultimately be used in future scientific endeavors and clinical applications, yet, the work presented herein should provide a solid foundation upon which greater and more profound advances can be made.

REFERENCES

[1] Andreas Diefenbach, Marco Colonna, and Shigeo Koyasu. Development, differentiation, and diversity of innate lymphoid cells. *Immunity*, 41(3):354–365, 2014.

[2] Eric Vivier, David Artis, Marco Colonna, Andreas Diefenbach, James P Di Santo, Gérard Eberl, Shigeo Koyasu, Richard M Locksley, Andrew NJ McKenzie, Reina E Mebius, et al. Innate lymphoid cells: 10 years on. *Cell*, 174(5):1054–1066, 2018.

[3] Meital Gury-BenAri, Christoph A Thaiss, Nicolas Serafini, Deborah R Winter, Amir Giladi, David Lara-Astiaso, Maayan Levy, Tomer Meir Salame, Assaf Weiner, Eyal David, et al. The spectrum and regulatory landscape of intestinal innate lymphoid cells are shaped by the microbiome. *Cell*, 166(5):1231–1246, 2016.

[4] Cécile Daussy, Fabrice Faure, Katia Mayol, Sébastien Viel, Georg Gasteiger, Emily Charrier, Jacques Bienvenu, Thomas Henry, Emilie Debien, Uzma A Hasan, et al. T-bet and Eomes instruct the development of two distinct natural killer cell lineages in the liver and in the bone marrow. *Journal of Experimental Medicine*, pages jem–20131560, 2014.

[5] Christoph SN Klose, Melanie Flach, Luisa Möhle, Leif Rogell, Thomas Hoyler, Karolina Ebert, Carola Fabiunke, Dietmar Pfeifer, Veronika Sexl, Diogo Fonseca-Pereira, et al. Differentiation of type 1 ILCs from a common progenitor to all helper-like innate lymphoid cell lineages. *Cell*, 157(2):340–356, 2014.

[6] Orr-El Weizman, Nicholas M Adams, Iona S Schuster, Chirag Krishna, Yuri Pritykin, Colleen Lau, Mariapia A Degli-Esposti, Christina S Leslie, Joseph C Sun, and Timothy E O'Sullivan. ILC1 confer early host protection at initial sites of viral infection. *Cell*, 171(4):795–808, 2017.

[7] Georg Gasteiger, Xiying Fan, Stanislav Dikiy, Sue Y Lee, and Alexander Y Rudensky. Tissue residency of innate lymphoid cells in lymphoid and nonlymphoid organs. *Science*, 350(6263):981–985, 2015.

[8] Michelle L Robinette, Anja Fuchs, Victor S Cortez, Jacob S Lee, Yaming Wang, Scott K Durum, Susan Gilfillan, Marco Colonna, Immunological Genome Consortium, et al. Transcriptional programs define molecular characteristics of innate lymphoid cell classes and subsets. *Nature Immunology*, 16(3):306–317, 2015.

[9] Dorothy K Sojka, Beatrice Plougastel-Douglas, Liping Yang, Melissa A Pak-Wittel, Maxim N Artyomov, Yulia Ivanova, Chao Zhong, Julie M Chase, Paul B Rothman, Jenny Yu, et al. Tissue-resident natural killer (NK) cells are cell lineages distinct from thymic and conventional splenic NK cells. *Elife*, 3:e01659, 2014.

[10] Olga Pikovskaya, Julie Chaix, Nyanza J Rothman, Amélie Collins, Yen-Hua Chen, Anna M Scipioni, Eric Vivier, and Steven L Reiner. Cutting edge: eomesodermin is sufficient to direct type 1 innate lymphocyte development into the conventional NK lineage. *The Journal of Immunology*, 196(4):1449–1454, 2016.

[11] Michael G Constantinides, Herman Gudjonson, Benjamin D McDonald, Isabel E Ishizuka, Philip A Verhoef, Aaron R Dinner, and Albert Bendelac. PLZF expression maps the early stages of ILC1 lineage development. *Proceedings of the National Academy of Sciences*, 112(16):5123–5128, 2015.

[12] Victor S Cortez, Anja Fuchs, Marina Cella, Susan Gilfillan, and Marco Colonna. Cutting edge: salivary gland NK cells develop independently of Nfil3 in steady-state. *The Journal of Immunology*, 192(10):4487–4491, 2014.

[13] Victor S Cortez, Luisa Cervantes-Barragan, Michelle L Robinette, Jennifer K Bando, Yaming Wang, Theresa L Geiger, Susan Gilfillan, Anja Fuchs, Eric Vivier, Joe C Sun, et al. Transforming growth factor-β signaling guides the differentiation of innate lymphoid cells in salivary glands. *Immunity*, 44(5):1127–1139, 2016.

[14] Victor S Cortez, Tyler K Ulland, Luisa Cervantes-Barragan, Jennifer K Bando, Michelle L Robinette, Qianli Wang, Andrew J White, Susan Gilfillan, Marina Cella, and Marco Colonna. SMAD4 impedes the conversion of NK cells into ILC1-like cells by curtailing non-canonical TGF-β signaling. *Nature Immunology*, 18(9):995–1003, 2017.

[15] Eugene Park, Swapneel Patel, Qiuling Wang, Prabhakar Andhey, Konstantin Zaitsev, Sophia Porter, Maxwell Hershey, Michael Bern, Beatrice Plougastel-Douglas, Patrick Collins, et al. Toxoplasma gondii infection drives conversion of NK cells into ILC1-like cells. *Elife*, 8:e47605, 2019.

[16] Laura K Mackay, Martina Minnich, Natasja AM Kragten, Yang Liao, Benjamin Nota, Cyril Seillet, Ali Zaid, Kevin Man, Simon Preston, David Freestone, et al. Hobit and Blimp1 instruct a universal transcriptional program of tissue residency in lymphocytes. *Science*, 352(6284):459–463, 2016.

[17] Binqing Fu, Yonggang Zhou, Xiang Ni, Xianhong Tong, Xiuxiu Xu, Zhongjun Dong, Rui Sun, Zhigang Tian, and Haiming Wei. Natural killer cells promote fetal development through the secretion of growth-promoting factors. *Immunity*, 47(6):1100–1113, 2017.

[18] Moriya Gamliel, Debra Goldman-Wohl, Batya Isaacson, Chamutal Gur, Natan Stein, Rachel Yamin, Michael Berger, Myriam Grunewald, Eli Keshet, Yoach Rais, et al. Trained memory of human uterine NK cells enhances their function in subsequent pregnancies. *Immunity*, 48(5):951–962, 2018.

[19] Dorothy K Sojka, Liping Yang, Beatrice Plougastel-Douglas, Darryl A Higuchi, B Anne Croy, and Wayne M Yokoyama. Cutting edge: local proliferation of uterine tissue-resident NK cells during decidualization in mice. *The Journal of Immunology*, 201(9): 2551–2556, 2018.

[20] April E Price, Hong-Erh Liang, Brandon M Sullivan, R Lee Reinhardt, Chris J Eisley, David J Erle, and Richard M Locksley. Systemically dispersed innate IL-13–expressing

cells in type 2 immunity. *Proceedings of the National Academy of Sciences*, 107(25): 11489–11494, 2010.

[21] Kazuyo Moro, Taketo Yamada, Masanobu Tanabe, Tsutomu Takeuchi, Tomokatsu Ikawa, Hiroshi Kawamoto, Jun-ichi Furusawa, Masashi Ohtani, Hideki Fujii, and Shigeo Koyasu. Innate production of TH 2 cytokines by adipose tissue-associated c-Kit$^+$ Sca-1$^+$ lymphoid cells. *Nature*, 463(7280):540–544, 2010.

[22] See Heng Wong, Jennifer A Walker, Helen E Jolin, Lesley F Drynan, Emily Hams, Ana Camelo, Jillian L Barlow, Daniel R Neill, Veera Panova, Ute Koch, et al. Transcription factor RORα is critical for nuocyte development. *Nature Immunology*, 13(3):229–236, 2012.

[23] Kazuyo Moro, Hiroki Kabata, Masanobu Tanabe, Satoshi Koga, Natsuki Takeno, Miho Mochizuki, Koichi Fukunaga, Koichiro Asano, Tomoko Betsuyaku, and Shigeo Koyasu. Interferon and IL-27 antagonize the function of group 2 innate lymphoid cells and type 2 innate immune responses. *Nature Immunology*, 17(1):76–86, 2016.

[24] Christoph Schneider, Jinwoo Lee, Satoshi Koga, Roberto R Ricardo-Gonzalez, Jesse C Nussbaum, Lucas K Smith, Saul A Villeda, Hong-Erh Liang, and Richard M Locksley. Tissue-resident group 2 innate lymphoid cells differentiate by layered ontogeny and in situ perinatal priming. *Immunity*, 50(6):1425–1438, 2019.

[25] Yuefeng Huang, Kairui Mao, Xi Chen, Ming-an Sun, Takeshi Kawabe, Weizhe Li, Nicholas Usher, Jinfang Zhu, Joseph F Urban, William E Paul, et al. S1p-dependent interorgan trafficking of group 2 innate lymphoid cells supports host defense. *Science*, 359(6371):114–119, 2018.

[26] Roberto R Ricardo-Gonzalez, Christoph Schneider, Chang Liao, Jinwoo Lee, Hong-Erh Liang, and Richard M Locksley. Tissue-specific pathways extrude activated ILC2s to disseminate type 2 immunity. *Journal of Experimental Medicine*, 217(4), 2020.

[27] Patrice Zeis, Mi Lian, Xiying Fan, Josip S Herman, Daniela C Hernandez, Rebecca Gentek, Shlomo Elias, Cornelia Symowski, Konrad Knöpper, Nina Peltokangas, et al. In situ maturation and tissue adaptation of type 2 innate lymphoid cell progenitors. *Immunity*, 53(4):775–792, 2020.

[28] Ari B Molofsky, Jesse C Nussbaum, Hong-Erh Liang, Steven J Van Dyken, Laurence E Cheng, Alexander Mohapatra, Ajay Chawla, and Richard M Locksley. Innate lymphoid type 2 cells sustain visceral adipose tissue eosinophils and alternatively activated macrophages. *Journal of Experimental Medicine*, 210(3):535–549, 2013.

[29] Jonathan R Brestoff, Brian S Kim, Steven A Saenz, Rachel R Stine, Laurel A Monticelli, Gregory F Sonnenberg, Joseph J Thome, Donna L Farber, Kabirullah Lutfy, Patrick Seale, et al. Group 2 innate lymphoid cells promote beiging of white adipose tissue and limit obesity. *Nature*, 519(7542):242–246, 2015.

[30] Min-Woo Lee, Justin I Odegaard, Lata Mukundan, Yifu Qiu, Ari B Molofsky, Jesse C Nussbaum, Karen Yun, Richard M Locksley, and Ajay Chawla. Activated type 2 innate lymphoid cells regulate beige fat biogenesis. *Cell*, 160(1-2):74–87, 2015.

[31] Takaharu Sasaki, Kazuyo Moro, Tetsuya Kubota, Naoto Kubota, Tamotsu Kato, Hiroshi Ohno, Susumu Nakae, Hirohisa Saito, and Shigeo Koyasu. Innate lymphoid cells in the induction of obesity. *Cell Reports*, 28(1):202–217, 2019.

[32] Roberto R Ricardo-Gonzalez, Steven J Van Dyken, Christoph Schneider, Jinwoo Lee, Jesse C Nussbaum, Hong-Erh Liang, Dedeepya Vaka, Walter L Eckalbar, Ari B Molofsky, David J Erle, et al. Tissue signals imprint ILC2 identity with anticipatory function. *Nature Immunology*, 19(10):1093–1099, 2018.

[33] Madelene W Dahlgren, Stephen W Jones, Kelly M Cautivo, Alexandra Dubinin, Jorge F Ortiz-Carpena, Sepideh Farhat, S Yu Kevin, Katharine Lee, Chaoqun Wang, Anna V Molofsky, et al. Adventitial stromal cells define group 2 innate lymphoid cell tissue niches. *Immunity*, 50(3):707–722, 2019.

[34] François Gerbe, Emmanuelle Sidot, Danielle J Smyth, Makoto Ohmoto, Ichiro Matsumoto, Valérie Dardalhon, Pierre Cesses, Laure Garnier, Marie Pouzolles, Bénédicte Brulin, et al. Intestinal epithelial tuft cells initiate type 2 mucosal immunity to helminth parasites. *Nature*, 529(7585):226–230, 2016.

[35] Michael R Howitt, Sydney Lavoie, Monia Michaud, Arthur M Blum, Sara V Tran, Joel V Weinstock, Carey Ann Gallini, Kevin Redding, Robert F Margolskee, Lisa C Osborne, et al. Tuft cells, taste-chemosensory cells, orchestrate parasite type 2 immunity in the gut. *Science*, 351(6279):1329–1333, 2016.

[36] Jakob Von Moltke, Ming Ji, Hong-Erh Liang, and Richard M Locksley. Tuft-cell-derived il-25 regulates an intestinal ILC2–epithelial response circuit. *Nature*, 529(7585): 221–225, 2016.

[37] Christoph Schneider, Claire E O'Leary, Jakob von Moltke, Hong-Erh Liang, Qi Yan Ang, Peter J Turnbaugh, Sridhar Radhakrishnan, Michael Pellizzon, Averil Ma, and Richard M Locksley. A metabolite-triggered tuft cell-ILC2 circuit drives small intestinal remodeling. *Cell*, 174(2):271–284, 2018.

[38] Jakob von Moltke, Claire E O'Leary, Nora A Barrett, Yoshihide Kanaoka, K Frank Austen, and Richard M Locksley. Leukotrienes provide an NFAT-dependent signal that synergizes with IL-33 to activate ILC2s. *Journal of Experimental Medicine*, 214 (1):27–37, 2017.

[39] ED Tait Wojno, LA Monticelli, SV Tran, T Alenghat, LC Osborne, JJ Thome, C Willis, A Budelsky, DL Farber, and D Artis. The prostaglandin D 2 receptor CRTH2 regulates accumulation of group 2 innate lymphoid cells in the inflamed lung. *Mucosal Immunology*, 8(6):1313–1323, 2015.

[40] John W McGinty, Hung-An Ting, Tyler E Billipp, Marija S Nadjsombati, Danish M Khan, Nora A Barrett, Hong-Erh Liang, Ichiro Matsumoto, and Jakob von Moltke. Tuft-cell-derived leukotrienes drive rapid anti-helminth immunity in the small intestine but are dispensable for anti-protist immunity. *Immunity*, 52(3):528–541, 2020.

[41] Jesse C Nussbaum, Steven J Van Dyken, Jakob Von Moltke, Laurence E Cheng, Alexander Mohapatra, Ari B Molofsky, Emily E Thornton, Matthew F Krummel, Ajay Chawla, Hong-Erh Liang, et al. Type 2 innate lymphoid cells control eosinophil homeostasis. *Nature*, 502(7470):245–248, 2013.

[42] Vânia Cardoso, Julie Chesné, Hélder Ribeiro, Bethania García-Cassani, Tânia Carvalho, Tiffany Bouchery, Kathleen Shah, Nuno L Barbosa-Morais, Nicola Harris, and Henrique Veiga-Fernandes. Neuronal regulation of type 2 innate lymphoid cells via neuromedin U. *Nature*, 549(7671):277–281, 2017.

[43] Christoph SN Klose, Tanel Mahlakõiv, Jesper B Moeller, Lucille C Rankin, Anne-Laure Flamar, Hiroki Kabata, Laurel A Monticelli, Saya Moriyama, Gregory Garbès Putzel, Nikolai Rakhilin, et al. The neuropeptide neuromedin U stimulates innate lymphoid cells and type 2 inflammation. *Nature*, 549(7671):282–286, 2017.

[44] Antonia Wallrapp, Samantha J Riesenfeld, Patrick R Burkett, Raja-Elie E Abdulnour, Jackson Nyman, Danielle Dionne, Matan Hofree, Michael S Cuoco, Christopher Rodman, Daneyal Farouq, et al. The neuropeptide NMU amplifies ILC2-driven allergic lung inflammation. *Nature*, 549(7672):351–356, 2017.

[45] Hiroyuki Nagashima, Tanel Mahlakõiv, Han-Yu Shih, Fred P Davis, Francoise Meylan, Yuefeng Huang, Oliver J Harrison, Chen Yao, Yohei Mikami, Joseph F Urban Jr, et al. Neuropeptide CGRP limits group 2 innate lymphoid cell responses and constrains type 2 inflammation. *Immunity*, 51(4):682–695, 2019.

[46] Antonia Wallrapp, Patrick R Burkett, Samantha J Riesenfeld, Se-Jin Kim, Elena Christian, Raja-Elie E Abdulnour, Pratiksha I Thakore, Alexandra Schnell, Conner Lambden, Rebecca H Herbst, et al. Calcitonin gene-related peptide negatively regulates alarmin-driven type 2 innate lymphoid cell responses. *Immunity*, 51(4):709–723, 2019.

[47] Kairui Mao, Antonio P Baptista, Samira Tamoutounour, Lenan Zhuang, Nicolas Bouladoux, Andrew J Martins, Yuefeng Huang, Michael Y Gerner, Yasmine Belkaid, and Ronald N Germain. Innate and adaptive lymphocytes sequentially shape the gut microbiota and lipid metabolism. *Nature*, 554(7691):255–259, 2018.

[48] Hiroaki Takatori, Yuka Kanno, Wendy T Watford, Cristina M Tato, Greta Weiss, Ivaylo I Ivanov, Dan R Littman, and John J O'Shea. Lymphoid tissue inducer–like cells are an innate source of IL-17 and IL-22. *Journal of Experimental Medicine*, 206 (1):35–41, 2009.

[49] Ju Qiu, Jennifer J Heller, Xiaohuan Guo, E Chen Zong-ming, Kamonwan Fish, Yang-Xin Fu, and Liang Zhou. The aryl hydrocarbon receptor regulates gut immunity through modulation of innate lymphoid cells. *Immunity*, 36(1):92–104, 2012.

[50] Jhimmy Talbot, Paul Hahn, Lina Kroehling, Henry Nguyen, Dayi Li, and Dan R Littman. Feeding-dependent VIP neuron–ILC3 circuit regulates the intestinal barrier. *Nature*, 579(7800):575–580, 2020.

[51] Lucille C Rankin, Mathilde JH Girard-Madoux, Cyril Seillet, Lisa A Mielke, Yann Kerdiles, Aurore Fenis, Elisabeth Wieduwild, Tracy Putoczki, Stanislas Mondot, Olivier Lantz, et al. Complementarity and redundancy of IL-22-producing innate lymphoid cells. *Nature Immunology*, 17(2):179–186, 2016.

[52] Elina A Kiss, Cedric Vonarbourg, Stefanie Kopfmann, Elias Hobeika, Daniela Finke, Charlotte Esser, and Andreas Diefenbach. Natural aryl hydrocarbon receptor ligands control organogenesis of intestinal lymphoid follicles. *Science*, 334(6062):1561–1565, 2011.

[53] Jacob S Lee, Marina Cella, Keely G McDonald, Cecilia Garlanda, Gregory D Kennedy, Manabu Nukaya, Alberto Mantovani, Raphael Kopan, Christopher A Bradfield, Rodney D Newberry, et al. Ahr drives the development of gut ILC22 cells and postnatal lymphoid tissues via pathways dependent on and independent of Notch. *Nature Immunology*, 13(2):144–151, 2012.

[54] Christoph SN Klose, Elina A Kiss, Vera Schwierzeck, Karolina Ebert, Thomas Hoyler, Yannick d'Hargues, Nathalie Göppert, Andrew L Croxford, Ari Waisman, Yakup Tanriver, et al. A T-bet gradient controls the fate and function of CCR6$^-$ RORγt$^+$ innate lymphoid cells. *Nature*, 494(7436):261–265, 2013.

[55] Sales Ibiza, Bethania García-Cassani, Hélder Ribeiro, Tânia Carvalho, Luís Almeida, Rute Marques, Ana M Misic, Casey Bartow-McKenney, Denise M Larson, William J Pavan, et al. Glial-cell-derived neuroregulators control type 3 innate lymphoid cells and gut defence. *Nature*, 535(7612):440–443, 2016.

[56] Eric Vivier, Serge A Van De Pavert, Max D Cooper, and Gabrielle T Belz. The evolution of innate lymphoid cells. *Nature Immunology*, 17(7):790, 2016.

[57] Reina E Mebius, Paul Rennert, and Irving L Weissman. Developing lymph nodes collect CD4$^+$ CD3$^-$ LTβ^+ cells that can differentiate to APC, NK cells, and follicular cells but not T or B cells. *Immunity*, 7(4):493–504, 1997.

[58] Gérard Eberl, Shana Marmon, Mary-Jean Sunshine, Paul D Rennert, Yongwon Choi, and Dan R Littman. An essential function for the nuclear receptor RORγt in the generation of fetal lymphoid tissue inducer cells. *Nature Immunology*, 5(1):64, 2004.

[59] Shinichiro Sawa, Marie Cherrier, Matthias Lochner, Naoko Satoh-Takayama, Hans Jörg Fehling, Francina Langa, James P Di Santo, and Gérard Eberl. Lineage

relationship analysis of RORγt$^+$ innate lymphoid cells. *Science*, 330(6004):665–669, 2010.

[60] Serge A van de Pavert, Manuela Ferreira, Rita G Domingues, Hélder Ribeiro, Rosalie Molenaar, Lara Moreira-Santos, Francisca F Almeida, Sales Ibiza, Inês Barbosa, Gera Goverse, et al. Maternal retinoids control type 3 innate lymphoid cells and set the offspring immunity. *Nature*, 508(7494):123–127, 2014.

[61] SP Spencer, C Wilhelm, Q Yang, JA Hall, N Bouladoux, A Boyd, TB Nutman, JF Urban, J Wang, TR Ramalingam, et al. Adaptation of innate lymphoid cells to a micronutrient deficiency promotes type 2 barrier immunity. *Science*, 343(6169):432–437, 2014.

[62] Djahida Bouskra, Christophe Brézillon, Marion Bérard, Catherine Werts, Rosa Varona, Ivo Gomperts Boneca, and Gérard Eberl. Lymphoid tissue genesis induced by commensals through NOD1 regulates intestinal homeostasis. *Nature*, 456(7221):507–510, 2008.

[63] Tetsuro Kobayashi, Benjamin Voisin, Elizabeth A Kennedy, Jay-Hyun Jo, Han-Yu Shih, Amanda Truong, Thomas Doebel, Keiko Sakamoto, Chang-Yi Cui, David Schlessinger, et al. Homeostatic control of sebaceous glands by innate lymphoid cells regulates commensal bacteria equilibrium. *Cell*, 176(5):982–997, 2019.

[64] Naoko Satoh-Takayama, Nicolas Serafini, Thomas Verrier, Abdessalem Rekiki, Jean-Christophe Renauld, Gad Frankel, and James P Di Santo. The chemokine receptor CXCR6 controls the functional topography of interleukin-22 producing intestinal innate lymphoid cells. *Immunity*, 41(5):776–788, 2014.

[65] Cedric Vonarbourg, Arthur Mortha, Viet L Bui, Pedro P Hernandez, Elina A Kiss, Thomas Hoyler, Melanie Flach, Bertram Bengsch, Robert Thimme, Christoph Hölscher, et al. Regulated expression of nuclear receptor RORγt confers distinct functional fates to NK cell receptor-expressing RORγt+ innate lymphocytes. *Immunity*, 33(5):736–751, 2010.

[66] Giuseppe Sciumé, Kiyoshi Hirahara, Hayato Takahashi, Arian Laurence, Alejandro V Villarino, Kentner L Singleton, Sean P Spencer, Christoph Wilhelm, Amanda C Poholek, Golnaz Vahedi, et al. Distinct requirements for T-bet in gut innate lymphoid cells. *Journal of Experimental Medicine*, 209(13):2331–2338, 2012.

[67] Lucille C Rankin, Joanna R Groom, Michaël Chopin, Marco J Herold, Jennifer A Walker, Lisa A Mielke, Andrew NJ McKenzie, Sebastian Carotta, Stephen L Nutt, and Gabrielle T Belz. The transcription factor T-bet is essential for the development of NKp46+ innate lymphocytes via the Notch pathway. *Nature Immunology*, 14(4): 389, 2013.

[68] Chao Zhong, Kairong Cui, Christoph Wilhelm, Gangqing Hu, Kairui Mao, Yasmine Belkaid, Keji Zhao, and Jinfang Zhu. Group 3 innate lymphoid cells continuously

require the transcription factor GATA3 after commitment. *Nature Immunology*, 17(2): 169, 2016.

[69] Erin C Zook and Barbara L Kee. Development of innate lymphoid cells. *Nature Immunology*, 17(7):775–782, 2016.

[70] Isabel E Ishizuka, Michael G Constantinides, Herman Gudjonson, and Albert Bendelac. The innate lymphoid cell precursor. *Annual Review of Immunology*, 34:299–316, 2016.

[71] Motonari Kondo, Irving L Weissman, and Koichi Akashi. Identification of clonogenic common lymphoid progenitors in mouse bone marrow. *Cell*, 91(5):661–672, 1997.

[72] Hisahiro Yoshida, Hiroshi Kawamoto, Sybil M Santee, Hiroyuki Hashi, Kenya Honda, Satomi Nishikawa, Carl F Ware, Yoshimoto Katsura, and Shin-Ichi Nishikawa. Expression of $\alpha 4\beta 7$ integrin defines a distinct pathway of lymphoid progenitors committed to T cells, fetal intestinal lymphotoxin producer, NK, and dendritic cells. *The Journal of Immunology*, 167(5):2511–2521, 2001.

[73] Cécilie Possot, Sandrine Schmutz, Sylvestre Chea, Laurent Boucontet, Anne Louise, Ana Cumano, and Rachel Golub. Notch signaling is necessary for adult, but not fetal, development of RORγt$^+$ innate lymphoid cells. *Nature Immunology*, 12(10):949–958, 2011.

[74] Xiaofei Yu, Yuhao Wang, Mi Deng, Yun Li, Kelly A Ruhn, Cheng Cheng Zhang, and Lora V Hooper. The basic leucine zipper transcription factor NFIL3 directs the development of a common innate lymphoid cell precursor. *Elife*, 3:e04406, 2014.

[75] Qi Yang, Fengyin Li, Christelle Harly, Shaojun Xing, Longyun Ye, Xuefeng Xia, Haikun Wang, Xinxin Wang, Shuyang Yu, Xinyuan Zhou, et al. TCF-1 upregulation identifies early innate lymphoid progenitors in the bone marrow. *Nature Immunology*, 16(10):1044–1050, 2015.

[76] Christelle Harly, Maggie Cam, Jonathan Kaye, and Avinash Bhandoola. Development and differentiation of early innate lymphoid progenitors. *Journal of Experimental Medicine*, 215(1):249–262, 2018.

[77] Christelle Harly, Devin Kenney, Gang Ren, Binbin Lai, Tobias Raabe, Qi Yang, Margaret C Cam, Hai-Hui Xue, Keji Zhao, and Avinash Bhandoola. The transcription factor TCF-1 enforces commitment to the innate lymphoid cell lineage. *Nature Immunology*, 20(9):1150–1160, 2019.

[78] Michael G Constantinides, Benjamin D McDonald, Philip A Verhoef, and Albert Bendelac. A committed hemopoietic precursor to innate lymphoid cells. *Nature*, 508(7496): 397, 2014.

[79] Yong Yu, Jason CH Tsang, Cui Wang, Simon Clare, Juexuan Wang, Xi Chen, Cordelia Brandt, Leanne Kane, Lia S Campos, Liming Lu, et al. Single-cell RNA-seq identifies

a PD-1^{hi} ILC progenitor and defines its development pathway. *Nature*, 539(7627): 102–106, 2016.

[80] Ai-Ping Mao, Isabel E Ishizuka, Darshan N Kasal, Malay Mandal, and Albert Bendelac. A shared Runx1-bound Zbtb16 enhancer directs innate and innate-like lymphoid lineage development. *Nature Communications*, 8(1):863, 2017.

[81] Thomas Hoyler, Christoph SN Klose, Abdallah Souabni, Adriana Turqueti-Neves, Dietmar Pfeifer, Emma L Rawlins, David Voehringer, Meinrad Busslinger, and Andreas Diefenbach. The transcription factor GATA-3 controls cell fate and maintenance of type 2 innate lymphoid cells. *Immunity*, 37(4):634–648, 2012.

[82] Marie Cherrier, Shinichiro Sawa, and Gérard Eberl. Notch, Id2, and RORγt sequentially orchestrate the fetal development of lymphoid tissue inducer cells. *Journal of Experimental Medicine*, 209(4):729–740, 2012.

[83] Sebastian Carotta, Swee Heng Milon Pang, Stephen L Nutt, and Gabrielle T Belz. Identification of the earliest NK-cell precursor in the mouse BM. *Blood*, 117(20):5449–5452, 2011.

[84] John W Fathman, Deepta Bhattacharya, Matthew A Inlay, Jun Seita, Holger Karsunky, and Irving L Weissman. Identification of the earliest natural killer cell–committed progenitor in murine bone marrow. *Blood*, 118(20):5439–5447, 2011.

[85] Adam K Savage, Michael G Constantinides, Jin Han, Damien Picard, Emmanuel Martin, Bofeng Li, Olivier Lantz, and Albert Bendelac. The transcription factor PLZF directs the effector program of the NKT cell lineage. *Immunity*, 29(3):391–403, 2008.

[86] Masaki Miyazaki, Kazuko Miyazaki, Kenian Chen, Yi Jin, Jacob Turner, Amanda J Moore, Rintaro Saito, Kenichi Yoshida, Seishi Ogawa, Hans-Reimer Rodewald, et al. The E-Id protein axis specifies adaptive lymphoid cell identity and suppresses thymic innate lymphoid cell development. *Immunity*, 46(5):818–834, 2017.

[87] Eleftheria E Rosmaraki, Iyadh Douagi, Claude Roth, Francesco Colucci, Ana Cumano, and James P Di Santo. Identification of committed NK cell progenitors in adult murine bone marrow. *European Journal of Immunology*, 31(6):1900–1909, 2001.

[88] Qi Yang, Laurel A Monticelli, Steven A Saenz, Anthony Wei-Shine Chi, Gregory F Sonnenberg, Jiangbo Tang, Maria Elena De Obaldia, Will Bailis, Jerrod L Bryson, Kristin Toscano, et al. T cell factor 1 is required for group 2 innate lymphoid cell generation. *Immunity*, 38(4):694–704, 2013.

[89] Timotheus YF Halim, Aric MacLaren, Mark T Romanish, Matthew J Gold, Kelly M McNagny, and Fumio Takei. Retinoic-acid-receptor-related orphan nuclear receptor alpha is required for natural helper cell development and allergic inflammation. *Immunity*, 37(3):463–474, 2012.

[90] Lisa A Mielke, Joanna R Groom, Lucille C Rankin, Cyril Seillet, Frederick Masson, Tracy Putoczki, and Gabrielle T Belz. TCF-1 controls ILC2 and NKp46$^+$ RORγt$^+$ innate lymphocyte differentiation and protection in intestinal inflammation. *The Journal of Immunology*, 191(8):4383–4391, 2013.

[91] Cyril Seillet, Lisa A Mielke, Daniela B Amann-Zalcenstein, Shian Su, Jerry Gao, Francisca F Almeida, Wei Shi, Matthew E Ritchie, Shalin H Naik, Nicholas D Huntington, et al. Deciphering the innate lymphoid cell transcriptional program. *Cell Reports*, 17 (2):436–447, 2016.

[92] Isabel E Ishizuka, Sylvestre Chea, Herman Gudjonson, Michael G Constantinides, Aaron R Dinner, Albert Bendelac, and Rachel Golub. Single-cell analysis defines the divergence between the innate lymphoid cell lineage and lymphoid tissue-inducer cell lineage. *Nature Immunology*, 17(3):269–276, 2016.

[93] Wei Xu, Dylan E Cherrier, Sylvestre Chea, Christian Vosshenrich, Nicolas Serafini, Maxime Petit, Pentao Liu, Rachel Golub, and James P Di Santo. An Id2RFP-Reporter Mouse Redefines Innate Lymphoid Cell Precursor Potentials. *Immunity*, 2019.

[94] Jennifer A Walker, Paula A Clark, Alastair Crisp, Jillian L Barlow, Aydan Szeto, Ana CF Ferreira, Batika MJ Rana, Helen E Jolin, Noe Rodriguez-Rodriguez, Meera Sivasubramaniam, et al. Polychromic Reporter Mice Reveal Unappreciated Innate Lymphoid Cell Progenitor Heterogeneity and Elusive ILC3 Progenitors in Bone Marrow. *Immunity*, 2019.

[95] Emma L Rawlins, Cheryl P Clark, Yan Xue, and Brigid LM Hogan. The Id2$^+$ distal tip lung epithelium contains individual multipotent embryonic progenitor cells. *Development*, 136(22):3741–3745, 2009.

[96] Yoshifumi Yokota, Ahmed Mansouri, Seiichi Mori, Seiichi Sugawara, et al. Development of peripheral lymphoid organs and natural killer cells depends on the helix-loop-helix inhibitor Id2. *Nature*, 397(6721):702, 1999.

[97] Markus D Boos, Yoshifumi Yokota, Gerard Eberl, and Barbara L Kee. Mature natural killer cell and lymphoid tissue–inducing cell development requires Id2-mediated suppression of E protein activity. *Journal of Experimental Medicine*, 204(5):1119–1130, 2007.

[98] Yuan Zhuang, Annette Jackson, Lihua Pan, Kang Shen, and Meifang Dai. Regulation of E2A gene expression in B-lymphocyte development. *Molecular Immunology*, 40(16): 1165–1177, 2004.

[99] Sylvestre Chea, Sandrine Schmutz, Claire Berthault, Thibaut Perchet, Maxime Petit, Odile Burlen-Defranoux, Ananda W Goldrath, Hans-Reimer Rodewald, Ana Cumano, and Rachel Golub. Single-cell gene expression analyses reveal heterogeneous responsiveness of fetal innate lymphoid progenitors to notch signaling. *Cell Reports*, 14(6): 1500–1516, 2016.

[100] David Allman, Arivazhagan Sambandam, Sungjune Kim, Juli P Miller, Antonio Pagan, David Well, Anita Meraz, and Avinash Bhandoola. Thymopoiesis independent of common lymphoid progenitors. *Nature Immunology*, 4(2):168–174, 2003.

[101] Qi Yang, Steven A Saenz, Daniel A Zlotoff, David Artis, and Avinash Bhandoola. Cutting edge: Natural helper cells derive from lymphoid progenitors. *The Journal of Immunology*, 187(11):5505–5509, 2011.

[102] Reina E Mebius, Toshihiro Miyamoto, Julie Christensen, Jos Domen, Tom Cupedo, Irving L Weissman, and Koichi Akashi. The fetal liver counterpart of adult common lymphoid progenitors gives rise to all lymphoid lineages, $CD45^+$ $CD4^+$ $CD3^-$ cells, as well as macrophages. *The Journal of Immunology*, 166(11):6593–6601, 2001.

[103] Jennifer K Bando, Hong-Erh Liang, and Richard M Locksley. Identification and distribution of developing innate lymphoid cells in the fetal mouse intestine. *Nature Immunology*, 16(2):153–160, 2015.

[104] Takashi Ebihara, Christina Song, Stacy H Ryu, Beatrice Plougastel-Douglas, Liping Yang, Ditsa Levanon, Yoram Groner, Michael D Bern, Thaddeus S Stappenbeck, Marco Colonna, et al. Runx3 specifies lineage commitment of innate lymphoid cells. *Nature Immunology*, 16(11):1124–1133, 2015.

[105] Maryam Ghaedi, Zi Yi Shen, Mona Orangi, Itziar Martinez-Gonzalez, Lisa Wei, Xiaoxiao Lu, Arundhoti Das, Alireza Heravi-Moussavi, Marco A Marra, Avinash Bhandoola, et al. Single-cell analysis of RORα tracer mouse lung reveals ILC progenitors and effector ILC2 subsets. *The Journal of Experimental Medicine*, 217(3), 2020.

[106] Jenny M Mjösberg, Sara Trifari, Natasha K Crellin, Charlotte P Peters, Cornelis M Van Drunen, Berber Piet, Wytske J Fokkens, Tom Cupedo, and Hergen Spits. Human il-25-and il-33-responsive type 2 innate lymphoid cells are defined by expression of crth2 and cd161. *Nature immunology*, 12(11):1055–1062, 2011.

[107] Jong-Eun Park, Laura Jardine, Berthold Gottgens, Sarah A Teichmann, and Muzlifah Haniffa. Prenatal development of human immunity. *Science*, 368(6491):600–603, 2020.

[108] Steven D Scoville, Bethany L Mundy-Bosse, Michael H Zhang, Li Chen, Xiaoli Zhang, Karen A Keller, Tiffany Hughes, Luxi Chen, Stephanie Cheng, Stephen M Bergin, et al. A progenitor cell expressing transcription factor rorγt generates all human innate lymphoid cell subsets. *Immunity*, 44(5):1140–1150, 2016.

[109] Naoko Satoh-Takayama, Sarah Lesjean-Pottier, Paulo Vieira, Shinichiro Sawa, Gerard Eberl, Christian AJ Vosshenrich, and James P Di Santo. Il-7 and IL-15 independently program the differentiation of intestinal $CD3^-$ $NKp46^+$ cell subsets from Id2-dependent precursors. *Journal of Experimental Medicine*, 207(2):273–280, 2010.

[110] Ai Ing Lim, Yan Li, Silvia Lopez-Lastra, Ralph Stadhouders, Franziska Paul, Armanda Casrouge, Nicolas Serafini, Anne Puel, Jacinta Bustamante, Laura Surace, et al. Systemic human ilc precursors provide a substrate for tissue ilc differentiation. *Cell*, 168 (6):1086–1100, 2017.

[111] Parinaz Aliahmad, Brian De La Torre, and Jonathan Kaye. Shared dependence on the DNA-binding factor TOX for the development of lymphoid tissue-inducer cell and NK cell lineages. *Nature Immunology*, 11(10):945–952, 2010.

[112] Corey R Seehus, Parinaz Aliahmad, Brian De La Torre, Iliyan D Iliev, Lindsay Spurka, Vincent A Funari, and Jonathan Kaye. Innate lymphoid cell development requires TOX-dependent generation of a common ILC progenitor. *Nature Immunology*, 16(6): 599, 2015.

[113] Duncan M Gascoyne, Elaine Long, Henrique Veiga-Fernandes, Jasper De Boer, Owen Williams, Benedict Seddon, Mark Coles, Dimitris Kioussis, and Hugh JM Brady. The basic leucine zipper transcription factor E4BP4 is essential for natural killer cell development. *Nature Immunology*, 10(10):1118–1124, 2009.

[114] Shintaro Kamizono, Gordon S Duncan, Markus G Seidel, Akira Morimoto, Koichi Hamada, Gerard Grosveld, Koichi Akashi, Evan F Lind, Jillian P Haight, Pamela S Ohashi, et al. Nfil3/E4bp4 is required for the development and maturation of NK cells in vivo. *Journal of Experimental Medicine*, 206(13):2977–2986, 2009.

[115] Theresa L Geiger, Michael C Abt, Georg Gasteiger, Matthew A Firth, Margaret H O'Connor, Clair D Geary, Timothy E O'Sullivan, Marcel R van den Brink, Eric G Pamer, Alan M Hanash, et al. Nfil3 is crucial for development of innate lymphoid cells and host protection against intestinal pathogens. *Journal of Experimental Medicine*, pages jem–20140212, 2014.

[116] Stefania Crotta, Annita Gkioka, Victoria Male, João H Duarte, Sophia Davidson, Ilaria Nisoli, Hugh JM Brady, and Andreas Wack. The transcription factor E4BP4 is not required for extramedullary pathways of NK cell development. *The Journal of Immunology*, 192(6):2677–2688, 2014.

[117] Cyril Seillet, Lucille C Rankin, Joanna R Groom, Lisa A Mielke, Julie Tellier, Michael Chopin, Nicholas D Huntington, Gabrielle T Belz, and Sebastian Carotta. Nfil3 is required for the development of all innate lymphoid cell subsets. *Journal of Experimental Medicine*, 211(9):1733–1740, 2014.

[118] Wei Xu, Rita G Domingues, Diogo Fonseca-Pereira, Manuela Ferreira, Helder Ribeiro, Silvia Lopez-Lastra, Yasutaka Motomura, Lara Moreira-Santos, Franck Bihl, Veronique Braud, et al. NFIL3 orchestrates the emergence of common helper innate lymphoid cell precursors. *Cell Reports*, 10(12):2043–2054, 2015.

[119] Beena Jeevan-Raj, Jasmine Gehrig, Mélanie Charmoy, Vijaykumar Chennupati, Camille Grandclément, Paolo Angelino, Mauro Delorenzi, and Werner Held. The

Transcription Factor Tcf1 Contributes to Normal NK Cell Development and Function by Limiting the Expression of Granzymes. *Cell Reports*, 20(3):613–626, 2017.

[120] Sandrine I Samson, Odile Richard, Manuela Tavian, Thomas Ranson, Christian AJ Vosshenrich, Francesco Colucci, Jan Buer, Frank Grosveld, Isabelle Godin, and James P Di Santo. GATA-3 promotes maturation, IFN-γ production, and liver-specific homing of NK cells. *Immunity*, 19(5):701–711, 2003.

[121] Ryoji Yagi, Chao Zhong, Daniel L Northrup, Fang Yu, Nicolas Bouladoux, Sean Spencer, Gangqing Hu, Luke Barron, Suveena Sharma, Toshinori Nakayama, et al. The transcription factor GATA3 is critical for the development of all IL-7Rα-expressing innate lymphoid cells. *Immunity*, 40(3):378–388, 2014.

[122] Nicolas Serafini, Roel GJ Klein Wolterink, Naoko Satoh-Takayama, Wei Xu, Christian AJ Vosshenrich, Rudi W Hendriks, and James P Di Santo. Gata3 drives development of RORγt$^+$ group 3 innate lymphoid cells. *Journal of Experimental Medicine*, pages jem–20131038, 2014.

[123] Shin-ichiro Ohno, Takehito Sato, Kazuyoshi Kohu, Kazuyoshi Takeda, Ko Okumura, Masanobu Satake, and Sonoko Habu. Runx proteins are involved in regulation of CD122, Ly49 family and IFN-γ expression during NK cell differentiation. *International Immunology*, 20(1):71–79, 2007.

[124] Masashi Tachibana, Mari Tenno, Chieko Tezuka, Machiko Sugiyama, Hisahiro Yoshida, and Ichiro Taniuchi. Runx1/Cbfβ2 complexes are required for lymphoid tissue inducer cell differentiation at two developmental stages. *The Journal of Immunology*, 186(3): 1450–1457, 2011.

[125] Danielle Califano, Jonathan J Cho, Mohammad N Uddin, Kyle J Lorentsen, Qi Yang, Avinash Bhandoola, Hongmin Li, and Dorina Avram. Transcription factor Bcl11b controls identity and function of mature type 2 innate lymphoid cells. *Immunity*, 43 (2):354–368, 2015.

[126] Jennifer A Walker, Christopher J Oliphant, Alexandros Englezakis, Yong Yu, Simon Clare, Hans-Reimer Rodewald, Gabrielle Belz, Pentao Liu, Padraic G Fallon, and Andrew NJ McKenzie. Bcl11b is essential for group 2 innate lymphoid cell development. *Journal of Experimental Medicine*, 212(6):875–882, 2015.

[127] Yong Yu, Cui Wang, Simon Clare, Juexuan Wang, Song-Choon Lee, Cordelia Brandt, Shannon Burke, Liming Lu, Daqian He, Nancy A Jenkins, et al. The transcription factor Bcl11b is specifically expressed in group 2 innate lymphoid cells and is essential for their development. *Journal of Experimental Medicine*, pages jem–20142318, 2015.

[128] Anja Fuchs, William Vermi, Jacob S Lee, Silvia Lonardi, Susan Gilfillan, Rodney D Newberry, Marina Cella, and Marco Colonna. Intraepithelial type 1 innate lymphoid cells are a unique subset of IL-12-and IL-15-responsive IFN-γ-producing cells. *Immunity*, 38(4):769–781, 2013.

[129] Chauncey J Spooner, Justin Lesch, Donghong Yan, Aly A Khan, Alex Abbas, Vladimir Ramirez-Carrozzi, Meijuan Zhou, Robert Soriano, Jeffrey Eastham-Anderson, Lauri Diehl, et al. Specification of type 2 innate lymphocytes by the transcriptional determinant Gfi1. *Nature Immunology*, 14(12):1229–1236, 2013.

[130] Erin C Zook, Kevin Ramirez, Xiaohuan Guo, Grant van der Voort, Mikael Sigvardsson, Eric C Svensson, Yang-Xin Fu, and Barbara L Kee. The ETS1 transcription factor is required for the development and cytokine-induced expansion of ILC2. *Journal of Experimental Medicine*, pages jem–20150851, 2016.

[131] Barbara L Kee. E and ID proteins branch out. *Nature Reviews Immunology*, 9(3): 175–184, 2009.

[132] Erin C Zook, Zhong-Yin Li, Yiying Xu, Renée F de Pooter, Mihalis Verykokakis, Aimee Beaulieu, Anna Lasorella, Mark Maienschein-Cline, Joseph C Sun, Mikael Sigvardsson, et al. Transcription factor ID2 prevents E proteins from enforcing a naive T lymphocyte gene program during NK cell development. *Science Immunology*, 3(22), 2018.

[133] Laura Chiossone, Julie Chaix, Nicolas Fuseri, Claude Roth, Eric Vivier, and Thierry Walzer. Maturation of mouse NK cells is a 4-stage developmental program. *Blood*, 113 (22):5488–5496, 2009.

[134] Rebecca B Delconte, Wei Shi, Priyanka Sathe, Takashi Ushiki, Cyril Seillet, Martina Minnich, Tatiana B Kolesnik, Lucille C Rankin, Lisa A Mielke, Jian-Guo Zhang, et al. The helix-loop-helix protein ID2 governs NK cell fate by tuning their sensitivity to interleukin-15. *Immunity*, 44(1):103–115, 2016.

[135] Walter K Mowel, Sam J McCright, Jonathan J Kotzin, Magalie A Collet, Asli Uyar, Xin Chen, Alexandra DeLaney, Sean P Spencer, Anthony T Virtue, EnJun Yang, et al. Group 1 innate lymphoid cell lineage identity is determined by a cis-regulatory element marked by a long non-coding RNA. *Immunity*, 47(3):435–449, 2017.

[136] Ai-Ping Mao, Michael G Constantinides, Rebecca Mathew, Zhixiang Zuo, Xiaoting Chen, Matthew T Weirauch, and Albert Bendelac. Multiple layers of transcriptional regulation by PLZF in NKT-cell development. *Proceedings of the National Academy of Sciences*, 113(27):7602–7607, 2016.

[137] Philip A Verhoef, Michael G Constantinides, Benjamin D McDonald, Joseph F Urban, Anne I Sperling, and Albert Bendelac. Intrinsic functional defects of type 2 innate lymphoid cells impair innate allergic inflammation in promyelocytic leukemia zinc finger PLZF–deficient mice. *Journal of Allergy and Clinical Immunology*, 137(2):591–600, 2016.

[138] Sjef Verbeek, David Izon, Frans Hofhuis, Els Robanus-Maandag, Hein Te Riele, Marc van de Watering, Mariette Oosterwegel, Anne Wilson, H Robson MacDonald, and Hans Clevers. An HMG-box-containing T-cell factor required for thymocyte differentiation. *Nature*, 374(6517):70–74, 1995.

[139] John L Johnson, Georgios Georgakilas, Jelena Petrovic, Makoto Kurachi, Stanley Cai, Christelle Harly, Warren S Pear, Avinash Bhandoola, E John Wherry, and Golnaz Vahedi. Lineage-determining transcription factor TCF-1 initiates the epigenetic identity of T cells. *Immunity*, 48(2):243–257, 2018.

[140] Werner Held, Hans Clevers, and Rudolf Grosschedl. Redundant functions of TCF-1 and LEF-1 during T and NK cell development, but unique role of TCF-1 for Ly49 NK cell receptor acquisition. *European Journal of Immunology*, 33(5):1393–1398, 2003.

[141] Nidhi Malhotra, Kavitha Narayan, Ok Hyun Cho, Katelyn E Sylvia, Catherine Yin, Heather Melichar, Mehdi Rashighi, Veronique Lefebvre, John E Harris, Leslie J Berg, et al. A network of high-mobility group box transcription factors programs innate interleukin-17 production. *Immunity*, 38(4):681–693, 2013.

[142] Zhong-Yin Li, Rosemary E Morman, Emma Hegermiller, Mengxi Sun, Elizabeth T Bartom, Mark Maienschein-Cline, Mikael Sigvardsson, and Barbara L Kee. The transcriptional repressor ID2 supports natural killer cell maturation by controlling TCF1 amplitude. *Journal of Experimental Medicine*, 218(6):e20202032, 2021.

[143] Kristine Germar, Marei Dose, Tassos Konstantinou, Jiangwen Zhang, Hongfang Wang, Camille Lobry, Kelly L Arnett, Stephen C Blacklow, Iannis Aifantis, Jon C Aster, et al. T-cell factor 1 is a gatekeeper for T-cell specification in response to Notch signaling. *Proceedings of the National Academy of Sciences*, 108(50):20060–20065, 2011.

[144] Akinola Olumide Emmanuel, Stephen Arnovitz, Leila Haghi, Priya S Mathur, Soumi Mondal, Jasmin Quandt, Michael K Okoreeh, Mark Maienschein-Cline, Khashayarsha Khazaie, Marei Dose, et al. Tcf-1 and HEB cooperate to establish the epigenetic and transcription profiles of $CD4^+$ $CD8^+$ thymocytes. *Nature Immunology*, 19(12): 1366–1378, 2018.

[145] Christelle Harly, Devin Kenney, Yueqiang Wang, Yi Ding, Yongge Zhao, Parirokh Awasthi, and Avinash Bhandoola. A Shared Regulatory Element Controls the Initiation of Tcf7 Expression During Early T Cell and Innate Lymphoid Cell Developments. *Frontiers in Immunology*, 11:470, 2020.

[146] Pier Paolo Pandolfi, Matthew E Roth, Alar Karis, Mark W Leonard, E Dzierzak, Frank G Grosveld, James Douglas Engel, and Michael H Lindenbaum. Targeted disruption of the GATA3 gene causes severe abnormalities in the nervous system and in fetal liver haematopoiesis. *Nature Genetics*, 11(1):40–44, 1995.

[147] Ken H Lieuw, Guo-long Li, Yinghui Zhou, Frank Grosveld, and James Douglas Engel. Temporal and spatial control of murine GATA-3 transcription by promoter-proximal regulatory elements. *Developmental Biology*, 188(1):1–16, 1997.

[148] Ganesh Lakshmanan, Ken H Lieuw, Kim-Chew Lim, Yi Gu, Frank Grosveld, James Douglas Engel, and Alar Karis. Localization of distant urogenital system-,

central nervous system-, and endocardium-specific transcriptional regulatory elements in the GATA-3 locus. *Molecular and Cellular Biology*, 19(2):1558–1568, 1999.

[149] Susan L Hasegawa, Takashi Moriguchi, Arvind Rao, Takashi Kuroha, James Douglas Engel, and Kim-Chew Lim. Dosage-dependent rescue of definitive nephrogenesis by a distant *Gata3* enhancer. *Developmental Biology*, 301(2):568–577, 2007.

[150] Takashi Moriguchi, Tomofumi Hoshino, Arvind Rao, Lei Yu, Jun Takai, Satoshi Uemura, Kazue Ise, Yasuhiro Nakamura, Kim-Chew Lim, Ritsuko Shimizu, et al. A *gata3* 3' distal otic vesicle enhancer directs inner ear-specific *gata3* expression. *Molecular and Cellular Biology*, 38(21), 2018.

[151] Elena Martynova, Maxime Bouchard, Linda S Musil, and Ales Cvekl. Identification of novel *Gata3* distal enhancers active in mouse embryonic lens. *Developmental Dynamics*, 247(11):1186–1198, 2018.

[152] Tomonori Hosoya, Takashi Kuroha, Takashi Moriguchi, Dustin Cummings, Ivan Maillard, Kim-Chew Lim, and James Douglas Engel. Gata-3 is required for early T lineage progenitor development. *Journal of Experimental Medicine*, 206(13):2987–3000, 2009.

[153] Chao-Nan Ting, Marilyn C Olson, Kevin P Barton, and Jeffrey M Leiden. Transcription factor GATA-3 is required for development of the T-cell lineage. *Nature*, 384 (6608):474–478, 1996.

[154] Sung-Yun Pai, Morgan L Truitt, Chao-Nan Ting, Jeffrey M Leiden, Laurie H Glimcher, and I-Cheng Ho. Critical roles for transcription factor GATA-3 in thymocyte development. *Immunity*, 19(6):863–875, 2003.

[155] Yunqi Wang, Ichiro Misumi, Ai-Di Gu, T Anthony Curtis, Lishan Su, Jason K Whitmire, and Yisong Y Wan. Gata-3 controls the maintenance and proliferation of T cells downstream of TCR and cytokine signaling. *Nature Immunology*, 14(7):714–722, 2013.

[156] Dong-Hong Zhang, Lauren Cohn, Prabir Ray, Kim Bottomly, and Anuradha Ray. Transcription factor GATA-3 is differentially expressed in murine Th1 and Th2 cells and controls Th2-specific expression of the interleukin-5 gene. *Journal of Biological Chemistry*, 272(34):21597–21603, 1997.

[157] Wei-ping Zheng and Richard A Flavell. The transcription factor GATA-3 is necessary and sufficient for Th2 cytokine gene expression in CD4 T cells. *Cell*, 89(4):587–596, 1997.

[158] Jinfang Zhu, Booki Min, Jane Hu-Li, Cynthia J Watson, Alex Grinberg, Qi Wang, Nigel Killeen, Joseph F Urban, Liying Guo, and William E Paul. Conditional deletion of *Gata3* shows its essential function in TH 1-TH 2 responses. *Nature Immunology*, 5 (11):1157–1165, 2004.

[159] Roel GJ Klein Wolterink, Nicolas Serafini, Menno van Nimwegen, Christian AJ Vosshenrich, Marjolein JW de Bruijn, Diogo Fonseca Pereira, Henrique Veiga Fernandes, Rudi W Hendriks, and James P Di Santo. Essential, dose-dependent role for the transcription factor *Gata3* in the development of IL-5^+ and IL-13^+ type 2 innate lymphoid cells. *Proceedings of the National Academy of Sciences*, 110(25):10240–10245, 2013.

[160] Christian AJ Vosshenrich, Marcos E García-Ojeda, Sandrine I Samson-Villéger, Valerie Pasqualetto, Laurence Enault, Odile Richard-Le Goff, Erwan Corcuff, Delphine Guy-Grand, Benedita Rocha, Ana Cumano, et al. A thymic pathway of mouse natural killer cell development characterized by expression of GATA-3 and CD127. *Nature Immunology*, 7(11):1217–1224, 2006.

[161] Chao Zhong, Mingzhu Zheng, Kairong Cui, Andrew J Martins, Gangqing Hu, Dan Li, Lino Tessarollo, Serguei Kozlov, Jonathan R Keller, John S Tsang, et al. Differential expression of the transcription factor GATA3 specifies lineage and functions of innate lymphoid cells. *Immunity*, 52(1):83–95, 2020.

[162] Sakie Hosoya-Ohmura, Yu-Hsuan Lin, Mary Herrmann, Takashi Kuroha, Arvind Rao, Takashi Moriguchi, Kim-Chew Lim, Tomonori Hosoya, and James Douglas Engel. An NK and T cell enhancer lies 280 kilobase pairs 3' to the *Gata3* structural gene. *Molecular and Cellular Biology*, 31(9):1894–1904, 2011.

[163] Sakie Ohmura, Seiya Mizuno, Hisashi Oishi, Chia-Jui Ku, Mary Hermann, Tomonori Hosoya, Satoru Takahashi, James Douglas Engel, et al. Lineage-affiliated transcription factors bind the *Gata3* Tce1 enhancer to mediate lineage-specific programs. *The Journal of Clinical Investigation*, 126(3):865–878, 2016.

[164] Jacques J Peschon, Philip J Morrissey, Kenneth H Grabstein, Fred J Ramsdell, Eugene Maraskovsky, Brian C Gliniak, Linda S Park, Steven F Ziegler, Dooglas E Williams, Carol B Ware, et al. Early lymphocyte expansion is severely impaired in interleukin 7 receptor-deficient mice. *The Journal of Experimental Medicine*, 180(5):1955–1960, 1994.

[165] Satoko Adachi, Hisahiro Yoshida, Kenya Honda, Kazushige Maki, Kaoru Saijo, Kohichi Ikuta, Takashi Saito, and Shin-Ichi Nishikawa. Essential role of IL-7 receptor alpha in the formation of Peyer's patch anlage. *International Immunology*, 10(1):1–6, 1998.

[166] Malay Mandal, Michael K Okoreeh, Domenick E Kennedy, Mark Maienschein-Cline, Junting Ai, Kaitlin C McLean, Natalya Kaverina, Margaret Veselits, Iannis Aifantis, Fotini Gounari, et al. Cxcr4 signaling directs Igk recombination and the molecular mechanisms of late B lymphopoiesis. *Nature Immunology*, 20(10):1393–1403, 2019.

[167] Qing Yu, Batu Erman, Jung-Hyun Park, Lionel Feigenbaum, and Alfred Singer. Il-7 receptor signals inhibit expression of transcription factors TCF-1, LEF-1, and RORγt: impact on thymocyte development. *The Journal of Experimental Medicine*, 200(6): 797–803, 2004.

[168] Jung-Hyun Park, Qing Yu, Batu Erman, Jacob S Appelbaum, Diego Montoya-Durango, H Leighton Grimes, and Alfred Singer. Suppression of IL7Rα transcription by IL-7 and other prosurvival cytokines: a novel mechanism for maximizing IL-7-dependent T cell survival. *Immunity*, 21(2):289–302, 2004.

[169] Hai-Chon Lee, Hirofumi Shibata, Shinya Ogawa, Kazushige Maki, and Koichi Ikuta. Transcriptional regulation of the mouse IL-7 receptor α promoter by glucocorticoid receptor. *The Journal of Immunology*, 174(12):7800–7806, 2005.

[170] Akifumi Abe, Shizue Tani-ichi, Soichiro Shitara, Guangwei Cui, Hisataka Yamada, Hitoshi Miyachi, Satsuki Kitano, Takahiro Hara, Ryo Abe, Yasunobu Yoshikai, et al. An enhancer of the IL-7 receptor α-chain locus controls IL-7 receptor expression and maintenance of peripheral T cells. *The Journal of Immunology*, 195(7):3129–3138, 2015.

[171] Cliff Y Yang, J Adam Best, Jamie Knell, Edward Yang, Alison D Sheridan, Adam K Jesionek, Haiyan S Li, Richard R Rivera, Kristin Camfield Lind, Louise M D'cruz, et al. The transcriptional regulators Id2 and Id3 control the formation of distinct memory $CD8^+$ T cell subsets. *Nature Immunology*, 12(12):1221–1229, 2011.

[172] Darshan N Kasal and Albert Bendelac. Multi-transcription factor reporter mice delineate early precursors to the ILC and LTi lineages. *Journal of Experimental Medicine*, 218(2), 2020.

[173] M Ryan Corces, Alexandro E Trevino, Emily G Hamilton, Peyton G Greenside, Nicholas A Sinnott-Armstrong, Sam Vesuna, Ansuman T Satpathy, Adam J Rubin, Kathleen S Montine, Beijing Wu, et al. An improved ATAC-seq protocol reduces background and enables interrogation of frozen tissues. *Nature Methods*, 14(10):959, 2017.

[174] Jason D Buenrostro, Beijing Wu, Howard Y Chang, and William J Greenleaf. Atac-seq: a method for assaying chromatin accessibility genome-wide. *Current Protocols in Molecular Biology*, 109(1):21–29, 2015.

[175] Aaron TL Lun and Gordon K Smyth. De novo detection of differentially bound regions for ChIP-seq data using peaks and windows: controlling error rates correctly. *Nucleic Acids Research*, 42(11):e95–e95, 2014.

[176] Jason D Buenrostro, Beijing Wu, Ulrike M Litzenburger, Dave Ruff, Michael L Gonzales, Michael P Snyder, Howard Y Chang, and William J Greenleaf. Single-cell chromatin accessibility reveals principles of regulatory variation. *Nature*, 523(7561):486–490, 2015.

[177] M Ryan Corces, Jason D Buenrostro, Beijing Wu, Peyton G Greenside, Steven M Chan, Julie L Koenig, Michael P Snyder, Jonathan K Pritchard, Anshul Kundaje, William J Greenleaf, et al. Lineage-specific and single-cell chromatin accessibility charts human hematopoiesis and leukemia evolution. *Nature Genetics*, 48(10):1193–1203, 2016.

[178] Sven Heinz, Christopher Benner, Nathanael Spann, Eric Bertolino, Yin C Lin, Peter Laslo, Jason X Cheng, Cornelis Murre, Harinder Singh, and Christopher K Glass. Simple combinations of lineage-determining transcription factors prime cis-regulatory elements required for macrophage and B cell identities. *Molecular Cell*, 38(4):576–589, 2010.

[179] Han-Yu Shih, Giuseppe Sciumè, Yohei Mikami, Liying Guo, Hong-Wei Sun, Stephen R Brooks, Joseph F Urban, Fred P Davis, Yuka Kanno, and John J O'Shea. Developmental acquisition of regulomes underlies innate lymphoid cell functionality. *Cell*, 165 (5):1120–1133, 2016.

[180] Difeng Fang, Kairong Cui, Gangqing Hu, Rama Krishna Gurram, Chao Zhong, Andrew J Oler, Ryoji Yagi, Ming Zhao, Suveena Sharma, Pentao Liu, et al. Bcl11b, a novel GATA3-interacting protein, suppresses Th1 while limiting Th2 cell differentiation. *Journal of Experimental Medicine*, 215(5):1449–1462, 2018.

[181] Chizuko Miyamoto, Satoshi Kojo, Motoi Yamashita, Kazuyo Moro, Georges Lacaud, Katsuyuki Shiroguchi, Ichiro Taniuchi, and Takashi Ebihara. Runx/Cbfβ complexes protect group 2 innate lymphoid cells from exhausted-like hyporesponsiveness during allergic airway inflammation. *Nature Communications*, 10(1):1–13, 2019.

[182] Hiroyuki Hosokawa, Maile Romero-Wolf, Qi Yang, Yasutaka Motomura, Ditsa Levanon, Yoram Groner, Kazuyo Moro, Tomoaki Tanaka, and Ellen V Rothenberg. Cell type–specific actions of Bcl11b in early T-lineage and group 2 innate lymphoid cells. *Journal of Experimental Medicine*, 217(1), 2020.

[183] Lai Wei, Golnaz Vahedi, Hong-Wei Sun, Wendy T Watford, Hiroaki Takatori, Haydee L Ramos, Hayato Takahashi, Jonathan Liang, Gustavo Gutierrez-Cruz, Chongzhi Zang, et al. Discrete roles of STAT4 and STAT6 transcription factors in tuning epigenetic modifications and transcription during T helper cell differentiation. *Immunity*, 32(6): 840–851, 2010.

[184] Le Cong, F Ann Ran, David Cox, Shuailiang Lin, Robert Barretto, Naomi Habib, Patrick D Hsu, Xuebing Wu, Wenyan Jiang, Luciano A Marraffini, et al. Multiplex genome engineering using CRISPR/Cas systems. *Science*, 339(6121):819–823, 2013.

[185] Katja Mohrs, Adil E Wakil, Nigel Killeen, Richard M Locksley, and Markus Mohrs. A two-step process for cytokine production revealed by IL-4 dual-reporter mice. *Immunity*, 23(4):419–429, 2005.

[186] Joo-Young Park, Devon T DiPalma, Juntae Kwon, Juliet Fink, and Jung-Hyun Park. Quantitative difference in PLZF protein expression determines iNKT lineage fate and controls innate CD8 t cell generation. *Cell Reports*, 27(9):2548–2557, 2019.

[187] Christine Mayr. Regulation by 3'-untranslated regions. *Annual Review of Genetics*, 51:171–194, 2017.

[188] Steven J Van Dyken, Jesse C Nussbaum, Jinwoo Lee, Ari B Molofsky, Hong-Erh Liang, Joshua L Pollack, Rachel E Gate, Genevieve E Haliburton, J Ye Chun, Alexander Marson, et al. A tissue checkpoint regulates type 2 immunity. *Nature Immunology*, 17 (12):1381–1387, 2016.

[189] Yisong Y Wan. Gata3: a master of many trades in immune regulation. *Trends in Immunology*, 35(6):233–242, 2014.

[190] Jinfang Zhu. Gata3 regulates the development and functions of innate lymphoid cell subsets at multiple stages. *Frontiers in Immunology*, 8:1571, 2017.

[191] Matthew J Gold, Frann Antignano, Timotheus YF Halim, Jeremy A Hirota, Marie-Renee Blanchet, Colby Zaph, Fumio Takei, and Kelly M McNagny. Group 2 innate lymphoid cells facilitate sensitization to local, but not systemic, TH2-inducing allergen exposures. *Journal of Allergy and Clinical Immunology*, 133(4):1142–1148, 2014.

[192] Timotheus YF Halim, Catherine A Steer, Laura Mathä, Matthew J Gold, Itziar Martinez-Gonzalez, Kelly M McNagny, Andrew NJ McKenzie, and Fumio Takei. Group 2 innate lymphoid cells are critical for the initiation of adaptive T helper 2 cell-mediated allergic lung inflammation. *Immunity*, 40(3):425–435, 2014.

[193] Koubun Yasuda, Takumi Adachi, Atsuhide Koida, and Kenji Nakanishi. Nematode-infected mice acquire resistance to subsequent infection with unrelated nematode by inducing highly responsive group 2 innate lymphoid cells in the lung. *Frontiers in Immunology*, 9:2132, 2018.

[194] Tracy SP Heng, Michio W Painter, Kutlu Elpek, Veronika Lukacs-Kornek, Nora Mauermann, Shannon J Turley, Daphne Koller, Francis S Kim, Amy J Wagers, Natasha Asinovski, et al. The Immunological Genome Project: networks of gene expression in immune cells. *Nature Immunology*, 9(10):1091–1094, 2008.

[195] Wing Fuk Chan, Hannah D Coughlan, Nadia Iannarella, Gordon K Smyth, Timothy M Johanson, Christine R Keenan, and Rhys S Allan. Identification and characterization of the long noncoding RNA Dreg1 as a novel regulator of *Gata3*. *Immunology and Cell Biology*, 99(3):323–332, 2021.

[196] Gangqing Hu, Qingsong Tang, Suveena Sharma, Fang Yu, Thelma M Escobar, Stefan A Muljo, Jinfang Zhu, and Keji Zhao. Expression and regulation of intergenic long noncoding RNAs during T cell development and differentiation. *Nature Immunology*, 14(11):1190–1198, 2013.

[197] Tomonori Hosoya, Ricardo D'Oliveira Albanus, John Hensley, Greggory Myers, Yasuhiro Kyono, Jacob Kitzman, Stephen CJ Parker, and James Douglas Engel. Global dynamics of stage-specific transcription factor binding during thymocyte development. *Scientific Reports*, 8(1):1–10, 2018.

[198] Liying Guo, Gang Wei, Jinfang Zhu, Wei Liao, Warren J Leonard, Keji Zhao, and William Paul. Il-1 family members and STAT activators induce cytokine production by Th2, Th17, and Th1 cells. *Proceedings of the National Academy of Sciences*, 106 (32):13463–13468, 2009.

[199] Morisada Hayakawa, Ken Yanagisawa, Shinsuke Aoki, Hiroko Hayakawa, Naoki Takezako, and Shin-ichi Tominaga. T-helper type 2 cell-specific expression of the ST2 gene is regulated by transcription factor GATA-3. *Biochimica et Biophysica Acta (BBA)-Gene Structure and Expression*, 1728(1-2):53–64, 2005.

[200] Irma Tindemans, Nicolas Serafini, James P Di Santo, and Rudi W Hendriks. Gata-3 function in innate and adaptive immunity. *Immunity*, 41(2):191–206, 2014.

[201] Gang Wei, Brian J Abraham, Ryoji Yagi, Raja Jothi, Kairong Cui, Suveena Sharma, Leelavati Narlikar, Daniel L Northrup, Qingsong Tang, William E Paul, et al. Genome-wide analyses of transcription factor GATA3-mediated gene regulation in distinct T cell types. *Immunity*, 35(2):299–311, 2011.

[202] Jinfang Zhu, Hidehiro Yamane, and William E Paul. Differentiation of effector CD4 T cell populations. *Annual Review of Immunology*, 28:445–489, 2009.

[203] Jun-ichi Furusawa, Kazuyo Moro, Yasutaka Motomura, Kazuo Okamoto, Jinfang Zhu, Hiroshi Takayanagi, Masato Kubo, and Shigeo Koyasu. Critical role of p38 and GATA3 in natural helper cell function. *The Journal of Immunology*, 191(4):1818–1826, 2013.

[204] Bobby WS Li, Dior MJM Beerens, Maarten D Brem, and Rudi W Hendriks. Characterization of group 2 innate lymphoid cells in allergic airway inflammation models in the mouse. In *Inflammation*, pages 169–183. Springer, 2017.

[205] Daniela Cipolletta, Markus Feuerer, Amy Li, Nozomu Kamei, Jongsoon Lee, Steven E Shoelson, Christophe Benoist, and Diane Mathis. Ppar-γ is a major driver of the accumulation and phenotype of adipose tissue T reg cells. *Nature*, 486(7404):549–553, 2012.

[206] Jonathan M Han, Dan Wu, Heather C Denroche, Yu Yao, C Bruce Verchere, and Megan K Levings. Il-33 reverses an obesity-induced deficit in visceral adipose tissue $ST2^+$ T regulatory cells and ameliorates adipose tissue inflammation and insulin resistance. *The Journal of Immunology*, 194(10):4777–4783, 2015.

[207] Kaori Mukai, Hajime Karasuyama, Kenji Kabashima, Masato Kubo, and Stephen J Galli. Differences in the importance of mast cells, basophils, IgE, and IgG versus that of $CD4^+$ T cells and ILC2 cells in primary and secondary immunity to *Strongyloides venezuelensis*. *Infection and Immunity*, 85(5), 2017.

[208] Koubun Yasuda, Taichiro Muto, Tatsukata Kawagoe, Makoto Matsumoto, Yuki Sasaki, Kazufumi Matsushita, Yuko Taki, Shizue Futatsugi-Yumikura, Hiroko Tsutsui, Ken J Ishii, et al. Contribution of IL-33–activated type ii innate lymphoid cells to pulmonary

eosinophilia in intestinal nematode-infected mice. *Proceedings of the National Academy of Sciences*, 109(9):3451–3456, 2012.

[209] Edgar Wingender. The TRANSFAC project as an example of framework technology that supports the analysis of genomic regulation. *Briefings in Bioinformatics*, 9(4): 326–332, 2008.

[210] Wenjun Ouyang, Max Löhning, Zhiguang Gao, Mario Assenmacher, Sheila Ranganath, Andreas Radbruch, and Kenneth M Murphy. Stat6-independent GATA-3 autoactivation directs IL-4-independent Th2 development and commitment. *Immunity*, 12(1): 27–37, 2000.

[211] Jinfang Zhu. T helper 2 (Th2) cell differentiation, type 2 innate lymphoid cell (ILC2) development and regulation of interleukin-4 (IL-4) and IL-13 production. *Cytokine*, 75 (1):14–24, 2015.

[212] Scott Barolo. Shadow enhancers: frequently asked questions about distributed cis-regulatory information and enhancer redundancy. *Bioessays*, 34(2):135–141, 2012.

[213] Catherine A Guenther, Bosiljka Tasic, Liqun Luo, Mary A Bedell, and David M Kingsley. A molecular basis for classic blond hair color in Europeans. *Nature Genetics*, 46 (7):748–752, 2014.

[214] Shruti Naik, Samantha B Larsen, Nicholas C Gomez, Kirill Alaverdyan, Ataman Sendoel, Shaopeng Yuan, Lisa Polak, Anita Kulukian, Sophia Chai, and Elaine Fuchs. Inflammatory memory sensitizes skin epithelial stem cells to tissue damage. *Nature*, 550(7677):475–480, 2017.

[215] Francis Poulin, Marcelo A Nobrega, Ingrid Plajzer-Frick, Amy Holt, Veena Afzal, Edward M Rubin, and Len A Pennacchio. In vivo characterization of a vertebrate ultraconserved enhancer. *Genomics*, 85(6):774–781, 2005.

[216] Paige Snider, Jana L Fix, Rhonda Rogers, Goldie Peabody-Dowling, David Ingram, Brenda Lilly, and Simon J Conway. Generation and characterization of Csrp1 enhancer-driven tissue-restricted Cre-recombinase mice. *genesis*, 46(3):167–176, 2008.

[217] Bosiljka Tasic, Simon Hippenmeyer, Charlene Wang, Matthew Gamboa, Hui Zong, Yanru Chen-Tsai, and Liqun Luo. Site-specific integrase-mediated transgenesis in mice via pronuclear injection. *Proceedings of the National Academy of Sciences*, 108 (19):7902–7907, 2011.

[218] Hirokazu Kurata, Hyun Jun Lee, Anne O'Garra, and Naoko Arai. Ectopic expression of activated stat6 induces the expression of Th2-specific cytokines and transcription factors in developing Th1 cells. *Immunity*, 11(6):677–688, 1999.

[219] Jinfang Zhu, Liying Guo, Cynthia J Watson, Jane Hu-Li, and William E Paul. Stat6 is necessary and sufficient for IL-4's role in Th2 differentiation and cell expansion. *The Journal of Immunology*, 166(12):7276–7281, 2001.

[220] Helena Stabile, Gianluca Scarno, Cinzia Fionda, Angela Gismondi, Angela Santoni, Massimo Gadina, and Giuseppe Sciumè. Jak/STAT signaling in regulation of innate lymphoid cells: the gods before the guardians. *Immunological Reviews*, 286(1):148–159, 2018.

[221] Timotheus YF Halim, You Yi Hwang, Seth T Scanlon, Habib Zaghouani, Natalio Garbi, Padraic G Fallon, and Andrew NJ McKenzie. Group 2 innate lymphoid cells license dendritic cells to potentiate memory TH 2 cell responses. *Nature Immunology*, 17(1):57–64, 2016.

[222] Nancy Noben-Trauth, Jane Hu-Li, and William E Paul. Il-4 secreted from individual naive $CD4^+$ T cells acts in an autocrine manner to induce Th2 differentiation. *European Journal of Immunology*, 32(5):1428–1433, 2002.

[223] Sven Heinz, Casey E Romanoski, Christopher Benner, and Christopher K Glass. The selection and function of cell type-specific enhancers. *Nature Reviews. Molecular Cell Biology*, 16(3):144, 2015.

[224] Jason D Buenrostro, Paul G Giresi, Lisa C Zaba, Howard Y Chang, and William J Greenleaf. Transposition of native chromatin for fast and sensitive epigenomic profiling of open chromatin, DNA-binding proteins and nucleosome position. *Nature Methods*, 10(12):1213–1218, 2013.

[225] Sascha Cording, Jasna Medvedovic, Emelyne Lécuyer, Tegest Aychek, François Déjardin, and Gérard Eberl. Mouse models for the study of fate and function of innate lymphoid cells. *European journal of immunology*, 48(8):1271–1280, 2018.

[226] Bernard C Lo, Diana Canals Hernaez, R Wilder Scott, Michael R Hughes, Samuel B Shin, T Michael Underhill, Fumio Takei, and Kelly M McNagny. The transcription factor rorα preserves ilc3 lineage identity and function during chronic intestinal infection. *The Journal of Immunology*, 203(12):3209–3215, 2019.

[227] Paul Krimpenfort, R De Jong, Y Uematsu, Z Dembic, S Ryser, H Von Boehmer, M Steinmetz, and A Berns. Transcription of T cell receptor beta-chain genes is controlled by a downstream regulatory element. *The EMBO journal*, 7(3):745–750, 1988.